‘Investigating the Mur ligases of *Streptococcus agalactiae* for the development of inhibitory fragments’

Rebecca Jane Steventon, MRes

A thesis submitted in partial fulfilment of the requirements for the degree of

Doctor of Philosophy in Life Sciences

University of Warwick
School of Life Sciences

November 2022

Table of Contents

Table of Figures

Table of Tables

Acknowledgments

I would like to thank my supervisors Prof. Chris Dowson and Dr. Allister Crow for their guidance, support and patience during my PhD and allowing me to freely explore ideas and new techniques. I would also like to thank Dr. Joe Eyermann and his lab for allowing me to spend some time in his lab and providing his guidance and chemistry knowledge to the project. I would like to thank Frank von Delft for providing the funding to pursue inhibitor screens, and Prof. Matthew Todd, Dr. Dana Klug and their team at UCL for working with us to screen potential inhibitory fragments.

Particular thanks goes to those individuals who have helped develop my skills and knowledge over the course of my PhD. This includes Dr. Adrian Lloyd for his advice and guidance throughout my PhD in matters of microbiological and enzymology, and Dr Jonathan Cook who provided guidance and support for DNA cloning. Further thanks go to Sarah Bennet and WISB for allowing me to use their facilities as an external user. I would also like to acknowledge the help of the Media Preparation Facility in The School of Life Sciences at the University of Warwick for the supply of all media and selected buffers during the course of this thesis.

I would also like to thank all members of C10 and IBRB 2.17 past and present for their support, advice and friendship throughout my PhD.

Special thanks goes to my family, who have supported my love and passion for science over the years, and to my partner, Nic, who was always there throughout all the long days and stressful moments, and without who I couldn't have completed this thesis.

Declaration

I hereby declare that I personally have carried out the work submitted in this thesis under the supervision of Prof. Chris Dowson (School of Life Sciences) and Dr. Allister Crow (School of Life Sciences) at the University of Warwick and Dr. Joe Eyermann at the Department of Chemistry, University of Cape Town, South Africa. Where work has been contributed to by other individuals, it is specifically stated in the text. This project was completed as part of the open-source Mur ligase project.

No part of this work has previously been summited to be considered for a degree or qualification. All sources of information are specifically acknowledged in the form of references.

Abstract

Streptococcus agalactiae is the leading cause of early onset neonatal sepsis, and with antibacterial resistance within *S. agalactiae* increasing, it is imperative that new antibacterial drugs are identified. Proteins involved in peptidoglycan formation are an attractive target for the development of novel antibacterial drugs. The Mur ligases form part of the cytosolic stages of peptidoglycan formation, and are responsible for the stepwise addition of amino acids that constructs the peptide component of the peptidoglycan. Due to their similar catalytic mechanism and three domain structure, the Mur ligases are a promising target for the development of new antibacterial compounds.

This project has focused on identifying multi-targeting inhibitory fragments that are able to target MurD and MurE from *S. agalactiae*. To achieve this, biochemical assays have been developed and optimized for high throughput screening of competitive inhibitory fragments targeted towards the Mur ligases. A targeted fragment screen was then developed using *in silico* screening to allow the repurposing of existing protein kinase inhibitors to target the ATP-binding site of the Mur ligases. Screening of potential inhibitory fragments was carried out, allowing the identification of multi-targeting inhibitory fragments. Previous studies have suggested that there may be complex formation amongst the Mur ligases. The ability of MurD and MurE from *S. agalactiae* to form a binary complex was investigated using a range of cloning and expressing systems, and biophysical techniques including Microscale Thermophoresis before possible structural arrangements were predicted using computational techniques.

It is anticipated that the multi-targeting inhibitors identified via the optimized assays within this work, alongside our better understanding of complex formation amongst the Mur ligases, may be used for the development of effective Mur ligases inhibitors in the future and new potential therapeutic approaches to the treatment of bacterial infection.

Abbreviations

Abbreviations used within this thesis follow the nomenclature laid out for authors by the Journal of Biological Chemistry. Any non-standard abbreviations are listed below.

ADPCP	β,γ-Methyleneadenosine 5’-triphosphate
ADPNP	Adenosine 5’-(β,γ-imido)triphosphate
AUC	Analytical UltraCentrifugation
EOS	Early Onset Sepsis
HRP	Horse radish peroxidase
IMAC	Immobilized metal-ion affinity chromatography
LOS	Late Onset Sepsis
MESG	7 methyl 6 thio guanosine
MRSA	Methicillin-resistant Staphylococcus aureus
MurNAc	N-Acetylmuramic acid
MSA	Multiple Sequence Alignment
MST	Microscale Thermophoresis
PEP	Phosphoenolpyruvate
PK/LDH	Pyruvate Kinase/Lactate Dehydrogenase
PNP	Purine nucleoside phosphorylase
SEC	Size Exclusion Chromatography
SEDS	Shape, Elongation, Division and Sporulation
SPR	Surface Plasmon Resonance
STPK	Serine-threonine protein kinases
TAE	Tris Acetate EDTA

Chapter 1

Thesis Introduction

1.1 *Streptococcus agalactiae*

Streptococcus agalactiae (*S. agalactiae*), also referred to as Group B streptococcus, is a Gram positive coccus [1]. *S. agalactiae* was first differentiated from other streptococci in the 1930s with human pathogenicity identified in 1938 [2]. Since the 1960s there have been increasing reports of invasive *S. agalactiae* infections, with *S. agalactiae* infections being a leading cause of neonatal infections; being responsible for pneumonia, septicaemia and meningitis [1]. *S. agalactiae* can also be a cause of mortality for immunocompromised adults and the elderly [3].

1.1.1 Polysaccharide capsule

The capsule of *S. agalactiae* is an important virulence factor. Due to different polysaccharide structures, nine different *S. agalactiae* serotypes have been identified [2]. Serotype Ia, Ib, II, III and V are responsible for the majority of invasive human disease, with serotype III being responsible for the majority of neonatal infection cases. The capsule provides protection for the bacteria preventing clearance from the host immune system via processes such as complement deposition and phagocytosis [4].

1.2 *S. agalactiae* infection in adults

S. agalactiae is a leading cause of early onset neonatal infection, with most cases arising due to the mother infecting the child with the bacteria during childbirth. Most mothers are asymptomatic carriers, with few developing symptoms of their own. However, a recent trend has started to emerge with a shift in more disease within nonpregnant adults due to *S. agalactiae* infection. Within the UK, incidence rates of invasive *S. agalactiae* infection within nonpregnant adults trebled between 1996 and 2010, with a incidence rate of 2.9/100 000 population in 2015/2016 [5]. *S. agalactiae* infection within adults is predominately seen within the ageing population or within adults with underlying health conditions, especially those who have *diabetes mellitus* [6]. *S. agalactiae* infection

within adults can lead to a multitude of clinical manifestations, including pneumonia, soft-tissue infection, septicaemia and meningitis [6].

1.3 Neonatal sepsis

S. agalactiae is one of the leading causes of early onset neonatal sepsis. Sepsis occurs when an infection spreads throughout the body, and the immune response results in systemic inflammation of tissues and organs. This spread of infection can be lethal, especially to neonates who have a reduced immune system to fight off the infection. Neonatal sepsis is defined as sepsis occurring within the first 28 days of life [7]. However, neonatal sepsis is normally defined as either early onset sepsis (EOS) or late onset sepsis (LOS) depending on when infection occurs within those 28 days. EOS is usually defined as infection occurring within the first 72 hours of life, however this can be extended up to a week in some studies and hospitals. LOS is defined as infection occurring after 72 hours or a week of life. This distinction is important, as EOS and LOS are usually caused by different bacteria, with EOS being caused by bacteria transmitted via the mother or during birth, whereas LOS bacteria are community acquired [7].

1.3.1 Incidence of EOS

The incidence rate of neonatal sepsis worldwide is roughly 2.5 cases per 1000 live births. Estimates of the incidence of EOS and LOS differ due to the different mechanisms of infection. EOS has a worldwide incidence rate of roughly 0.75 cases per 1000 live births, with most countries showing similar figures [8–11]. True incidence rates for EOS are hard to determine due to the fact that many studies have different criteria for whether a birth is included in the values, especially in areas where most births take place within the community, but only hospital births are included in the numbers.

1.3.2 Mortality rate

It is estimated that worldwide, 36% of neonatal deaths are due to invasive neonatal infections [12]. Determining true mortality rates for EOS is tricky due to the

same issues that arise from trying to determine true incidence rates. Estimated mortality rates for EOS in Europe is 13%, with a similar rate being seen in the USA [12]. Oceania and Africa show slightly higher estimated mortality rates of 16% and 17.2% respectively [13,14]. The mortality rate of EOS in Asia is harder to determine, with rates between 10.4% and 34.4% being given [15].

1.4 Antibiotic treatment and emergence of antibiotic resistance

Typically within the UK, when neonatal sepsis has been identified, therapy is commenced before a causative organism is identified. This means that the common treatment plan is antibiotic intervention. Commonly therapeutic intervention for EOS within the UK consists of empiric antibiotic combinations. The first line therapy within the UK consists of the antibiotic combination of 50 mg/ kg/ dose amoxicillin with 50 mg/ kg/ dose cefotaxime if MRSA is not suspected [16]. If MRSA is suspected or the first line therapy is not an option then an antibiotic combination of 50 mg/ kg cefotaxime with 15 mg/ kg vancomycin is given [16]. The majority of EOS pathogens that are responsible for neonatal sepsis within the UK are susceptible to the most commonly used antibacterial combinations. Cefotaxime shows a susceptibility rate of 98%, while amoxicillin and cefotaxime shows a susceptibility rate of 95%. Amoxicillin and gentamicin, another antibiotic combination commonly used to treat EOS within the UK, shows a susceptibility rate of 96% [17]. Cefotaxime and amoxicillin currently have breakpoints of 0.25 mg/L against *S. agalactiae* [18], allowing them to still be considered as effective treatments for EOS. When *S. agalactiae* infection is identified within adults, a similar antibiotic treatment is considered with penicillin being the first line treatment. Other beta-lactam antibiotics are also considered such as ampicillin, cephalosporins and carbapenems [2].

However, antibiotic resistance is becoming a problem for treating *S. agalactiae*. Within the USA, 46% of *S. agalactiae* isolates within a study were found to be resistant to erythromycin, and 20% were resistant to clindamycin [19]. Within Asia, erythromycin resistance and clindamycin resistance within *S. agalactiae* is estimated to be 40%. Within Europe, 18% of *S. agalactiae* appear to be erythromycin resistant, and 16% resistant to clindamycin [20]. Within the UK, 15%

of invasive *S. agalactiae* infections in 2010 were resistant to erythromycin [21]. Erythromycin currently has a breakpoint of 0.5 mg/L against *S. agalactiae*, allowing it to still be considered as a possible treatment for *S. agalactiae* infection [18]. However, vancomycin currently has a breakpoint of 2 mg/L against *S. agalactiae*, while clindamycin currently has a breakpoint of 1 mg/L against *S. agalactiae* [18]. These breakpoints indicate that these antibiotics are becoming less effective for treatment of *S. agalactiae* infection. These increasing rates of antibiotic resistance make it essential that new antibiotics are developed to tackle *S. agalactiae* infections. One way of doing this is to develop new molecules that are able to effectively target bacterial components, such as the proteins involved in peptidoglycan formation.

1.5 Peptidoglycan

Peptidoglycan is an essential component of bacterial cell walls. Peptidoglycan used to be thought of as an inert structure surrounding bacterial cells but has been found to be a highly complex macromolecule that is dynamic and constantly being remodelled. Peptidoglycan consists of the simple building blocks of GlcNAc and MurNAc pentapeptide, with glycan chains being built of alternating units of these two-building blocks [22]. These linear glycan chains then become interlinked by short peptides. This interlinking between the chains creates a macromolecular mesh which has a high tensile strength and rigidity. This strength and rigidity help maintain the structural integrity of the bacterial cell wall. The bacterial cell wall is essential for bacterial survival via its ability to help maintain bacterial cell shape as well as offer mechanical resistance and insulation from differences in osmotic pressure [23].

1.5.1 Formation

Peptidoglycan formation is a multistep process that occurs within the cytoplasm, inner membrane and periplasm of a bacterial cell as seen in **Figure 1.1**. It begins with the formation of UDP-GlcNAc. UDP-GlcNAc is formed from fructose-6-phosphate via a four step process which is catalysed via GlmS, GlmM and GlmU

[23,24]. UDP-GlcNAc is then converted to UDP-MurNAc via two enzymes; MurA and MurB. MurA is a transferase enzyme which transfers an enolpyruvate from phosphoenolpyruvate onto UDP-GlcNAc. MurB acts as a reductase enzyme by reducing the enolpyruvate moiety to a D-lactoyl. After the UDP-MurNAc component has been formed, a stepwise addition of amino acids occurs. This is carried out by four Mur ligases, resulting in the formation of the UDP-MurNAc pentapeptide [24,25].

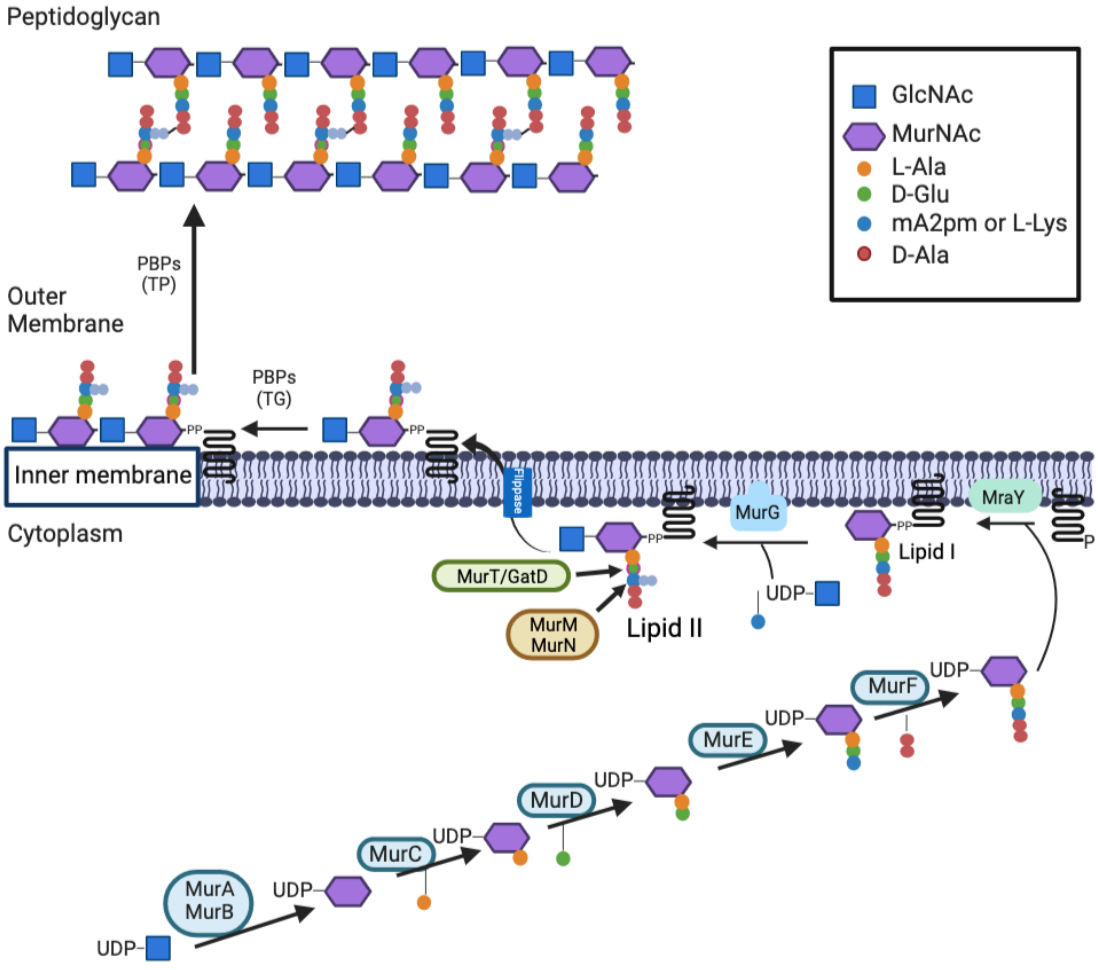

Figure 1. 1: A schematic representation of the cytoplasmic, inner membrane and periplasmic steps of the formation of peptidoglycan.

Within the cytoplasm, UDP-GlcNAc is converted to UDP-MurNAc via MurA and MurB. UDP-MurNAc passes through four Mur ligases to form UDP-MurNAc-pentapeptide. MraY and MurG then generate Lipid I and Lipid II which is then flipped to the periplasmic space. Within the periplasmic space penicillin binding proteins polymerise Lipid II into long glycan chains. Image generated via Biorender.

Phospho-MurNAc pentapeptide is then transferred to undecaprenyl phosphate by MraY, a membrane bound protein, to form undecaprenyl

pyrophosphoryl MurNAc pentapeptide (Lipid I). MurG than generates Lipid II via the addition of N-acetylglucosamine to the C-4 position of the MurNAc sugar ring of Lipid I generating undecaprenyl pyrophosphoryl MurNAc (GlcNAc) pentapeptide. At this point in *Streptococcus* the stem peptide C-1 glutamate is amidated via the enzyme complex MurT/GatD [26], and the stem peptide is branched by the construction of a serine-alanine or alanine-alanine dipeptide to the ε -amino group of the stem peptide lysine via MurM and MurN [27]. This is then flipped to the periplasm through the actions of the flippase, MurJ [24,25,28].

Polymerisation of these Lipid II monomers then occurs via transglycosylation in reactions catalysed by either bifunctional penicillin binding proteins or SEDS [29] proteins. Penicillin binding proteins are also responsible for the transpeptidation that allows cross linking of the glycan strands to occur. The formation of peptidoglycan occurs in the overwhelming majority of bacteria[30], although the thickness of the peptidoglycan layers varies. Gram negative bacteria have a peptidoglycan layer between 3-6 nm while Gram positive bacteria possess a peptidoglycan layer with a thickness of between 10-20 nm, with a greater level of cross-linking [24].

1.5.2 Antibiotic targets and current antibiotics

Peptidoglycan is absent in higher eukaryotes [31], making it an attractive target for antibacterial agents [25]. Many antibiotics exist which are able to target and interfere with the correct biosynthesis and assembly of peptidoglycan, as seen in **Figure 1.2**. There are two main antibiotics that are able to target the cytoplasmic stages of peptidoglycan formation. Fosfomycin is able to mimic the substrate phosphoenolpyruvate and bind in its place to MurA thereby inhibiting the first Mur enzyme involved in peptidoglycan formation. Fosfomycin is able to bind to MurA via a thioether bond to the key residue Cys115 thereby inhibiting the first committed step of peptidoglycan synthesis. Fosfomycin is a broad spectrum bactericidal antibiotic, and is highly effective against Gram-positive pathogens [32]. The other antibiotic targets the D-Ala-D-Ala ligase and the D-Ala racemase. Inhibition of these enzymes starves the bacteria of D-Ala, preventing the

biosynthesis of peptidoglycan. D-cycloserine is an example of such an inhibitor, which acts as a reversible competitive inhibitor, acting as a suicide substrate[25,33].

Antibacterial compounds also exist which are able to target the membrane associated stages of peptidoglycan formation. There are a number of naturally occurring inhibitors that are able to act against MraY, such as tunicamycin. However, there is a lack of specificity within these inhibitors due to the structural similarity between MraY and human GlcNAc-1-phosphate transferases, allowing the inhibitors to act against both, preventing it from being used as an antibiotic [34].

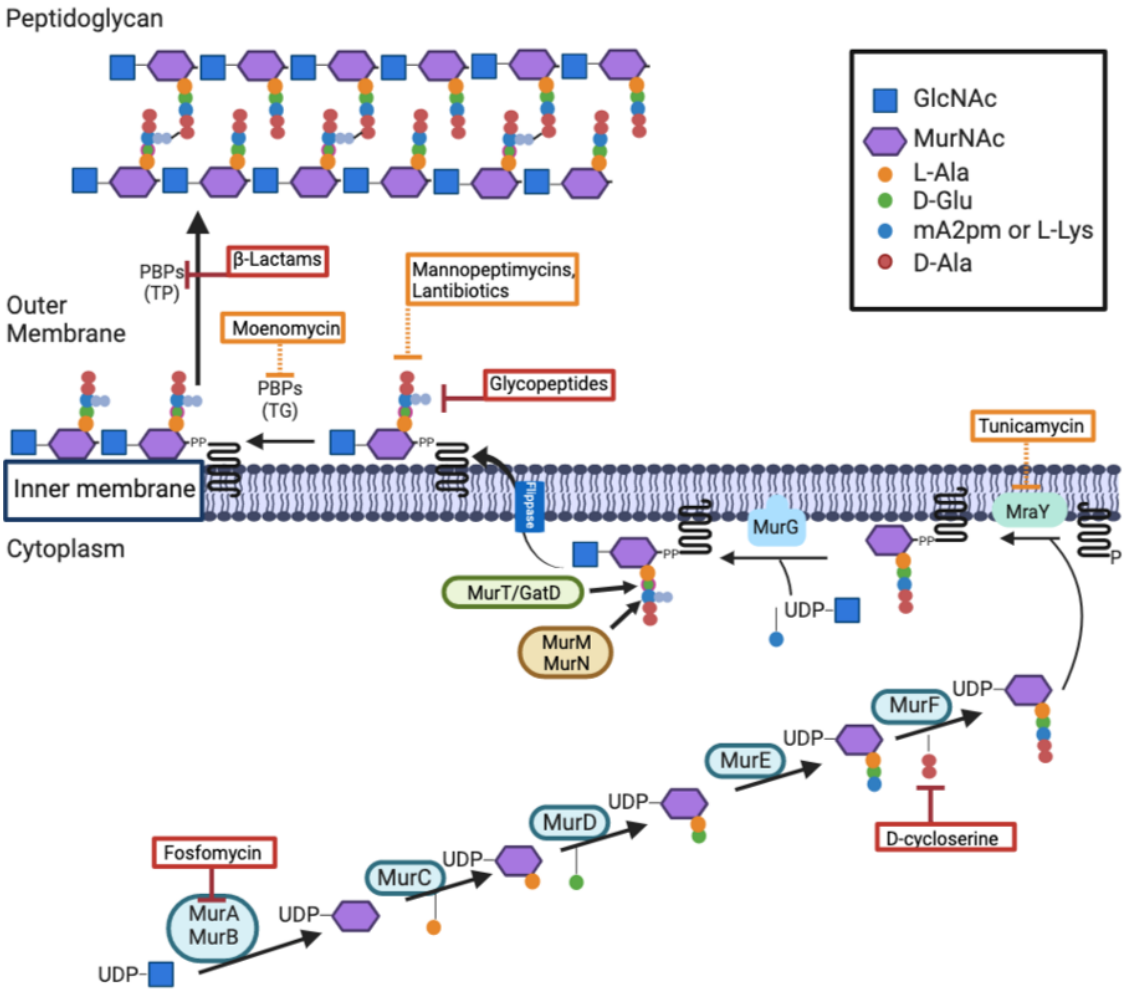

Figure 1. 2: Schematic diagram of the formation of peptidoglycan with antibiotic targets identified

Many antibacterial compounds exist which can target and interfere with the correct biosynthesis and assembly of peptidoglycan. Antibacterial compounds are shown here at the stage of formation that they inhibit. Antibacterial compounds used to treat human pathogens are shown in red. Antibacterial compounds in development or not in use against human pathogens are shown in orange. Image generated via Biorender.

Three classes of antibacterial compounds exist which are able to target Lipid II; mannopeptimycins, lantibiotics, and glycopeptide antibiotics. Mannopeptimycins are characterised by a cyclic ring structure formed of six amino acids in alternating D- and L- configurations, and bind to Lipid II, sequestering it preventing bacterial cell wall synthesis [35,36].

Lantibiotics contain the rare thioether amino acids of lanthionine and/or 3-methyllanthionine and are split into two types dependent on their mode of action and structure. Type A lantibiotics are able to form pores in the cytoplasmic membrane of bacteria, allowing for the rapid efflux of small metabolites from the cell, leading to cell death. Nisin, a Type A lantibiotic, uses Lipid II as a docking molecule to be able to bind to the bacterial membrane to aid in the formation of pores [37]. Type B lantibiotics comprise of rigid, globular peptides that either have no net charge or a net negative charge. Mersacidin, a Type B lantibiotic, is able to bind to Lipid II and inhibit cell wall biosynthesis [38,39].

Glycopeptide antibiotics are glycosylated non-ribosomal peptides with unique tricyclic or tetracyclic heptapeptide cores. The heptapeptide backbone of the glycopeptide generally binds to the C-terminal L-Lys-D-Ala-D-Ala of Lipid II inhibiting the transglycosylation step of peptidoglycan formation, as with vancomycin [40]. Other glycopeptide antibacterial compounds, such as ramoplanin, potentially target the disaccharide head group of Lipid II [41]. Targeting Lipid II leads to a weakened cell wall, and subsequently the cell undergoes cytolysis and cell death [42,43].

Moenomycin antibacterial compounds are able to target the transglycosylation stage of peptidoglycan formation. Moenomycins interact with the transmembrane domain of PBPs to prevent the transglycosylation of Lipid II [44]. Moenomycins are potent antibacterials, with minimum inhibitory concentrations ranging from 1 ng/mL to 100 ng/L. Currently the only moenomycin in use is Flavomycin, which is used within animal feed [45].

Antibiotics that target the penicillin binding proteins are some of the most widely used antibiotic agents. β-lactams inhibit bacterial cell wall synthesis by binding to penicillin binding proteins, leading to acylation of the active site serine of these enzymes thereby preventing their transpeptidase activity [46]. β-lactams have a ring structure that mimics the D-Ala-D-Ala moiety of the pentapeptide terminal

allowing them to act as substrate for the enzyme during the acylation phase of cross-link formation, preventing peptide bond formation and cross-linking from occurring [47].

One step of peptidoglycan formation with virtually no targeted antibiotics is the stepwise addition of amino acids onto the UDP-MurNAc component which is controlled by the Mur ligases.

1.6 Mur Ligases

1.6.1 Role within peptidoglycan formation

Within the cytoplasmic steps of peptidoglycan formation, the stepwise addition of amino acids onto UDP-MurNAc occurs through the actions of the Mur enzymes as seen in **Figure 1.3**. There are four Mur enzymes; MurC, MurD, MurE and MurF, which are all ATP- dependent amino acid ligases [25].

MurC is the first ligase in the pathway and is responsible for the addition of the first amino acid onto the newly formed UDP-MurNAc. MurC adds L-Ala to UDP-MurNAc generating UDP-MurNAc-L-Ala. MurD, the second ligase in the pathway, catalyses formation of a peptide bond formation between the α -amino group of D-Glu and the α -carboxyl of the L-alanyl moiety of UDP-MurNAc-L-Ala yielding UDP-MurNAc-L-Ala-D-Glu.

MurE is the only Mur ligase which has a substrate specificity that differs between bacteria. Typically, MurE catalyses the addition of meso-diaminopimelic (DAP) to the γ -glutamyl carboxyl of UDP-MurNAc-L-Ala-D-Glu within Gram negative bacteria, Gram positive bacillus and mycobacteria. Within Gram positive bacteria, MurE catalyses the addition of L-Lys to UDP-MurNAc-L-Ala-D-Glu. The addition of this amino acid is very important for the survival of the bacteria, as the third residue is involved in the cross-linking of the peptidoglycan macromolecule, and any 'wrong' addition would result in cell lysis [48].

MurF is the final Mur ligase and catalyses the addition of a dipeptide composed of D-amino acids, generating the final peptidoglycan precursor of UDP-MurNAc-pentapeptide. This addition of a dipeptide is crucial for peptidoglycan formation as the dipeptide bond provides the energy required for glycan strand

cross linking within the periplasm, where there is no ATP [22]. Generally, MurF catalyses the addition of D-Ala-D-Ala, however, MurF is able to catalyse the addition of many dipeptide substrates in the D conformation such as D-Ala-D-Lac. The ability to catalyse the addition of various dipeptide substrates is crucial for high-level resistance to vancomycin which is specific in its recognition of the D-alanyl-D-alanine of peptidoglycan precursors. Substitution of this dipeptide with D-alanyl-D-lactate furnishes peptidoglycan precursors that are not recognised by vancomycin, leading to clinically significant resistance to this antibiotic [25].

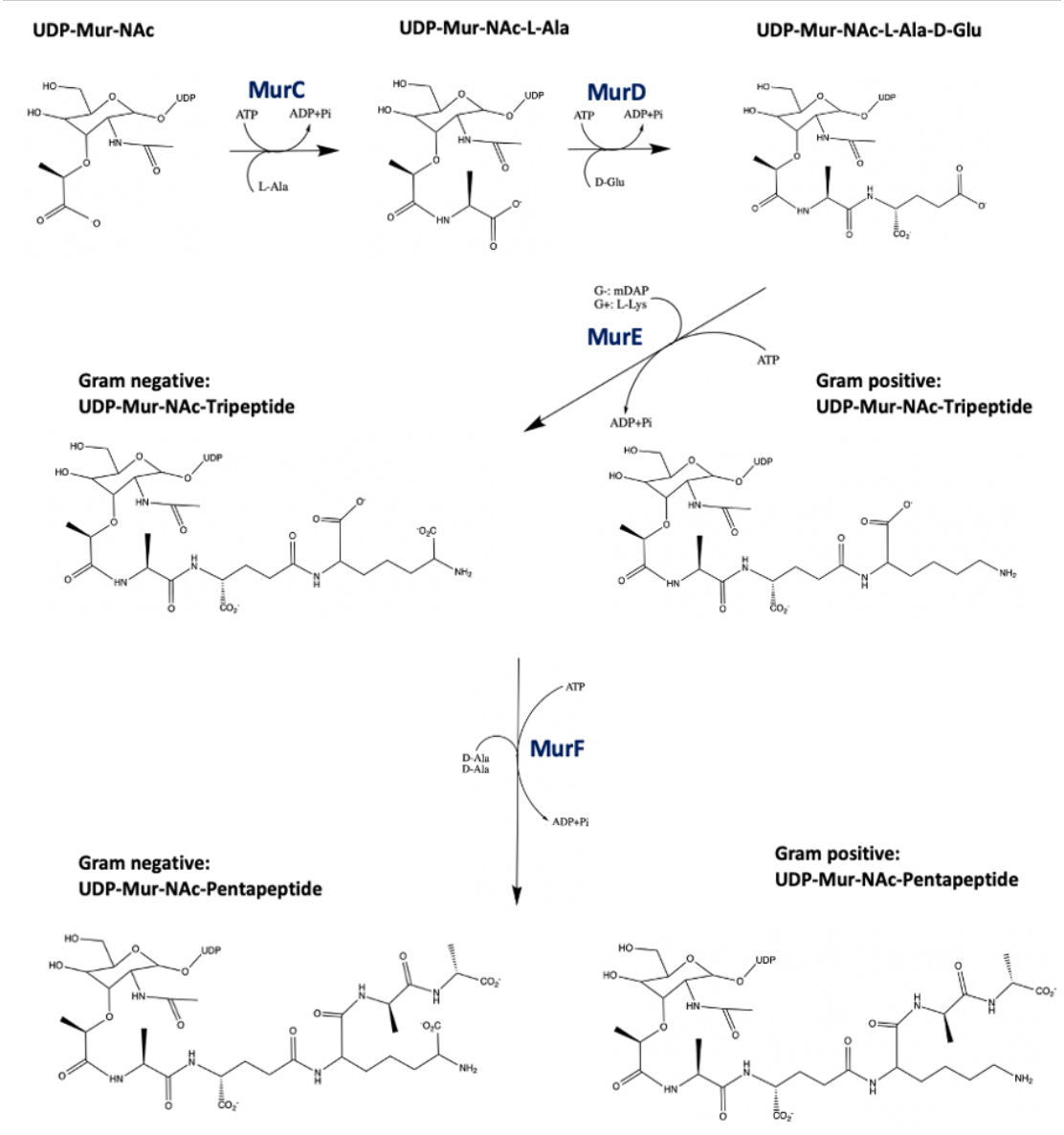

Figure 1. 3: Formation of UDP-MurNAc-pentapeptide by the Mur ligases.

MurC is the initial enzyme which converts UDP-MurNAc to UDP-MurNAc-L-Ala via the addition of L-Ala. MurD then adds D-Glu to the moiety. MurE then either ligates mA2pm or L-Lys before MurF catalyses the final addition of D-Ala-D-Ala.

1.6.2 Regulation of the Mur ligase pathway

The activity of the Mur ligases, and overall peptidoglycan formation is subject to regulation within the bacterial cell. As can be seen from **Figure 1.4,** substrates and products within the Mur ligase stages of peptidoglycan formation can act as inhibitors of the enzymes involved, leading to a regulation of the formation of peptidoglycan.

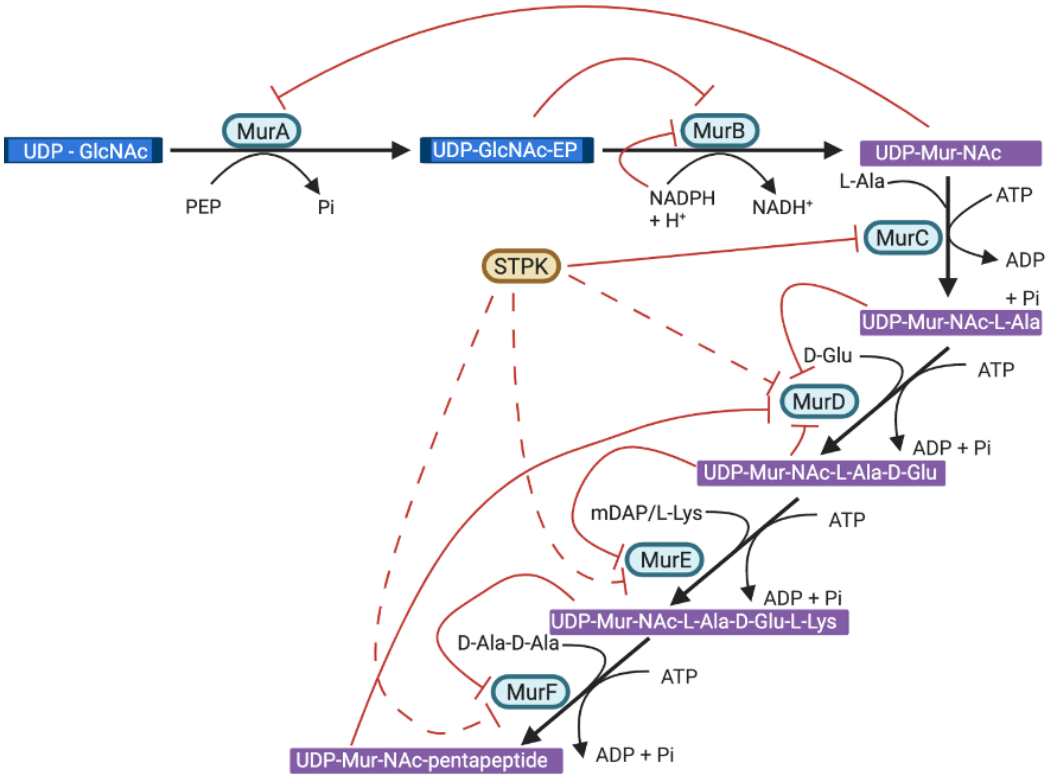

Figure 1. 4: Schematic diagram of the regulation of the Mur ligase pathway

Within peptidoglycan formation, the Mur ligase steps are subject to regulation. Various substrates and products act as inhibitors of enzymes within the pathway, leading to negative feedback loops and regulation of the activity of the enzymes. Routes of inhibition are shown in red. Predicted inhibition are shown in dashes. Image generated via biorender.

The activity of MurA is regulated via a negative feedback loop of the product of MurB, UDP-Mur-NAc. An accumulation of this product of MurB causes inhibition of the activity of MurA, potentially via binding within the active site of MurA [49]. UDP-Mur-NAc is able to act as an inhibitor of both MurA substrates, PEP and UDP-GlcNAc, although the method of inhibition is still unknown [49]. This level of regulation may prevent unwarranted peptidoglycan formation as MurA acts as the

first committed step of peptidoglycan formation. This level of regulation can be exploited via antibiotics that target MurC as inhibition of MurC could cause a build-up of its substrate UDP-MurNAc, allowing for secondary inhibition of MurA.

The activity of MurB is regulated via its own substrates, UDP-GlcNAc-enolpyruvate and NADPH. UDP-GlcNAc-EP can act as a strong competitive substrate inhibitor of MurB, while NADPH acts as a weak competitive substrate inhibitor [50]. Inhibition via NADPH and UDP-GlcNAc-EP appears to be pH-dependent, with UDP-GlcNAc-EP exhibiting less inhibition as the pH becomes more basic, while inhibition via NADPH becomes more pronounced as the pH becomes more basic [50]. This regulation may allow an antibiotic that binds in a similar fashion to UDP-GlcNAc-EP or NADPH to be used as an inhibitor of the activity of MurB.

Within peptidoglycan formation, the Mur ligases activity can be regulated via their own respective UDP-MurNAc substrates. Within gram negative bacteria, UDP-MurNAc-L-Ala is able to act as a substrate inhibitor of MurD [51]. UDP-MurNAc-L-Ala-D-Glu can act as a substrate inhibitor of MurE [52], while UDP-MurNAc-L-Ala-D-Glu-L-Lys/DAP can act as a substrate inhibitor of MurF [53]. MurD activity can also be regulated either via its own UDP-MurNAc product, UDP-MurNAc-L-Ala-D-Glu, or via the final product of the Mur ligase pathway, UDP-MurNAc-pentapeptide [53,54]. Substrate inhibition can be exploited within antibiotic development via the development of compounds that target the UDP-MurNAc binding site.

Serine-threonine protein kinases (STPKs) are responsible for the phosphorylation of multiple bacterial proteins resulting in the regulation of various bacterial systems. STPKs have been found to interact with all the Mur ligases [55]. The STPK PknA, has been found to cause the phosphorylation of MurC *in vitro* resulting in a decrease in the activity of MurC [56]. Phosphorylation of the Mur ligases represents a key mechanism in the regulation of peptidoglycan formation, and a key mechanism for antibiotic design. Development of a compound that can interact with the residues that undergo phosphorylation could reduce activity of the Mur ligases.

1.6.3 Mechanism of action

Mur ligases all have similar catalytic mechanisms which rely on the conversion of ATP to ADP and inorganic phosphate. The breaking of the phosphate bond provides the energy required to catalyse the ligation of amino acids onto a growing peptide chain. A set binding order is followed, beginning with ATP, followed by the uridine nucleotide substrate and ending with the amino acid or dipeptide [57,58]. The reaction follows an ordered kinetic mechanism, beginning with the activation by phosphorylation of the carboxyl group of the nucleotide via ATP as seen in **Figure 1.5**.

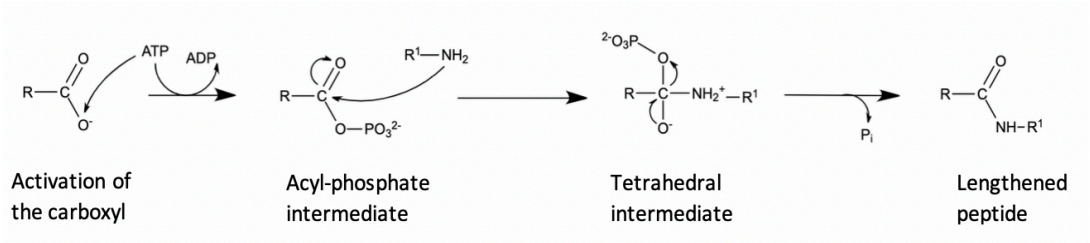

Figure 1. 5: The catalytic mechanism shared by the Mur ligases.

The reaction begins with the activation of the carboxyl group via ATP, which leads to the formation of an acyl-phosphate intermediate. A nucleophilic attack by the amino acid lead to the formation of a tetrahedral intermediate, which then breaks down into the lengthened peptide and P_i.

Catalysis requires juxtaposition of two Mg^{2+} ions, one located between the β- and γ- phosphate groups of ATP, the other between ADP and the uridine nucleotide substrate to bridge the negatively charged groups of ATP and the uridine nucleotide substrate[58]. The Mg^{2+} polarizes the γ -phosphate-oxygen bond of ATP, increasing its reactivity to nucleophilic attack by the carboxyl of the UDP-MurNAc precursor. This leads to phosphorylation of the UDP MurNAc carboxylate group to form an acyl-phosphate intermediate. Subsequently, an S_n2 nucleophilic attack by the amino group of the condensing amino acid or dipeptide then occurs, resulting in the formation of a peptide bond and a tetrahedral transition state which collapses on expulsion of the phosphate to form the lengthened peptide for the next stage of peptidoglycan intermediate formation [58].

1.6.4 Structure of the Mur ligases

The four Mur ligases all share a similar three domain structure, with each Mur ligase comprising of a N-terminal domain, central domain and C-terminal domain, with an active structure being present at the common domain interface [59] as seen in **Figure 1.6**.

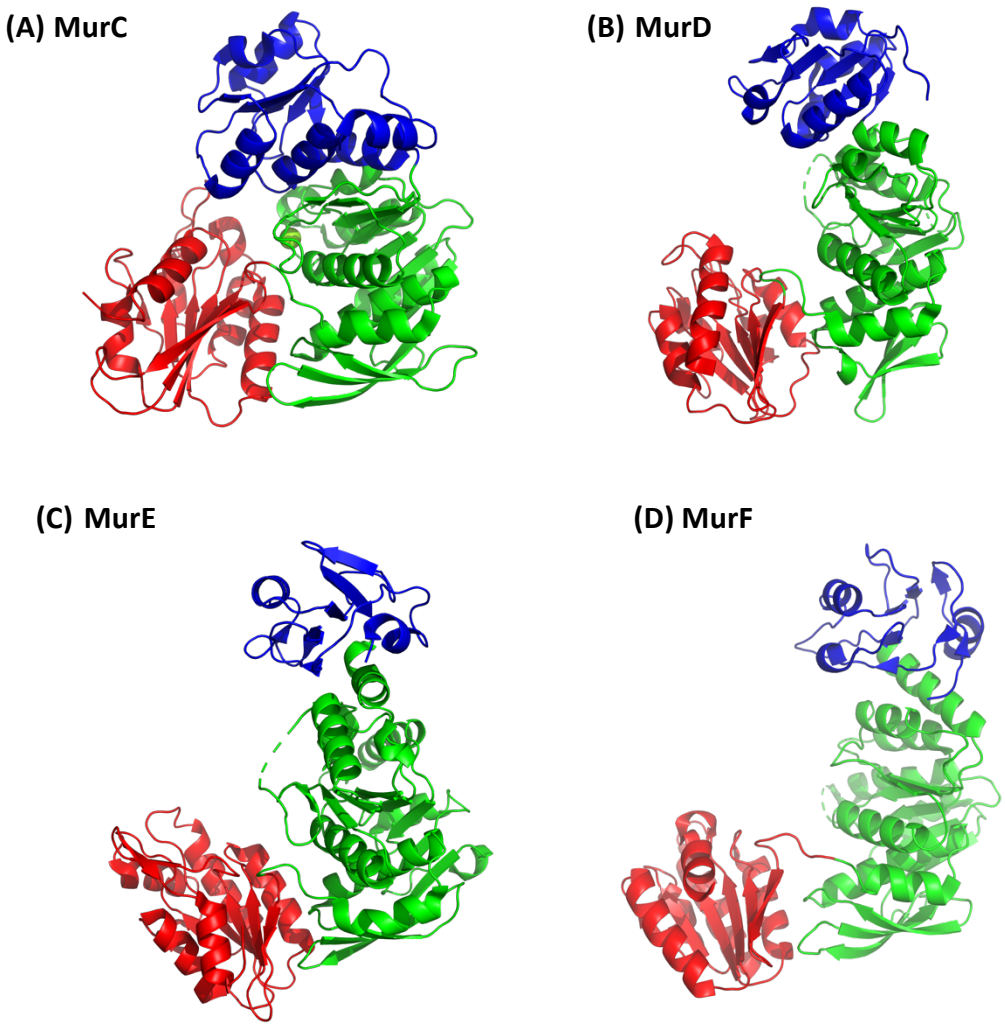

Figure 1. 6: Models of the structures of the four Mur ligases.

The Mur ligases all have a similar three domain structure as seen here. The N-terminal domain is seen in blue, the central domain in green and the C-terminal domain in red. Structures shown are *E.coli* proteins. MurC (PDB: 2F00), MurD (PDB:1E0D), MurE (PDB:7B53), MurF (PDB:1GG4)

The N-terminal domain is responsible for the binding of the uridine nucleotide substrate. For the *Escherichia coli (E. coli)* Mur ligases, the N-terminal

consists of a five-stranded parallel β-sheet which is surrounded by α helices; two in MurE, three in MurF and four in MurC and MurD [60,6162,63]. The N-terminal of MurC and MurD is reminiscent of the Rossmann dinucleotide-binding fold. Within MurC and MurD there are two hydrophobic loops and a diphosphate-binding pocket with a glycine-rich dinucleotide loop which forms a cleft which the UDP moiety of the uridine nucleotide substrate can bind within. The ribose hydroxyl groups, and uracil ring of the nucleotide substrate are anchored to the N-terminal domain via hydrogen bonding while the lactyl side-chain is able to extend towards the catalytic centre of the ligase, and interact with a Mg^{2+} ion [63,64]. To accommodate the longer substrate, MurE and MurF bind the nucleotide substrate in an alternate manner. The diphosphate moiety of the UDP forms four hydrogen bonds with a long loop that extends towards the C-terminal. The uracil ring of the UDP also binds via hydrogen bonding within the N-terminal [60,61].

The central domain is responsible for the binding of ATP. Within MurD, MurE and MurF it consists of a six-stranded parallel β sheet, while in MurC this is a seven-stranded β sheet. The β sheet is surrounded by α helices; four in MurC, seven in MurD and MurE and eight in MurF. The domain is also flanked by a smaller antiparallel three-stranded β sheet [58,60,61,62,63]. The central domain contains a Glu and His residue that are important for the co-ordination of the Mg^{2+} ions that the UDP moiety binds to [64].

The final domain is the C-terminal where the amino acid substrate binds. This domain contains a Rossman dinucleotide-binding fold and consists of a six-stranded β sheet with five parallel and one anti-parallel β strands, and is surrounded by five α helices [60,61,62,63]. The C-terminal domain contains a loop that becomes inserted into the active site allowing for correct orientation of the amino acid. Within the C-terminal domain there is a well conserved Arg residue that interacts with the amino acid and the α-phosphate of ATP, with the C-terminal domain playing a critical role in the capping of the ATP-binding site [58,59,62].

1.6.5 Conformational change

The Mur ligases undergo a conformational change from an 'open' substrate free structure to a 'closed' structure once substrates have bound. This 'closed' structure is also sometimes referred to as the 'active' conformation as it is only in this position that the amide bond formation can occur. During the conformational change the C-terminal domain undergoes a rigid body rotation allowing it to be brought towards the N-terminal and central domain. The capping of ATP by the C-terminal domain appears to induce this conformational change, and allows for the binding of the nucleotide substrate. A final rotation of the C-terminal domain then causes the enzyme to enter its active 'closed' conformation [63].

Due to their longer nucleotide substrates, MurE and MurF have to undergo a more pronounced domain rotation allowing for a wider interdomain cleft for the substrate to bind to [63]. These enzymes position the nucleotide substrate further from the active site allowing the peptide tail to fold up against the central domain. The ATP and nucleotide substrate are then brought together into the correct orientation to form the acyl-phosphate intermediate. The amino acid substrate is then bound, and correctly orientated allowing for the nucleophilic attack to occur. This then results in the stabilization of the tetrahedral transition state, lowering the activation barrier and accelerating catalysis [58–61,63].

It has been suggested that there is a requirement that ATP is bound to the Mur ligase in order to initiate the domain movement [65]. However, a study carried out by Sink et al suggests that domain movement may be dependent on more than just the binding of ligands [66]. Within this study, an intermediate conformation of MurD was identified in the absence and presence of ligands. The importance of the carbamoylation of Lys198 in MurD was considered a reason why the conformational change did not occur upon the binding of the ligands. Within their ligand bound structure, Lys198 was not carbamoylated, but within previously identified closed structures, Lys198 was carbamoylated, thus presenting a reason why a closed conformation was not observed [66]. Residue 198 plays an important role within the Mur ligases as it helps to stabilize Mg^{2+}, which is essential for the correct binding of ligands and enzymatic activity of the Mur ligases. This study

presents the idea that the conformational change that the Mur ligases undergo may contain more transition states than previously thought, and so further experimentation is required to fully understand the conformational change that occurs within the Mur ligases.

1.6.6 Conservation of Mur ligases

The Mur ligases have a similar three domain structure, undergo similar conformational changes, and follow the same binding order and mechanism of action. This level of similarity could be due to the high level of homology between the residues found within certain regions of the Mur ligases. Around 10-20% of the primary sequence of the Mur ligases is identical [67], with four regions of homology being described as critical for activity; Region I contains the nucleotide binding motif involved in ATP binding, region II is an extended domain in the middle of the protein, region III contains a dyad of acidic residues, and region IV is a patch of hydrophobic residues [68]. These domains are highlighted in the sequences in **Figure 1.7**.

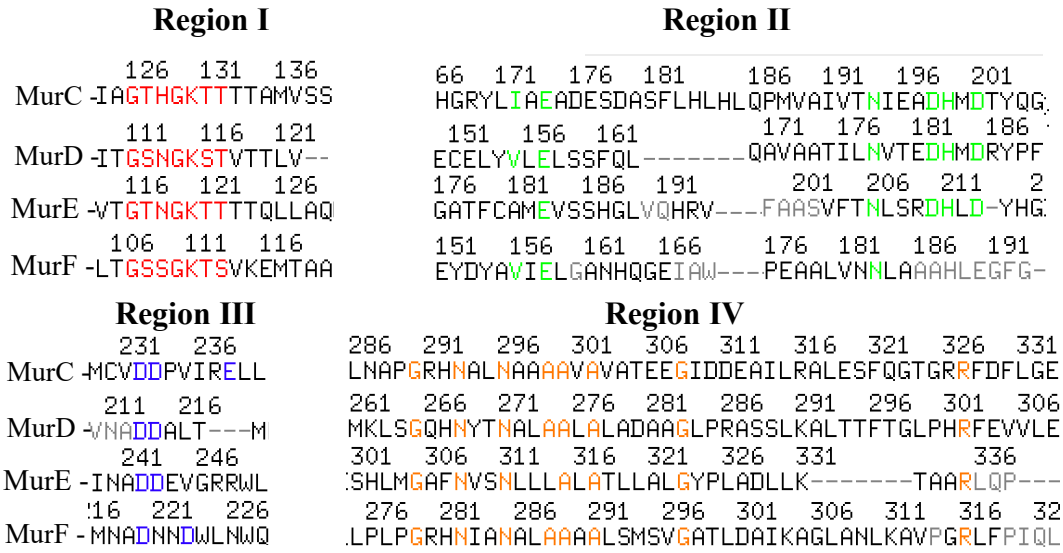

Figure 1. 7: Alignment of the conserved amino acids within Mur ligases.

There are 4 regions within the sequences of the E. coli Mur ligases that are conserved throughout the family. Region I (shown in red), Region II (shown in green), Region III (shown in blue) and Region IV (shown in orange).

The ATP-binding pocket contained within region I is the most well conserved active site throughout the Mur ligase family, with a consensus sequence of GXXGKT/S being identified as being present within the ATP binding pocket of Mur ligases [65,69]. Region II is an extended domain that contains a glutamic acid and histidine that are conserved throughout the Mur ligases, with the histidine being flanked by acidic amino acids [68].

1.6.7 Antibiotic target

For many years the Mur ligases have been an antibacterial target. This is due to their essential role in peptidoglycan formation, as well as the fact that they have no mammalian counterparts making them unique bacterial targets. There are many areas that antibiotics can target within the Mur ligases such as the binding site of the uridine nucleotide substrate, the catalytic mechanism, and the ATP-binding site, the amino acid binding site and exploiting the conformational change that occurs.

Some promising inhibitors have been identified over the years such as 5-benzylidenethiazolidin-4-one compounds that are able to target multiple Mur ligases by preventing the binding of their uridine nucleotide substrates. They are able to inhibit the Mur ligases by binding to residues that flank the UDP-MurNAc binding site, and have been shown to have IC_{50} values between 2 and 6 μM [70].

Phosphinate inhibitors can mimic the structure of the the tetrahedral transition state of the mur ligase directly prior to its collapse to form a new peptide bond with the incoming amino acid. The phosphinate is comprised of a dipeptide analogue linked to a uridine diphosphate by a hydrophobic spacer and can act as an inhibitor of the first transition state. These inhibitors can target multiple Mur ligases with IC_{50} values in the micromolar range [71,72]. Benzene 1,3-dicarboxylic acid derivatives are also able to act as transition state analogue inhibitors with micro molar inhibitors against all four Mur ligases having been identified [73].

The conformational change that the Mur ligases undergo from a closed to an open structure can present opportunities for antibacterial targets, especially as we continue to develop our knowledge of the exact amino acids involved. Cyanothiophene inhibitors have been developed that are able to target this within

MurF, and have IC_{50} values in the nanomolar and micromolar range. These inhibitors bind at the interface between the three structural domains and induce interdomain closure yielding the 'closed' conformation of the ligase in the absence of ligands [74,75].

However, even though many promising inhibitors with IC_{50} values in the nanomolar and micromolar range have been identified, no new antibiotics that are able to target the Mur ligases *in vivo* in wild type cells have been identified. This could be due to issues with insufficient accumulation of drugs within the bacteria due to permeability barriers or the impact of efflux pumps [76]. Indeed, it has been possible to isolate potent inhibitors of *E. coli* and *Pseudomonas aeruginosa (P. aeruginosa)* MurC with nanomolar IC_{50} values that are impotent as antibiotics unless targeted at mutated strains that lack efflux capacity [77]. More recently it has been suggested that inhibitors are unable to act efficiently *in vivo* because the Mur ligases are forming a complex within the cytoplasm. If the Mur ligases are forming a complex within the cytoplasm this would mean that intermediates may be channelled through the complex, making it harder for antibiotics to preferentially bind in the place of substrates. A complex formation may also mean that binding locations targeted by the inhibitors are hidden and inaccessible *in vivo*.

1.7 Mur Ligase Complex

The Mur ligases have been a target for antibacterial studies for many years, and yet very few antibiotics that are able to act against any of the Mur ligases involved in the stepwise addition of amino acids have been identified that are active against wild type strains. One contributory factor to this issue that has been proposed is that within the cytoplasm, the Mur ligases form a complex which is significantly reducing the inhibitory potency of inhibitors targeting these enzymes[78]. If a complex is formed within the cytoplasm, this could obscure the targets of known inhibitors preventing them being able to function *in vivo.* A complex could also mean that substrates are sequestered within the complex meaning their local concentrations are much higher than previously identified preventing inhibitors from competing at suitable drug levels [78]. Understanding if a complex is forming

and how could help in the development of inhibitory molecules against the Mur ligases, or complex formation itself.

1.7.1 Role of complex formation within bacteria

The role of protein complexes within bacteria is wide and varied. Within bacteria, protein complexes exist whereby activity of the proteins is only present when the proteins are in complex together, such as with the GatD/MurT enzyme complex that allows for lipid II amidation [26]. Other protein complexes exist to help regulate the activity of a protein. Although the Mur ligases have been seen to be active independently, complex formation may still play a role in the activity and regulation of the activity of the Mur ligases within the cytoplasm. Protein complexes may also exist to aid in the sequestering of substrates to increase the activity of the pathway. Sequestering of the UDP intermediate within a Mur ligase complex could increase the activity of the peptidoglycan pathway.

1.7.2 Complex formation of MurT/GatD

The MurT/GatD complex is responsible for the amidation of lipid II, and may provide an insight into the potential formation of a Mur ligase complex. MurT is similar in sequence to the substrate binding domains of the Mur ligases and contains a middle and C-terminal domain typical of the Mur ligase family, with MurF from *E. coli* its closest structural homology [79]. A study carried out by Nöldeke et al identified a complex formation between MurT and GatD that occurs between GatD and the MurT C-terminal [79], suggesting a possible interface within other Mur ligases that may be involved in complex formation. Nöldeke et al also observed that in the absence of Lipid II, the complex appeared to be in an open conformation, but there was flexibility within the complex to allow for a closed conformation upon binding of Lipid II [79]. It is known that upon binding of substrates, the Mur ligases undergo a conformational change whereby the C-terminal undergoes a rigid body rotation allowing it to be brought towards the N-terminal and central domain. The flexibility within the complex formation between MurT and GatD suggests that this

conformational change may still be able to occur within the Mur ligases while in complex formation.

1.7.3 Interaction of Mur ligases with MreB

Understanding of how the Mur ligases may be interacting within a complex is limited. A study carried out by Divakaruni et al investigated the cellular localisation of the Mur ligases. MurC, MurE, and MurF were all seen to localise in a similar cellular location, exhibiting a banded localisation pattern which was perpendicular to the long axis of the cell. This localisation was dependent though on there being intact MreB cables, and when MreB polymerization was inhibited by A22, the Mur ligases were redistributed to the midcell or poles of the cell [80].

The interaction of MreB and the Mur ligases was further studied by Favini-Stabile et al. Using SPR spectroscopy where MreB was immobilized on a CM5 sensor chip, interactions between MreB and the Mur ligases from *Thermotoga maritima (T. maritima)* were determined. MurD, MurE and MurF all appeared to be interacting partners of MreB. Using this method, interactions between MurD, MurE and MurF with MurG were also established. However, when MurF was immobilized and the same experiment run with MurD and MurE, no signal could be detected. Pull down assays were also used to assess the interactions between the Mur ligases themselves, with no interaction being seen [81].

These studies suggested that the Mur ligases were unable to interact with each other, but could interact with MurG or MreB, potentially using these proteins as a backbone for complex formation.

1.7.4 Interaction between Mur ligases

A recent study carried out by Miyachiro et al investigated whether any of the Mur ligases from *Streptococcus pneumoniae (S. pneumoniae)* were able to form binary complexes. Binary complex formation amongst the Mur ligases was investigated via chemical cross-linking. Mass spectrometry was then used to identify the peptides which were potentially involved in these interactions. Using this methodology, the peptides potentially involved in the binary complex

formation between MurC - MurF and MurD – MurF were determined. Using analytical ultracentrifugation, the ability of MurC-MurD, MurC-MurF and MurD-MurF to form binary complexes was further investigated, with all showing the formation of binary globular complexes. These results showed that the Mur ligases could interact with each other without the presence of other potential binding partners [82].

1.7.5 Fusion Mur ligases

Along with experimental evidence of complex formation, evolutionary evidence can be used to help predict the likelihood of complex formation amongst the Mur ligases. A study carried out by Laddomada et al investigated the presence of a fusion of the MurE and MurF proteins within *Bordetella pertussis (B. pertussis)*. Within the *B. pertussis* genome, the MurE and MurF proteins are fused into a single transcript, with a 20 amino acid linker present between the MurE and MurF genes. These proteins when expressed produced an elongated molecule with two distant active sites. Expression of these fusion proteins yielded a bifunctional molecule, with both MurE and MurF being active within this fusion form. The presence of an active fusion of MurE and MurF could point to the ability of these two proteins to form an active binary complex within bacteria where they are not fused within the genome [83].

1.7.6 Differences in interacting partners

Whether the Mur ligases can form a complex is still controversial. Previous studies appear to contradict each other regarding whether an additional structural protein is required for complex formation amongst the Mur ligases. One suggestion as to why differing results have been seen is that *S. pneumoniae*, unlike *T. maritima* does not encode MreB, and so is unable to use this protein to help form a Mur ligase complex. This suggestion could mean that bacteria that do not encode MreB are able to form the complex independently of structural proteins such as MreB. Another suggestion could be that Gram positive and Gram negative bacteria form the complex in different ways, with Gram negative bacteria requiring a structural

protein such as MreB or MurG for complex formation, while Gram positive bacteria are able to form a complex with just the Mur ligases. Further studies will be needed to determine whether the Mur ligases can form a complex, and what proteins are required for complex formation. Understanding if, and how complex formation occurs within bacteria could greatly influence the development of future antibacterial agents targeted towards the Mur ligases.

1.8 Project Aims and Outline

Antibiotic resistance is a growing global threat which requires immediate attention by the global scientific community. The development of new antibiotics is desperately required in order to tackle the growing number of antibiotic resistant bacterial strains [84]. The Mur ligases have been a target for new antibiotic studies for many years due to their role in peptidoglycan formation and lack of human counterpart. The similar catalytic mechanism and structure of Mur ligases presents a unique opportunity to develop multi targeted inhibitors that will help to reduce the emergence of resistance to antibiotics. This thesis aims to optimise and develop methodologies that will improve our ability to identify novel inhibitory fragments designed via *in silico* screening, along with summarising and contributing to the current understanding of complex formation amongst the Mur ligases, using *S. agalactiae* as a model organism. Specifically, the work described herein aimed to:

1. Develop and utilise biochemical assays to screen and identify inhibitory fragments targeted towards the Mur ligases of *S. agalactiae* to help identify novel starting points for the development of antibacterial compounds.
2. Generate a better understanding of the predicted ability of the Mur ligases to form complexes using computational modelling.
3. Characterise the formation of a binary complex between MurD and MurE from *S. agalactiae* using a range of cloning and expressing system including pET DUET dual expression, and biophysical techniques including Microscale Thermophoresis and activity assays.

Chapter 2

Development and optimization of an assay for identifying low affinity binding fragments for the Mur ligases

1. Introduction and Aims

The Mur ligases have been studied for many years as a potential therapeutic target, with multiple trials undertaken to try and design antibacterial agents [85]. Due to the essential nature of the role performed by these enzymes in bacteria, identification of inhibitory fragments targeted towards the Mur ligases as a route towards development of novel antibacterials formed the main aim of this project.

Biochemical assays are one technique used for determining the inhibitory effects of fragments. Within Warwick, Dr Adrian Lloyd has designed assays that allow the activity of the Mur ligases to be coupled to a secondary reaction that can then be tracked photometrically. These assays allow binding fragments to be tested for their inhibitory effects within a simple, repeatable assay. Optimization of the assay for specific proteins allows for the best chance of detecting inhibitory fragments. The assay can also be optimized and adapted depending on where the inhibitory fragments are targeted towards.

This chapter aimed to confirm previous work done within the Dowson group. Determination of the optimal conditions for *S. agalactiae* MurD within existing assays was carried out with a focus on targeted fragments screens. Development of a stopped assay based on an existing assay was also carried out.

2. Materials and Methods

2.1 Media

The composition of the culture medias used for the growth of proteins are described in **Table 2.1**. Selective media was supplemented with either 50 mg/L Kanamycin or 100 mg/L Ampicillin. For media containing agar, antibiotics were added at 50°C and poured into sterile Petri dishes.

Name	Composition
LB Broth	10 g Tryptone, 5 g Sodium Chloride, 5 g Yeast extract, prepared to 1 L in water and autoclaved
SOC	20 g Tryptone, 0.5 g Sodium Chloride, 5 g Yeast extract, 0.2 g Potassium Chloride, 3.6 g Glucose, 1 g Magnesium Chloride, prepared to 1 L with double distilled water and autoclaved
2YT	16 g Tryptone, 5 g Sodium Chloride, 10 g Yeast extract, prepared to 1 L in water and autoclaved

Table 2. 1: Composition of media

2.2 Buffers and solutions

All chemicals used were of analytical grade unless otherwise stated. MilliQ pure water was used to make all buffers. Composition of protein buffers used for purification and storage are summarised in **Table 2.2**. Buffers were stored at 4°C for up to 1 month.

Name	Composition
	General Buffers
TAE	40 mM Tris acetate, 1 mM EDTA
SDS PAGE	1.2 M Triethanolamine, 0.8 M Tricine, 2.0% (w/v) sodium dodecyl sulfate, pH 8.2
Sample Buffer	62.5 mM Tris-HCl pH 6.8, 2.5% (w/v) SDS, 0.002% (v/v) Bromophenol Blue, 0.7135 M β-mercaptoethanol, 10% (v/v) glycerol
	Purification of Mur ligases
Buffer A	50 mM HEPES, 40 mM Imidazole, 150 mM NaCl
Buffer B	50 mM HEPES, 250 mM Imidazole, 150 mM NaCl
Storage Buffer	20 mM HEPES, 150 mM NaCl
	Purification of UDP-MurNAc-L-Ala
Working Buffer	0.25 M Hepes, 50 mM $MgCl_2$, pH 7.6
Buffer A	10 mM ammonium acetate, pH 7.6
Buffer B	1 M ammonium acetate, pH 7.6
	Activity assay
Storage Buffer 2	30 mM HEPES pH7.6, 50 mM KCl, 1 mM $MgCl_2$, 3 mM DTT, 0.2 mM protease inhibitor, 2 μM Leupeptin, 2 μM peptin, 50% glycerol

Table 2. 2: Composition of buffers

2.3 Protein Expression and Purification

2.3.1 Expression of Protein

Proteins were over expressed in BL21 *E. coli* strains using isopropyl-D-1-thiogalactopyranoside (IPTG) induction. A sample from a glycerol stock containing the gene of interest was introduced into a 15 mL LB broth containing the relevant antibiotic and incubated overnight at 37°C at 180 RPM.

15 mL of the overnight pre-culture was used to inoculate 1 L of 2YT broth containing the relevant antibiotic and was incubated at 37°C at 180 RPM until an OD_{600nm} of 0.5-0.7 was reached. IPTG was added to each 1 L culture to a final concentration of 1 mM and cultures were then incubated at 37°C at 180 RPM for 4 hours. Cells were harvested via centrifugation at 6,000 x g for 10 minutes at 4°c. The supernatant was discarded, and the cell pellets collected before being flash frozen with liquid nitrogen and being stored at -20°C overnight.

2.3.2 Preparation of cell lysates

The cell pellets were thawed and resuspended in 150 mL of Buffer A supplemented with DNase and lysozyme. The cell suspension was evenly resuspended by homogenisation and then passed through a cell disruptor twice at 30kpsi at 4°C to lyse the cells. Centrifugation of the cells was then carried out at 30,000xg for 30 minutes at 4°C to remove the cell debris and clarify the lysate.

2.3.3 Protein Purification

Proteins with a poly-histidine (x6) affinity tag were purified by immobilised metal affinity chromatography (IMAC) which was carried out at 4°c. The cell lysate was passed over a nickel charged IMAC column at a flow rate of 1 mL/min which had been pre-equilibrated in Buffer A. The column was then attached to an AKTA before 3 column volumes of Buffer A were used to wash the column and remove any unbound protein. The protein was then eluted from the column using Buffer B. The concentration of Buffer B was increased in 10% increments with each new increment occurring either after 3 column volumes had passed through the column or there was no further change in the absorbance of the eluate until 100% Buffer B

was achieved. Fractions correlating to an increase at 280 nm were then analysed by SDS Page Analysis.

2.3.4 SDS Page Analysis

Proteins were separated and visualised under denaturing conditions by Sodium dodecyl sulphate-Polyacrylamide Gel Electrophoresis (SDS-PAGE) with a 10% resolving gel. Protein samples for analysis were prepared in sample buffer (**Table 2.2**). Gels were loaded into a Mini-PROTEAN tetra system (Bio-Rad) unit and 12 μL of the protein samples and 4 μL of colour protein standard broad range calibration ladder (NEB) were loaded into respective wells. Gels were run in TAE buffer (**Table 2.2**) for 45 minutes at 180V. SDS-PAGE gels were stained with instant blue (Expedeon) overnight. SDS-PAGE gels were then washed with water 3 times to remove excess staining before being imaged with a Gel Box (Vilber).

2.3.5 Protein Quantification

Buffer exchange was carried out either using a PD-10 column (GE Healthcare) following manufacturer's guidance, or via overnight dialysis. Protein containing fractions identified via SDS-PAGE analysis were pooled and the buffers exchanged from Buffer B to a storage buffer. To determine protein concentrations a Nanodrop ND-1000 spectrophotometer (Nanodrop Technologies) was used. Protein absorbance at 280 nm was measured against a storage buffer blank, and protein concentration determined using the molecular weight and molar extinction coefficient of the protein. Concentration of protein samples was carried out by centrifugal ultracentrifugation using 30,000 molecular-weight cut off (MWCO) Vivaspin centrifugal concentrator (Sartorius). Protein was loaded into the concentrator and centrifuged at 3000xg at 4°C until the desired concentration was achieved.

2.4 Cloning of MurD

Synthetic DNA was ordered from IDT (gBlocks) and was codon optimised where appropriate and restriction site sequences added. The N-terminal hexa-histidine tagged *S. agalactiae* MurD was then cloned into inPUC then pET28 by Dr Jonathan Cook.

2.4.1 Transformation of Competent Cells

Transformation of chemically competent cells was carried out using NEB5 *E. coli* BL21 (DE3). Cryo-preserved competent cells were thawed on ice before being mixed with ligated DNA provided by Dr Jonathan Cook. Cells were incubated on ice for 30 minutes before being heat shocked via incubation at 42˚C for 30 seconds. A further 5 minute incubation on ice was carried out before the cells were added to Super Optimal broth with Catabolite repression (SOC medium) to a final volume 10 times the original cell suspension volume. Cells were incubated at 37°C for one hour at 180 RPM before being plated on selective LB agar.

2.4.2 Construct Validation

Plasmid DNA constructs were verified via Genewiz sequencing. 80-100 ng of DNA was sent with relevant primers. Construct maps were then generated via Snapgene.

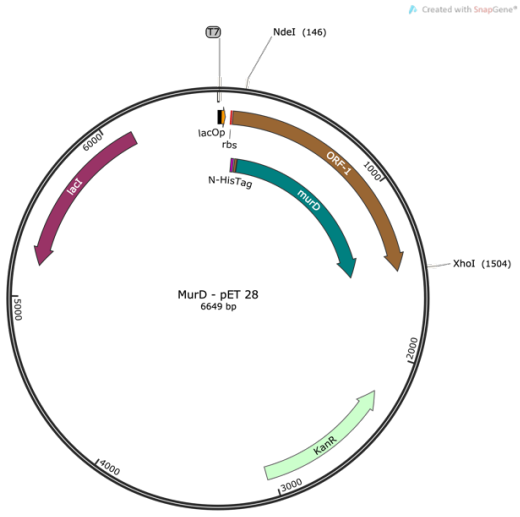

Figure 2. 1: Construct map of S. agalactiae MurD within pET 28

Construct map of *S. agalactiae* MurD. *S. agalactiae* MurD was cloned into open reading frame 1 of pET 28 using restriction enzyme digest. Restriction enzyme sites used were NdeI and XhoI. Construct map was generated via Snapgene.

2.4.3 Protein Purification

Protein purification of MurD from *S. agalactiae* was carried out following the methodology described in **Section 2.3**.

2.5 Synthesis of UDP-MurNAc-L-Ala

Synthesis of UDP-MurNAc-L-Ala was carried out following the methodology previously stated in 'Characterization of tRNA-dependent peptide bond formation by MurM in the synthesis of Streptococcus pneumoniae peptidoglycan' [27].The synthesis of UDP-MurNAc-L-Ala requires the sequential addition of all reagents into a 2 mL Eppendorf which is then incubated at 37°C overnight. The synthesis mixture contained the following components (final concentrations): 125 mM phosphoenolpyruvate (PEP) from a 1 M PEP stock made in 5x working buffer (Table 2), 1x working buffer from a 5x working buffer solution (including volume used in PEP addition), 1 mM dithiothreitol (DTT), 50 mM KCl, 8.22 mM UDP-GlcNAc, 0.21 mg/mL *E. coli* MurA, 1.24 mg/mL *P. aeruginosa* MurB, 0.2 mM $NADP^+$, 1.48 u/mL IDH, 26 mM DL-isocitrate, 6 mM ATP, 5.53 u/mg rabbit muscle Pyruvate kinase, 0.24 mg/mL *P. aeruginosa* MurC, and 35 mM L-Ala. The final volume of the synthesis was 2 mL.

2.5.1 Purification of UDP-MurNAc-L-Ala

The purification of UDP-MurNAc-L-Ala was carried out using a Source 30Q column. The synthesis mixture was removed from the 37°C incubator and stored on ice. To remove the proteins from the UDP-MurNAc-L-Ala, the contents of the Eppendorf was transferred to a Vivaspin20 10,000 MWCO centrifugal concentrator (Sartorius). The Eppendorf was rinsed with 3 aliquots of 1 mL sterile water which was also added to the concentrator which was then centrifuged at 4500rpm for 45 minutes at 4°c.

A Source 30Q column was attached to an AKTA before being washed at room temperature with 10 column volumes sterile water at a flow rate of 1 mL/min. The column was then equilibrated with 8 column volumes Buffer B and 10 column volumes Buffer A. The sample was loaded onto the column and washed through

with 10 column volumes of Buffer A. The intermediate was then eluted using a gradient of Buffer B. 10 mL fractions were collected and the elution of the desired UDP MurNAc product was followed via the absorbance of the column eluate at 280 nm and 254 nm. Fractions likely to contain the desired UDP MurNAc species were identified as those with an A_{254}/A_{260} ratio of ~2.6, typical of a uridine 5'-diphosphate containing species [86]. The appropriate fractions were collected and placed into a round bottomed flask. The contents of the flask were frozen using liquid nitrogen and lyophilised overnight to remove the ammonium acetate from the sample. The sample was resuspended in 30 mL of filtered water, frozen with liquid nitrogen and freeze dried again, with this step being repeated until the ammonium acetate had been removed. Once a loose powder of sample had been formed, it was transferred to a falcon tube and resuspended in 2 mL of filtered water before being frozen with liquid nitrogen and freeze dried, a process that was repeated 5 times. The final powder was resuspended in 200 μl of sterile water and concentration of UDP MurNAc determined at 260 nm using an extinction coefficient for the uracil chromophore within the molecule of 10,000 $M^{-1}.cm^{-1}$ [86].

2.6 Pyruvate Kinase/Lactate Dehydrogenase Coupled Assay for Mur ligases

Enzyme activity as defined by the rate of ADP production from ATP was confirmed using a Pyruvate Kinase/Lactate Dehydrogenase (PK/LDH) assay. The PK/LDH assay was carried out in a Cary 100 UV/Vis spectrophotometer in a total reaction volume of 200 μL at 37°c. The reaction mixture contained the following components (final concentrations): 50 mM HEPES (pH7.6), 10 mM $MgCl_2$, 300 μM NADH, 25 mM KCl, 1 mM DTT, 2 mM PEP, 1 μL per 100 μL PK/LDH (Stock solution of 6-10 U mL^{-1} PK and 9-14 U mL^{-1} LDH), 2 mM ATP, 100 μM UDP-MurNAc-L-Ala, 1 mM D-Glu and 50 nM MurD. A Cary 100 UV/Vis spectrophotometer was run using Cary WinUV kinetics software at 37°c. All components barring one substrate were added to a Hellman Analytics High Precision QUARTZ cuvette and mixed. A background rate was determined at 340 nm. The final substrate was added to start the reaction and the reaction was monitored at 340 nm as a decline in absorbance as a consequence of the consumption of the NADH chromophore. The gradient of the

slope of the initial rate of catalysis was determined using the tracking function within the software.

2.7 MESG coupled assay

Enzyme activity as defined by the rate of phosphate production from ATP was followed using a 7 methyl 6 thio guanosine (MESG)- coupled assay, which has an extinction coefficient of 10,000 $M^{-1}.cm^{-1}$ [87]. The MESG coupled assay was carried out in either a Cary 100 UV/Vis spectrophotometer at a total reaction volume of 200 μL at 37°c, or within a Varioskan Flash plate reader at a total reaction volume of 50 μL in 384 well microtitre plates. The reaction mixture contained the following components (final concentrations): 50 mM HEPES (pH7.6), 10 mM $MgCl_2$, 1 mM DTT, 50 mM KCl, 400 μM MESG, 100 U per mL purine nucleoside phosphorylase (PNP), 250 μM ATP, 1 mM D-Glu, 50 μM UDP-MurNAc-L-Ala and 100 nM Mur ligase. Assays were carried out with the Cary 100 UV/Vis spectrophotometer run using Cary WinUV kinetics software set at 37°c, or within a Varioskan Flash plate reader set at 37°c. All components barring one substrate were added and mixed and a background rate was determined at 360 nm. The final substrate was added to start the reaction, either manually or via the injection system of the Varioskan Flash, and the reaction was followed at 360 nm as an increase in absorbance. The gradient of the slope of the initial rate was determined using the tracking function within the software of the Cary 100 UV/Vis spectrophotometer or manually. K_m determinations for ATP, UDP-MurNAc-L-Ala and D-Glu were carried out using this assay. When K_m was being determined the concentrations for all components remained the same apart from the concentration of the component for which K_m was being determined. The reaction was then carried out using the same protocol as previously described. Nucleotide substitutes were run in place of ATP, with all other components remaining at either K_m or constant levels. The IC_{50} value for ADPNP and ADPCP were determined using this assay. ADPNP/ADPCP were added to the component mixture before the recording of the background rate of the reaction.

2.8 Stopped MESG coupled assay

The ability of a stopped MESG coupled assay to determine protein activity in the absence and presence of inhibitors was determined. The stopped MESG coupled assay was carried out in either a Cary spectrophotometer at a total reaction volume of 200 μL at 37°c, or within a Varioskan Flash plate reader at a total reaction volume of 50 μL. The reaction mixture contained the following components (final concentrations): 50 mM HEPES (pH7.6), 2 mM $MgCl_2$, 1 mM DTT, 50 mM KCl, 400 μM MESG, 250 μM ATP, 1 mM D-Glu, 50 μM UDP-MurNAc-L-Ala and 50 nM Mur ligase. All components barring one substrate were added and mixed and a background rate was determined at 360 nm. The final substrate was added to start the reaction and allowed to run for the initial rate period before the reaction was quenched with 10 mM EDTA. A background absorbance was determined photometrically at 360 nm before PNP was added. Absorbance change was followed at 360 nm until the end point was achieved. The absorbance change was then determined.

3. Results

3.1 Inactivity of previously cloned MurD from *S. agalactiae*

MurD from *S. agalactiae* had previously been cloned, expressed and purified within the Dowson laboratory. However, further purification experiments produced a low yield of MurD with no improvement from expression trials. Activity assays, using a spectrophotometer, were carried out on the purified MurD, along with a *P. aeruginosa* MurD species. Activity was seen within the assay for the MurD from *P.* a*eruginosa* but the MurD from *S. agalactiae* was lacking activity as seen in **Figure 2.2.**

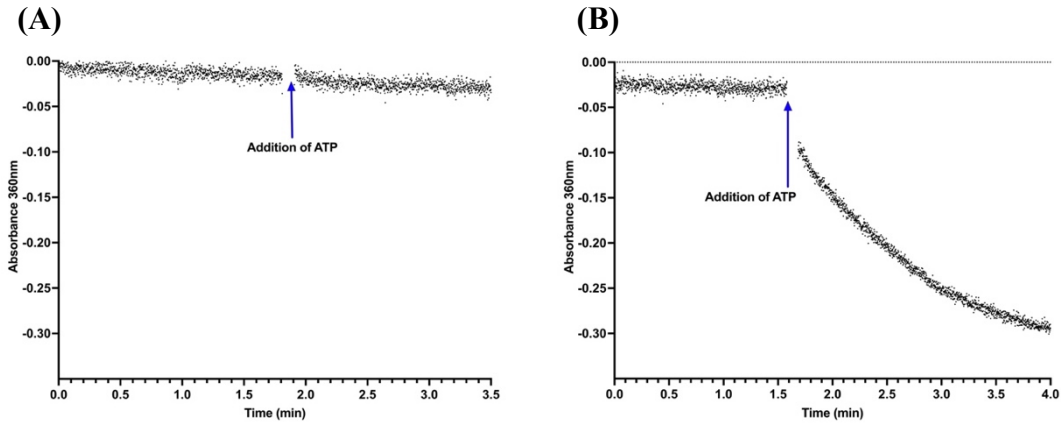

Figure 2. 2: Activity assay of MurD shows a lack of activity for the MurD clone from S. agalactiae

Activity of different MurD proteins was determined via a PK/LDH coupling reaction. Addition of ATP should induce the Mur ligase reaction, resulting in the formation of ADP. ADP is rephosphorylated by pyruvate kinase generating pyruvate which is reduced to lactate with NADH via lactate dehydrogenase. Consumption of NADH causes a decrease in absorbance at 340 nm. Final protein concentration was 5µg/ml of MurD for *S. agalactiae* and *P. aeruginosa*. (A) Activity trace of MurD from *S. agalactiae.* No activity was seen after the addition of ATP. (B) Activity trace of MurD from *P. aeruginosa.* Activity was seen after the addition of ATP.

3.2 Previously cloned MurD from *S. agalactiae* lacks an alpha helix

To determine why there was a lack of activity with the *S. agalactiae* MurD clone, sequencing of the MurD plasmid was performed. A point deletion was identified at nucleotide 1302 that resulted in the appearance of a stop codon, highlighted in **Figure 2.3A**. This caused the truncation of the protein sequence by removal of the last 18 amino acids, which when mapped to the MurD structure (PDB: 3LK7) comprised the final alpha helix of the structure, as seen in **Figure 2.3B**.

The lack of activity meant that this construct could not be used within the project and a new full-length clone of MurD had to be produced.

(A)

```
S. agalactiae.   1101 AGATATCACTGGACTTAAACATATGGTTGTTTTAGGGGAATCGGCATCTC   1150
                      ||||||||||||||||||||||||||||||||||||||||||||||||||
Dom_S.agalact    1101 AGATATCACTGGACTTAAACATATGGTTGTTTTAGGGGAATCGGCATCTC   1150

S. agalactiae.   1151 GAGTAAAACGTGCTGCACAAAAAGCAGGAGTAACTTATAGCGATGCTTTA   1200
                      ||||||||||||||||||||||||||||||||||||||||||||||||||||
Dom_S.agalact    1151 GAGTAAAACGTGCTGCACAAAAAGCAGGAGTAACTTATAGCGATGCTTTA   1200

S. agalactiae.   1201 GATGTTAGAGATGCGGTACATAAAGCTTATGAGGTGGCACAACAGGGCGA   1250
                      |||||||||||||||||||||||||.|||||||||||||||||||||||||
Dom_S.agalact    1201 GATGTTAGAGATGCGGTACATAAAGCGTATGAGGTGGCACAACAGGGCGA   1250

S. agalactiae.   1251 TGTTATCTTGCTAAGTCCTGCAAATGCATCATGGGACATGTATAAGAATT   1300
                      ||||||||||||||||||||||||||||||||||||||||||||||||||||
Dom_S.agalact    1251 TGTTATCTTGCTAAGTCCTGCAAATGCATCATGGGACATGTATAAGAATT   1300

S. agalactiae.   1301 TCGAAGTCCGTGGTGATGAATTCATTGATACTTTCGAAAGTCTTAGAGGA   1350
                      |||
Dom_S.agalact    1301 T-GA----------------------------------------------   1303

S. agalactiae.   1351 GAGTAA   1356

Dom_S.agalact    1304 ------   1303
```

(B)

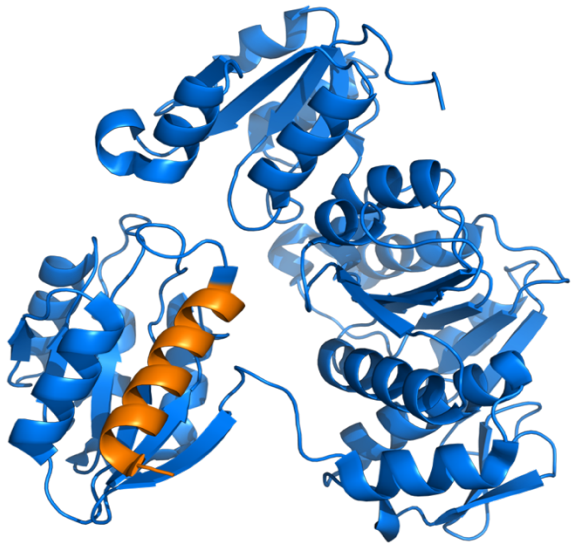

Figure 2. 3: A point mutation led to the deletion of an alpha helix

Using BLAST, the sequence of the previously cloned MurD (Dom_S.agalact) was compared to the known sequence of MurD from *S. agalactiae (S. agalactiae)*. (A) At position 1302, within the previously cloned MurD, a point deletion of a cytosine had occurred, resulting in the formation of a STOP codon. (B) A Pymol model of MurD from the *S. agalactiae* MurD crystal structure (PDB: 3LK7) with the deleted alpha helix shown in orange.

3.3 *S. agalactiae* MurD protein purification and activity

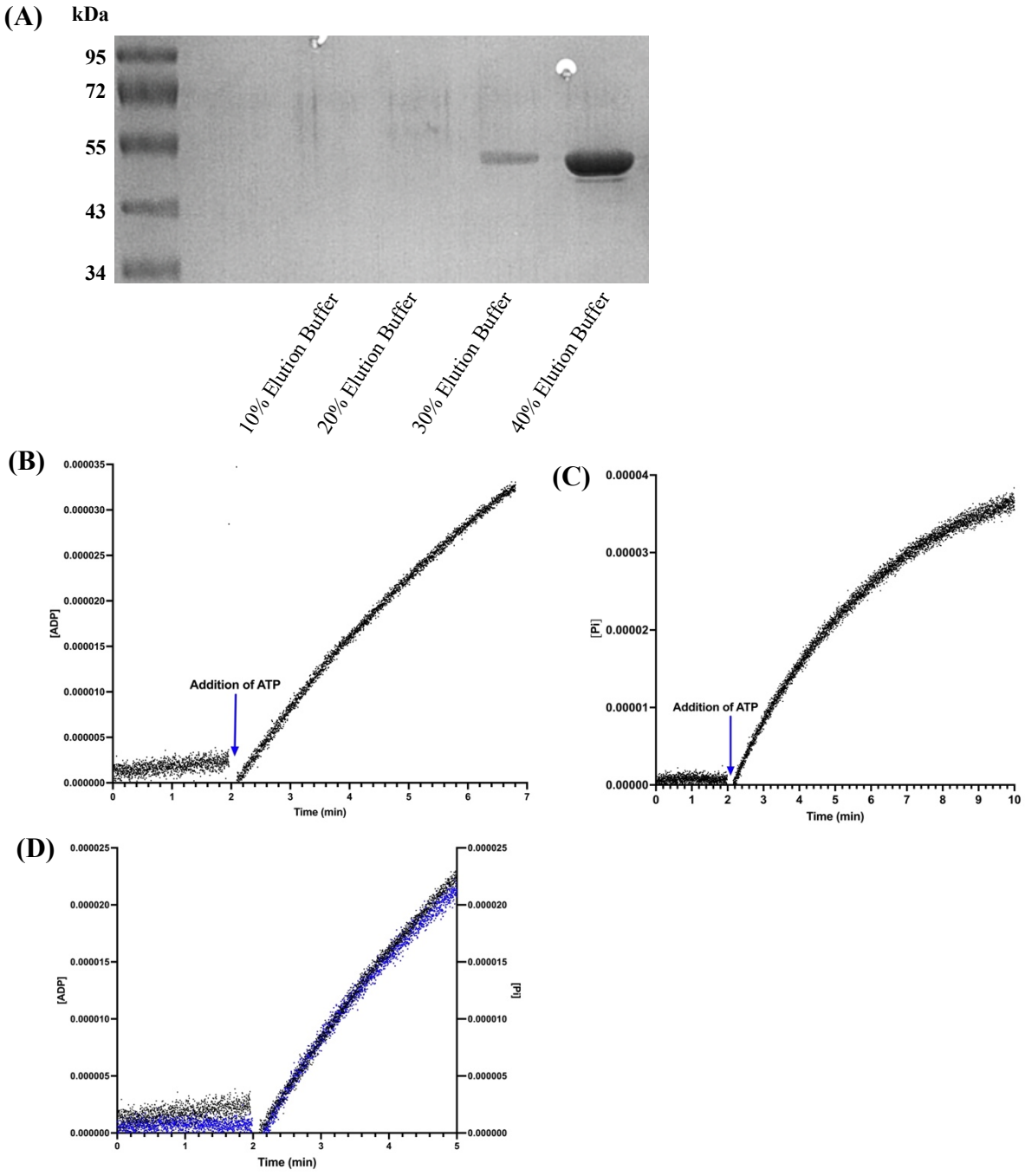

Figure 2. 4: Purification and activity assay of purified MurD from S. agalactiae

MurD from *S. agalactiae* was purified and its activity determined via activity assays. (A) SDS-PAGE analysis of IMAC-purified *S. agalactiae* MurD (predicted molecular weight: 49.8 kDa)(B) Activity of MurD within a PK/LDH assay. (C) Activity of MurD within a MESG coupled assay. (D) Comparison of activity of MurD from S. agalactiae in a PK/LDH assay (black) and a MESG coupled assay (blue).MurD was at an [assay] of 100nM. Addition of ATP induced the activity of the Mur ligase.

To be able to develop and optimise an *S. agalactiae* MurD assay, an active form of *S. agalactiae* MurD was required. An N- terminal hexa-histidine tagged *S. agalactiae* MurD was cloned into pET28a by Dr Jonathan Cook (School of Life Sciences, University of Warwick). Following sequence conformation, the vector was then transformed into competent *E. coli BL21 (DE3)* cells for protein expression. Protein purification was carried out using IMAC purification via a nickel column and the purity of the protein was assessed via SDS-PAGE, as shown in **Figure 2.4a**. Pure protein was obtained via this method with a clear band being seen at around 50 kDa, consist with the predicted subunit molecular weight of 49.8 kDa. Purified protein was tested for activity within a PK/LDH coupled assay and a MESG coupled assay using a spectrophotometer. The purified protein was active within both assays, as seen in **Figure 2.4b and Figure 2.4c,** with the rate of ADP release equal to the rate of phosphate release as seen in **Figure 2.4D**.

3.4 Optimization of a MESG coupled assay for MurD from *S. agalactiae*

S. agalactiae MurD was seen to be active in both a PK/LDH coupled assay and a MESG coupled assay. Both assays rely on coupling the Mur ligase reaction to a secondary reaction that can be tracked photometrically. The PK/LDH coupled assay relies on the production of ADP to convert phosphoenolpyruvate to pyruvate via pyruvate kinase. The pyruvate is then converted to lactate via lactate dehydrogenase, which requires the oxidation of NADH to NAD^+. This cascade can be seen in **Figure 2.5**.

NADH contains a quinone ring and can absorb light at 340 nm. However, when NADH is oxidised to NAD^+ a pyridine ring is formed which is aromatic and does not absorb light at 340 nm. This loss of absorption allows the reaction to be tracked photometrically. The decrease in absorbance at 340 nm on conversion of NADH to NAD^+, is stoichiometric with the production of ADP by the Mur ligase reaction thus allowing the decrease in absorption to be linked to the activity of the Mur ligase.

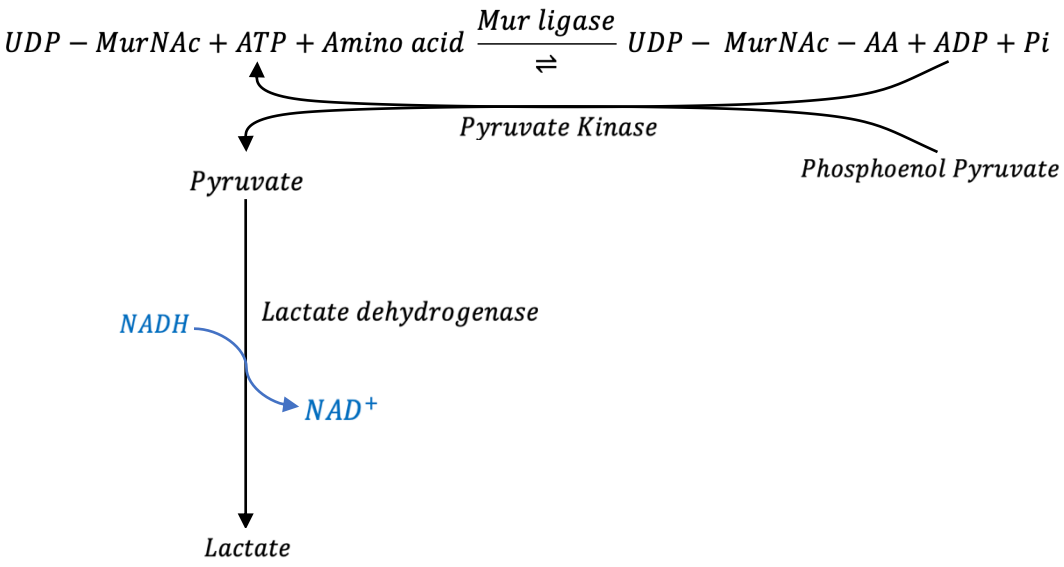

Figure 2. 5: Diagram to show the coupling reaction during the PK/LDH coupled assay

The Mur ligase reaction results in the conversion of ATP to ADP. The release of ADP initiates a secondary reaction that converts phosphoenol pyruvate to pyruvate via the actions of pyruvate kinase. The pyruvate is then converted to lactate via lactate dehydrogenase, which requires the oxidation of NADH. The oxidation of NADH (shown in blue), causes an absorbance decrease at 340 nm, which can be equated to the activity of the Mur ligase during the initial rate period of the Mur ligase reaction.

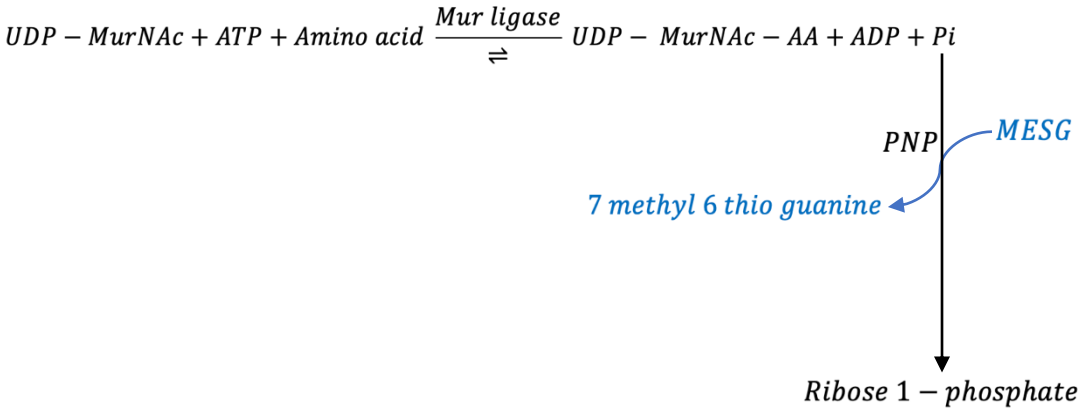

Figure 2. 6: Diagram to show the coupling reaction within a MESG coupled assay

The Mur ligase reaction results in the conversion of ATP to ADP and phosphate. This free phosphate can be converted to ribose 1-phosphate via PNP, which also converts MESG to 7-methyl 6 thio guanine. The conversion of MESG to 7-methyl 6 thio guanine (shown in blue), results in an absorbance increase at 360 nm, which can be equated to the activity of the Mur ligase during the initial rate period of the Mur ligase reaction.

Instead of relying on the production of ADP, a MESG coupled assay converts the free phosphate formed during the Mur ligase reaction to ribose 1-phosphate via the actions of PNP, acting upon MESG to convert it to 7-methyl 6 thio guanine, as seen

in **Figure 2.6**. 7-methyl 6 thio guanine absorbs light at 360 nm, whereas MESG absorbs light at 330 nm. An increase in absorbance at 360 nm corresponds to the conversion of MESG to 7-methyl 6 thio guanine, which is taken to be stoichiometric with the production of phosphate during the Mur ligase reaction, thus allowing assay of activity of the Mur ligase.

Both assays allow for the tracking of Mur ligase activity by equating absorbance change to activity. However, for the purposes required within this project, the MESG coupled assay was more suitable. The MESG coupled assay only required the addition of a single secondary reaction, whereas the PK/LDH assay relied on a two-step secondary reaction, which may potentially result in more interference within the assay from inhibitory compounds. Another benefit of the MESG coupled assay is that it does not rely on the production of ADP, instead tracking the production of free phosphate. Therefore, this assay would function in the presence of other alternative nucleotides such as CTP or GTP, which should have higher K_m's allowing for lower affinity binding fragments to be identified within the assay.

3.4.1 The MESG coupled assay is reliant on the production of free phosphate

Within an MESG coupled assay, the activity of the Mur ligase was tracked via the coupling of the Mur ligase reaction to a secondary reaction that was reliant on the production of free phosphate. To confirm that the secondary reaction was

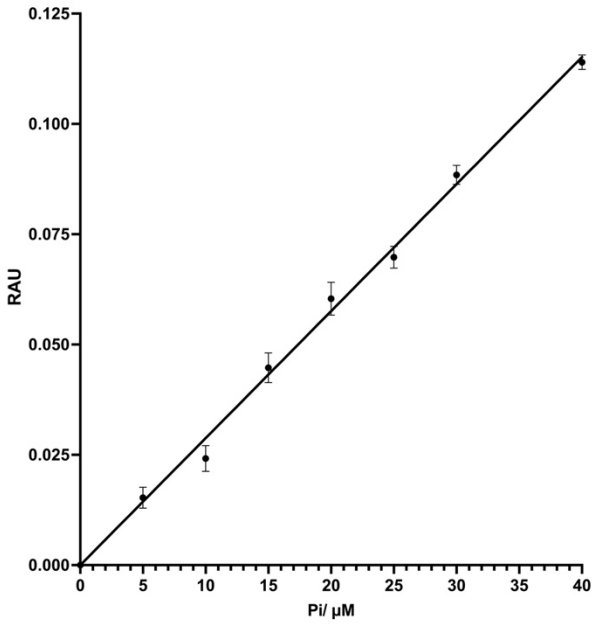

Figure 2. 7: Secondary coupled reaction is reliant on the presence of free phosphate

The activity of the secondary coupled reaction was tracked in the presence of various phosphate concentrations. The initial rate of the reaction was determined and plotted against phosphate concentration. A linear relationship was observed between phosphate concentration and initial rate.

reliant on the presence of free phosphate within our assay system, the secondary reaction was run in the presence of various phosphate concentrations via a Plate reader. As can be seen from **Figure 2.7**, a linear relationship between phosphate concentration and initial activity rate was seen, with a gradient of 2879 $M^{-1}.cm^{-1}$, confirming that the secondary reaction was reliant on the presence of free phosphate within our assay system.

3.4.2 The MESG coupled assay can track Mur enzyme activity

The secondary assay system of the MESG coupled assay was shown to be able to effectively track the presence of free phosphate. The ability of the secondary assay system to be coupled to the Mur ligase reaction and effectively track the activity of the Mur ligase via the production of free phosphate was then confirmed. The MESG coupled assay was run, via a Plate reader, in the presence of various *S. agalactiae* MurD concentrations and the initial rate determined.

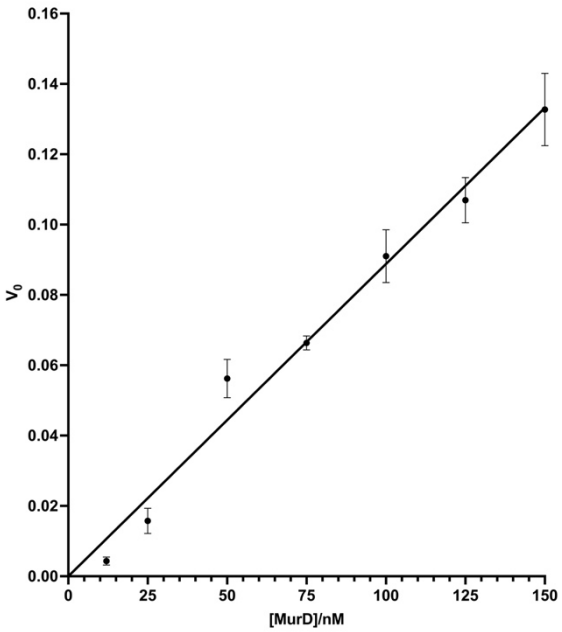

Figure 2. 8: MESG coupled reaction is reliant on MurD concentration

The activity of *S. agalactiae* MurD was determined via the MESG coupled assay. The assay was tracked in the presence of various MurD concentrations. The initial rate of the reaction was determined and plotted against MurD concentration. A linear relationship was observed between MurD concentration and initial rate.

As can be seen from **Figure 2.8**, a linear relationship was seen between MurD concentration and the initial rate determined via the assay. A linear relationship showed that the MESG coupled assay was effectively following the activity of the Mur ligase during the initial rate period without limiting the rate of the reaction catalysed by MurD. Extrapolation of this relationship to the origin of the graph

indicated the rates being measured were strictly dependent on the presence of MurD.

3.4.3 MurD requires the presence of all substrates for activity

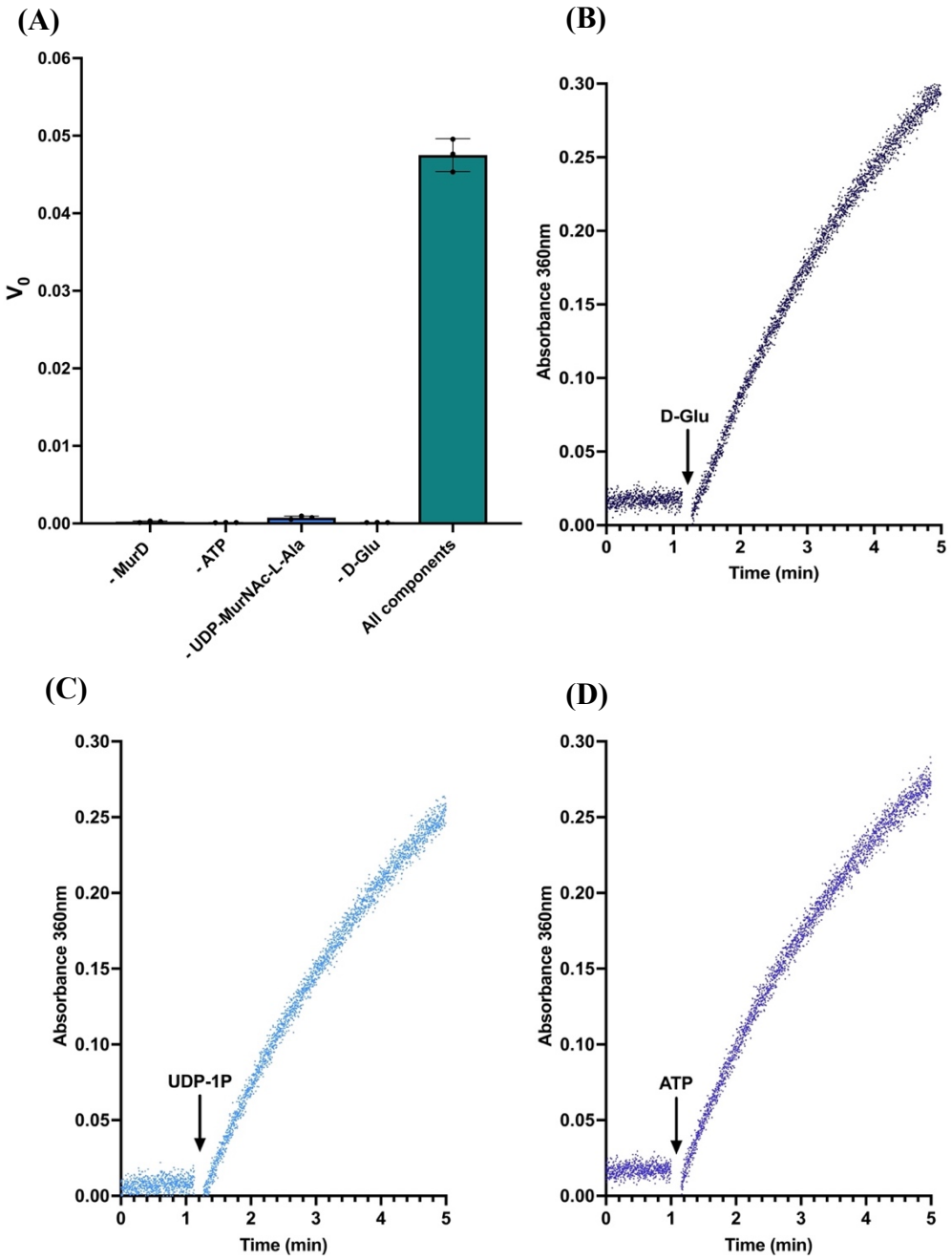

Figure 2. 9: The activity of MurD relies on the presence of all three substrates

The activity of MurD was tracked using a MESG coupled assay. All components of the assay were incubated at 37^0c barring one substrate which was added after 1 minute. No activity was seen within any of the assays until all three substrates were present. (A) Comparison of initial rate when individual substrates were omitted and when all substrates were present. (B) D-Glu added after 1 minute. (C) UDP-MurNAc-L-Ala added after 1 minute. (D) ATP added after 1 minute.

The Mur ligases require three substrates for activity – a UDP-MurNAc intermediate, a nucleotide and a relevant amino acid. To determine whether the presence of all substrates was required for the activity of *S. agalactiae* MurD during the MESG coupled assay, the assay was run via a spectrophotometer, in the absence of a substrate or the ligase. The absorbance change was followed and the initial rate was determined. The initial rates were compared to the initial rate when all substrates were present, as seen in **Figure 2.9A**. As can be seen in **Figure 2.9A**, no initial rate was seen when a substrate or the ligase was omitted. When the omitted substrate was introduced to the assay, an activity rate could be seen, as shown in **Figure 2.9B,C and D**. These results showed that within the assay, MurD from *S. agalcatiae* required the presence of all substrates for activity to be detected.

3.4.4 Determination of the K_m values for substrates for MurD from *S. agalactiae*

MurD from *S. agalactiae* required the presence of all three substrates for activity. Typically each Mur ligase will display a hyperbolic dependence of initial velocity upon each substrate, with the exception of those instances where substrate inhibition is observed [52]. Under a given set of conditions, these relationships can be defined by two constants, K_m and V_{max}. V_{max} relates to the initial velocity of the enzyme at infinite substrate concentration, whereas the K_m relates to the concentration of substrate at which the rate is at half maximal [88]. The Michaelis Menten equation describes the relationship between initial velocity and substrate concentration [S]:

$$V_0 = \frac{Vmax.[S]}{Km + [S]}$$

With multi-substrate enzymes, these parameters are determined at fixed finite concentrations of co-substrates, and so these constants are denoted with the superscript ‘App’ for apparent.

The major aim of this chapter was to develop assays suitable for the detection of weakly binding fragments targeted towards the substrate binding sites of the Mur ligases. Competition for this binding site via an inhibitor can be described by the relationship between initial velocity (V_i) and substrate concentration in the presence of a concentration of inhibitor [I]:

$$V_i = \frac{Vmax.[S]}{Km.\left(1 + \frac{[I]}{Ki}\right) + [S]}$$

In the presence of a competitive inhibitor, the K_m is increased by a factor of (1 + [I]/Ki) where Ki is the dissociation constant of inhibitor from the enzyme. The degree of competitive inhibition, when defined as 1-(V_i/V_0) can be determined via the combination of the two previous equations:

$$Inhibition = 1 - \left\{\frac{Km + [S]}{Km.\left(1 + \frac{[I]}{Ki}\right) + [S]}\right\}$$

By setting theoretical values for Ki of 2 mM and inhibitor of 100 mM, the impact on K_m over a 105-fold variation of substrate concentration can be simulated in GraphPad Prism.

As seen in **Figure 2.10**, the ability of an assay to identify a competitive inhibitor is dependent on substrate concentration and K_m value. A decreasing substrate concentration and an increasing K_m value can significantly improve the ability of an assay to detect a weakly competitive inhibitor. The estimation of the K_m is an essential pre-requisite for the development of assays directed towards the identification of competitive inhibitors.

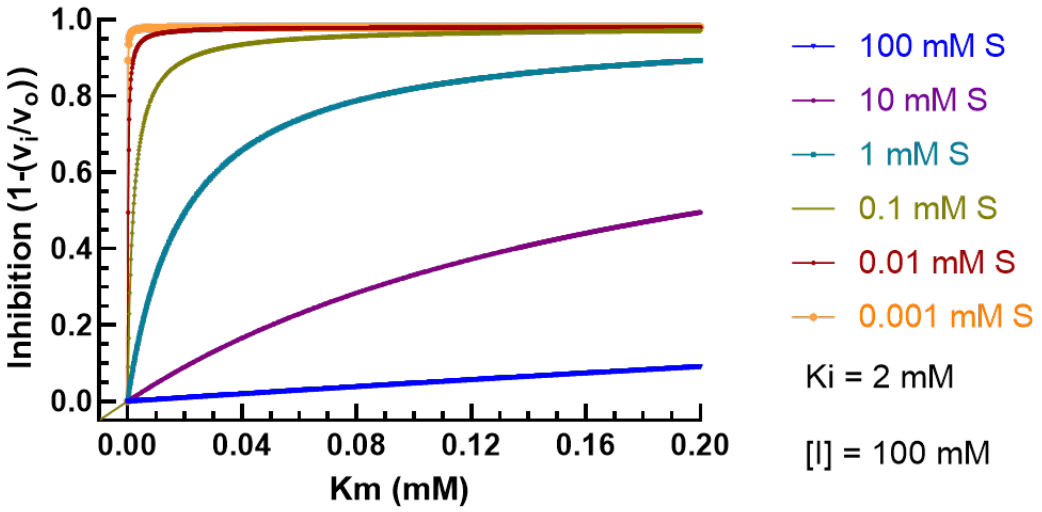

Figure 2. 10: Ability of assay to identify competitive inhibitors is dependent on Km value
Simulation of the impact of increasing Km and substrate concentration on inhibition by an inhibitor at a final concentration of 100 mM with a Ki of 2 mM. Km values were increased with a 0.0002 increment.

The dependence of *S. agalactiae* MurD activity on ATP, D-Glu and UDP-MurNAc-L-Ala concentrations was determined at constant concentrations while the other substrates remained unvaried (250 µM ATP, 1 mM D-Glu, 50 µM UDP-MurNAc-L-Ala respectively) using a MESG coupled assay at 100 nM MurD *S. agalactiae.*

The concentration of the substrate being investigated was varied to allow for the determination of the apparent values of V_{max} and K_m for the three substrates. The data was fitted by non-linear regression within GraphPad to the Michaelis Menten equation allowed for the formation of hyperbolic graphs as seen in **Figure 2.11**, which allowed for the determination of the required constants as seen in **Table 2.3.**

	ATP	UDP-MurNAc-L-Ala	D-Glu
K_m^{App}(µM)	47.1 +/- 6.5	13.3 +/-2	97.8 +/- 9.4
V_{max}^{App} (µM Pi/ min^{-1})	121.4 +/- 4.4	116.6 +/- 6.2	114.7 +/- 3.3
K_{cat}^{App} (s^{-1})	20.2	19.4	21.5
K_{cat}^{App}/ K_m^{App}	0.42	1.46	0.22

Table 2. 3: Kinetic parameters for substrates against MurD from S. agalactiae
The kinetic determinations of all substrates for MurD from *S. agalactiae* was determined using a MESG coupled assay. MurD was at a concentration of 100 nM.

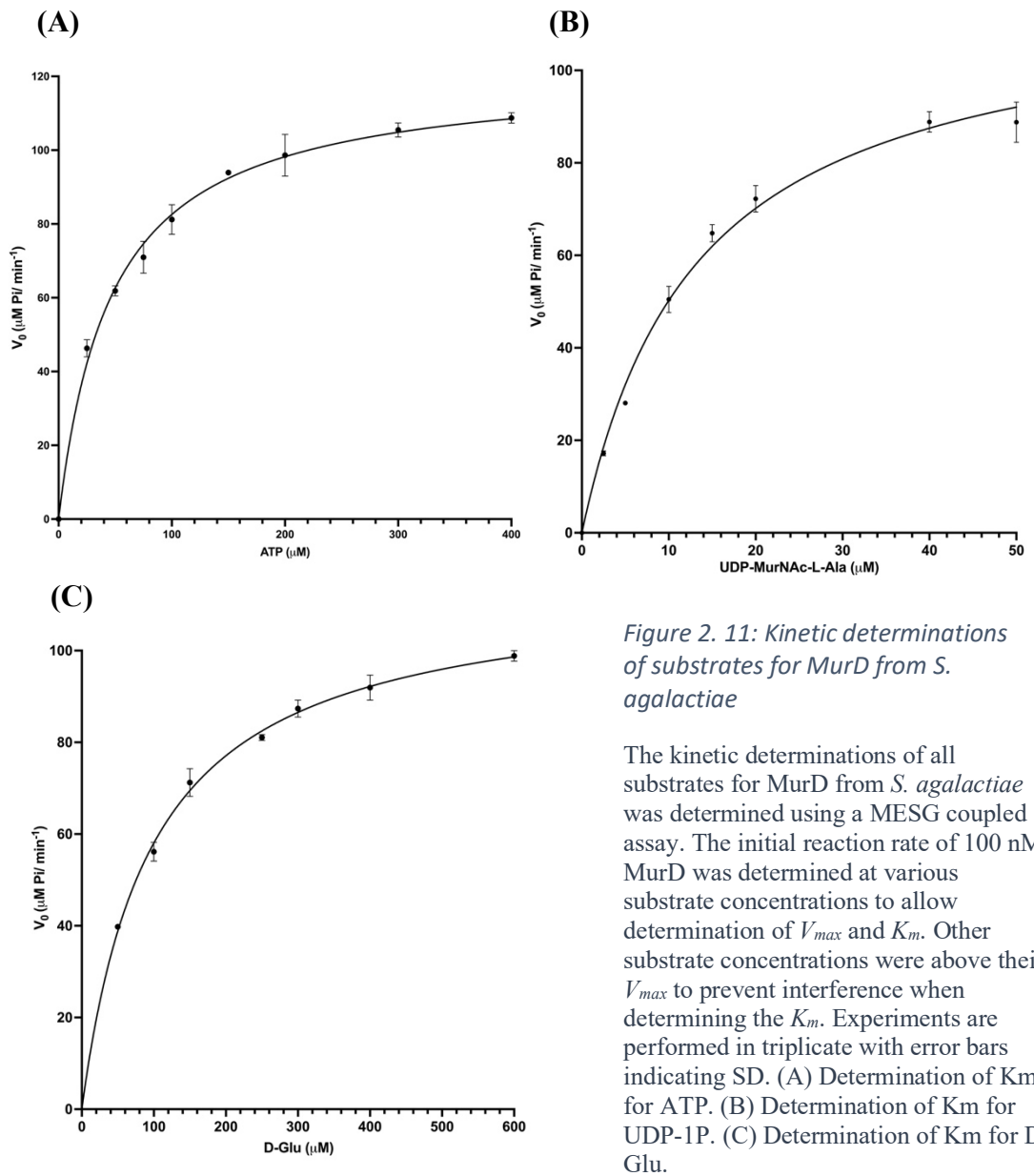

Figure 2. 11: Kinetic determinations of substrates for MurD from S. agalactiae

The kinetic determinations of all substrates for MurD from *S. agalactiae* was determined using a MESG coupled assay. The initial reaction rate of 100 nM MurD was determined at various substrate concentrations to allow determination of V_{max} and K_m. Other substrate concentrations were above their V_{max} to prevent interference when determining the K_m. Experiments are performed in triplicate with error bars indicating SD. (A) Determination of Km for ATP. (B) Determination of Km for UDP-1P. (C) Determination of Km for D-Glu.

3.4.5 Positive control inhibitors for a Mur ligase assay

To determine whether inhibition via fragments could be established using an MESG coupled assay, a positive control inhibitor was selected. β,γ-Methyleneadenosine 5′-triphosphate (ADPCP) and adenosine 5′-(β,γ-imido)triphosphate (ADPNP) are ATP analogues that are non-hydrolysable by virtue of replacement of the oxygen atom between the β and γ phosphorous atoms of ATP with a methylene and an amido group in ADPCP and ADPNP respectively, as seen in

Figure 2.12. ADPCP and ADPNP may have the potential to bind to the ATP-binding site of the Mur ligases in place of ATP, preventing activity.

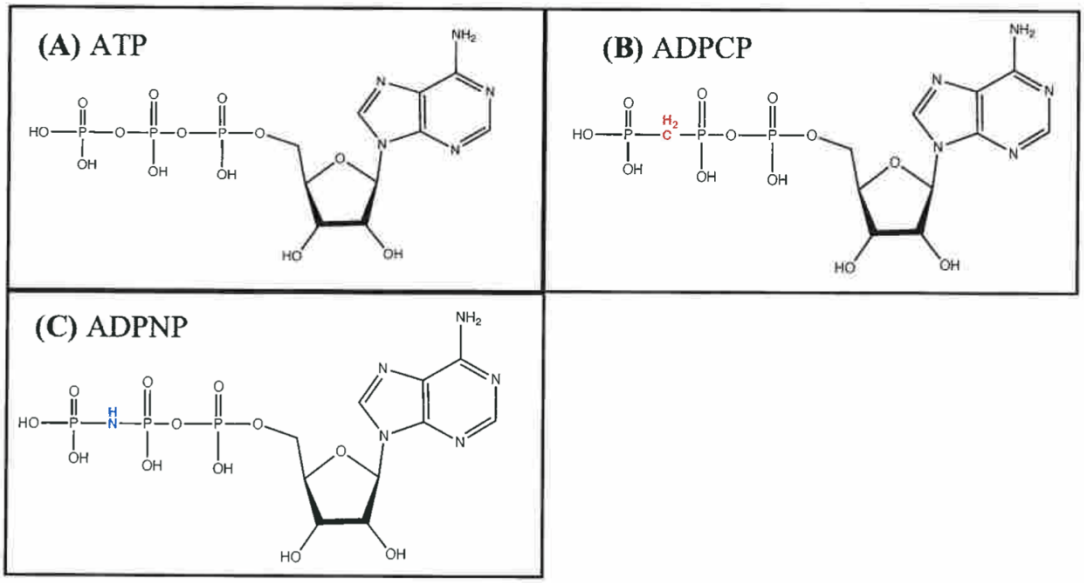

Figure 2. 12: Structures of ATP analogue inhibitors

Structural formulae of ATP and ATP analogue inhibitors. (A) ATP (B) ADPCP. The oxygen has been replaced with a methylene group (shown in red). (C) ADPNP. The oxygen has been replaced with an amido group (shown in blue).

3.4.5.1 ADPNP and ADPCP can act as inhibitors of MurD from *S. agalactiae*

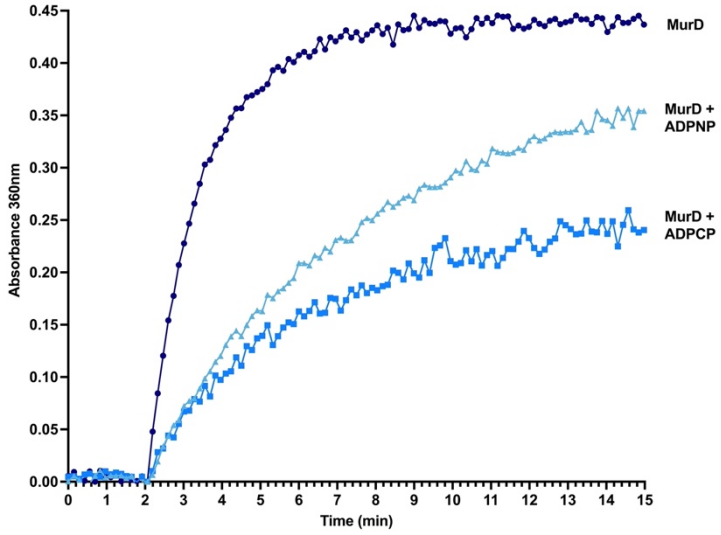

Figure 2. 13: ADPNP and ADPCP can act as inhibitors of MurD from S. agalactiae

The inhibitory effects of ADPNP and ADPCP were determined using a MESG coupled assay. The assay was run at V_{max} concentrations of substrate in the presence or absence of 50 μM ADPNP or 50 μM ADPCP, and the initial reaction rate of MurD tracked after the addition of D-Glu. A decrease in the initial rate of MurD shows that ADPNP and ADPCP were acting as inhibitors of MurD from *S. agalactiae*.

To determine if ADPNP and ADPCP were able to inhibit the activity of MurD from *S. agalactiae*, an MESG coupled assay in the absence and presence of each compound was run via a spectrophotometer. As can be seen from **Figure 2.13**, activity of MurD was reduced in the presence of both ADPNP and ADPCP, confirming that these compounds can act as inhibitors of MurD within a MESG coupled assay. ADPCP is more chemically stable than ADPNP, and so would be used as a positive control inhibitor of the Mur ligases during inhibitory fragment testing.

3.4.5.2 ADPCP has an IC_{50} value of 24.2 μM against MurD from *S. agalactiae*

ADPCP was shown to be able to act as a positive control inhibitor of MurD from *S. agalactiae* within a MESG coupled assay. For all inhibitors, an IC_{50} value can be determined. The IC_{50} value relates to the concentration of inhibitor required to achieve a 50% inhibition of enzyme activity within the assay. The MESG coupled assay was carried out for MurD from *S. agalactiae* in the presence of various ADPCP concentrations using a Plate reader. The initial rate was determined and plotted against ADPCP concentration. As can be seen from **Figure 2.14**, the initial rate of MurD from *S. agalactiae* decreases as the concentration of ADPCP increases, with an IC_{50} value of 24.2 $^{+}/_{-}$ 7.6 μM being determined.

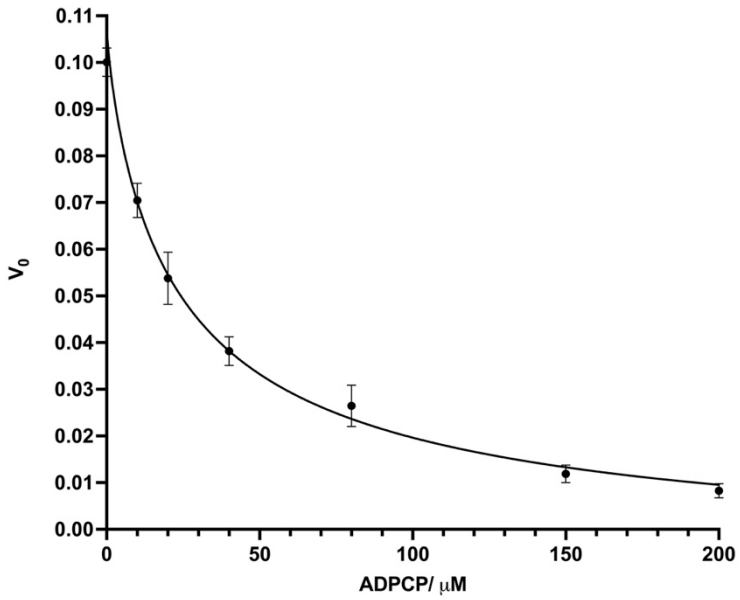

Figure 2. 14: ADPCP has an IC50 value of 24.2 μM against MurD from S. agalactiae
The IC_{50} of ADPCP against MurD was determined using a MESG coupled assay. Substrate concentrations were at their K_m values. The concentration of ADPCP was increased and the initial rate of MurD determined. The IC_{50} value was determined as the concentration of ADPCP that reduced activity of MurD by 50%. All experiments were run in triplicate with error bars indicating SD.

3.4.5.3 ADPCP has a Ki value of 11.7 μM against MurD from *S. agalactiae*

The IC_{50} value for an inhibitor can vary based on enzyme and substrate concentration. To overcome this issue, the IC_{50} value can be related to the affinity of the inhibitor via an absolute inhibition constant, K_i [89]. The K_i value of ADPCP against MurD from *S. agalactiae* can be determined using the Cheng-Prusoff equation describing the relationship between IC_{50} and K_i for a simple competitive inhibitor [89]:

$$K_i = \frac{IC_{50}}{1+\frac{[S]}{K_m}}$$

where [S] is the fixed substrate concentration and K_m is the Michaelis constant. In this equation, the K_i will always be lower than the IC_{50}, as the IC_{50} is divided by a number greater than 1. ADPCP was shown to act as an inhibitor of MurD, and as an ATP analogue was likely to be competitive with ATP binding. Therefore, substituting the K_m^{App} value for ATP (47.1 μM), the concentration of ATP used (50 μM) and the observed IC_{50} of 24.2 μM into the equation allowed for the computation of a Ki for ADPCP for ATP-competitive inhibition of MurD from *S. agalactiae* of 11.7 μM.

3.4.5.4 Z prime score of a MESG coupled assay

ADPCP was shown to be able to act as an inhibitor of MurD from *S. agalactiae* within a MESG coupled assay, suggesting that the MESG coupled assay could be used to establish the inhibitory effects of unknown fragments. The final step in evaluating the assay for use within high throughput screening was assessing its effectiveness to distinguish between positive and negative controls. One way to determine this effectiveness is via a Z prime score [90]. By running an assay in the presence (positive) and absence (negative) of a positive inhibitor control for the assay system, the Z prime score can provide a numerical value for the effectiveness of the assay for distinguishing inhibition. The Z prime score takes into account the difference between the means of the positive control and the negative control, (the

'dynamic range') as well as the difference between set standard deviation values of the positive and negative controls, (the 'separation band'), as seen in **Figure 2.15**.

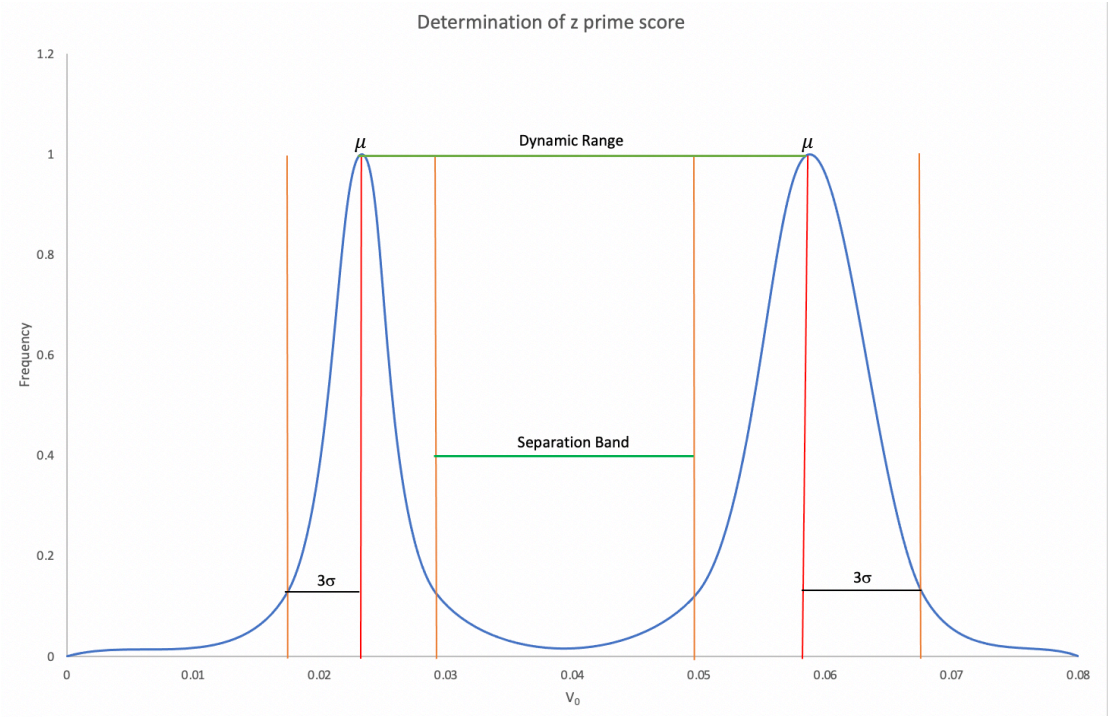

Figure 2. 15: Schematic diagram of the determination of a Z prime score

The Z prime score is determined by comparing the dynamic range to the separation band. A Z prime score between 0.5 and 1 is indicative of an assay able to effectively determine inhibition.

The Z prime score is defined as the ratio of the separation band to the dynamic range, and can be calculated using the equation [90]:

$$Z = 1 - \frac{(3\sigma_s + 3\sigma_c)}{(\mu_s - \mu_c)}$$

Where σ indicates the standard deviation, μ indicates the mean, s indicates sample and c indicates control. Using this equation, a value between negative infinity and 1 can be achieved. A value above 0.5 is considered a very good assay, and a value above 0 an acceptable assay [91].

To determine the Z prime score of the MESG coupled assay, the initial rate for MurD in the presence and absence of ADPCP at its IC_{50} value were compared across 10 repeats using a plate reader. The mean value and standard deviations were

determined, to allow the determination of the Z prime score, as seen in **Table 2.4**. The Z prime score was determined to be 0.86, indicating that the activity assay could identify inhibitors accurately.

	MurD	MurD + ADPCP
Mean	0.1715	0.07765
Standard Deviation	0.00316	0.00118
Z prime Score	$Z = 1 - \frac{(3\ x\ 0.00316) + (3\ x\ 0.00118)}{(0.1715 - 0.07765)}$ $Z = 0.86$	

Table 2. 4: Determination of the Z prime score for ADPCP within a MESG coupled assay against MurD from S. agalactiae

The Z prime score was determined by calculating the mean V_0 for MurD in the presence and absence of ADPCP, along with the standard deviation of the means. The Z prime was then calculated using the formula shown. A Z prime score of 0.86 was determined for ADPCP against MurD from *S. agalactiae* within a MESG coupled assay.

3.5 Optimization of existing assay for fragments targeted towards the ATP-binding site

Optimization steps of the MESG coupled assay have focused on the Mur ligase in the presence of its standard substrates. However, if inhibitory fragments are targeted towards the binding site of a substrate it may be beneficial to run the assay with an alternative. An alternative substrate may have a higher K_m, which would make the assay more sensitive to fragments targeted towards the binding site of that substrate, as fragments are likely to have low binding affinities. One area inhibitory fragment sets may be targeted towards is the ATP-binding site of the Mur ligases. Finding an alternative nucleotide with a higher K_m for the Mur ligases would be a useful optimization of the assay for potential inhibitory screens.

3.5.1 MurD from *S. agalactiae* lacks activity with alternative nucleotides

A variety of nucleotides that have previously been shown to be active against MurC, and having higher K_m values than ATP (A. Lloyd Pers. Commun) were chosen to be tested against MurD from *S. agalactiae*. GTP and ITP are purine-based nucleotides that contain a double bonded oxygen in place of the NH_2 present in

ATP, shown in **Figure 2.16**. CTP maintains the NH_2 group but is a pyrimidine rather than purine-based nucleotide, as seen in **Figure 2.16**.

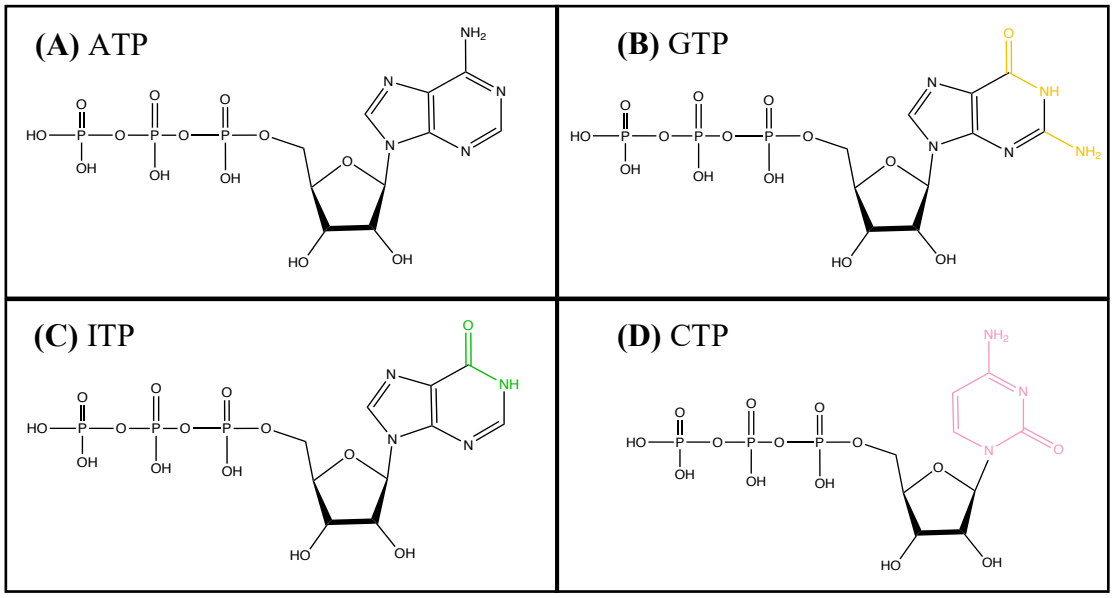

Figure 2. 16: Structural formulas of ATP and alternative nucleotides

Structural formulas of alternative nucleotides tested against MurD from *S. agalactiae.* (B) GTP is a purine nucleoside that contains an NH_2 group as well as a doubled bonded oxygen (shown in orange). (C) ITP is a purine nucleoside that contains a double bonded oxygen in place of an NH_2 group (shown in green). (D) CTP is a pyrimidine nucleoside that contains an NH_2 group and a double bonded oxygen (shown in pink).

The activity of MurD from *S. agalactiae* was compared between ATP, and the three alternative nucleotides using a MESG coupled assay in a spectrophotometer. As can be seen from **Figure 2.17,** activity of MurD could only be established in the presence of ATP, with no activity for MurD being seen in the presence of the three alternative nucleotides after the addition of D-Glu.

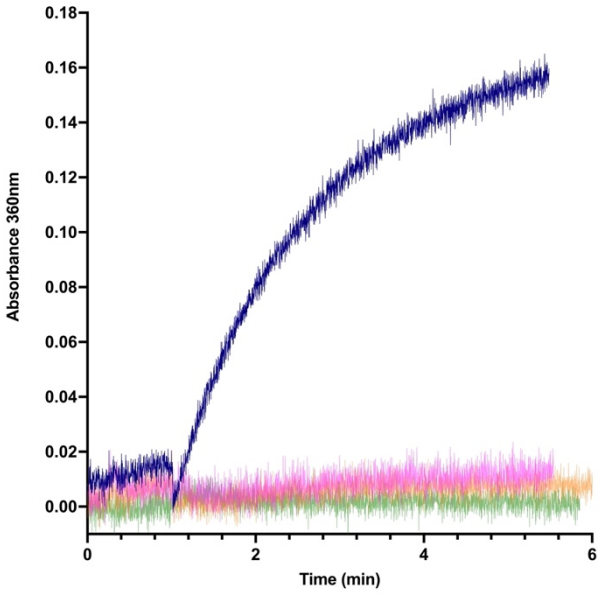

Figure 2. 17: MurD from S. agalactiae lacks activity in the presence of alternative nucleotides

Using a MESG coupled assay the activity of MurD was determined in the presence of various nucleotides. The activity rate after the addition of D-Glu was followed spectrophotometrically at 360 nm. Alternative nucleotides were tested at 1 mM, while all other substrates were at their K_m concentrations as observed in the presence of ATP. ATP is shown in blue, GTP shown in orange, ITP shown in green and CTP shown in pink. MurD showed no detectable activity with the alternative nucleotides.

3.5.2 MurD as an enzyme lacks activity with alternative nucleotide

Mur ligases have been shown in vitro to be able to utilise alternative nucleotides for activity. However, it appeared that MurD from *S. agalactiae* was inactive in the presence of alternative nucleotides. This could be due to greater nucleotide triphosphate specificity. To determine where the specificity lies, the ability of MurE from *S. agalactiae* and MurD from *P. aeruginosa* to use alternative nucleotides within a MESG coupled assay was determined via a spectrophotometer. MurE from *S. agalactiae* could use all three alternative nucleotides for activity as seen in **Figure 2.18A**, but MurD from *P. aeruginosa* showed no activity with any of the alternative nucleotides, seen in **Figure 2.18B**. These results suggest a high level of substrate specificity for ATP within MurD as an enzyme compared to GTP,ITP and CTP.

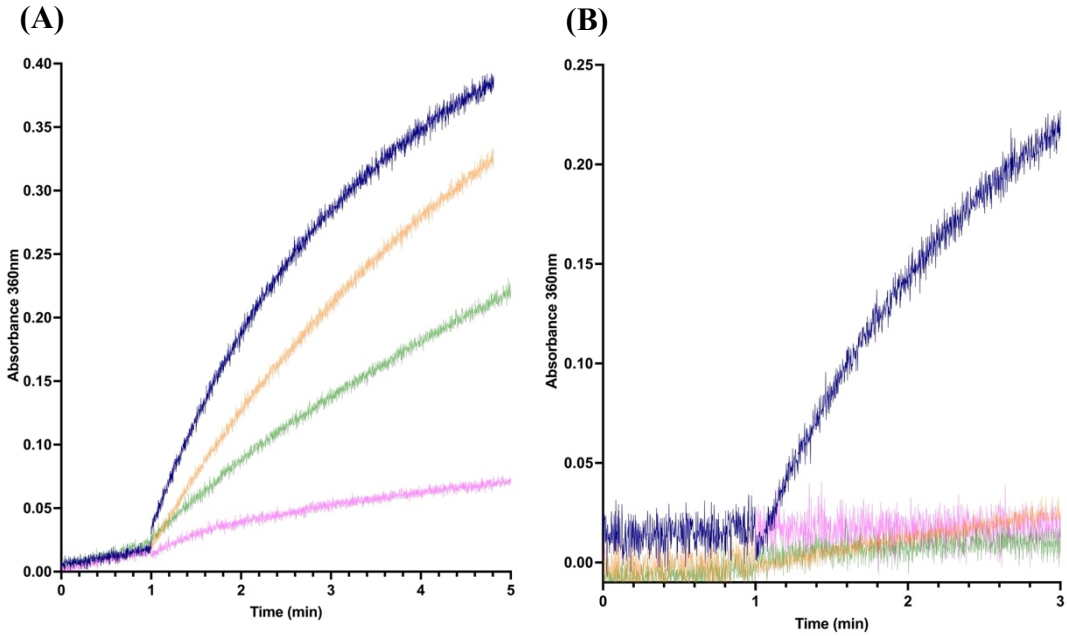

Figure 2. 18: MurD as an enzyme lacks activity with alternative nucleotides

Using a MESG coupled assay, the ability of 50 nM MurE from *S. agalactiae* and 50 nM MurD from *P. aeruginosa* to use alternative nucleotides was established. The activity rate after the addition of amino acid was followed spectrophotometrically at 360 nm. Alternative nucleotides were tested at 1 mM, all other substrates were at their K_m concentration. ATP is shown in blue, GTP shown in orange, ITP shown in green and CTP shown in pink. (A) MurE from *S. agalactiae* shows activity with all nucleotides tested. (B) MurD from *P. aeruginosa* shows no detectable activity with any nucleotides apart from ATP.

3.5.3 MurD is unable to hydrolyse alternative nucleotides

The lack of activity of MurD with the alternative nucleotides could have been due to an inability of the alternative nucleotides to bind to the ATP-binding site of MurD. Alternatively, the lack of activity could have been due to the inability of MurD to hydrolyse the alternative nucleotides once bound. In order to determine which was occurring, a competition assay with the alternative nucleotides and ATP was run using a spectrophotometer, where the concentration of the alternative nucleotide was increased in relation to the ATP concentration. If the nucleotides were able to bind in place of ATP but were unable to be hydrolysed by MurD, then a decrease in activity would be seen. However, if the alternative nucleotides were unable to bind, the activity would remain the same irrespective of how much alternative nucleotide was introduced into the assay. Using a MESG coupled assay, the ratio of [Alternative nucleotide]: [ATP] was gradually increased and the activity of MurD from *S. agalactiae* determined. As can be seen from **Figure 2.19**, the activity of MurD decreases as the concentration of all alternative nucleotides increases. This suggests that MurD was able to bind all three alternative nucleotides but was unable to hydrolyse them, resulting in a lack of activity.

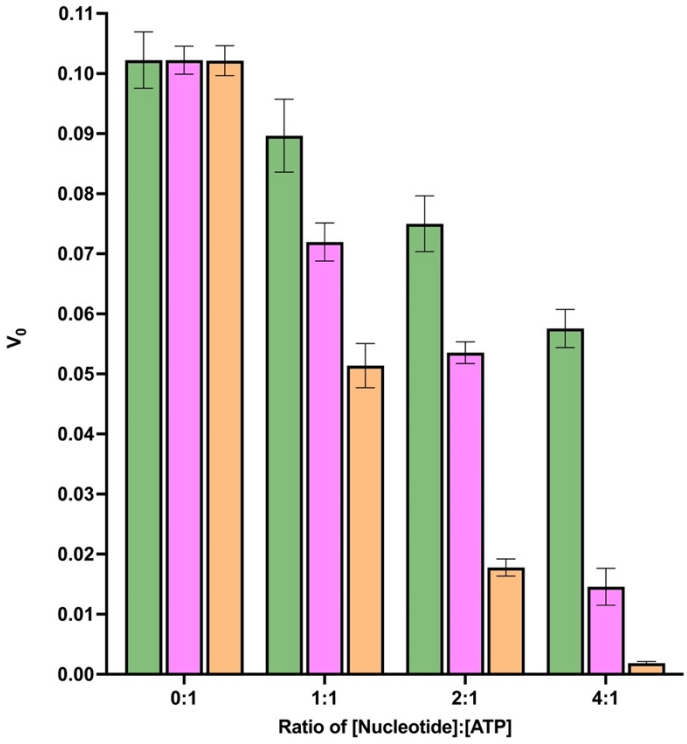

Figure 2. 19: MurD lacks the ability to hydrolyse alternative nucleotides

Using a MESG coupled assay, the ability of 50 nM MurD from *S. agalactiae* to bind or hydrolyse alternative nucleotides was established. Substrates were at their K_m concentrations. Alternative nucleotides were introduced alongside ATP at a concentration that was in relation to the ATP concentration, and the initial rate of MurD determined. GTP shown in orange, ITP shown in green and CTP shown in pink. MurD could bind all three alternative nucleotides to varying degrees but is unable to hydrolyse them.

3.5.4 Deoxy-ATP can act as an alternative nucleotide for MurD

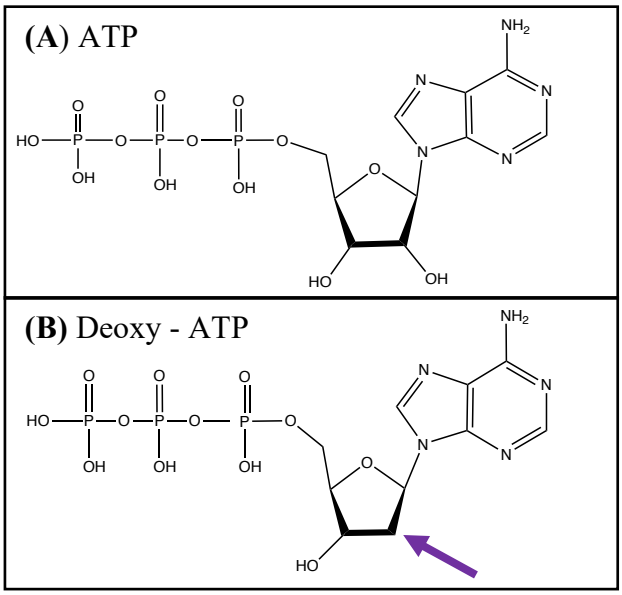

Figure 2. 20: Skeletal formula of ATP and Deoxy-ATP

Skeletal formula of ATP and deoxy-ATP. Deoxy-ATP maintains the adenine ring of ATP but lacks an OH group on the ribose sugar, highlighted by the purple arrow.

MurD from *S. agalactiae* was unable to hydrolyse the alternative nucleotides when the adenine base was changed. 2'-deoxyadenosine triphosphate (deoxy-ATP) retains the adenine base but removes the 2' OH group from the ribose sugar, as shown in **Figure 2.20**.

This could mean that MurD would be able to use deoxy-ATP as an alternative nucleotide to ATP. Using a MESG coupled assay on a spectrophotometer, the activity of MurD from *S. agalactiae* in the presence of deoxy-ATP was determined. As can be seen from **Figure 2.21**, an activity rate could be seen for MurD in the

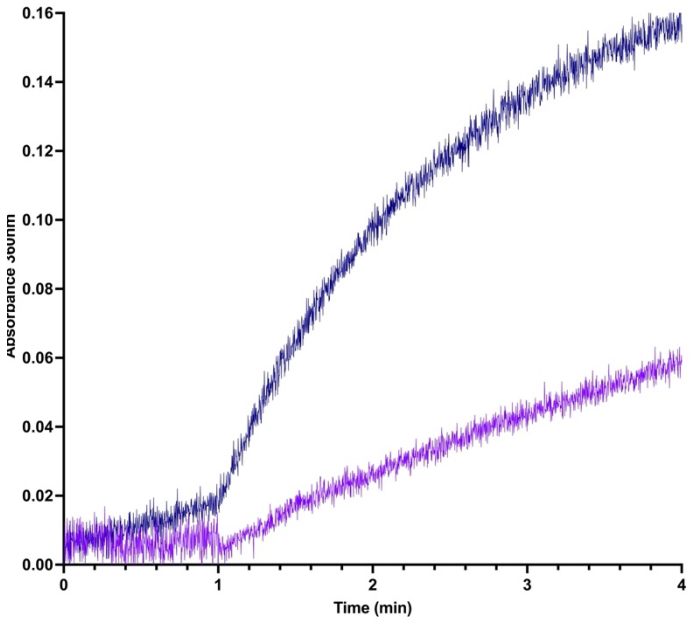

Figure 2. 21: MurD can use deoxy-ATP as an alternative nucleotide

Using a MESG coupled assay, the ability of MurD to utilise deoxy-ATP as an alternative nucleotide was established. All substrates were present at their K_m values, and deoxy-ATP was run at 200µM. The activity rate after the addition of D-Glu was tracked spectrophotometrically at 360 nm. MurD was able to utilise deoxy-ATP, with a reduced activity rate, making it a suitable alternative nucleotide.

presence of deoxy-ATP, suggesting that deoxy-ATP may be able to act as a suitable alternative nucleotide for MurD within targeted fragment screens.

As MurD was able to use deoxy-ATP as an alternative nucleotide, the K_m of deoxy-ATP was established to determine if deoxy-ATP had a higher K_m than ATP against MurD from *S. agalactiae*, which would make it more effective in targeted fragment screens. Using a MESG coupled assay on a Plate reader, the activity of 80 nM MurD from *S. agalactiae* at increasing concentrations of deoxy-ATP were assayed. The resulting initial rates were plotted against deoxy-ATP concentration. The data was plotted and then fitted by non-linear regression within GraphPad to the Michaelis Menten equation resulted in the graph seen in **Figure 2.22**. As can be seen from **Table 2.5**, the K_m of deoxy-ATP with MurD from *S. agalactiae* was determined to be 476.1 $^{+}/_{-}$ 81.2 μM.

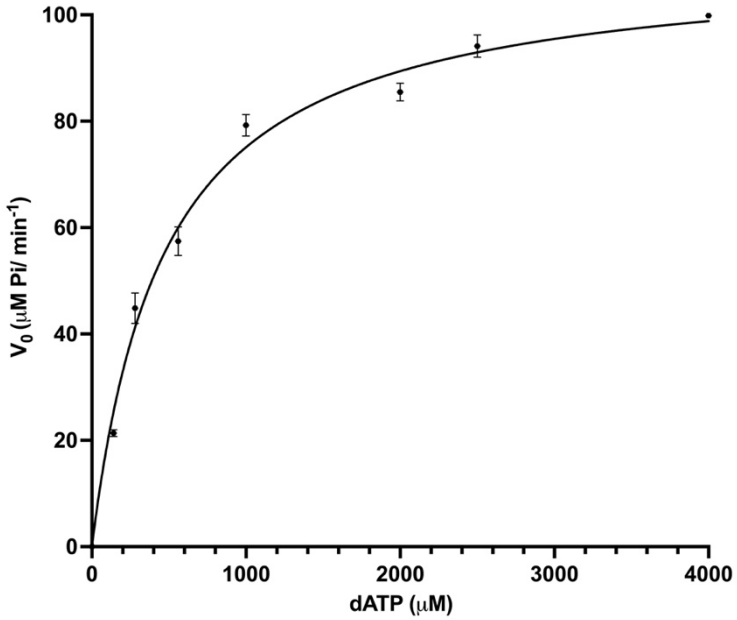

Figure 2. 22: The Km for deoxy-ATP for MurD from S. agalactiae is 477 μM

The K_m for deoxy-ATP for MurD *from S. agalactiae* was determined using a MESG coupled assay. The initial reaction rate of MurD was determined at various deoxy-ATP concentrations to allow determination of V_{max} and K_m. Other substrate concentrations were above their V_{max} to prevent interference when determining the K_m. Experiments are performed in triplicate with error bars indicating SD.

	K_m^{App}(μM)	V_{max}^{App} (μM Pi/ min^{-1})	K_{cat}^{App} (s^{-1})	K_{cat}^{App}/ K_m^{App}
Deoxy-ATP	476.1 $^{+}/_{-}$ 74	110.7 $^{+}/_{-}$ 5.3	23	0.05

Table 2. 5: Kinetic determinations for deoxy- ATP for MurD from S. agalactiae

The kinetic determinations of deoxy -ATP for MurD from *S. agalactiae* was determined using a MESG coupled assay. MurD was at a concentration of 80 nM.

3.6 Development of a stop point assay for Mur ligase activity

Previously used assays have relied upon a secondary coupled reaction running concurrently with the primary Mur ligase reaction. This requires the components of the secondary reaction to be at high concentrations to allow the consumption of phosphate generated during the initial rate period of the Mur ligase reaction to be fast enough to not itself be rate limiting. This makes the assay expensive when scaled up to run high throughput screening of fragments. Other issues with scaling up this version of the assay for high throughput screening were the amount of data interpretation required for each assay. Typically, continuous assay plate-reader rate data comprised of up to 1000 data points which required manual analysis for each individual run of the assay, making data analysis extremely inefficient.

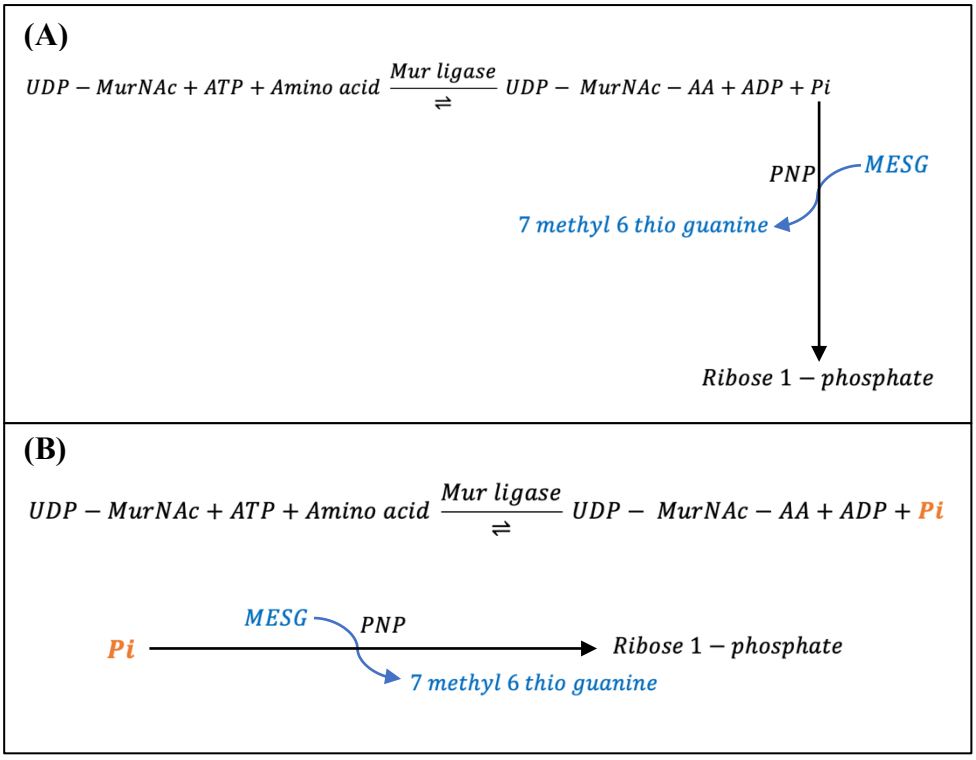

Figure 2. 23: Diagram to compare the set-up of a MESG coupled assay and a stopped MESG assay Previously used assays relied on the coupling reaction running concurrently with the Mur ligase reaction. Within a stop point assay, the coupling reaction would be run after the Mur ligase reaction. (A) In previously used assays, all reactions would be running simultaneously; as the Mur ligase converts its substrates into its UDP intermediate and free phosphate, the phosphate would immediately be used by the coupling reaction to convert MESG into 7 methyl 6 thio guanine. resulting in an absorbance change at 360 nm. (B) In a stopped assay, the Mur ligase reaction would occur, converting the substrates into the UDP intermediate product and free phosphate. The Mur ligase reaction would then be stopped before the free phosphate formed would be used within the coupling reaction to convert MESG into 7 methyl 6 thio guanine resulting in an absorbance change at 360 nm.

Additionally, following V_0 requires the very initial portion of the assay to be tracked with a large amount of data points to make it as accurate as possible, therefore precluding the testing of a large number of samples simultaneously.

To combat these issues, a stop point assay could be designed whereby the coupling reaction and Mur ligase reaction are run consecutively. This would mean running the Mur ligase reaction over the initial rate period before stopping the reaction. The free phosphate formed during the initial rate period of the Mur ligase reaction could then be used within the coupling reaction which would be tracked to its end point to give the initial rate of the ligase, as seen in **Figure 2.23**.

By tracking the end point of the coupling reaction, the requirement to collect a large volume of data points during the initial stage of the reaction to get an accurate rate of the Mur ligase activity is removed. Running the coupling reaction separately also removes the requirement of having the coupling reaction components at high concentrations to keep pace with the Mur ligase reaction during its initial rate period. Instead, the coupling reaction components can be decreased reducing the cost of the assay. In order to design a stopped assay, a stopping agent that could stop Mur ligase activity, but not affect the secondary assay was required. Comparison of the recordable initial rate of the ligase across both assays would also need to be carried out. Furthermore, the effect of dropping the coupling reaction components on the recordable initial rate of the Mur ligase would need to be determined to conclude if a stop point assay was a viable alternative to the existing assays.

3.6.1 EDTA inhibits the MurD reaction within an assay

In order to develop a stop point assay, the first step was to determine if the Mur ligase reaction could be stopped during the initial rate period in order to be able to separate the Mur ligase reaction from the coupling reaction. Mur ligases require the presence of Mg^{2+} to form the magnesium-chelate of ATP. Ethylene diamine tetra acetic acid (EDTA) can chelate divalent cations, and so would be able to chelate the Mg that is present in the buffer of the assay. Removing the Mg from the buffer system would stop the Mur ligases from binding their substrates,

effectively preventing their activity. EDTA and EDTA in complex with Mg do not absorb at 360 nm and so any change in absorption seen would be due to the effect EDTA was having on the Mur ligase reaction. The activity of MurD from *S. agalactiae* was tracked photometrically via a MESG coupled assay on a spectrophotometer with a reduced Mg concentration of 2 mM. Once the initial rate period had occurred, 10 mM EDTA , in a 5 to 1 ratio to Mg, was introduced into the assay. After introduction of EDTA into the assay system a plateau in absorbance was observed, as seen in **Figure 2.24**. A plateau in absorbance suggests that there was no longer any phosphate being produced within the assay system for the PNP to act upon to convert MESG to 7 methyl 6 thio guanine suggesting that there was no longer any activity of MurD.

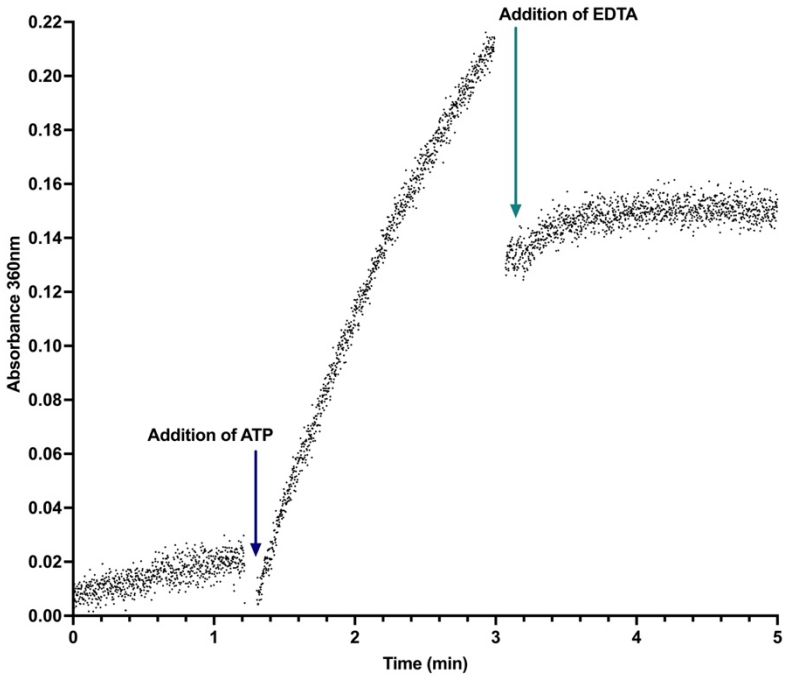

Figure 2. 24: EDTA is able to stop activity of MurD from S. agalactiae

Using a MESG coupled assay, the ability of EDTA to impede the reaction of MurD from *S. agalactiae* was determined. The MESG coupled assay was run using standard conditions with substrates at their K_m values. The Mur ligase reaction was initiated with ATP and the initial rate of the reaction tracked spectrophotometrically. After a minute and a half of tracking the initial rate, a final concentration of 10 mM EDTA was added. A plateau in absorbance shows that the MurD reaction is impeded by the addition of EDTA.

To confirm that the addition of EDTA was affecting the activity of the Mur ligase reaction, and not the ability of the coupling system to track the free

phosphate, the coupling assay was run in the presence of EDTA on a Plate reader. As can be seen from **Figure 2.25**, a linear relationship between V_0 and [Phosphate] was still seen in the presence of EDTA. The gradient of the line was determined to be 2719 $M^{-1}cm^{-1}$, which was not statistically different to the gradient of the MESG assay in the absence of EDTA, as seen in **Section 3.4.1**, suggesting that the addition of EDTA was effectively stopping the Mur ligase reaction only.

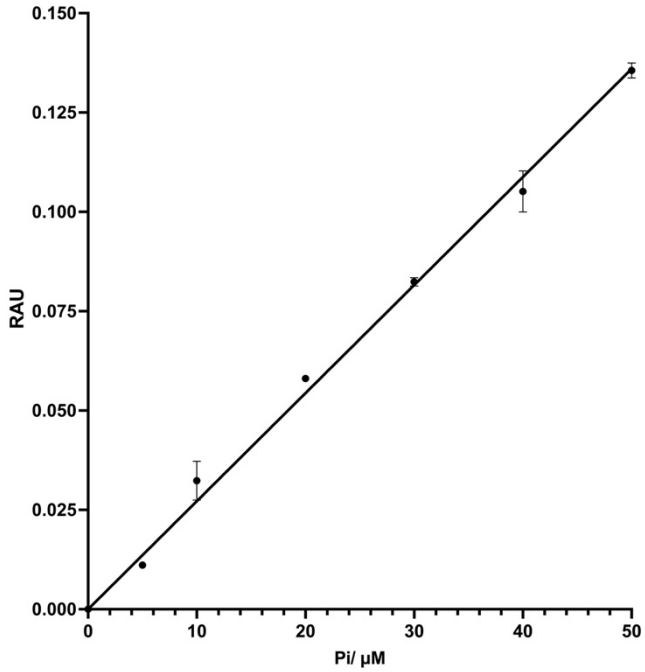

Figure 2. 25: EDTA does not affect the secondary coupling system

The activity of the secondary coupled reaction in the presence of EDTA was determined. The initial rate of the reaction at various phosphate concentrations was determined. Initial rate was plotted against phosphate concentration. A linear relationship was observed between phosphate concentration and initial rate, showing the addition of EDTA was not affecting the secondary assay system.

3.6.2 The initial rate of *S. agalactiae* MurD can be determined within a stop point assay

As EDTA was able to stop the activity of MurD but caused no effect on the ability of the secondary system to use free phosphate, EDTA could be used as a stopping agent allowing the separation of the Mur ligase reaction from the secondary reaction. However, the effect of stopping the Mur ligase reaction with EDTA and then running the secondary reaction separately on the measurable V_0 of the Mur ligase had to be determined. To understand the effect stopping the reaction and running the secondary reaction separately had on the recordable V_0, the V_0 of MurD from *S. agalactiae* was determined via a MESG coupled assay on a spectrophotometer and compared to the V_0 determined using the stopped MESG assay on a spectrophotometer, as seen in **Figure 2.26**.

The V_0 of MurD within a MESG coupled assay was determined to be 0.1/min, while within the stop point assay it was determined to be 0.098/min. These results were not statistically significantly different, suggesting that the addition of EDTA, and the uncoupling of the reaction did not influence the measurable V_0 of *S. agalactiae* MurD, suggesting that accumulation of phosphate in the stopped assay (which did not occur in the continuous variant of the assay) did not inhibit MurD catalysis.

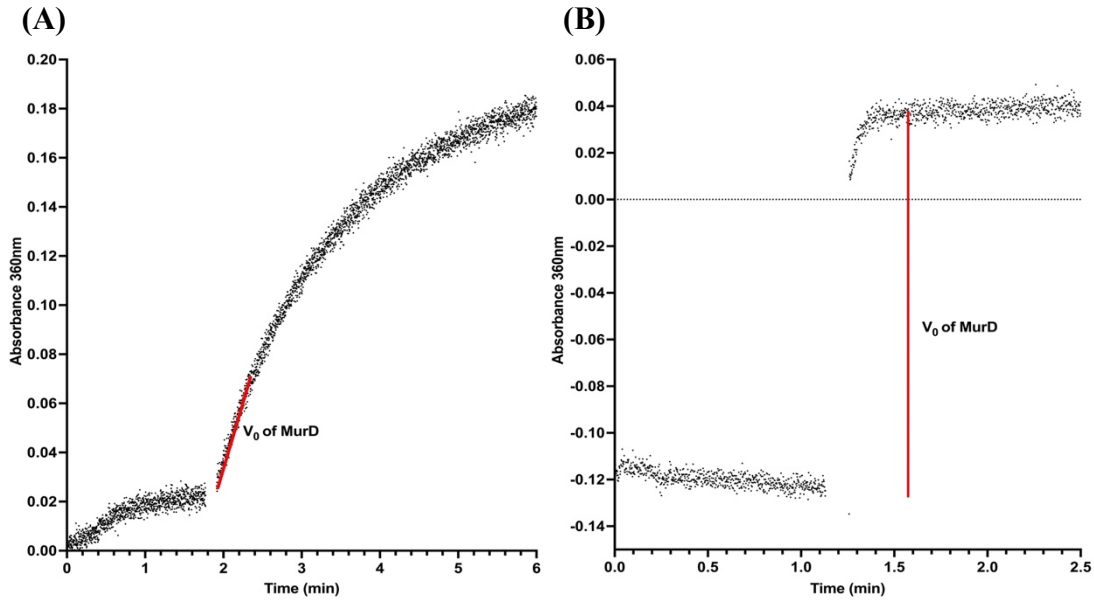

Figure 2. 26: Comparison of the measurable V_0 of MurD between a MESG coupled assay and a stop point assay

The measurable V_0 of MurD from *S. agalactiae* was compared between a MESG coupled assay and a stop point assay. Experiments were run in triplicate with an example run shown. (A) Using a MESG coupled assay, under K_m conditions, the V_0 of MurD from *S. agalactiae* was determined, highlighted with a red line. The V_0 was determined to be 0.1/min. (B) Using a stop point assay, under K_m conditions, the V_0 of MurD from *S. agalactiae* was determined, highlighted with a red line. The V_0 was determined to be 0.098/min.

3.6.3 Reduction of PNP levels has no significant effect on V_0

Previously the coupling reaction components were present within the assay at concentrations that would not interfere with the determination of the V_0 of the Mur ligase. This meant the components were at concentrations that allowed for there to be an excess within the assay, allowing all the phosphate produced by Mur ligase activity to be immediately consumed by PNP, allowing for accurate determination of the activity of the Mur ligase. This however, meant the assay was expensive to run for high throughput screening. By reducing the concentration of

PNP, the assay could become more cost effective for high throughput screening. To ensure reducing the secondary coupling enzyme did not affect the recordable V_0 of the Mur ligase, the stopped assay was run in the presence of various PNP concentrations on a spectrophotometer, and the MurD V_0 was determined. As can be seen from **Figure 2.27**, reducing the PNP concentration caused no statistically significant difference on the recordable V_0 of MurD from *S. agalactiae.*

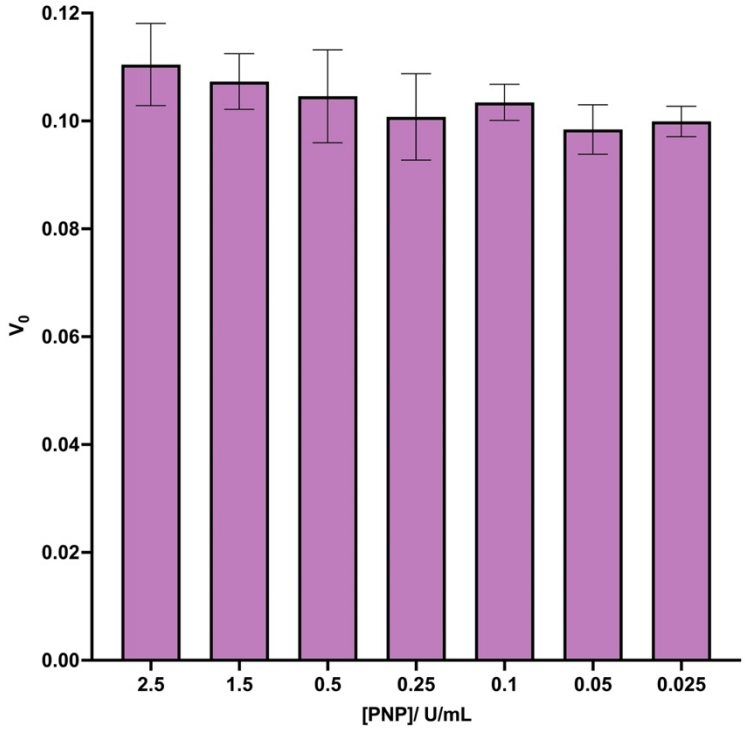

Figure 2. 27: Reducing PNP concentration causes no significant effect on V_0 of MurD from S. agalactiae

The measurable V_0 of MurD from *S. agalactiae* was determined at various PNP concentrations. Using a stop point assay with all substrates at their K_m values the V_0 of MurD from *S. agalactiae* was determined at various PNP concentrations. Reducing the PNP concentration caused no significant effect on the measurable V_0 of MurD.

3.6.4 Quality of assay for high throughput screening

The stopped MESG assay was developed to improve upon the existing assays to facilitate screening for inhibitory fragments. The stopped MESG assay would allow more fragments to be tested simultaneously, requiring less data analysis, and being more cost effective than existing assays. However, the effectiveness of the assay for determining inhibition would need to be established before it could be used for screening of inhibitory fragments.

3.6.4.1 Inhibition of the MurD reaction within a stopped MESG assay

One way to determine the effectiveness of the stopped MESG assay to identify inhibitors was to test a known inhibitor within the assay. ADPCP was already shown to act as an inhibitor within a MurD assay. The stopped MESG assay was run in the

presence and absence of ADPCP on a spectrophotometer and the V_0 determined. As can be seen from **Figure 2.28**, ADPCP reduced the V_0 of *S. agalactiae* MurD by greater than 30%.

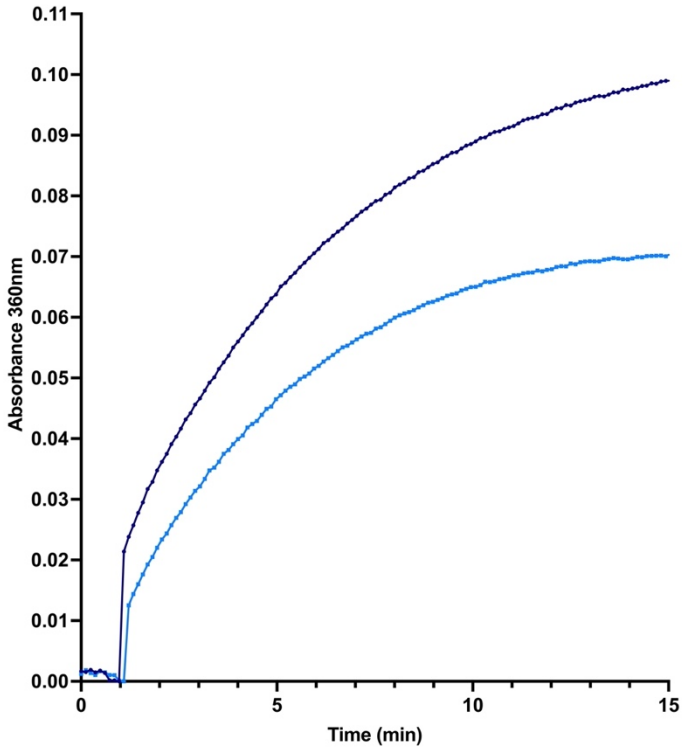

Figure 2. 28: ADPCP can act as an inhibitor of MurD within a stop point assay

The activity of MurD from *S. agalactiae* was tracked using a stop point assay in the absence and presence of 10 μM ADPCP. The Mur ligase reaction was run in the presence or absence of ADPCP for the initial rate period before being quenched with EDTA. The secondary coupling reaction was then initiated by PNP and tracked spectrophotometrically at 360 nm. Absence of ADPCP shown in dark blue, presence shown in light blue.

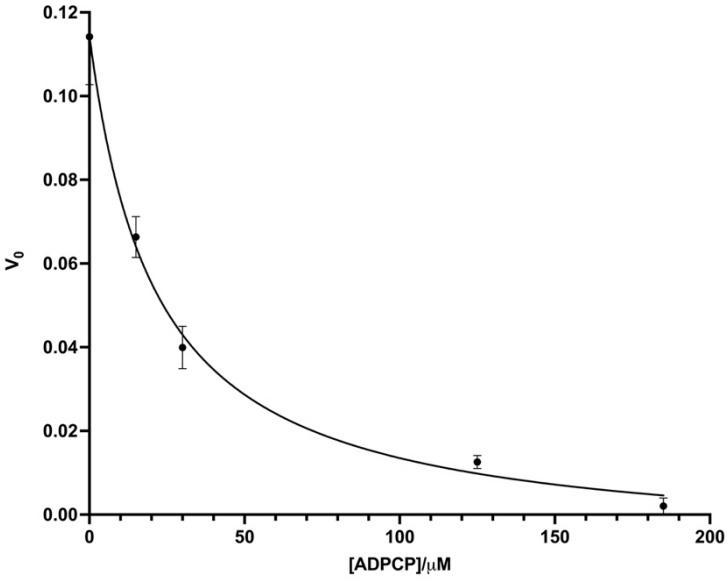

Figure 2. 29: ADPCP has an IC_{50} value of 22.8 μM against MurD from S. agalactiae within a stop

The IC_{50} value of ADPCP against MurD was determined using a stop point assay. Substrate concentrations were at their K_m values. The concentration of ADPCP was increased and the initial rate of MurD determined. The IC_{50} value was determined as the concentration of ADPCP that reduced activity of MurD by 50%. All experiments were run in triplicate with error bars indicating SD.

ADPCP was still able to inhibit *S. agalactiae* MurD within a stopped assay, and so the IC_{50} value of ADPCP was determined. The V_0 of *S. agalactiae* MurD was determined at varying concentrations of ADPCP via a Plate reader. The impact of increasing ADPCP concentration of MurD V_0 was then established. As can be seen from **Figure 2.29**, ADPCP had an IC_{50} of 22.8 $^{+}/_{-}$ 7.5 μM which was not statistically different from that seen within existing assays (24.2 $^{+}/_{-}$ 7.6 μM, **Section 3.4.5.2**) .

3.6.4.2 Z prime score for assay shows high level of effectiveness for determining inhibition

The effectiveness of the stopped MESG assay to determine inhibition was also determined by calculating the Z prime score. A Z prime score between 0.5 and 1 shows a high level of effectiveness within the assay for determining inhibition. To determine the Z prime score of the stopped MESG assay, the V_0 for MurD from *S. agalactiae* in the presence and absence of ADPCP at its IC_{50} value within a stopped MESG assay were compared. 10 repeats were run via a Plate reader. The mean value and standard deviations were determined, to allow the determination of Z prime score, as seen in **Table 2.6**. The separation band was then divided by the dynamic range to determine that the Z prime score for the assay was 0.73. This Z prime score was able to show that the assay would be effective in determining the inhibitory effects of fragments.

	MurD	MurD + ADPCP
Mean	0.11	0.048
Standard Deviation	0.0013	0.0042
Z prime Score	$Z = 1 - \frac{(3\ x\ 0.0013) + (3\ x\ 0.0042)}{(0.11 - 0.048)}$ $Z = 0.73$	

Table 2. 6: Z prime score determination within a stopped assay

The Z prime score was determined by calculating the mean V_0 for MurD in the presence and absence of ADPCP, along with the standard deviation of the means. The Z prime was then calculated using the formula shown. A Z prime score of 0.73 was determined for ADPCP against MurD from *S. agalactiae* within a stopped assay.

4. Conclusions and Future Direction

4.1 Optimization of biochemical assays required for inhibitory fragment identification

Activity assays can be used to biochemically test fragments for their ability to inhibit the activity of a protein [92]. By optimising the activity assays developed for the Mur ligases, a system was produced that would provide the greatest opportunity for identifying inhibitory fragments. Identification of the K_m values for the substrates allowed optimization of the assay for the identification of competitive inhibitors [92]. Identifying a positive control inhibitor, ADPCP, provided a standardized control to which all inhibitory fragments could be compared to. Determination of a Z prime score of 0.86 for ADPCP within the assay confirmed that the assay has been optimized to a standard consistent with other published assays used for the identification of inhibitors [93,94]. These optimization steps produced an assay that was at a stage that it could be used for screening inhibitory fragments.

4.2 Nucleotide specificity of MurD could act as a starting point for future antibacterial development

During the optimization of the activity assay, it was determined that MurD shows a high level of nucleotide specificity. Activity assays in the presence of GTP, ITP and CTP showed that MurD lacked activity with these alternative nucleotides. Further experiments identified that MurD from *S. agalactiae* was, however, able to bind these nucleotides. Understanding the difference in binding that occurs between ATP and these alternative nucleotides, which resulted in *S. agalactiae* MurD being unable to hydrolyse the nucleotide could provide a starting place for the development of inhibitory fragments targeted towards the ATP-binding site of MurD. Understanding the binding mode of fragments that inhibit the activity of a protein, and how binding differs from the intended substrate is a key technique in the development of inhibitory compounds. Understanding which residues to target to prevent activity allows for the development and optimization of inhibitory compounds targeted towards a specific region of a protein. This approach has previously been used by Hameed et al to improve fragments targeted towards the ATP-binding site of MurC from *E. coli* and *P. aeruginosa* [77].Crystal structures of *S. agalactiae* MurD bound to ATP and the alternative nucleotides could reveal

different binding modes that might suggest new routes for the development of MurD inhibitors.

4.3 Use of stopped assays for high-throughput screening

By converting the current activity assay into a stopped assay, limitations of the current assay system for high throughput screening could be overcome. The introduction of an enzyme quenching step within an assay is a common technique used for the conversion of an assay system into one suitable for high throughput screening, as seen by Sullivan et al introducing $ZnSO_4$ to quench purine enzymes and form a suitable high throughput assay screen for purine biosynthesis [95]. Conversion of the current assay system into a stopped assay reduced the requirement for data collection within the initial rate period of the assay, as well as reduced the data analysis after collection, allowing the assay to become more efficient to run and analyse, a key requirement for high throughput screens [96]. Conversion to a stopped assay also allowed the assay to become more cost effective by allowing a reduction in the concentration of the secondary coupling enzyme, PNP. These alterations allowed for an assay that can complete multiple runs within a day allowing for the testing of large numbers of inhibitory fragments per day, a hallmark of high throughput screening [92]. Limitations were still present within the stopped assay, such as sensitivity and the interference of fragments at the recorded absorbance, aspects which were tackled within the fluorometric assay described in **Chapter 5.**

Chapter 3

Identification of μM inhibitory fragments that can target multiple Mur ligases

1. Introduction and Aims

The Mur ligases are attractive targets for the development of new antibiotics due to their presence in all bacterial species, with no eukaryotic counterpart [64]. Developing new antibiotics is a daunting task, and there are many ways in which to start the process. One approach is by using screening of small chemical scaffolds (fragment screening), which if inhibitory, can act as the initial building blocks which can be further elaborated to improve binding potency [97], and deliver *in vivo* activity, which can hopefully lead to effective antibiotic development.

Fragment screening is now a well-established starting point for the development of inhibitory compounds. The initial stages of fragment screening can be carried out *in silico* or via X-ray crystallography. X-ray crystallography is a biophysical technique that can be used to identify fragments that are able to bind to a protein of interest and structurally characterise such an interaction. XChem is a service developed by Diamond that allows users to screen fragments via X-ray crystallography. XChem involves soaking a protein of interest with a fragment screen before determining the crystal structure of the protein in the presence of the fragment [98] .This allows for the characterization of the binding of fragments to the macromolecular target. Fragments that appear to bind in an area of interest can then be developed and tested further, either biochemically or via another XChem screen, allowing the enhancement of selectivity and potency as inhibitors of target activity.

XChem is able to identify fragments that are able to bind to a protein of interest, however, a biochemical approach is required to determine if bound fragments can inhibit the activity of the protein. Activity assays can be used to establish the effect fragments have on the activity of the protein, and determine which fragments have inhibitory effects.

This chapter describes the use of XChem, which was carried out by our collaborators at University College London (UCL) and Diamond within the open-source Mur Ligase project, to identify binding fragments to MurD from *S. agalactiae*. Biochemical assays were then carried out on the fragments, to identify the inhibitory effects of these fragments on MurD from *S. agalactiae.* Assay

interference checks were then completed, before fragments were tested for their ability to act as dual inhibitors and target Mur ligases from other bacteria. Further enzymological analysis was carried out on inhibitory fragments to determine the IC_{50} values.

2. Materials and Methods

2.1 XChem

An XChem fragment screen was carried out by Dr Dana Klug at UCL. A Diamond-SGC-iNEXT Poised (DSI-poised) fragment library [99], consisting of ~ 768 fragments at 500 mM in d6-DMSO was screened against apo MurD from *S. agalactiae*. Further experimental details can be obtained by contacting Dr Dana Klug.

2.2 Stopped MESG assay

Fragments were biochemically tested for inhibition via a stopped MESG assay. Fragments were provided in powdered form and diluted to a stock concentration of 10 mM in DMSO. In a final volume of 50 μL, 1 mM of fragment was incubated with the relevant concentration of Mur ligase, in the presence of 50 mM HEPES (pH7.6), 2 mM $MgCl_2$, 1 mM DTT, 50 mM KCl, 400 μM MESG, and the relevant substrates barring ATP for 10 minutes. The assay was then initiated with 50 μM ATP and allowed to run for the initial rate period before the reaction was quenched with 10 mM EDTA. A background absorbance was determined photometrically via the Varioskan plate reader (ThermoFisher) at 360 nm before 24.2 U per litre PNP was added. Absorbance change was tracked at 360 nm for 40 minutes to allow the end point to be achieved. The absorbance change was then determined. Each fragment was run in triplicate in the presence and absence of the Mur ligase to determine background rate. Background rates were removed from the final activity rate for each fragment. The activity rate was compared to control groups of 10% $^{V}/_{V}$ DMSO and 5 μM ADPCP. Assays were carried out at 37°c.

To determine the inhibitory activity of fragments against MurD from *S. agalactiae*, 100 nM MurD was incubated with 1 mM of fragment in the presence of 60 μM UDP-MurNac-L-Ala and 250 μM D-Glu. To determine the inhibitory activity of fragments against MurE from *S. agalactiae,* 100 nM MurE was incubated with 1 mM of fragment in the presence of 60 μM UDP-MurNac-L-Ala-D-Glu and 200 μM L-Lys. To determine the inhibitory activity of fragments against MurE from *P. aeruginosa,* 100 nM MurE was incubated with 1 mM of fragment in the presence of 60 μM UDP-MurNac-L-Ala-D-Glu and 200 μM DAP.

2.3 Secondary coupling system assay

In a final concentration of 50 μL, 400 μM MESG, 50 mM HEPES (pH7.6), 1 mM $MgCl_2$, 1 mM DTT, and 50 mM KCl were incubated with 1 mM fragment and the absorbance change at 360 nm was followed in a Varioskan plate reader (ThermoFisher) over the course of 10 minutes. 130 μM $Na(H_2)PO_4$ was then introduced and the absorbance change at 360 nm was followed over the course of 5 minutes. 24.2 U per litre PNP was then introduced and the absorbance change at 360 nm was followed for 40 minutes to allow the end point to be attained. The absorbance change for each stage was then determined and compared to a control group of 10% $^{V}/_{V}$ DMSO. Assays were carried out at 37°c.

3. Results

3.1 XChem of DSI-Poised fragment library against Mur ligases

In order to identify fragments that bind to the Mur ligases, XChem was carried out via our collaborating partners at UCL and Diamond. The initial fragment screen was carried out using a DSI-poised fragment library screen produced by Diamond Light source. The DSI-poised fragment library was designed to allow rapid and cheap follow-up synthesis of fragment hits by having fragments that contained at least one functional group that could be synthesised using well-characterised reactions [99]. The library consisted of 768 fragments that were present at a concentration of 500 mM in deuterated-DMSO. The library was screened against apo MurD from *S. agalactiae* and apo MurE from *E. coli* at Diamond and the results were interpreted by Dr Dana Klug at UCL.

3.1.1 Identification of binding pocket within apo MurD from *S. agalactiae*

The XChem fragment screen against apo MurD from *S. agalactiae,* run by our collaborators at Diamond and UCL, identified 4 hits, as shown in **Figure 3.1**. These fragments were identified as binding to a pocket adjacent to the ATP-binding site, as shown in the XChem generated structure in **Figure 3.2A.**

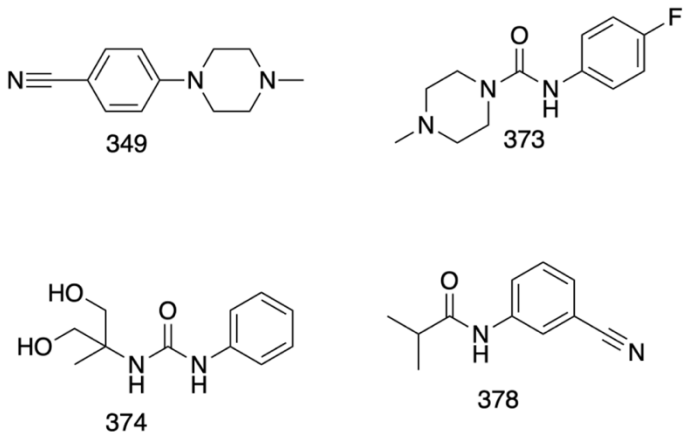

Figure 3. 1: Structural formula of four hits from the DSI-poised fragment library identified to bind to MurD from S. agalactiae

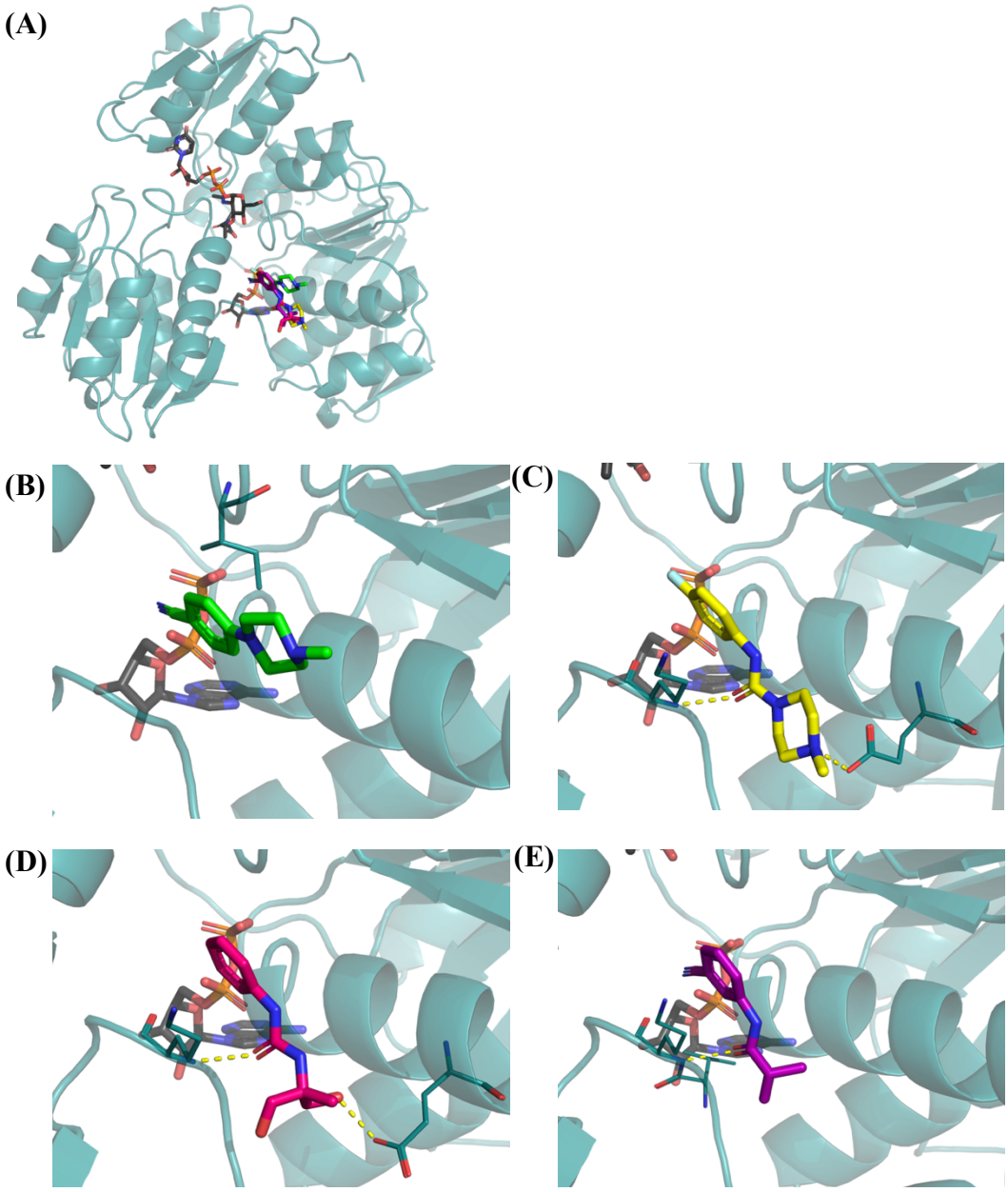

Figure 3. 2: Four fragments were identified to bind within a pocket adjacent to the ATP-binding site

Four fragment hits were identified to bind to apo MurD from *S. agalactiae* via an XChem fragment screen. Fragments were identified to bind to a pocket adjacent to the ATP-binding site. (A) All 4 fragments are shown bound within this binding site. UMA is shown bound as well. (B)Fragment 349. (C) Fragment 373. Forms an interaction between the nitrogen and Glu132, and between the oxygen and Lys311. (D) Fragment 374.Forms an interaction between the hydroxyl group and Glu132, and the oxygen and Lys311. (E) Fragment 378. Forms an interaction between the oxygen and Lys311.

Fragment 349 was unable to form hydrogen interactions, as seen in the XChem interaction in **Figure 3.2B**, but likely formed van der Waal interactions**.** As seen in the XChem interaction in **Figure 3.2C**, fragment 373 formed an interaction between

the piperazine nitrogen and Glu132 as well as an interaction between the carbonyl oxygen of 373 and the Lys311 peptide bond amide nitrogen. Fragment 374 formed interactions with Glu132 and Lys311, with an interaction between the propane diol hydroxyl group and Glu132, and the carbonyl oxygen of 374 and the Lys311 peptide bond amide nitrogen, as seen in the XChem interaction in **Figure 3.2D.** Fragment 378 was also able to form hydrogen bonds through its carbonyl oxygen atom and Val 310 and Lys311 as seen in the XChem interaction in **Figure 3.2E.** These fragments were all suitable building blocks for the development of a fragment screen that elaborated and built upon these parental fragments with the aim of targeting the binding site present within MurD from *S. agalactiae*.

3.1.2 Production of elaborated fragment screen

Based on the parental fragments 349, 373 and 378 an elaborated fragment screen containing seventy-eight fragments was produced by Dr Dana Klug. The elaborated fragment screen contained analogues of the parental fragments, such as piperazine analogues, aryl analogues and sulphonamide analogues. A full list of the elaborated fragment screen can be found in **Supplementary 1,** and further information on its development can be found under the issue 'Follow up for the fragment hits for MurD Ligase' within the open source Mur ligase project GitHub.

3.2 Determination of inhibition of MurD activity by fragments via biochemical assay

As the parental fragments were binding to a pocket adjacent to the *S. agalactiae* MurD ATP-binding site, these fragments and those within the elaborated fragment screen derived from the parental fragments may have had no effect on activity of the ligase and may be unable to cause inhibition. To determine the effect these fragments had on the activity of MurD, a biochemical approach was required.

3.2.1 Identification of inhibitory fragments targeted against MurD from *S. agalactiae*

In order to determine the effect the elaborated fragments had on the activity of MurD, a stopped MESG assay was used, which was validated in **Chapter 2**. Our

collaborators at UCL and Diamond produced the constituent fragments of the elaborated screen which were typically reconstituted in 100% ($^{v}/_{v}$) DMSO. However, fragments 779, 784, 790, 799 and 806 of the elaborated screen could not be reconstituted, and so were not tested biochemically. The ability of the reconstituted fragments to inhibit the activity of *S. agalactiae* MurD was then determined using the stopped MESG assay. Fragments were incubated at a final concentration of 1 mM with *S. agalactiae* MurD prior to initiation of the activity assay. The activity of MurD in the presence of fragments was compared to a control of the activity in the presence of 10% ($^{v}/_{v}$) DMSO alone. The percentage activity of MurD in the presence of fragments was determined, as seen in **Figure 3.3**. A positive control inhibitor of ADPCP was also used to confirm inhibition within the assay system. As can be seen from **Figure 3.3**, the fragments had a varied effect on the activity of MurD.

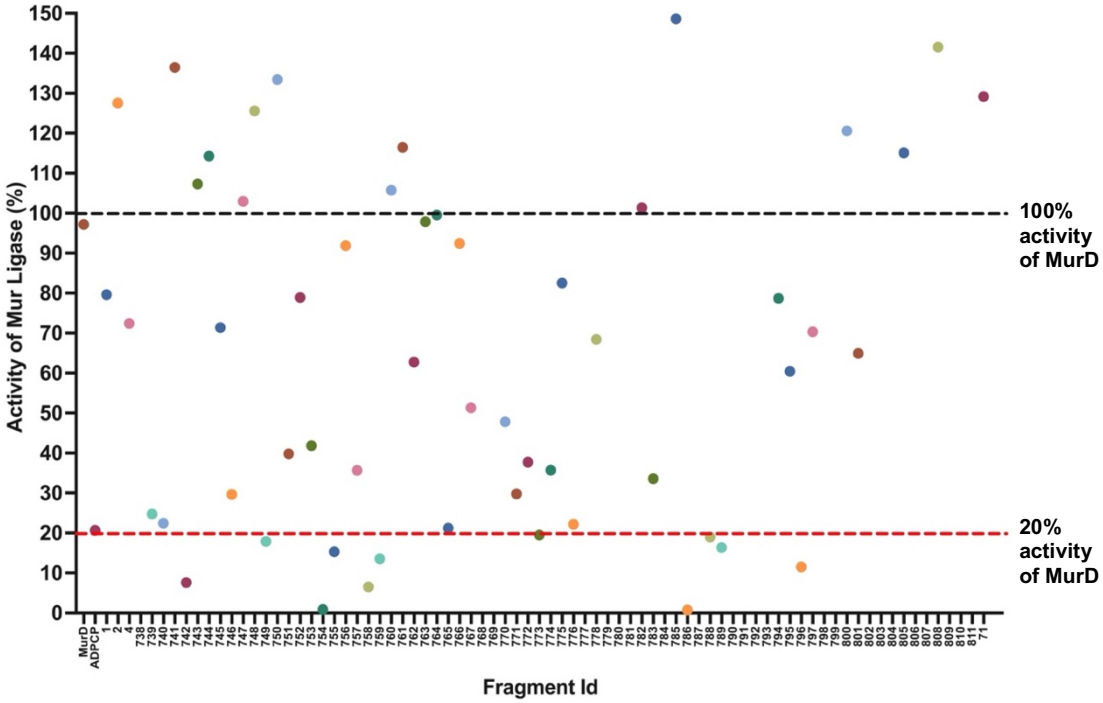

Figure 3. 3: Activity of MurD in the presence of elaborated fragments

The ability of the elaborated fragments to inhibit the activity of MurD from *S. agalactiae* was determined via a stopped MESG assay. Fragments were incubated at a final concentration of 1 mM with 100 nM MurD before activity of MurD was determined. Activity of MurD in the presence of fragments was compared to a control group of DMSO and the percentage activity of MurD determined and plotted. All fragments were run in triplicate with a triplicate background rate being removed from the activity rate. The mean percentage activity of compounds was plotted. Black line indicates 100% activity of MurD. Red line indicates 20% activity of MurD.

Thirty two fragments were able to reduce activity of MurD by 25% or more. Twenty four fragments were able to reduce activity by 50% or more. Twenty three fragments caused an increase in activity of MurD, with seven increasing activity to a level greater than that shown on **Figure 3.3.** Triplicate activity levels can be seen in **Supplementary 2**. Eighteen fragments produced activity that fell outside of the range of the graph, either due to an increase in activity or a negative activity rate after removal of the background rate, as seen in **Figure 3.4**. Extreme values above 100% and below 0% of control values could have been due to interference with the assay components, precipitation of the fragment within the assay or natural absorbance by the fragment at 360 nm. Due to their activity rates falling outside a range that was deemed acceptable for interference within the assay, greater than 150% activity of MurD and below -10% activity of MurD, the ability of these fragments to inhibit the activity of MurD could not be determined within this assay system, and so were removed from further studies.

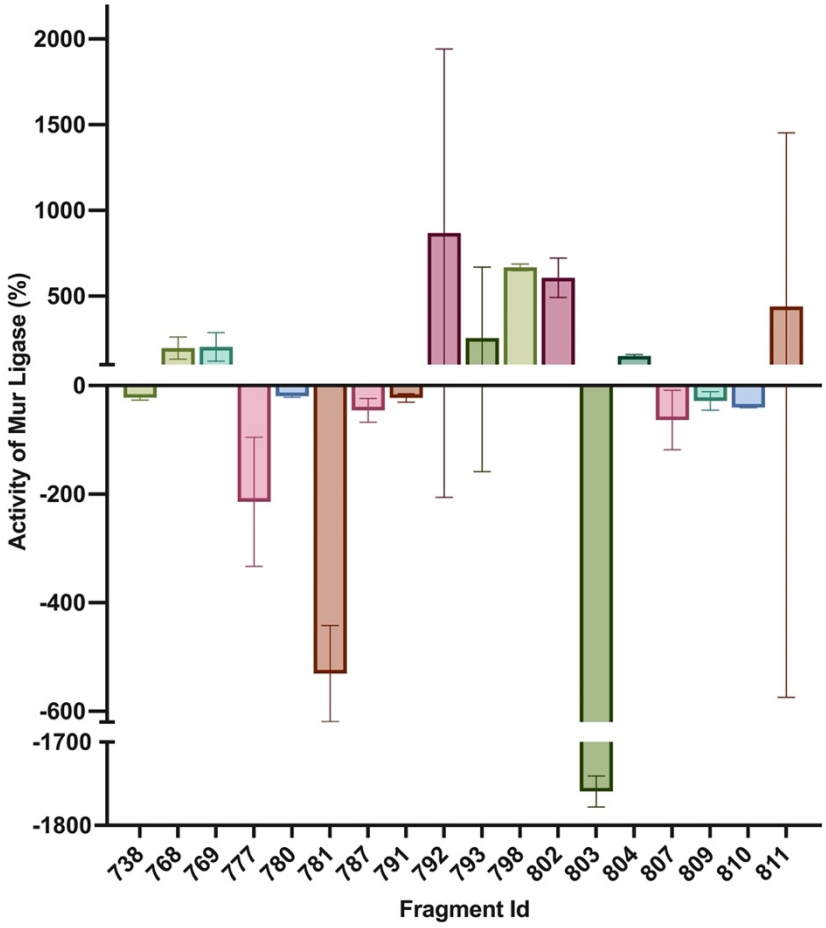

Figure 3. 4: Eighteen fragments produced rates outside standard range
Eighteen elaborated fragments produced rates outside the acceptable range for the assay. Fragments were incubated at a final concentration of 1 mM with 100 nM MurD before activity of MurD was determined. Activity of MurD in the presence of fragments was compared to control assays in the presence of DMSO and the percentage activity of MurD determined and plotted. All fragments were run in triplicate with a triplicate background rate being removed from the activity rate. The mean is plotted with triplicate repeat data shown with error bars showing SD.

A threshold of an 80% reduction in activity of MurD was set for fragments to be considered as inhibitors of MurD activity within this study. As can be seen from **Figure 3.3** and **Figure 3.5**, eleven fragments satisfied this criterion. Fragments 754 and 786 were able to almost completely inhibit MurD within the assay, as seen in **Figure 3.5**. These eleven fragments were therefore selected for further validation.

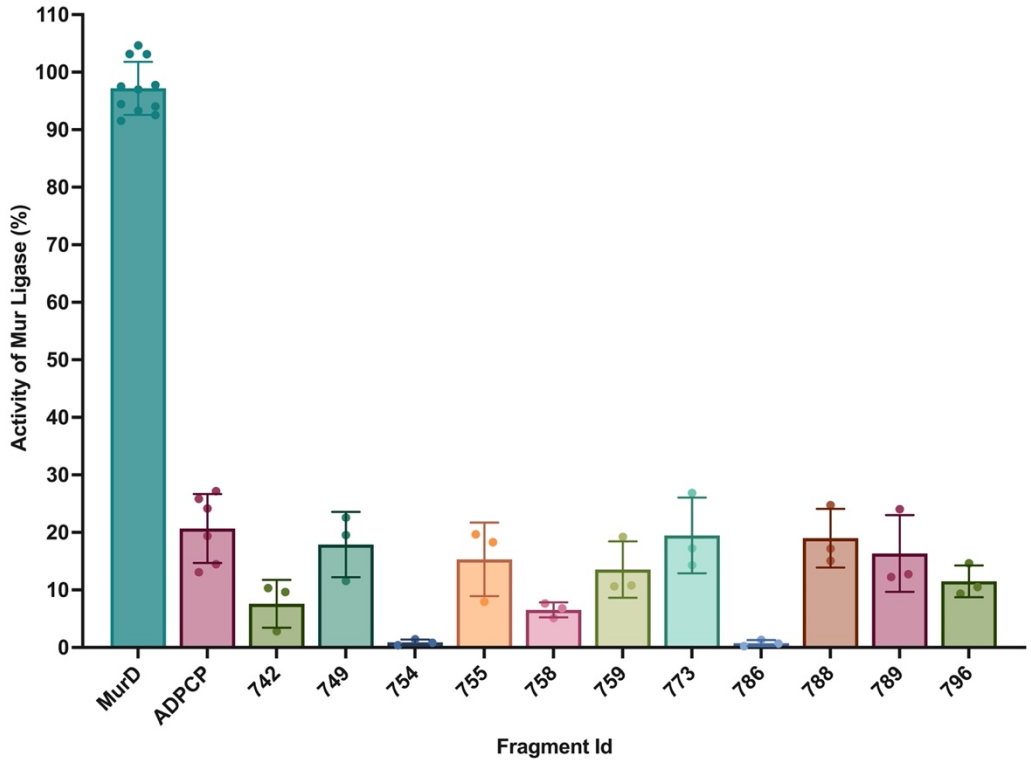

Figure 3. 5: Eleven fragments can act as inhibitors of MurD

Eleven elaborated fragments were able to reduce the activity of MurD from *S. agalactiae* by 80% or more. Fragments were incubated at a final concentration of 1 mM with 100 nM MurD before activity of MurD was determined. Activity of MurD in the presence of fragments was compared to a control group of DMSO and the percentage activity of MurD determined and plotted. All fragments were run in triplicate with a triplicate background rate being removed from the activity rate. The mean is plotted with triplicate repeat data shown with error bars showing SD.

3.3 Six fragments cause interference with assay system resulting in false positives

Initial screening of the elaborated fragments identified eleven fragments that were able to reduce the activity of MurD by 80% or more. If however, the fragments interfered with any of the assay components, it could have resulted in a reduced absorbance change which would have been interpretated as a reduction in activity due to inhibition of MurD by the fragment. To determine if any of the fragments had behaved in this manner, the fragments were tested against the

assay components, phosphate and PNP. The fragments were incubated at 1 mM final concentration with the assay components, phosphate and PNP, and the absorbance was tracked at 360 nm. The absorbance change for each fragment in the presence of the components was determined and compared to a control group of MurD in the presence of 10% ($^{v}/_{v}$) DMSO. The statistical difference in results was determined using a Welch's T-test.

As can be seen from **Figure 3.6,** fragment 786 interacted with the assay components resulting in a large increase in absorbance change at 360 nm. Fragments 758 and 796 both caused statistically significant increases in absorbance change in the presence of the assay components, with p values of 0.023 and 0.0163 respectively. All three fragments also caused statistically significant increases in the range of data. An increase in absorbance change in the presence of the assay components could suggest that the fragments were interacting with the MESG present converting it to its corresponding free base 2-amino-6-mercapto-7-methylpurine, which absorbs at 360 nm. A reduction in the MESG available within the assay for PNP to act upon could result in a reduction in absorbance change after activity, leading to a false positive recording of inhibition via the fragments. Fragment 788 caused a significant decrease in absorbance in the presence of the assay components. A decrease in absorbance change may also represent an interference with the assay components.

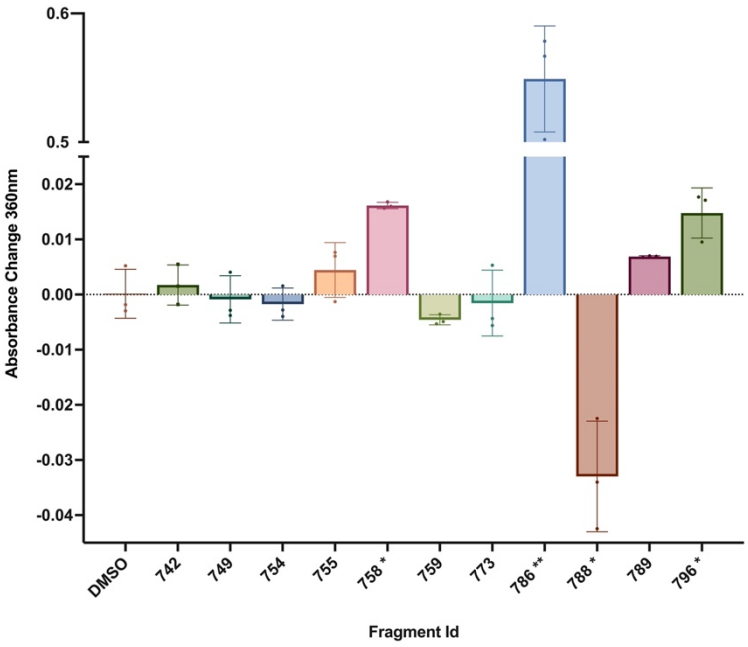

Figure 3. 6: Fragments 758, 786 and 796 show interference with the assay

Fragments that had reduced activity of MurD in initial screening were tested for their effect on the assay components. Fragments 786, 758 and 796 caused significant increases in absorbance compared to the control group. 788 caused a significant decrease in absorbance compared to the control group. All experiments were run in triplicate with mean results being plotted, with individual data points shown. Error bars show SD.

Phosphate is generated and used within a stopped MESG assay to determine the activity of the Mur ligase. Interaction of the fragments with the phosphate thus generated could result in false positive recordings of inhibition. The effect the fragments had on the absorbance change after the addition of phosphate was determined.

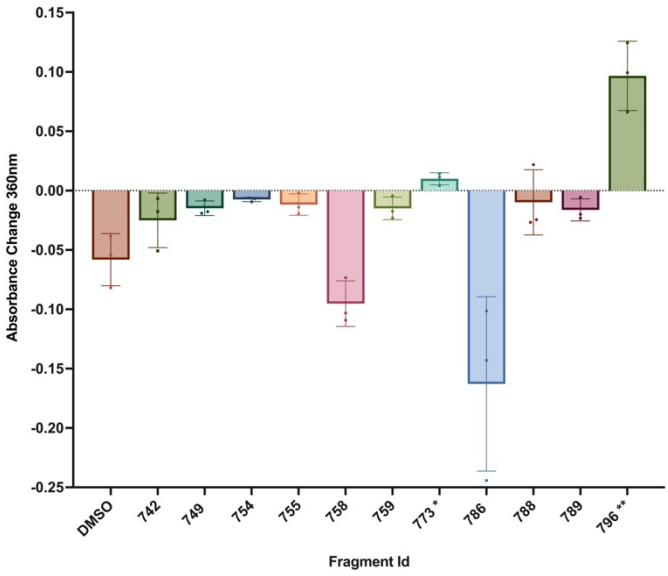

Figure 3. 7: Fragments 773 and 796 show interference with phosphate

Fragments that had reduced activity of MurD in initial screening were tested for their effect on phosphate. Fragments 773 and 796 caused significant increases in absorbance change compared to the control group. All experiments were run in triplicate with mean results being plotted, with individual data points shown. Error bars show SD.

As can be seen from **Figure 3.7,** fragments 773 and 796 caused statistically significant increases in the absorbance change at 360 nm when phosphate was present, with p values of 0.0278 and 0.0024 respectively. A significant difference in the absorbance change suggests that the fragment was interacting with the phosphate present. This could result in a change in the phosphate concentration present within the sample. Activity of MurD was determined via the amount of phosphate present within the sample after the MurD reaction was quenched. Altering the amount of phosphate present within the sample could result in a reduction in absorbance change after activity, leading to a false positive recording of inhibition via the fragments.

The final check carried out was to determine the effect the fragments had on the ability of PNP to convert phosphate to ribose-1 phosphate and MESG to 2-amino-6-mercapto-7-methylpurine to result in an absorbance change at 360 nm. As can be seen from **Figure 3.8**, fragments 755, 758 and 786 caused statistically significant decreases in the absorbance change at 360 nm, with fragment 755

having a p value of 0.0086, fragment 758 a p value of 0.02 and fragment 786 having a p value of 0.0011. A decrease in the absorbance change after the addition of PNP suggested that these fragments were interfering with the coupling enzyme PNP, preventing it from being able to convert phosphate to ribose-1 phosphate and MESG to 2-amino-6-mercapto-7-methylpurine. This resulted in a decreased absorbance change which was used to determine activity of MurD, and so gave false positive readings of inhibition for these fragments.

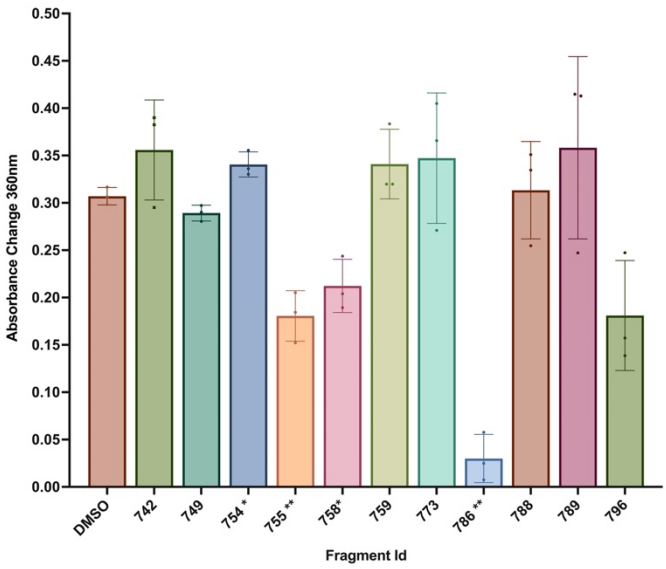

Figure 3. 8: Fragments 755 and 786 show interference with PNP

Fragments that had reduced activity of MurD in initial screening were tested for their effect on PNP. Fragments 755 and 786 caused significant decreases in absorbance change compared to the control group. Fragment 754 caused a significant increase in absorbance change compared to the control group. All experiments were run in triplicate with mean results being plotted, with individual data points shown. Error bars show SD.

Across the three experiments, six fragments caused interference with the assay system. Fragments 758 and 786 caused statistically significant increases in absorbance in the presence of the assay components as well as statistically significant decreases in activity after the addition of PNP. Due to this interference, the ability of these fragments to inhibit the activity of MurD could not be determined within this assay system. Fragment 773 and fragment 796 caused statistically significant increases in absorbance in the presence of phosphate, with fragment 796 causing a statistically significant increase in absorbance in the presence of the assay components. Due to this interference, the ability of fragments 773 and 796 to inhibit the activity of MurD could not be determined within this assay system. Fragment 755 caused a statistically significant decrease in activity after the addition of PNP. Due to this interference, the ability of fragment 755 to inhibit the activity of MurD could not be determined within this assay

system. The interference with the assay system by these fragments meant that the inhibition data generated via the initial screen relating to them was unreliable and so inhibition of MurD with these fragments could not be established, and so they were not considered further.

3.4 The binding pocket within MurD from *S. agalactiae* is present within MurE from *S. agalactiae*

Fragments that were able to reduce activity of MurD from *S. agalactiae* by 80% or more, and passed the assay interference checks were then screened for inhibition of *S. agalactiae* MurE activity. The Mur ligases share a similar catalytic mechanism and 3 domain structure [23] and therefore inhibitors that can inhibit the activity of one Mur ligase may potentially be able to inhibit the activity of another. The parental fragments that the elaborated screen was based upon bound to a pocket within MurD from *S. agalactiae* that was adjacent to the ATP binding pocket. To determine if this pocket was present within MurE from *S. agalactiae*, a homology model of MurE generated by SWISS-MODEL was aligned to the structure of MurD (PDB: 3LK7). As can be seen from the alignment of the predicted structure of MurE and the known structure of MurD in **Figure 3.9**, the alpha helices that line the pocket were in similar positions in both MurD and MurE.

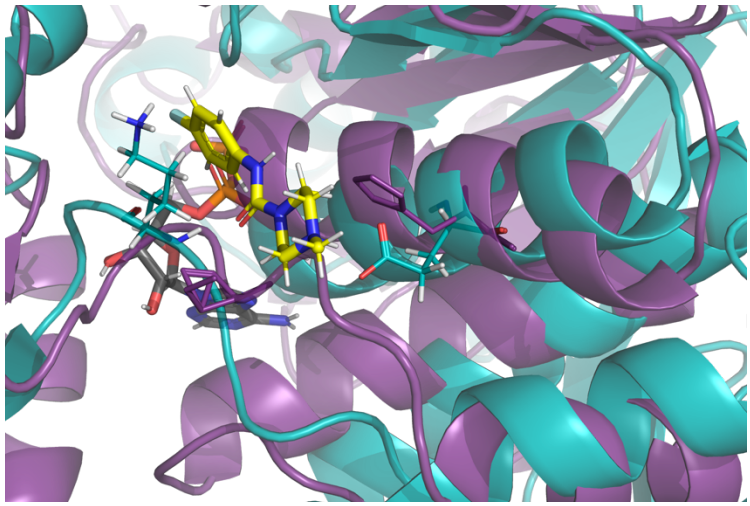

Figure 3. 9: Alignment of binding pocket within MurD to MurE from S. agalactiae

Alignment of MurD from *S. agalactiae* and MurE from *S. agalactiae*. The binding pocket where the parental fragments bound to MurD is aligned to MurE. There is a similar structure between both proteins. Interacting residues within MurD are aligned to residues with MurE. Glu132 is aligned to His132, while Lys311 is aligned to Pro330. MurD is shown in green, while MurE is shown in purple. Fragment 373 is shown bound within the binding pocket.

A flexible region within the MurE homology model was seen to intrude into the binding pocket for the fragments, which might interfere with the binding of the fragments to this area of the protein.

Sequence alignment of MurE from *S. agalactiae* to MurD from *S. agalactiae* showed a 38% sequence similarity within the pocket. Within MurD, Glu132 and Lys311 were involved in forming interactions with the parental fragments. The corresponding residues within MurE from *S. agalactiae* were His132 and Pro330, as seen in **Figure 3.9**. The switch from the negatively charged Glu residue to the positively charged His residue may result in fragments being unable to bind within this pocket. The change in interacting residues may hinder the binding of certain fragments within this binding site, but a similar structure within the binding pocket may still allow certain fragments to bind and inhibit the activity of MurE from *S. agalactiae.*

3.5 Identification of fragments that can inhibit MurD and MurE from *S. agalactiae*

The presence of a binding pocket within MurE from *S. agalactiae* that is similar in structure to the binding pocket within MurD from *S. agalactiae* suggests that the fragments identified to have inhibitory effects against MurD from *S. agalactiae* may also be able to bind and inhibit the activity of MurE from *S. agalactiae*. The fragments that were identified to reduce activity of MurD by 80% or more and showed no assay interference were screened against MurE from *S. agalactiae* using a stopped MESG assay. Validation of assay for MurE was carried out, see **Supplementary 3**. Fragments were incubated at a final concentration of 1 mM with 100 nM MurE from *S. agalactiae* prior to initiation of the activity assay. The activity rate of MurE in the presence of fragments was compared to a control group where 10% ($^{v}/_{v}$) DMSO was present, and the percentage activity of MurE in the presence of fragments relative to their absence was determined, as seen in **Figure 3.10**. A positive control inhibitor of ADPCP was also used to confirm inhibition within the assay system. As can be seen from **Figure 3.10**, all the fragments were able to inhibit the activity of MurE. Fragment 749 was only able to reduce activity of MurE by 35%, but all other fragments were able to reduce activity by 70% or more, and

so were considered significant inhibitors of MurE. Of the five fragments identified as inhibitors of MurD, four were considered as dual inhibitors of MurD and MurE from *S. agalactiae.*

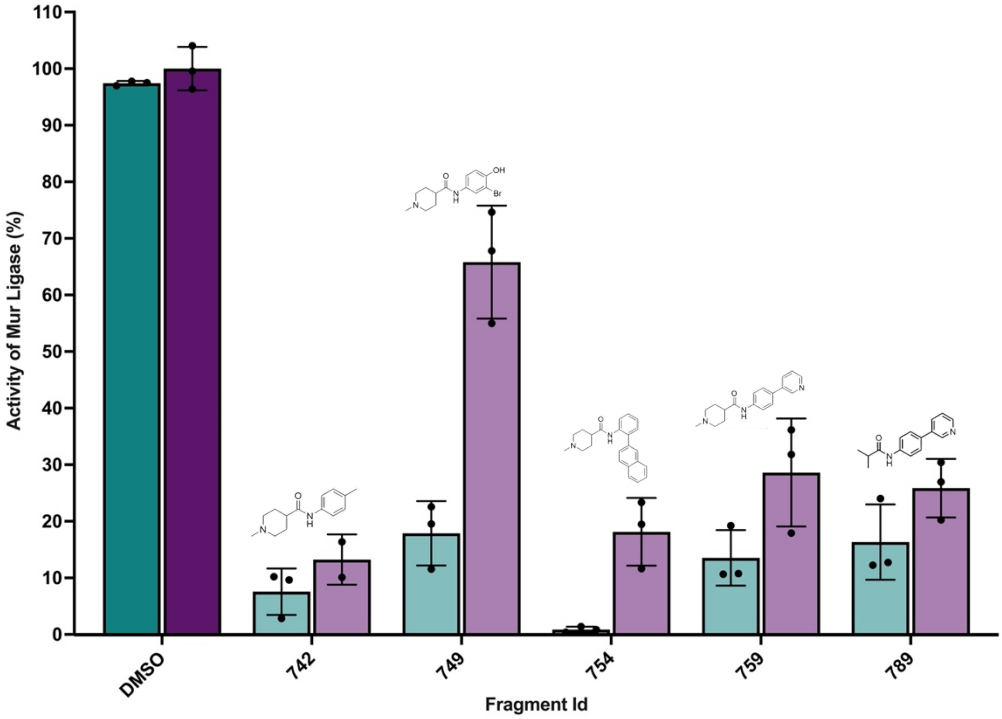

Figure 3. 10: Four fragments can act as inhibitors of MurE from S. agalactiae

Fragments that had reduced activity of MurD in initial screening were tested for their effect on MurE from *S. agalactiae*. Fragment 749 was only able to reduce activity of MurE by 35%. All other fragments were able to reduce activity by 70% or more. All fragments were run in triplicate with a triplicate background rate being removed from the activity rate. The mean is plotted with triplicate repeat data shown with error bars showing SD. Skeletal formula of fragment present. Activity of MurD shown in blue, activity of MurE shown in purple.

3.6 The binding pocket within MurD from *S. agalactiae* is present within MurE from *P. aeruginosa*

The Mur ligases have very similar catalytic mechanisms and domain structure. This similarity is present across the four Mur ligases, across bacterial species. Across differing bacterial species, MurE changes which amino acid it links to the UDP-intermediate. Typically, MurE catalyses the addition of meso-DAP to UDP-MurNAc-L-Ala-D-Glu within Gram negative bacteria, bacilli and mycobacteria. Within other Gram positive bacteria, MurE is able to catalyse the addition of L-Lys to UDP-MurNAc-L-Ala-D-Glu [48]. The difference in amino acid addition may affect the way in which inhibitors are able to target and inhibit MurE from various bacteria. Due to

the clinical significance of Gram-negative infection, it was important to investigate whether this difference would affect the ability of inhibitors identified from the elaborated fragment screen, to additionally target MurE from *P. aeruginosa* where L-Lysine, utilised by *S. agalactiae* was now replaced by meso-DAP.

The structure of MurE from *P. aeruginosa* was aligned to that of MurD from *S. agalactiae* to predict if the binding pocket that the parental fragments were identified to bind to within MurD from *S. agalactiae* was present within the structure. The structure of MurE from *P. aeruginosa* was taken from Alphafold (AF-Q59650-F1) and aligned to the structure of MurD from *S. agalactiae* (PDB:3LK7) within Pymol.

As can be seen from the alignment of the predicted structure of MurE and the known structure of MurD in **Figure 3.11,** the binding pocket is present within MurE from *P. aeruginosa*. Sequence alignment of MurE from *P. aeruginosa* to MurD from *S. agalactiae* showed a 75% sequence similarity within the pocket. Within MurD, Glu132 and Lys311 were involved in forming interactions with the parental fragments. The corresponding residues within MurE from *P. aeruginosa* were Glu129 and Ala307 as seen in **Figure 3.11**.

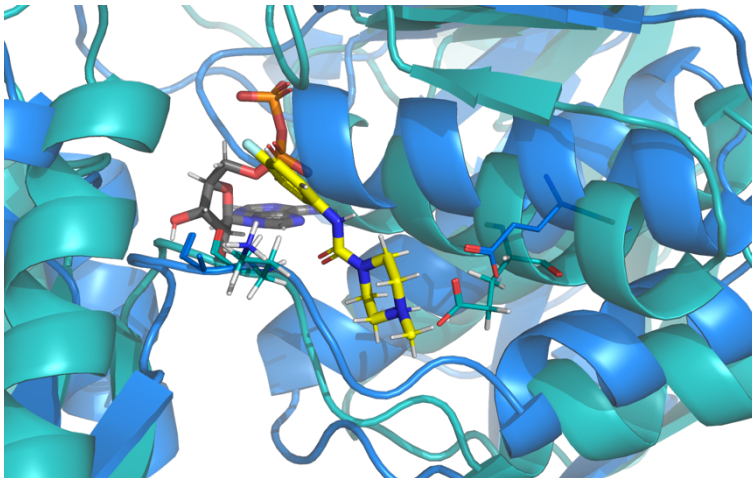

Figure 3. 11: Alignment of binding pocket within MurD to MurE from P. aeruginosa

Alignment of MurD from *S. agalactiae* and MurE from *P.aeruginosa*. The binding pocket where the parental fragments bound to MurD is aligned to MurE. There is a similar structure shared by both proteins. Interacting residues within MurD are aligned to residues with MurE. Glu132 is aligned to Glu129, while Lys311 is aligned to Ala307. MurD is shown in green, while MurE is shown in blue. Fragment 373 is shown bound within the binding pocket.

The change from a Lys residue to an Ala residue may hinder the binding of certain fragments within this binding site, but a similar structure within the binding pocket may still allow certain fragments to bind and inhibit the activity of MurE from *P. aeruginosa*, allowing for the potential identification of fragments that can target Mur ligases across bacterial species.

3.7 Identification of fragments that can inhibit MurE from *S. agalactiae* and MurE from *P. aeruginosa*

Structural alignment of the *P. aeruginosa* MurE to the *S. agalactiae* MurD structure identified a similar binding pocket where the parental fragments originally bound to. Fragments identified to inhibit MurD and MurE from *S. agalactiae* might also bind and inhibit the activity of MurE from *P. aeruginosa*. To determine if fragments that had been identified to reduce activity of MurD and MurE from *S. agalactiae* by 70% or more were able to act as inhibitors of MurE from *P. aeruginosa,* a stopped MESG assay was run in the presence of fragments against MurE from *P. aeruginosa*. Fragments were incubated at a final concentration of 1 mM with 100 nM MurE from *P. aeruginosa* prior to initiation of the activity assay. The activity rate of MurE in the presence of fragments was compared to a control assay where 10% ($^{v}/_{v}$) DMSO was added in place of a fragment, and the percentage activity of MurE in the presence of fragments relative to that in their absence was determined, as shown in **Figure 3.12**. A positive control inhibitor of ADPCP at 5 μM was also used to confirm inhibition within the assay system. Fragments 742 and 789 did not significantly impact the activity of MurE, as seen in **Figure 3.12**. Fragments 759 and 754 were able to reduce activity by around 50%.

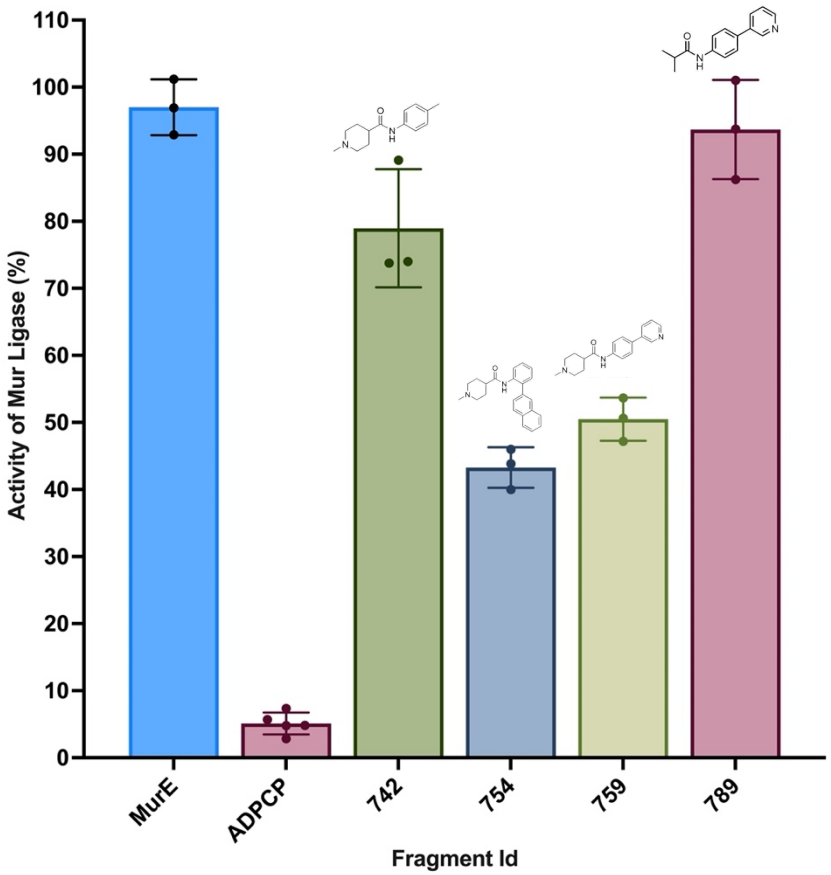

Figure 3. 12: Lack of inhibition by fragments against MurE from P. aeruginosa

Fragments that had reduced activity of MurD and MurE from *S. agalactiae* were tested for their effect on MurE from *P. aeruginosa*. Fragments 742 and 789 caused no significant difference in MurE activity compared to the control. All fragments were run in triplicate with a triplicate background rate being removed from the activity rate. The mean is plotted with triplicate repeat data shown with error bars showing SD.

A comparison of the effect the four fragments had on the activity of the three ligases can be seen in **Figure 3.13**. All fragments were more effective at reducing the activity of the *S. agalactiae* ligases compared to the *P. aeruginosa* ligase. All fragments were more effective at reducing activity of MurD compared to MurE from *S. agalactiae*.

These results suggest that the binding and action of these fragments was better targeted towards *S. agalactiae*, and particularly MurD. These fragments were based on parental fragments that bound to a pocket adjacent to the ATP-binding site within MurD from *S. agalactiae*. The way in which the fragments were produced was biased towards the specific residues present within this binding site in MurD, and so fragments may be unable to interact with the residues present in the binding site of MurE. The binding site may be in a slightly different conformation in

MurE compared to MurD due to the domain movements that occurred when substrates bind to Mur ligases [66], preventing the fragments from binding as well to the MurE ligases.

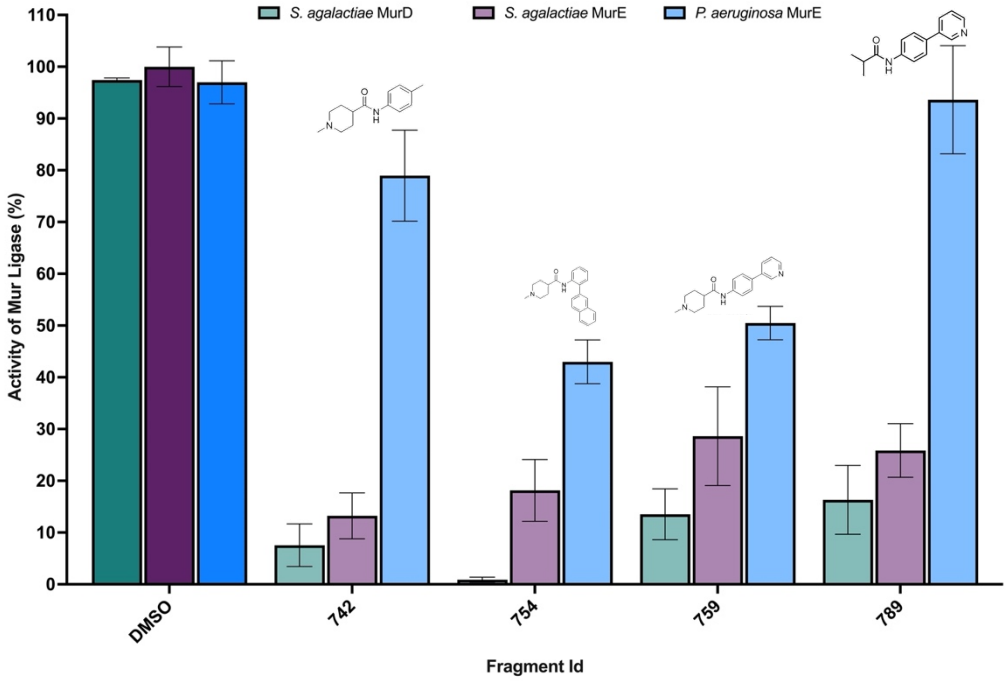

Figure 3. 13: Comparison of activity of ligases in the presence of fragments
Activity of ligases was determined using a stopped MESG assay in the presence of fragments. Activity of MurD is shown in green, activity of MurE from *S. agalactiae* is shown in purple and activity of MurE from *P. aeruginosa* is shown in blue. All fragments were run in triplicate with a triplicate background rate being removed from the activity rate. The mean is plotted with triplicate repeat data shown with error bars showing SD.

3.8 Identification of fragments with micromolar IC_{50}s against MurD from *S. agalactiae*

Fragments were identified to inhibit MurD from *S. agalactiae* at 1 mM concentration. To develop a better understanding of the inhibitory potency of the fragments, dose response curves were generated to determine the concentration of fragment required to inhibit the activity of enzyme by half [100]. An IC_{50} can provide a measure by which to compare the efficacy of the fragments. To determine the IC_{50} of the fragments, the stopped MESG assay was run at various concentrations of fragment against MurD from *S. agalactiae*. The activity of MurD was determined in the absence and then presence of increasing concentrations of fragments, and the remaining activity, relative to that in the absence of fragment was plotted against the log concentration of fragment. As seen in **Figure 3.14,** Fragment 742 had an IC_{50}

of 107 +/- 15 μM against MurD from *S. agalactiae.* Fragments 754 and 789 also had similar IC_{50} values of 93 +/- 13 μM and 147 +/- 25 μM respectively. Fragment 759 had the lowest IC_{50} of 22 +/- 2.5 μM against MurD from *S. agalactiae*. Fragment 759 reduced the activity of MurD by 50% at the lowest fragment concentration, making it the most attractive fragment for future studies.

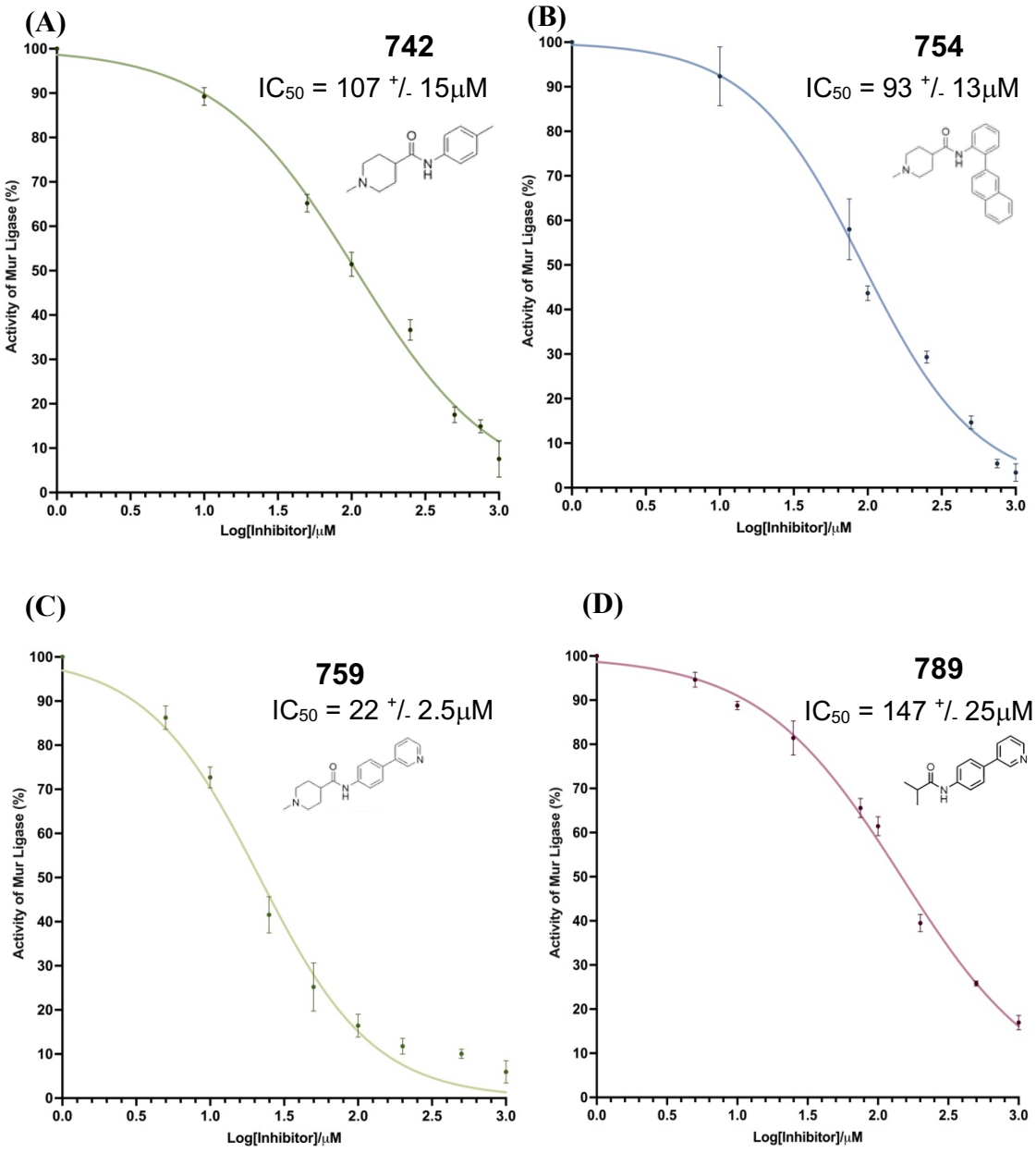

Figure 3. 14: Dose response curves for inhibitory fragments against MurD from S. agalactiae
The IC_{50} of 4 fragments hits were identified using a stopped MESG assay. Various concentrations of fragment were incubated with MurD from *S. agalactiae* before activity of MurD was established. Activity was then plotted against log fragment concentration and the IC_{50} determined. (A) IC_{50} determination of fragment 742. (B) IC_{50} determination of fragment 754. (C) IC_{50} determination of fragment 759. (D) IC_{50} determination of fragment 789. All fragments were run in triplicate with a triplicate background rate being removed from the activity rate. The mean is plotted with error bars showing SD. A variable response curve was the plotted via PRISM.

4. Conclusions and Future Direction

4.1 Use of X-Chem for the design of novel inhibitory fragments

Biophysical and biochemical techniques can be used to identify fragments that are able to bind and inhibit the Mur ligases. Our collaborators at Diamond and UCL were able to use XChem to identify four parental fragments from a DSI-poised fragment library that were able to bind to a pocket adjacent to the ATP-binding site of MurD from *S. agalactiae*. An elaborated fragment screen produced by our collaborators at UCL based upon these hits was evaluated for inhibition of MurD activity. Identification of a parental scaffold provides a useful starting point for the development of an elaborated fragment screen; providing structural information upon which fragments can be based. This can lead to the development of fragments that already have high levels of potency against their intended target which have a greater potential for becoming antibacterial fragments. This approach was taken in the development of a selective inhibitor of the oncogenic B-Raf kinase which possessed potent antimelanoma activity, which was developed from an XChem screen of a poised library and elaborated fragments [97]. Biochemical screening of the elaborated fragment set developed by UCL identified five fragments that had inhibitory effects against MurD from *S. agalactiae*, providing five fragment scaffolds which can act as a good starting points for the development of antibacterial compounds.

4.2 Assay interference and its effects on fragment screening

Biochemical techniques such as activity assays can provide information on the inhibitory effects of fragments. However, there are limitations to every assay, and sometimes false positives occur. To determine whether false positive results occurred within the fragment screen, the effect the fragments had on the assay components, phosphate and PNP were taken into consideration when determining whether the fragments were having an inhibitory effect on MurD. Fragments that caused significant differences in absorbance change in the presence of these components compared to the control group of DMSO were ruled out as inhibitors as their true effects on MurD activity could not be determined within our assay.

This approach prevented the inclusion of false positive results within our final evaluations but may have led to the removal of inhibitory fragments.

Fragments that themselves absorb at 360 nm may have been ruled out within the initial screen. To overcome this issue, all fragments could be retested within another assay system that does not track absorbance at 360 nm, such as the amplex red assay, which was used for high throughput screening of NOX inhibitors [101], and is described in **Chapter 5.** Fragments that cause interference with the assay system were removed from further studies but may have the ability to inhibit the activity of the protein. To overcome this issue, fragments could be retested within another assay system that does not use the same secondary assay system to determine activity, such as a PK/LDH assay which was used to determine inhibition of D-Ala: D-Ala by D-cycloserine[33]. By changing the absorbance at which the assay is tracked, and changing the secondary assay system, any fragments that do absorb at 360 nm or interfere with the assay components could be accurately tested for their ability to inhibit the activity of MurD.

4.3 Development of multi-targeting inhibitors

Of the five fragments identified to inhibit the activity of MurD from *S. agalactiae*, four were identified as having dual inhibitory effects; being able to inhibit the activity of MurE from *S. agalactiae* as well as MurD from *S. agalactiae*. Two fragments were identified as having cross bacterial inhibitory effects; with fragments 754, and 759 reducing the activity of MurE from *P. aeruginosa* by 50% or more. An antibacterial compound that can target multiple Mur ligases may be possible based upon these results. An antibacterial compound that can bind to multiple targets is becoming considered more therapeutically advantageous compared to a highly specific compound due to the potential to prevent emergence of antibiotic resistance. The development of multi-targeting fragments able to bind to the Mur ligases is not a novel concept, with previously identified multi-targeting Mur ligases inhibitors with IC_{50}s ranging from 59 μM to 368 μM against MurC- MurF from *E. coli* being identified by Hrast et al [102]. The ability of a fragment to have

cross-species targeting abilities is less common and provides an interesting starting point for future studies into these fragments.

Further elaboration of these fragments will need to be carried out to improve their potency and their ability to enter the bacterial cell. Elaboration of the inhibitory fragments is currently being undertaken by our collaborators at UCL. Once these more elaborated fragments have been produced, their ability to inhibit the activity of the Mur ligases can be reaffirmed via biochemical assays before the ability of the fragments to entre the bacterial cell are confirmed via minimum inhibitory concentration experiments.

4.4 Targeting novel pockets for the development of inhibitory fragments

The original XChem screen carried out by our collaborators identified parental fragments that were able to bind to a pocket adjacent to the ATP-binding site of MurD. Allosteric binding sites are an attractive target for the development of novel inhibitors as they offer alternative mechanisms for enzyme inhibition. However, within the development of inhibitory compounds targeted towards the Mur ligases, inhibitory compounds are mostly targeted towards either the catalytic site of the Mur ligases, such as with phosphinate inhibitors that were shown to target the active site of MurE [72], or target the binding site of the substrates, such as targeting the ATP-binding site of *E. coli* MurD [103]. Identification of inhibitory fragments binding to a novel pocket of the Mur ligases could provide a new starting point for the development of antibacterial compounds.

Confirmation of the binding mode of these fragments needs to be carried out to continue their development into an antibacterial compound. Crystallographic studies could be carried out to confirm if the fragments are still binding within the novel pocket identified within the original XChem screen. Biochemical assays could be carried out to identify if the fragments are acting in a competitive manner towards any of the substrates.

Chapter 4

Identification of inhibitory fragments via *in silico* screening and biochemical assays

1. Introduction and Aims

Fragment screening is a well-established starting place for the development of inhibitory compounds. The initial stages of fragment screening can be carried out *in silico* or via X-ray crystallography. *In silico* screening, a computational technique for identifying potential binding fragments, involves using prediction software to identify fragments that may have the potential to bind to a protein of interest. *In silico* screening allows for the screening of large collections of fragments against multiple proteins without the cost and time associated with biophysical techniques such as XChem or SPR [104,105].

In silico screening can identify fragments that may have the potential to bind to a protein of interest and inhibit its activity. Once a fragment list has been generated via *in silico* screening, experimental techniques can be used to establish the true binding potential and inhibitory effects of the fragments. A biochemical approach, such as activity assays, can be used to determine if fragments can inhibit the activity of the protein.

This chapter describes the development of an *in silico* screen and the steps taken to identify a target area within the Mur ligases. A suitable fragment library was established that could be used within a targeted *in silico* screen against the Mur ligases. Examination of the fragment set generated via the *in silico* screen identified issues within the fragment set that led to another *in silico* screen being carried out. Biochemical assays were then carried out on the fragment set, which was identified via the second *in silico* screen, to identify the inhibitory effects on MurD and MurE from *S. agalactiae.* The *in silico* screening and evaluation of *in silico* results was done in collaboration with Dr Joe Eyermann, of H3D department of the University of Cape Town, South Africa and latterly of Northeastern University, Boston, MA, USA.

2. Material and Methods

2.1 Use of Pymol to compare structures and visually inspect fragments

Pymol (The PyMOL Molecular Graphics System, Version 2.2, Schrödinger, LLC.) was used to compare structural alignments, sequence alignments and fragment alignments. Structures were imported into Pymol either by fetching via their Protein Data Bank (PDB) ID (https://www.rcsb.org/), from downloaded Crystallographic Information Files (CIF), or PDB files generated via Glide [106]. Alignments were generated via the align function of Pymol either for the whole molecule or specified areas. Residues of interest were shown in line function with important elements shown in the standard setting colour scheme. Polar contacts between important residues and substrates or fragments were predicted via the find polar contacts function of Pymol either for the whole substrate/fragment or important elements.

2.2 Structural Sequence Alignment

Structural sequence alignments between the Mur ligases and kinases were run using the pairwise structure alignment software within the RCSB Protein Databank [107]. The PDB ID of a Mur ligase and a kinase were entered into the pairwise structure alignment software, before a jFATCAT (flexible) alignment was run using default settings. A jFATCAT (flexible) alignment detects and aligns fragment pairs based on similarities in local geometry, while allowing for the introduction of 'twists' into the alignment to allow for protein flexibility within the comparison. The sequence alignment of the two proteins was visualised using the flexible alignment tab. The structural alignment was visualised by downloading the superimposed structures and comparing them using Pymol.

2.3 Production of fragment library

A kinase fragment library was generated via the Schrodinger Scaffold Decomposition tool. 3861 kinase inhibitor complexes were identified via PDB and papers which were then inputted into the scaffold software. A fragment list was generated via the scaffold software by breaking down the known inhibitor

structures into large scaffolds via the removal of side chains from ring structures. Large scaffolds were then split into sub scaffolds by removal of linkers between rings, if a fused ring was not present. A final list of scaffolds was then generated which was used for the fragment screen.

2.4 *In silico* screen using Glide

An *in silico* screen was run using the Glide software from Schrodinger. The PDB files chosen for each run were processed using the protein preparation wizard, converting them into files which were more suitable for ligand binding within Glide. During the protein preparation, water molecules that were not directly involved within the active site were deleted. After protein preparation was complete, a receptor grid was generated. A receptor grid defined the space in which ligand binding was carried out by the software. A receptor grid centred on the ATP-binding site of the Mur ligases was established. Specific constraints determined to be important for binding were set. H-bond constraints were used within both *in silico* screens to specific that a receptor-ligand hydrogen bond must be formed for Glide to consider the fragment a 'hit'. One H-bond constraint set was between asparagine 271 of MurD from *E. coli,* or equivalent asparagine in other bacteria, and the receptor protein. For the second *in silico* screen, a second constraint that a receptor-ligand hydrogen bond needed to form within the area of lysine 115 within MurD of *E. coli*, or equivalent lysine in other bacteria was also included. The ligands to be docked were then loaded into the system and the docking job established.

2.5 Stopped MESG assay

Fragments identified via the *in silico* screen were purchased from Enamine and shipped to Warwick at 50 mM concentration in 100% DMSO. Full fragment list is shown in **Supplementary 4.** Fragments were biochemically tested for inhibition of MurD from *S. agalactiae* within a stopped MESG assay. In a final volume of 50 μL, 1 mM of fragment was incubated with 80 nM MurD from *S. agalactiae* in the presence of 50 mM HEPES (pH7.6), 2 mM $MgCl_2$, 1 mM DTT, 50 mM KCl, 400 μM MESG, 30 μM UDP-MurNAc-L-Ala and 300 μM Deoxy-ATP for 10 minutes. The assay

was then initiated with 150 μM D-Glu and allowed to run for the initial rate period before the reaction was quenched with 10 mM EDTA. A background absorbance was determined photometrically via the ClarioStar plate reader (ThermoFisher) at 360 nm before 24.2 U per litre PNP was added. Absorbance change was tracked at 360 nm for 40 minutes to allow the end point to be achieved. The absorbance change was then determined. Each fragment was run in triplicate in the presence and absence of MurD to determine a background rate. Background rates were removed from the final activity rate for each fragment. The rates obtained in the presence of inhibitors were compared to control groups of 10% ($^{v}/_{v}$) DMSO and 30 μM ADPCP. All stages of the assay were carried out at 37°c.

In order to identify dual inhibitory fragments, a stopped MESG assay was carried out in the presence of MurE from *S. agalactiae*. 80 nM MurE was incubated with fragments at a final concentration of 1 mM in the presence of 75 μM UDP-MurNac-L-Ala-D-Glu and 20 μM ATP, before activity was initiated with 300 μM L-Lys.

2.6 Assay interference checks

To determine if inhibition identified via the stopped MESG assay was due to interference with the secondary coupling system, assays to determine the effect fragments had on the secondary coupling components was carried out. In a final concentration of 50 μL, 400 μM MESG, 50 mM HEPES (pH7.6), 2 mM $MgCl_2$, 1 mM DTT, and 50 mM KCl was incubated with 1 mM fragment and the absorbance change at 360 nm was tracked photometrically over the course of 10 minutes. 130 μM $Na(H_2)PO_4$ was then introduced and the absorbance change at 360 nm was tracked photometrically over the course of 10 minutes. 10 mM EDTA was then introduced and the absorbance change at 360 nm was tracked photometrically over the course of 10 minutes. 24.2 U per litre PNP was then introduced and the absorbance change at 360 nm was tracked photometrically for 40 minutes to allow the end point to be achieved. The absorbance change for each stage was then determined and compared to a control group of 10% ($^{v}/_{v}$) DMSO. All stages of the assay were carried out at 37°C within a ClarioStar plate reader (ThermoFisher).

3. Results

In order to run a targeted *in silico* screen against the Mur ligases, certain criteria had to be established. A domain or binding pocket within the Mur ligases that is well conserved and can be targeted via fragments had to be identified. An initial data set for the fragments that would be predicted to bind to the designated domain or binding pocket would also need to be established. Finally, specific residues that could be targeted via the fragment set within the designated domain or binding pocket were established before the *in silico* screen was carried out.

3.1 The Mur ligases have a high level of similarity within their ATP binding pockets

A domain or binding pocket within the Mur ligases that could be targeted via the *in silico* fragment screen had to be determined. To effectively target multiple Mur ligases within the fragment screen, an area that is well conserved across multiple Mur ligases and across bacterial species needed to be identified. Consultation of Eveland et al and Bouhss et al[68,69], suggested a large level of consensus within the structure and sequence of the ATP binding pocket of the Mur ligases. By overlaying the known structures of MurC, MurD, MurE and MurF from *E. coli*, and overlaying the known structures of MurD from *E. coli*, *S. agalactiae* and *Staphylococcus aureus (Sta. aureus)* it was seen that the secondary structure of the ATP binding pocket has a high level of similarity across the Mur ligases and different species, as seen in **Figure 4.1**. Across the Mur ligases, a difference of less than 1 Å was seen between three residues involved in the ATP-binding site of the Mur ligases, as seen in **Figure 4.1A**. A difference of less than 2 Å was seen between these three residues within the ATP-binding site of MurD across bacterial species, as seen in **Figure 4.1B**.

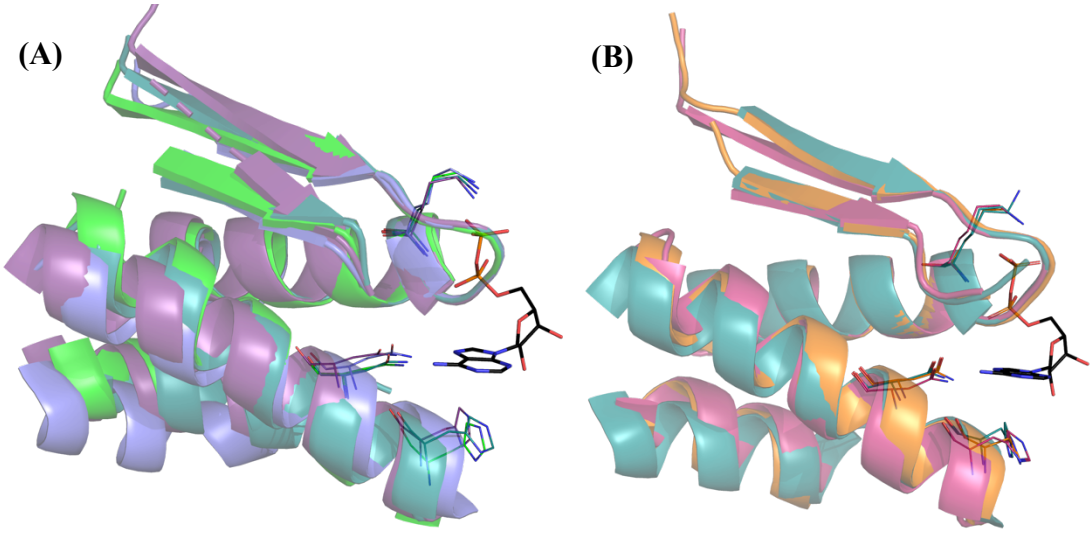

Figure 4. 1: Pymol diagrams to show the high level of similarity within the ATP binding pocket of various Mur ligases

Pymol diagrams showing the ATP binding pocket of the Mur ligases overlayed to show the high level of similarity. A lysine, histidine and asparagine are shown to compare distance between amino acids involved in the ATP-binding site. (A) ATP binding pocket of MurC (purple), MurD (teal), MurE (blue) and MurF (green) from *E.coli* overlayed to show the high level of similarity across the Mur ligases. (B) ATP binding pocket of MurD from *E.coli* (pink), *S. agalactiae* (teal) and *Sta. aureus*(orange) overlayed to show the high level of similarity across bacterial species.

As seen in **Figure 4.1**, there is a high degree of structural similarity within the ATP-binding site of the Mur ligases. To determine whether this similarity was also present within the amino acid sequences of the Mur ligases, sequence alignments of the Mur ligases was carried out using EMBOSS-Needle. The full amino acid sequences of the proteins determined to have structural similarity within their ATP-binding site were compared using EMBOSS-Needle and regions of amino acids that corresponded to areas of structural similarity were highlighted and the percentage sequence identity determined, as seen in **Figure 4.2**. All Mur ligases showed at least 30% sequence identity of the residues involved in ATP binding apart from area 3 in *E. coli* C: *E. coli* E, as shown in **Figure 4.2.** MurD across bacterial species showed a greater level of sequence similarity when compared to the Mur ligases across *E. coli*, with MurE showing the lowest sequence similarity within an area. The percentage sequence identity of amino acid sequences suggests that the Mur ligases have a high level of similarity within their amino acid sequences of the ATP-binding site.

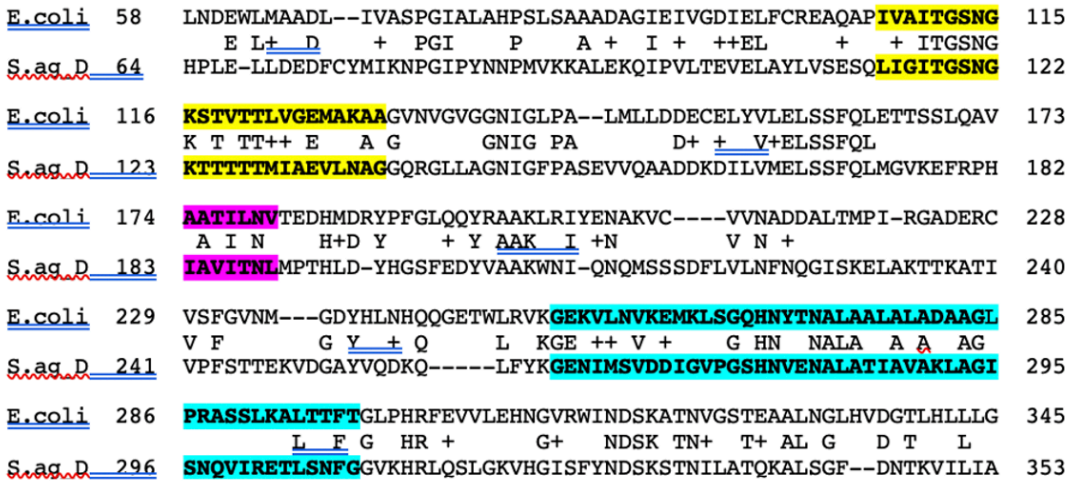

	Sequence Identity Coverage (%)		
	1	**2**	**3**
***S. ag* D: *E. coli* D**	50	43	35
***S. ag* D: *S. au* D**	42	71	37
***E. coli C*: *E. coli* D**	33	30	35
***E. coli C*: *E. coli* E**	42	57	17
***E. coli C*: *E. coli* F**	33	43	35

Figure 4. 2: Sequence similarity between the Mur ligases is present within the ATP-binding site

Sequence alignment of Mur ligases determined percentage positive sequence coverage in areas seen to have structural similarity within the ATP-binding site. (A) Example of a sequence alignment between MurD from *E. coli* and *S. agalactiae*. The three areas previously seen to be involved in the ATP-binding site and to have structural similarity are highlighted. (B) Sequence identity coverage for the three areas identified to be involved in ATP binding and to have structural similarity across bacterial species, and across the Mur ligases.

It has previously been seen that the Mur ligases contain a nucleotide binding motif within the ATP binding pocket which consists of a consensus sequence of GXXGKT/S [69]. This consensus sequence was present within all the Mur ligases previously seen to have structural and sequence similarity, as seen in **Table 4.1**. The structural similarity, sequence similarity and the presence of a consensus sequence within the ATP-binding site of the Mur ligases suggests that fragments targeted towards these areas could target multiple Mur ligases across multiple bacterial species. For this reason, the ATP-binding site was chosen as the area into which the *in silico* screen would be targeted for binding fragments.

	Location of consensus sequence
MurC	121 126 131 136 IGIAIAGTHGKTTTTAMVSSI'
MurD	106 111 116 121 : IVAITGSNGKSTVTTLVGEMI
MurE	111 116 121 126 .VGVTGTNGKTTTTQLLAQWS
MurF	101 106 111 116 : RVVALTGSSGKTSVKEMTAA:
E. coli D	106 111 116 121 'IVAITGSNGKSTVTTLVGEM
S. agalactiae D	116 121 126 131 GITGSNGKTTTTTMIAEVI
S. aureus D	111 116 121 126 : APIIAVTGTNGKTTVTSLIGI

Table 4. 1: A consensus sequence is well conserved across the 4 Mur ligases as well as across bacterial species

The ATP binding pocket of the Mur ligases contains a conserved nucleotide binding motif, consisting of a consensus sequence of GXXGKT/S, highlighted in red. This sequence is conserved across all four Mur ligases, as shown here across *E.coli* as well as across bacterial species, shown here in MurD across *E.coli, S. agalcatiae* and *S. aureus.*

3.2 Determination of kinases inhibitors as a targeted fragment screen

With the ATP-binding site being determined as the target within the Mur ligases for the *in silico* screen, the fragment data set needed to be determined. The basis of a fragment set can be varied, with previous screens being run using existing drugs as the fragment basis [108], previous inhibitor screens acting as the basis or natural substances providing a fragment set [109]. In order to effectively target the ATP-binding site of the Mur ligases, a fragment set based upon drugs that have previously been seen to target the ATP-binding site of a protein would be a good starting point. Drugs that are able to target the ATP-binding site of kinases have previously been used as the basis for determining new antibacterial development, with kinase inhibitors being seen to effectively target the ATP-binding site of biotin carboxylase [110]. Kinase inhibitors have also previously been used to effectively inhibit the activity of the Mur ligases, although not via binding to the ATP-binding site of the Mur ligases [102]. In order to determine if kinase inhibitors would be an effective starting point for the development of a fragment screen, the structural

similarity between the ATP-binding site of kinases and the Mur ligases was evaluated. Structural similarity between the Mur ligases and kinases was determined using structural pairwise alignment software available via PDB. Areas of structural alignment were then aligned to the full Mur ligase and kinase structures, and analysed in Pymol, as seen in **Figure 4.3.**

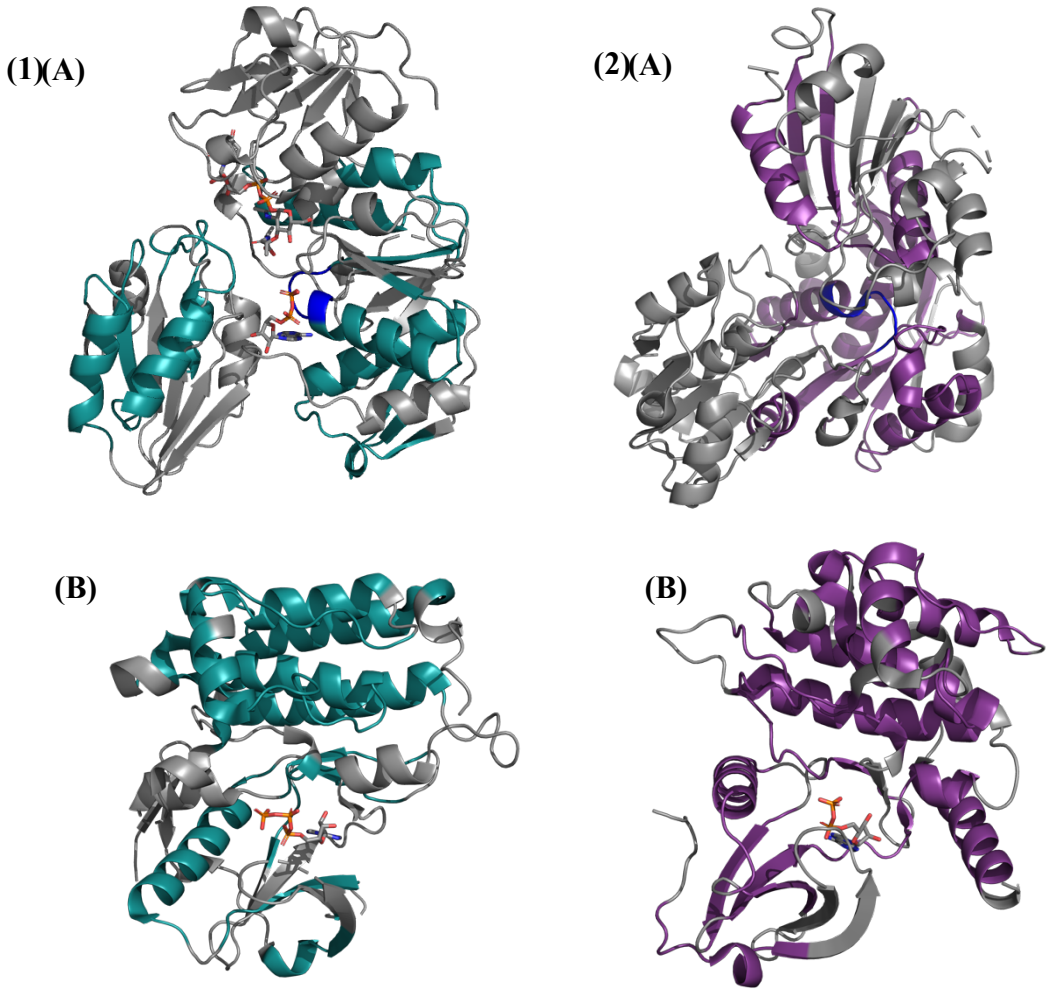

Figure 4. 3: Structural alignment of Mur ligases to kinases

Structural sequence alignment of Mur ligases to kinases was carried out to determine areas of similarities. Areas of structural alignment were determined via a pairwise structural alignment. Areas of structural alignment were highlighted on the full protein structure within Pymol. The ATP-binding site of the Mur ligases and kinases fall within areas of structural similarity. The ATP binding consensus motif within the Mur ligases falls within a region of structural similarity with the kinase, and is highlighted in blue. (1) Structural sequence alignment of MurD from *E.coli (A)* (PDB: 2UAG) and ALK tyrosine kinase from *Homo Sapiens (B)*(PDB: 6CDT). Areas of structural similarity are highlighted in green. (2) Structural sequence alignment of MurC from *E.coli(A)* (PDB: 2F00) and Human MST3 kinase from *Homo Sapiens* (PDB: 3A7H). Areas of structural similarity are highlighted in purple.

The ATP-binding site of the Mur ligases was seen to have structural similarity with the kinases, with the consensus sequence of the ATP-binding site being present in an area of structural similarity, as seen in **Figure 4.3A**. When aligned, the areas of structural similarity also fell in an area within the kinases which is involved in ATP binding, as seen in **Figure 4.3B.** The structural similarity between the ATP-binding sites of the Mur ligases and kinases suggested that fragments based on kinase inhibitors may be able to effectively target the ATP-binding site of the Mur ligases.

3.3 There is a high degree of similarity in interactions formed during ATP binding between the Mur ligases and kinases

Structural similarity between the Mur ligases and kinases had been established. In order to determine if kinase inhibitors targeted towards the ATP-binding site would be able to correctly interact with the ATP-binding site of the Mur ligases, determination of the interactions that form between ATP and the surrounding residues in the Mur ligases and kinases had to be established. Using known structures of the Mur ligases and known structures of kinases bound to ATP, the residues involved in forming interactions with ATP within each protein could be established.

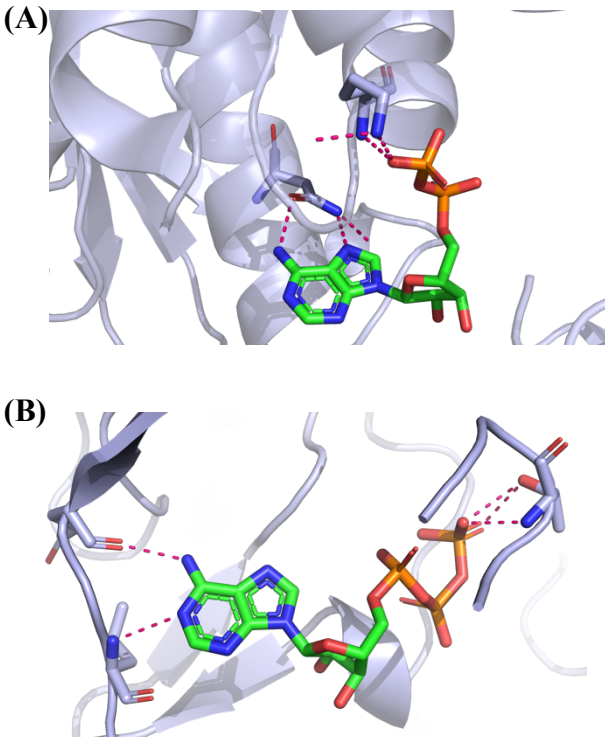

Figure 4. 4: ATP forms similar interactions with residues present in the Mur ligases and kinases

ATP forms interactions within the hinge region of kinases which are similar to those seen between ADP and the ATP-binding site of the Mur ligases (A) Hydrogen bonds formed between ADP and surrounding residues in MurD (PDB: 2UAG). (B) Hydrogen bonds formed between ATP and surrounding residues in Human cyclin-dependent kinase 2 (PDB: 1HCK). The ATP/ADP adenosine moiety is shown in green where the oxygen is highlighted in red, nitrogen is highlighted in blue and phosphorus in orange. Interactions are shown with red dotted lines.

As can be seen from **Figure 4.4A**, within the ATP-binding site of the Mur ligases a hydrogen bond is formed between the NH_2 of the adenosine ring and the oxygen of Asn271, while the nitrogen of Asn271 forms a hydrogen bond with the neighbouring nitrogen on the adenosine ring. The phosphate groups of the ATP can form multiple interactions with surrounding residues. An interaction can form between the nitrogen of residue Lys115 and the second phosphate group present, as seen in **Figure 4.4A.** Similar interactions were seen between ATP and the kinase. A hydrogen bond forms between the oxygen of residue Glu81 and the nitrogen of the adenosine ring, as shown in **Figure 4.4B**. A second hydrogen bond is also able to form between another nitrogen of the adenosine ring and residue Leu83 of the kinase. The final phosphate of the ATP can form a hydrogen bond with residue Thr14 within the kinase as seen in **Figure 4.4B**.

The similarity in the interactions that occur between ATP and the residues present within the ATP-binding site of the Mur ligases and kinases suggests that inhibitors that can bind to the ATP-binding site of a kinase may also be able to bind to the ATP-binding site of the Mur ligases.

3.4 Building the fragment library from known kinase inhibitors

Similarity between the structure of the ATP-binding site of Mur ligases to the ATP-binding site of kinases, and similarity in the interactions formed between ATP within the ATP-binding site of both proteins allowed kinase inhibitors to be used as the basis of the fragment set for the *in silico* screen. To build a fragment library, the structures of known kinase inhibitors had to be sourced. This was achieved by researching papers of kinase inhibitors [111] as well as searching PDB for kinases with inhibitors bound to the ATP-binding site. 3861 kinase inhibitors were identified and these were then broken down into fragment size. Inhibitors were broken down into fragments using the Schrodinger Scaffold Decomposition tool which identified 'ring systems' in the kinase inhibitor complexes, as shown in **Figure 4.5**. A known kinase inhibitor [112], such as that seen in **Figure 4.5A** can be broken down into ring systems via the decomposition tool, as shown in **Figure 4.5B**.

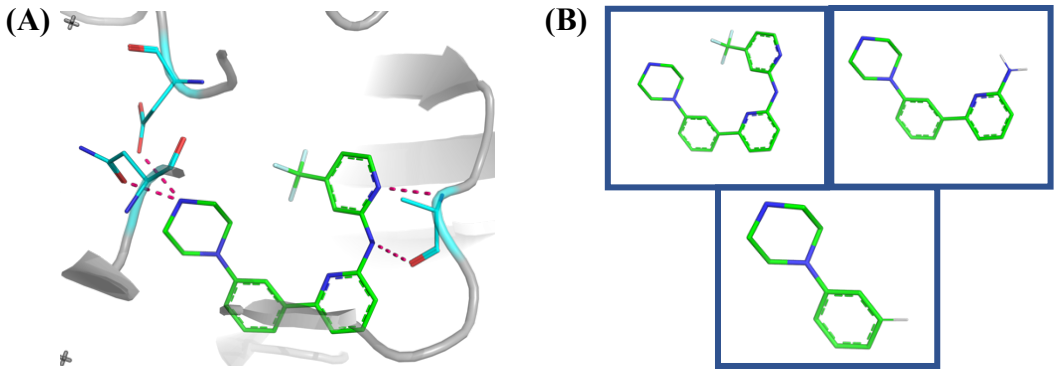

Figure 4. 5: Fragments were designed based on existing kinase inhibitors

To generate a fragment library, PDB files of kinases with inhibitors bound were found and the inhibitors broken down into fragments. (A) PDB 4F4P shows an inhibitor (shown in green) bound to a kinase. (B) Inhibitor was broken down into fragments for the screen.

The inhibitors and fragments were collated into one fragment library. The library was processed by the LigPrep software of Glide [113], generating multiple structures from each input structure with various tautomers, sterochemistries and ring conformations being produced. Structure files for all fragments were produced which could then be used within *in silico* screening.

3.5 Identification of residues to target within the ATP-binding site of the Mur ligases

Similarity in the interactions formed between ATP within the ATP-binding site of both Mur ligases and kinases allowed kinase inhibitors to be used as the basis of the fragment set for the *in silico* screen. The next step in setting up the targeted *in silico* screen was to determine the exact residues to which binding must occur for the fragment to be considered a 'hit'. Within the ATP-binding site of the Mur ligases, residues which form interactions which are similar to that formed between ATP and the hinge region of the kinase would be most suited for targeting via the *in silico* screen. Within the kinase ATP-binding site, a hydrogen bond is formed between the NH_2 group of the adenosine of ATP and an oxygen on a neighbouring residue. Targeting the residue within the Mur ligases which is able to hydrogen bond to this NH_2 group would provide an interaction point for the fragments which is similar across both proteins. This interacting residue was determined by identifying the

polar contacts between ADP and MurD from *E. coli* (PDB:2UAG) within Pymol. As can be seen from the known structure in **Figure 4.6,** residue Asn271 in MurD from *E. coli* is able to form a hydrogen bond with the NH_2 group of the adenosine ring of ATP.

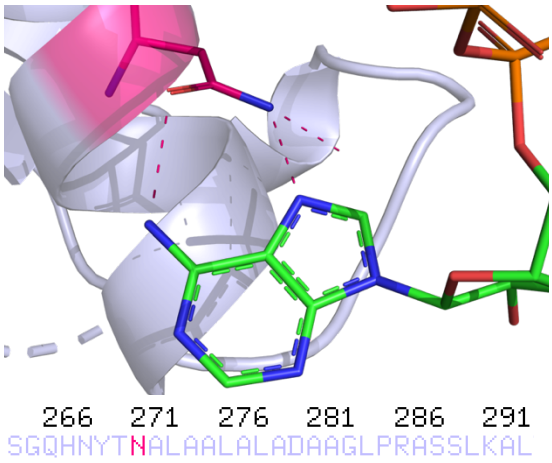

Figure 4. 6: Asn271 forms a hydrogen bond with the NH_2 group of the adenosine ring

ATP forms a hydrogen bond between the NH_2 group of the adenosine ring and Asparagine 271 of MurD *E.coli*. ATP is shown in green, with the asparagine being highlighted in pink within the secondary structure and within the amino acid sequence. PDB ID: 2UAG.

To be an interacting residue of value within the *in silico* screen, the Asn residue must be well conserved across the Mur ligases and bacterial species. Comparison of the sequence of the previously studied Mur ligases showed that the Asn is well conserved across bacterial species and the Mur ligases, as seen in the structural alignment in **Figure 4.7**, and so could be used as a target within the *in silico* screen.

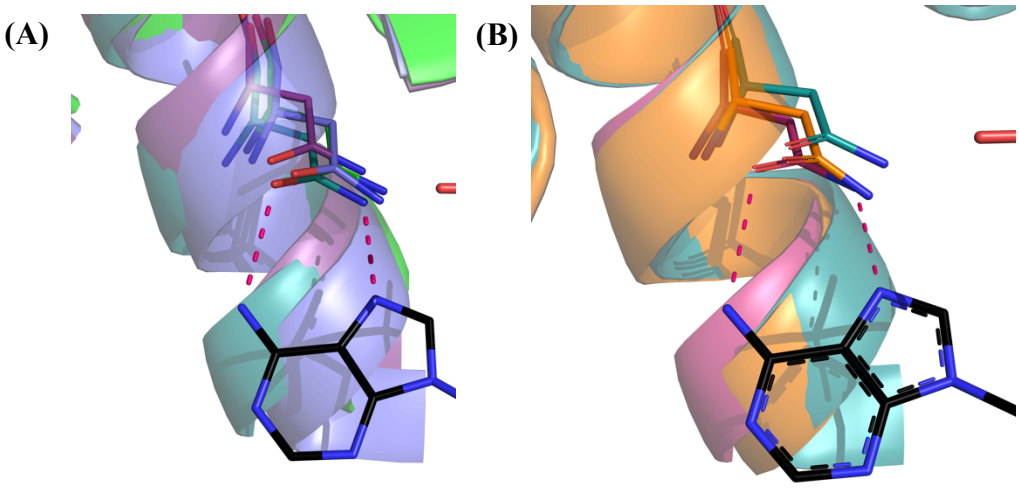

Figure 4. 7: The Asparagine that forms a hydrogen bond with ATP is well conserved across Mur ligases and bacterial species

Pymol diagrams showing the asparagine that forms a hydrogen bond to the adenosine ring of ATP is well conserved across Mur ligases and bacterial species (A) The asparagine is present within MurC (purple), MurD (teal), MurE (blue) and MurF (green) from *E.coli*. (B) The asparagine is present within MurD from *E.coli* (pink), *S. agalactiae* (teal) and *Sta. aureus*(orange).

Within the kinase ATP-binding site, other interactions are also formed between the final phosphate group of ATP and the oxygen and nitrogen groups of residue Thr14. Targeting the residue within the Mur ligases which is able to hydrogen bond to one of the phosphates would provide an interaction point for the fragments which is similar across both proteins. This interacting residue was determined by identifying the polar contacts between ADP and MurD from *E. coli* (PDB:2UAG) within Pymol.

As can be seen from the known structure in **Figure 4.8A,** residue Lys115 within MurD from *E. coli* is able to form an interaction with the oxygen of the phosphate group of ADP. To be an interacting residue of value within the *in silico* screen, the Lys residue must be well conserved across the Mur ligases and bacterial species.

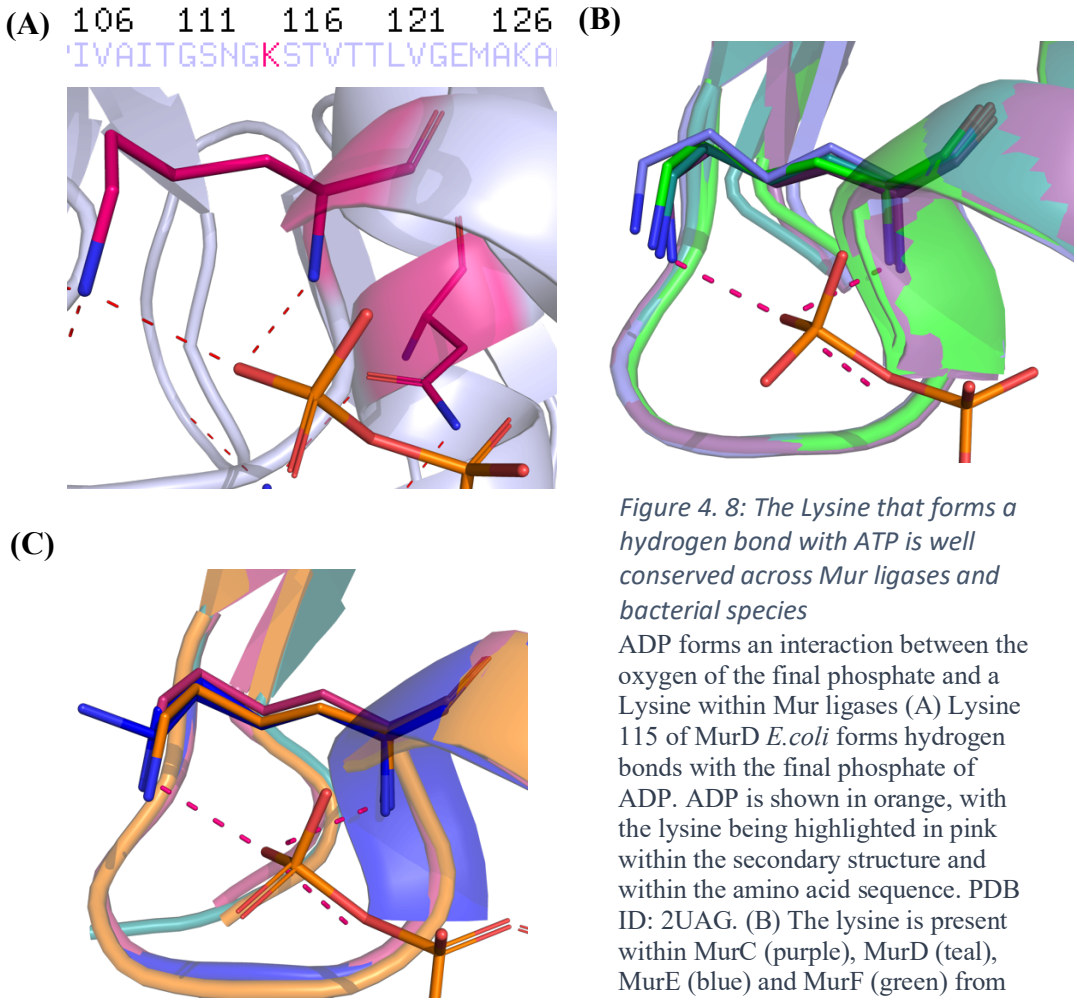

Figure 4. 8: The Lysine that forms a hydrogen bond with ATP is well conserved across Mur ligases and bacterial species

ADP forms an interaction between the oxygen of the final phosphate and a Lysine within Mur ligases (A) Lysine 115 of MurD *E.coli* forms hydrogen bonds with the final phosphate of ADP. ADP is shown in orange, with the lysine being highlighted in pink within the secondary structure and within the amino acid sequence. PDB ID: 2UAG. (B) The lysine is present within MurC (purple), MurD (teal), MurE (blue) and MurF (green) from *E.coli*. (B) The lysine is present within MurD from *E.coli* (pink), *S. agalactiae* (teal) and *Sta. aureus*(orange).

Comparison of the sequence of the previously studied Mur ligases showed that the Lys115 is well conserved across bacterial species and the Mur ligases and so could be used as a target within the *in silico* screen, as seen in the structural alignments in **Figure 4.8B** and **Figure 4.8C**. As both the asparagine and lysine are well conserved across Mur ligases and form interactions with ATP similar to the interactions seen between ATP and eukaryotic protein kinases, Lys 115 and Asn 271 were selected for targeting within the *in silico* screen.

3.6 Evaluation of existing PDB files of Mur ligases for use within the Glide software

In order to run the *in silico* screen, suitable Mur ligase structures would need to be chosen that would act as the target for the fragments to bind to. PDB structures provide detailed information on ligands bound within the structure, resolution of the structure and the organism that the protein came from, and so PDB structures were chosen as the starting point for determining suitable Mur ligase structures. The first step in determining suitable Mur ligase structures was to determine which Mur ligases the screen would be targeted towards. The targeting of two Mur ligases within the screen increased the chances of finding a multi targeting fragment. Previous work at Warwick had investigated the ability of fragments to bind and inhibit the activity of MurD, and so MurD was chosen as one of the targets to be able to continue to build on previous work. Dr Eyermann had previous experience working with MurC and so this was chosen as the second Mur ligase.

With the Mur ligases chosen that would be targeted via the screen, other criteria could now be set. The structure of the Mur ligase would need to consist of only one chain. The presence of a secondary chain within the structure could result in a change in the folding of the protein at the point of contact which may affect the ability of the fragments to bind to the target. The final criterion was that for this screen, an ATP equivalent would need to be bound to the ATP-binding site of the Mur ligase. The presence of a molecule within the target site for the fragments would aid in setting up the targeted *in silico* screen. With the Mur ligases chosen, and the criteria set, a list of potential PDB files could be generated, as seen in **Table 4.2**.

MurC	**1P3D**	**4HV4**	**6CAU**	
MurD	**2UAG**	**3UAG**	**5A5F**	**2JFG**

Table 4. 2: Potential PDB files that could be used within the in silico screen

In order to run the *in silico* screen, a suitable protein structure needed to be determined. Using set criteria; that something must be bound within the ATP-binding site, and the structure must only contain one chain, a list of potentially suitable PDB files was generated.

From these potential PDB files, it was decided to use 6CAU for MurC and 5A5F from MurD. For MurD, all PDB files were from *E. coli* and had resolutions of less than 2 angstroms. Therefore, 5A5F was chosen as it was the newest entry. For MurC, all three PDB files came from three different bacteria; 1P3D, 4HV4 and 6CAU described the *Haemophilus influenzae*, *Yersinia pestis* and *Acinetobacter baumannii* MurC structures respectively. 1P3D was ruled out as it contained a mutation. 4HV4 was ruled out as it is from a biothreat pathogen and not a WHO priority pathogen or a Warwick pathogen and so 6CAU was used for the screen.

3.7 Use of Glide to identify fragments that have the potential to target the ATP-binding site of MurC and MurD

With the PDB files that would act as the structures for the screen chosen, along with the production of the fragment set, and determination of the residues that would be targeted via the screen, the *in silico* screen could be run. The *in silico* screen was run using the Glide software from Schrödinger. The chosen PDB files were inserted into the software, and a grid was formed around the ATP-binding site before the ADP was removed. The grid allowed the binding of the fragments to be targeted towards a specific region within the protein. Within the grid, further constraints could be placed, to further target the fragments. The previously identified residues, the conserved asparagine 271 and lysine 115 (*E. coli* numbering), were set as binding constraints for the fragments. By setting the binding to these residues as constraints, only fragments that were able to bind in some capacity to the residue would be returned as a hit. Due to the size of some of the fragments, some fragments may have been unable to form hydrogen bonds to both the lysine and asparagine. Therefore a priority was placed upon the binding

constraints, with the ability of the fragment to form a hydrogen bond to the asparagine being placed as a higher priority, allowing fragments that only form this hydrogen bond to be returned as hits. With the grid in place, and constraints set, the 12,000 fragments identified via LigPrep could be run within the *in silico* screen.

3.8 Evaluation of fragments identified via the screen

For the initial *in silico* run, 12,000 fragments were targeted towards the ATP-binding site of MurD (5A5F) using the Glide software from Schrodinger. Of the 12,000 fragments, 4,000 were found to bind within the desired region under the constraints set. For these 4,000 fragments, the molecular weight of the fragment, and its glide score were taken into account for deciding the top 100 fragments that would be passed onto the second run.

3.8.1 Top hits were determined via their Le score, molecular weight and glidemodel score

After the initial run, 4,000 fragments were returned as potentially being able to bind within the ATP-binding site of MurD under the set constraints. In order to determine the top hits from these fragments, the molecular weight and the glidemodel score were taken into account to determine the Le score of each fragment. The Le score, glidemodel score and molecular weight of each fragment were then taken into consideration when determining the top hits from the screen.

The molecular weight of the fragment was taken into consideration when determining the top hits of the screen as the smaller the molecular weight, the more likely the fragment is to have high ligand efficiency. Smaller fragments provide better opportunities for development of the fragments into compounds at a later stage. A cut-off point of 600 MW was set for the fragment screen, with fragments with a molecular weight of less than 600 being considered for the second run.

The glidemodel score is a score generated via the Glide software. The score helps to predict binding affinity via the ligand binding free energy [114]. The score takes into account many factors including van der Waals energy, ionic charges on

groups as well as penalizing or rewarding interactions that are known to influence ligand binding [114]. The system was optimized for docking accuracy and binding affinity prediction. As the glidemodel approximated ligand binding free energy, the more negative the score, the tighter the potential binding of the fragment was. A cut-off value for the glidemodel score of -50 was set, with fragments having a glidemodel of less than -50 being considered for the second run.

The Le score for each fragment was determined by dividing the glidemodel score by the molecular weight of the fragment. This score was used to predict which fragments were most likely to bind to the ATP-binding site. An Le score cut-off of -0.2 was set with fragments having an Le score of less than -0.2 being considered for the second run.

With cut-off values set, the 4,000 fragments were analysed, and the top 100 fragments were chosen to be run through a second fragment screen against MurC (6CAU) using the same constraints as previously set against MurD. These 100 fragments had glidemodel scores ranging from -197 to -82, with Le scores ranging from -0.398 to -0.227. After the second run, 80 fragments were found to bind to both MurD and MurC under the set constraints. These fragments were then analysed for their glidemodel score and Le score again before undergoing visual inspection.

3.8.2 Fragments existing as tautomers are unlikely to act as inhibitors of the Mur ligases

Visual inspection of the fragments that were able to bind to both MurC and MurD was carried out to identify issues which may prevent the fragments from being able to act as inhibitors of the Mur ligases. Inspection of the fragments identified the presence of tautomers within the fragments. Tautomers are isomers that can convert between each other with the movement of a proton via the rearrangement of a double bond [115]. Protons can freely move between two positions via the rearrangement of the double bond, but the proton will favour one position, allowing a dominant tautomer to exist [115]. The LigPrep software used in the production of the fragment data set produced fragments with multiple tautomeric forms. When visual inspection of the fragments was carried out, a

certain number of fragments were seen to contain a nitrogen within a ring structure, which would tautomerise, as seen in the predicted interaction in **Figure 4.9**.

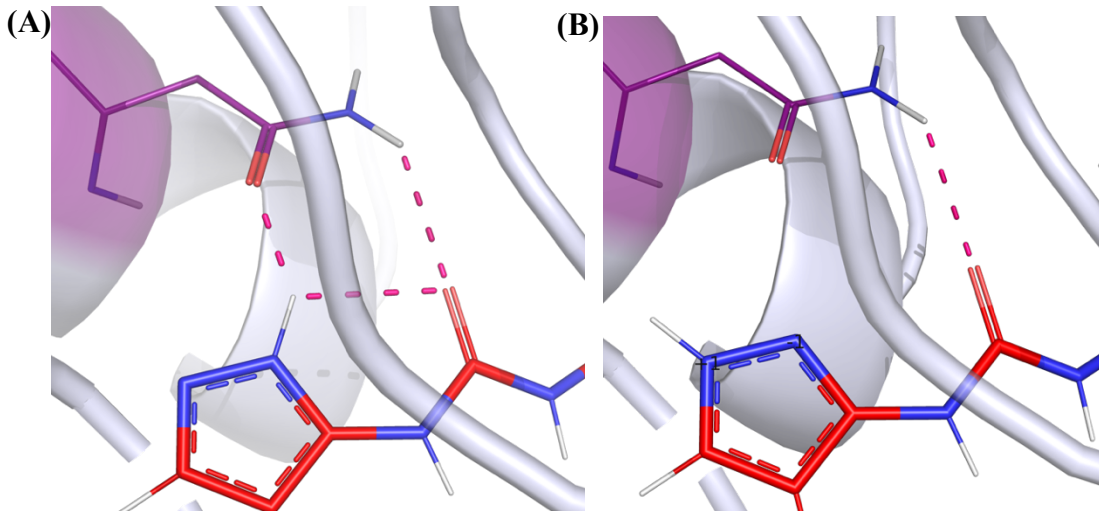

Figure 4. 9: Fragments existing as tautomers were unlikely to act as inhibitors

Upon visual inspection, fragments were identified to contain tautomers. Fragments containing tautomers were seen to mostly fall into the unfavoured state, and the favoured state would break the hydrogen bonds set as criteria for the fragment screen, making them less likely to be able to act as inhibitors of the Mur ligases. One of these fragments is shown here bound to MurD (PDB: 5A5F), with the fragment shown in red and the asparagine shown in purple. (A) The nitrogen is present in the tautomer provided by Glide. In this tautomer, the nitrogen is able to form a hydrogen bond to the oxygen of the asparagine. (B) The nitrogen is present in the naturally occurring tautomer. The nitrogen is no longer able to form the hydrogen bond with the asparagine.

Inspection of the fragments identified certain fragments that contained unfavourable tautomers. The favoured tautomers of these fragments were unable to form hydrogen bonds to the asparagine, which had been set as a constraint within the screen, as seen in the predicted interactions in **Figure 4.9**. The inability to form the required hydrogen bonds to the asparagine meant these fragments were less likely to be able to act as inhibitors and so were removed from the list of hits from the fragment screen.

3.8.3 Fragments with flexible middle regions unlikely to form predicted interactions

Visual inspection of the fragments that were able to bind to both MurC and MurD was carried out to identify flexible regions within the fragments. Flexible regions within fragments can increase the negative effects of the binding entropy of the fragment-protein complex, making them less favourable binding partners for the protein. Fragments were considered to have flexible middle regions if they contained more than three carbons in a row within the backbone, such as that seen in the predicted fragment layout shown in **Figure 4.10**. Flexible regions may also prevent favourable interactions occurring, such as the hydrogen bond between the fragment and the conserved lysine. Due to increased negative effects of flexible regions and the potential for favourable interactions to be broken due to flexible regions, fragments containing flexible regions were considered to be unable to act as inhibitors of the Mur ligases and so were removed from the list of hits from the fragment screen.

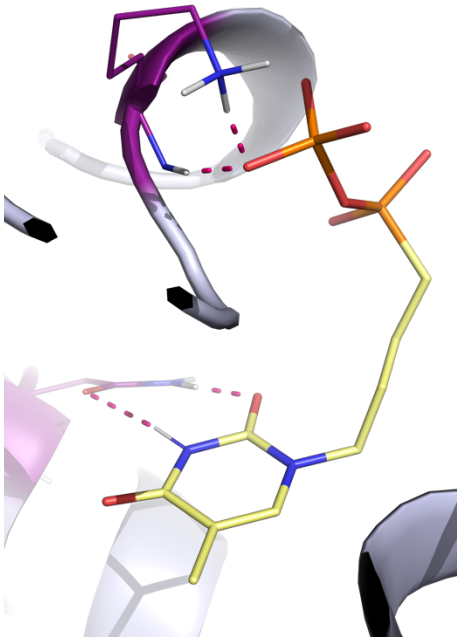

Figure 4. 10: Fragments with flexible middle regions were unlikely to act as inhibitors

Upon visual inspection it was seen that certain fragments contained flexible middle regions that made them unsuitable as potential inhibitors. Flexible regions increase the binding entropy and reduce the potential for accurate binding. One of these fragments is shown here bound to MurD (PDB: 5A5F). The conserved asparagine and lysine are shown in purple, with interactions between residues and fragments shown in red. The middle region consists of 4 carbons in a chain, making it very flexible and unsuitable as a potential inhibitor.

3.8.4 Commercial availability of fragments

After visual inspection of the fragments and removal of any fragments that contained unfavourable tautomers or flexible regions, the remaining fragments were compiled and compared to look for similar features, as shown in the predicted fragment layout in **Figure 4.11**. Fragments that contained similar structures were visually inspected for their ability to form interactions with residues present within the ATP-binding site of MurD and MurC. Fragments that formed more favourable interactions were kept and a final list of fragments compiled. In order to biochemically test the fragments to determine their inhibitory effects, the fragments would need to be produced or ordered via a commercial source. The final fragment list was inputted into the Enamine store database to determine the commercial availability of the fragments. Many fragments were not commercially available and required specialist production. Specialist production of the fragments would not have been cost effective for a high throughput biochemical screen. Another *in silico* screen would need to be carried out to produce commercially available fragments that were suitable for a high throughput biochemical screen.

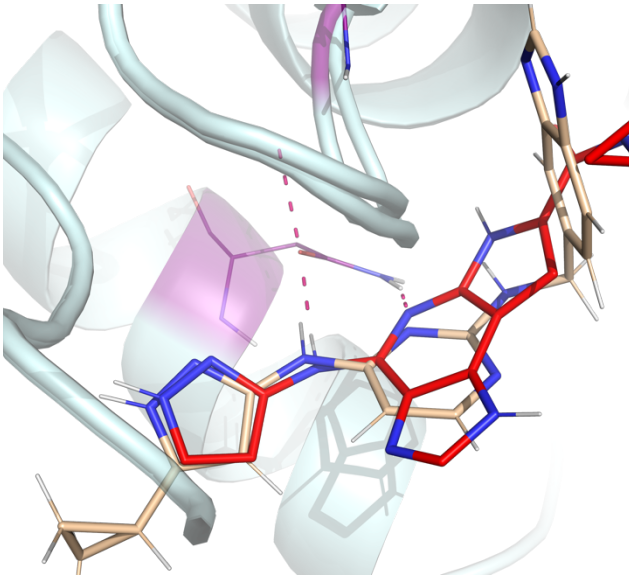

Figure 4. 11: Comparison of fragments to identify similar regions

Upon visual inspection it was seen that certain fragments contained similar features. Two fragments are shown here bound to MurC (PDB: 6CAU). Both fragments contain a ring structure containing a nitrogen that forms a hydrogen bond to the asparagine with a neighbouring nitrogen forming another hydrogen bond to the asparagine.

3.9 High throughput screen of commercially available kinase inhibitory fragments

A second *in silico* fragment screen was carried out by Dr Eyermann. Instead of developing a fragment library, a commercially available Enamine kinase inhibitor library was used to prevent the issue of commercial availability preventing biochemical testing of the fragments. The second *in silico* screen was carried out against MurD and MurE, instead of MurC and MurD. This switch in protein targeting was made due to the availability of proteins for biochemical testing of the fragments, once a final fragment set had been established. For MurD, two PDB structure files were used within the *in silico* screen. An *E. coli* structure of MurD in complex with UDP-MurNAc-L-Ala with ADP bound within the ATP binding pocket (PDB: 5A5F), along with an *S. agalactiae* structure of MurD which has nothing bound within the ATP binding pocket (PDB: 3LK7) were used within the screen. The second MurD structure was included as previous work at Warwick in collaboration with H3D department of the University of Cape Town, South Africa had focused on *S. agalactiae* as a priority pathogen associated with neonatal sepsis and so MurD from this organism was chosen to be included within the second screen. The MurE structure used within the screen came from *E. coli* and has nothing bound within the ATP binding pocket (PDB: 1E8C).

Before docking was carried out, an initial constraint was placed on the 40,000 fragments contained within the Enamine kinase inhibitor library, limiting the fragment molecular weight to less than 350 to reduce the number of fragments that would be run through the *in silico* screen against the Mur ligases. The previous constraints of docking within the ATP-binding site and forming hydrogen bonds to the asparagine present within the ATP-binding site were used within the *in silico* screen. From this fragment screen, 724 fragments were found to bind to at least one of the three proteins and satisfy the constraints placed upon them. Fragments were then visually inspected using the same criteria as previously used; satisfactory tautomer arrangement, and level of flexibility within the backbone. 624 fragments met the constraints placed upon them, and contained no unnatural tautomers or flexibility within the backbone. These 624 fragments were then commercially produced by Enamine to allow biochemical testing to be carried out.

3.10 Identification of inhibitory fragments targeted against MurD from *S. agalactiae*

The fragments identified to potentially bind to the ATP-binding site of the Mur ligases via the *in silico* screen were produced by Enamine. 624 fragments were shipped to Warwick at 50 mM concentration in 100% DMSO in 364 well plates ready to be tested biochemically. *In silico* screening predicted what fragments may be able to bind to the ATP-binding site of the Mur ligases. Biochemically testing the fragments within an activity assay would provide information on the ability of the fragments to bind and inhibit the activity of a Mur ligase.

In order to determine the effect the fragments had on the activity of MurD from *S. agalactiae*, a stopped MESG assay was used. The activity rate of 80 nM *S. agalactiae* MurD in the presence of fragments at a final assay concentration of 1 mM was compared to a control group of 10% ($^{v}/_{v}$) DMSO, and the percentage activity of MurD in the presence of fragments was determined, as seen in

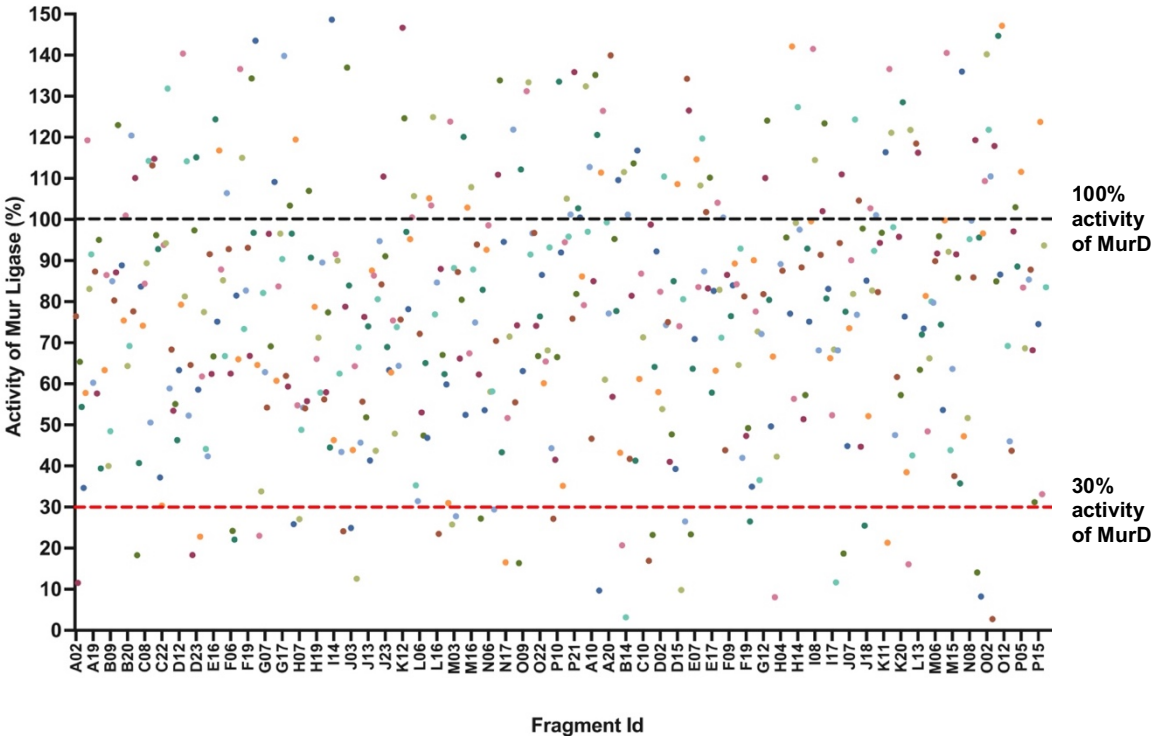

Figure 4. 12: Activity of MurD in the presence of Enamine fragments

The ability of the fragments to inhibit the activity of MurD from *S. agalactiae* was determined via a stopped MESG assay. Fragments were incubated at a final concentration of 1 mM with 80 nM MurD for 10 minutes at 37^{0}c before activity of MurD was determined. Activity of MurD in the presence of fragments was compared to a control group of DMSO and the percentage activity of MurD determined and plotted. All fragments were run in triplicate with a triplicate background rate average being removed from the individual replicate activity rates. The mean percentage activity of compounds was plotted. Black line indicates 100% activity of MurD. Red line indicates 30% activity of MurD.

Figure 4.12. A positive control inhibitor of 30 μM ADPCP was also used to confirm inhibition within the assay system. As can be seen from **Figure 4.12**, the fragments had a varied effect on the activity of MurD.

One hundred and forty two fragments precipitated in the conditions of the assay, and so activity of MurD could not be established in the presence of these fragments. Twenty one fragments stimulated MurD activity by over 150 %. This could have been due to interference with the assay components, or natural absorbance by the fragment at 360 nm. Two hundred and twenty three fragments were able to reduce activity of MurD by 25% or more. Ninety six fragments were able to reduce activity by 50% or more. One hundred and one fragments caused an increase in activity of MurD to no more than 150%. Triplicate activity levels can be seen in **Supplementary 5**. A threshold of a 70% reduction in activity was used as a cut-off point for considering fragments as inhibitors of *S. agalactiae* MurD activity.

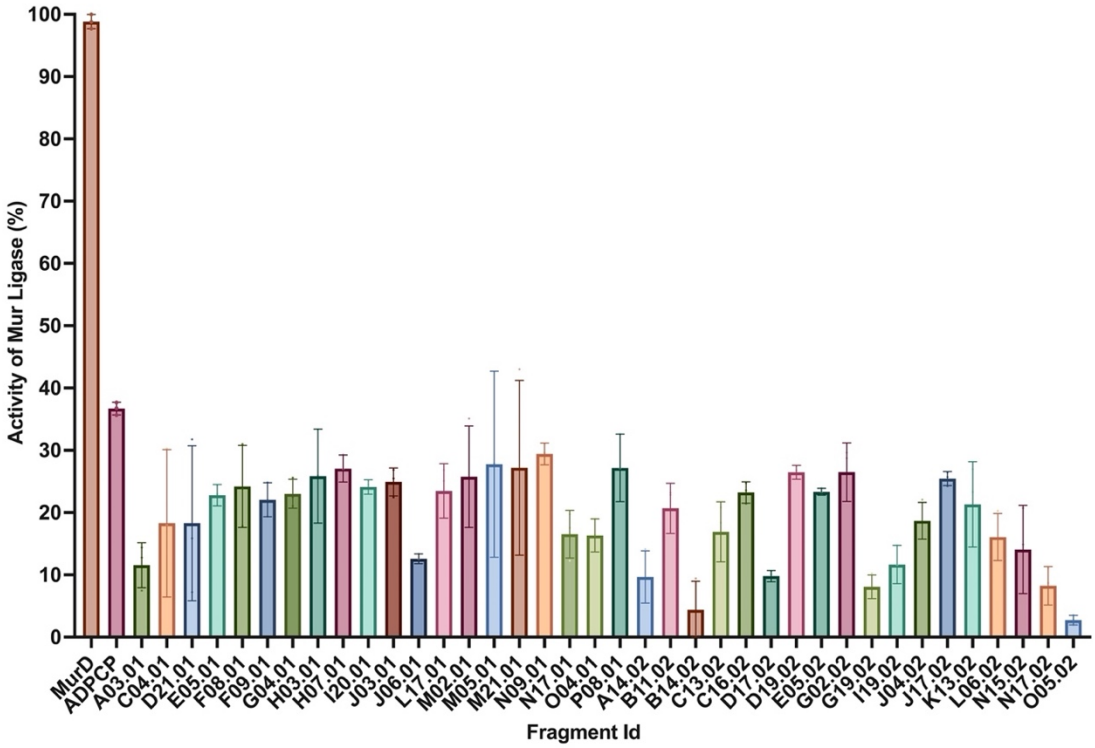

Figure 4. 13: 38 fragments can act as inhibitors of MurD

38 Enamine fragments were able to reduce the activity of MurD from *S. agalactiae* by 70% or more. Fragments were incubated at a final concentration of 1 mM with MurD before activity of MurD was determined. Activity of MurD in the presence of fragments was compared to a control group of DMSO and the percentage activity of MurD determined and plotted. All fragments were run in triplicate with a triplicate background rate being removed from the activity rate. The mean is plotted with triplicate repeat data shown with error bars showing SD.

As can be seen from **Figure 4.12** and **Figure 4.13**, thirty eight fragments satisfied this criterion. Fragments B14.02 and O05.02 were able to reduce activity of MurD within the assay by more than 95%, as seen in **Figure 4.13**. These thirty eight fragments were seen to inhibit the activity of MurD from *S. agalactiae* within this assay, and so were selected for further validation.

3.11 Certain fragments cause interference with assay system resulting in false positives

Initial screening of the Enamine fragments identified thirty eight fragments that were able to reduce the activity of MurD from *S. agalactiae* by 70% or more. The reduction in activity was determined by tracking an absorbance change at 360 nm. This absorbance change was dependent on the PNP-catalysed phosphorolysis of MESG to generate ribose -1 phosphate and methyl thioguanine. If the fragments interfered with any of these components, it could have resulted in a reduced absorbance change which would have been interpretated as a reduction in activity due to inhibition of MurD by the fragment. To determine if any of the fragments had produced false positive results, the fragments were tested against the assay components, phosphate, the stopping agent EDTA and PNP. The fragments were incubated at 1 mM final concentration with the assay components and the absorbance tracked at 360 nm. After 10 minutes, phosphate was introduced, and the absorbance monitored at 360 nm for 10 minutes before EDTA was introduced. The absorbance was followed at 360 nm for 10 minutes before PNP was introduced and the absorbance followed until an end point had been reached. The absorbance change, and absorbance range for each fragment in the presence of the components was determined and compared to a control group of DMSO.

As can be seen from **Figure 4.14A,** fragments A03.01, C04.01, H03.01, D21.01, D17.02, and I19.02 all caused an increase in absorbance change at 360 nm. These fragments also all had a large range in their absorbance readings as seen in **Figure 4.14B**. An increase in absorbance change in the presence of the assay components could suggest that the fragments were interacting with the MESG present, converting it to methyl thioguanine, which absorbs at 360 nm.

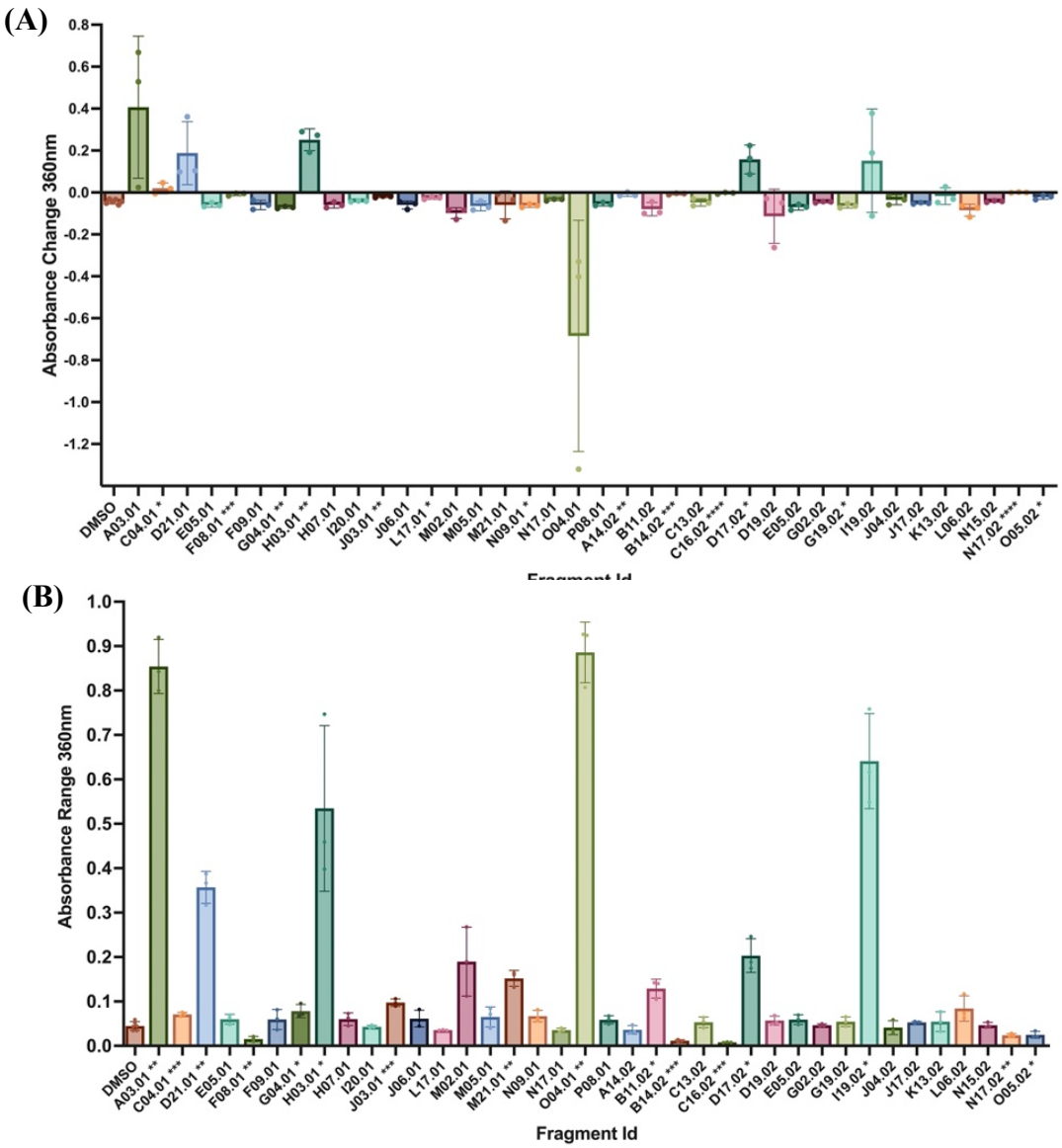

Figure 4. 14: Fragments interfere with the assay components

Fragments that had reduced activity of MurD in initial screening were tested for their effect on the assay components. (A) The absorbance change after the addition of assay components in the presence of fragments was determined. (B) The absorbance range after the addition of assay components in the presence of fragments was determined. All experiments were run in triplicate with mean results being plotted, with individual data points shown. Error bars show SD.

A reduction in the MESG available within the assay for PNP to act upon could result in a reduction in absorbance change after activity, leading to a false positive recording of inhibition via the fragments. Fragment O04.01 had a large range in its absorbance readings and showed a large decrease in absorbance change at 360 nm. A large range could suggest that the fragment was causing precipitation within the assay which affected the ability of the plate reader to record the absorbance of the

assay. Due to their interference with MESG, the ability of these fragments to inhibit the activity of MurD could not be determined within this assay system, and so were removed from further studies.

Phosphate was generated and used within the stopped MESG assay to determine the activity of the Mur ligase. Interaction of the fragments with the phosphate present could result in false positive recordings of inhibition.

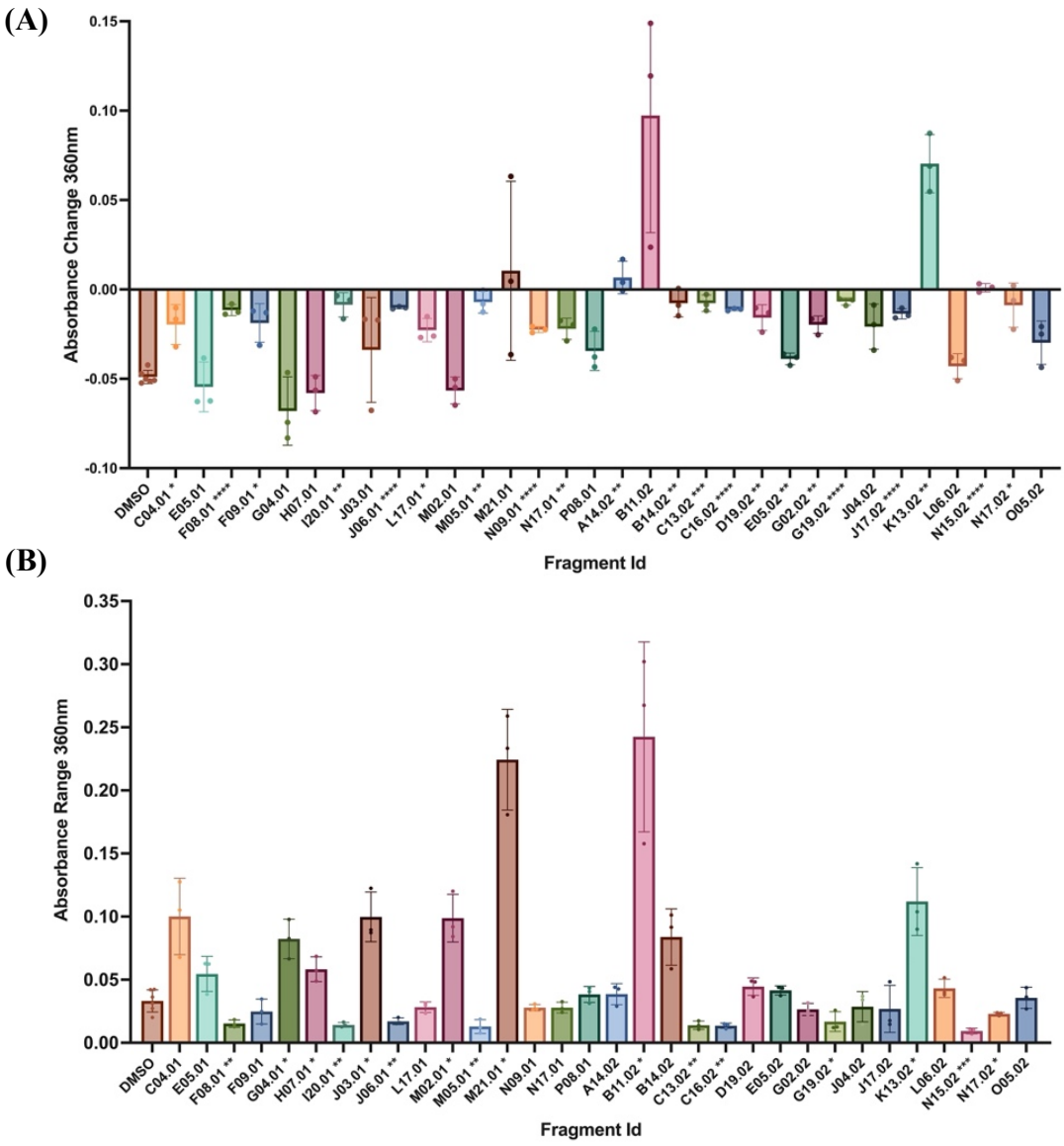

Figure 4. 15: Fragments interfered with the phosphate present within the assay

Fragments that had reduced activity of MurD in initial screening were tested for their effect on phosphate. (A) The absorbance change after the addition of assay components in the presence of fragments was determined. (B) The absorbance range after the addition of assay components in the presence of fragments was determined. All experiments were run in triplicate with mean results being plotted, with individual data points shown. Error bars show SD.

The effect the fragments had on the absorbance change, and absorbance range after the addition of phosphate was determined. As can be seen from **Figure 4.15A,** fragments M21.01, A14.02, B11.02 and K13.02 all caused an increase in the absorbance change after the addition of phosphate. Fragments M21.01, B11.02 and K13.02 all had a significant range in their absorbance readings as seen in **Figure 4.15B**. An increase in the absorbance change, and absorbance range suggests that the fragment was interacting with the phosphate present. This could result in a change in the phosphate concentration present within the sample. Activity of MurD was determined via the amount of phosphate present within the sample after the MurD reaction was quenched. Altering the amount of phosphate present within the sample could result in a reduction in absorbance change after activity, leading to a false positive recording of inhibition via the fragments. Due to their interference with phosphate detection, the ability of these fragments to inhibit the activity of MurD cannot be determined within this assay system, and so were removed from further studies.

EDTA was used to quench the activity of MurD within the assay. Interaction of the fragments with the EDTA present could result in false positive recordings of inhibition. The effect the fragments had on the absorbance change, and absorbance range after the addition of EDTA was determined. As can be seen from **Figure 4.16A**, fragments L17.01 and O05.02 caused an increase in absorbance change after the addition of EDTA. Fragment C04.01 caused a significant decrease in absorbance change, along with having a significant increase in absorbance range, as seen **in Figure 4.16A** and **Figure 4.16B**. A significant difference in the absorbance change, and absorbance range suggests that the fragment was interacting with the EDTA present. Due to their interference with EDTA, the ability of these fragments to inhibit the activity of MurD cannot be determined within this assay system, and so were removed from further studies.

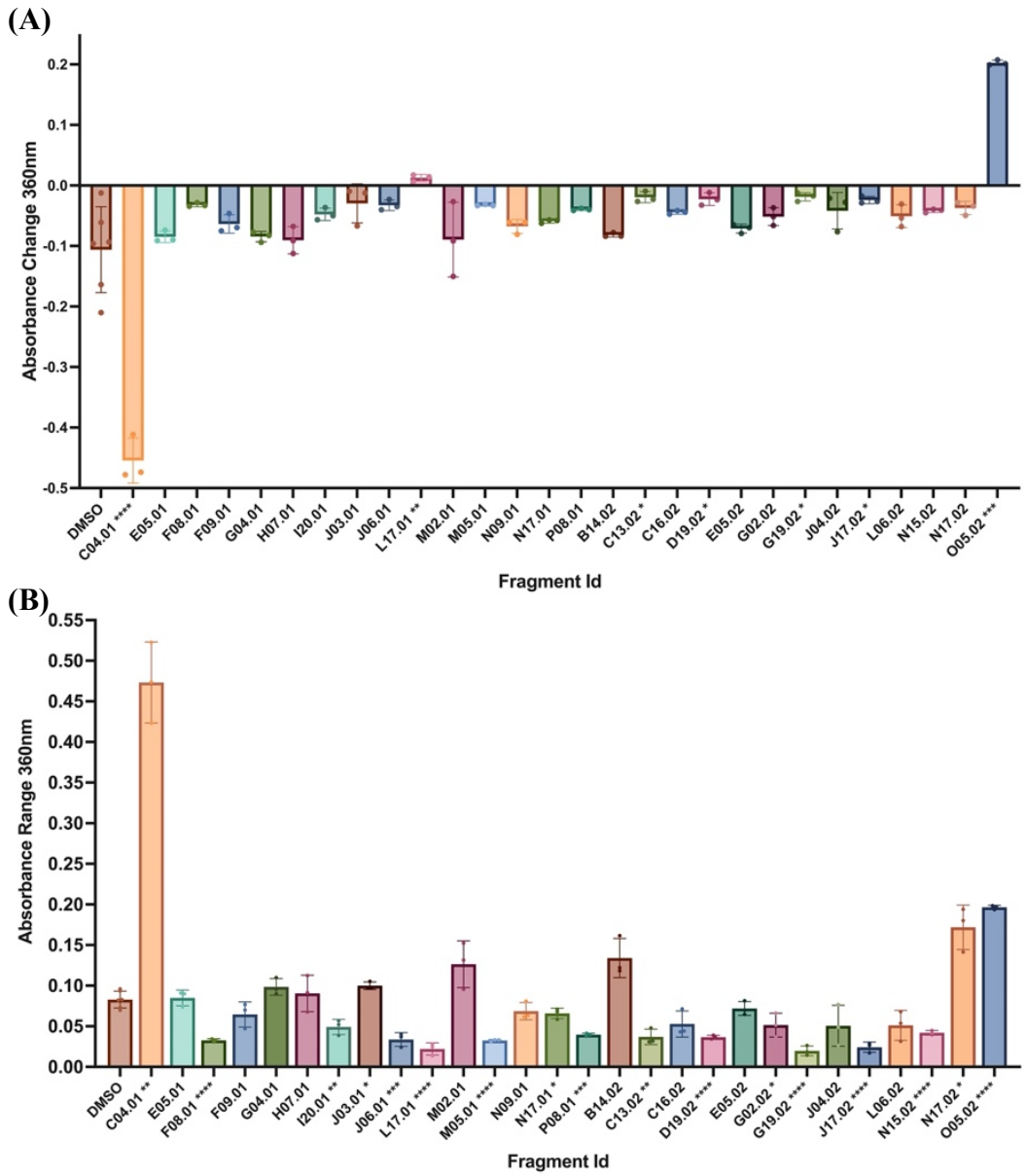

Figure 4. 16: Fragments interfered with the EDTA present within the assay

Fragments that had reduced activity of MurD in initial screening were tested for their effect on EDTA. (A) The absorbance change after the addition of assay components in the presence of fragments was determined. (B) The absorbance range after the addition of assay components in the presence of fragments was determined. All experiments were run in triplicate with mean results being plotted, with individual data points shown. Error bars show SD.

The final check carried out was to determine the effect the fragments had on the ability of PNP to convert phosphate to ribose-1 phosphate and MESG to methyl thioguanine to result in an absorbance change at 360 nm. As can be seen from **Figure 4.17**, fragments E05.01, F08.01, H07.01, M05.01, J17.02 caused statistically significant decreases in the absorbance change at 360 nm. A decrease in the absorbance change after the addition of PNP suggested that these fragments were

interfering with the coupling enzyme PNP, preventing it from being able to convert phosphate to ribose-1 phosphate and MESG to methyl thioguanine. Prevention of the conversion of MESG may have resulted in a decreased absorbance change which was used to determine activity of MurD, giving false positive readings of inhibition for these fragments. Due to their interference with PNP, the ability of these five fragments to inhibit the activity of MurD from *S. agalactiae* could not be determined within this assay system, and so were removed from further studies.

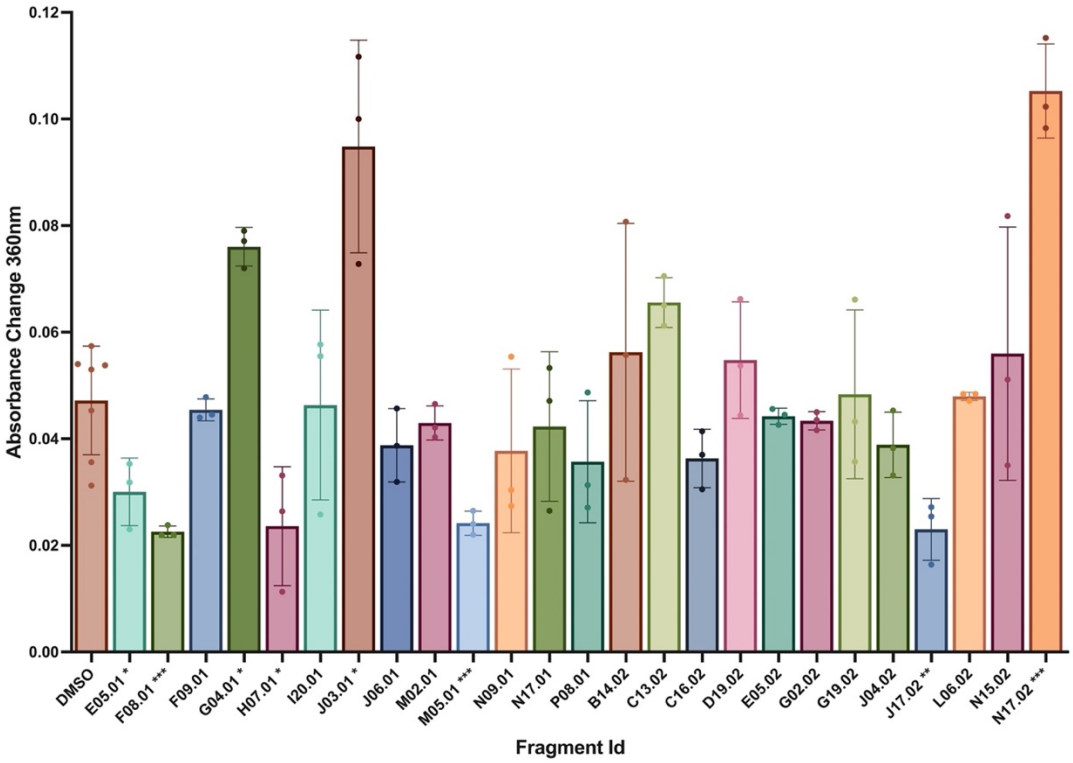

Figure 4. 17: Fragments interfered with PNP present in assay

Fragments that had reduced activity of MurD in initial screening were tested for their effect on PNP. Five fragments caused significant decreases in absorbance change compared to the control group. All experiments were run in triplicate with mean results being plotted, with individual data points shown. Error bars show SD.

3.12 Inhibitory fragments share similar binding features

Fragments that were able to reduce activity of MurD from *S. agalactiae* by 70% or more, and passed the assay interference checks were then analysed for similarity in structure and binding ability to MurD. As can be seen from **Table 4.3,** eleven

fragments contained a double ring structure similar to that of the adenine base of ATP.

Fragment Id	Fragment Structure	Percentage Activity of MurD
M02.01	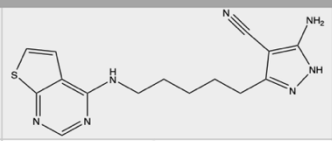	28%
N09.01	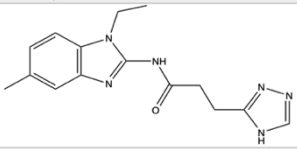	29%
G04.01	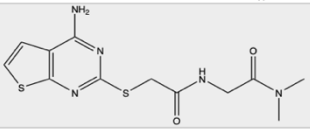	23%
J03.01	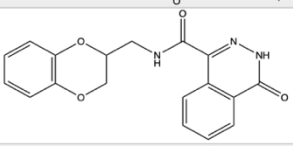	24%
J06.01	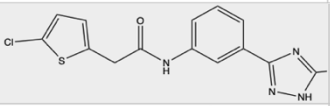	12%
P08.01	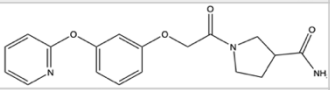	27%
F09.01	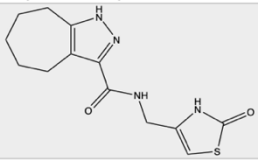	20%
N17.01	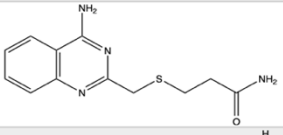	16%
I20.01	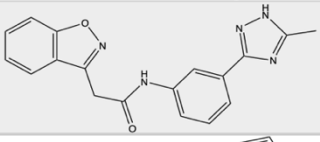	24%
G02.02	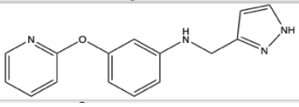	30%

Fragment Id	Fragment Structure	Percentage Activity of MurD
J04.02	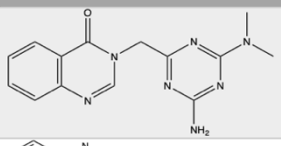	19%
E05.02	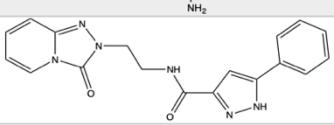	23%
L06.02	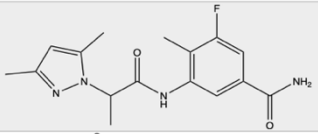	15%
C13.02	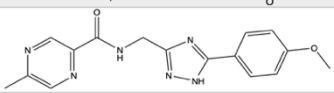	16%
B14.02	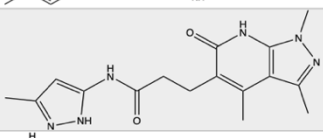	4%
N15.02	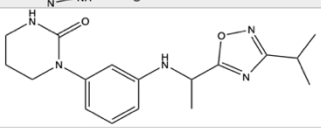	14%
C16.02	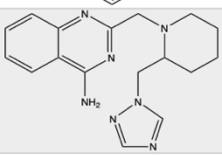	23%
N17.02	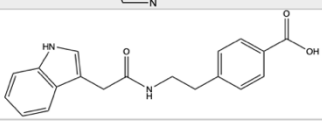	7%
D19.02	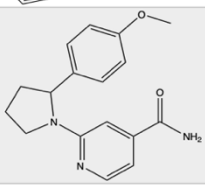	26%
G19.02	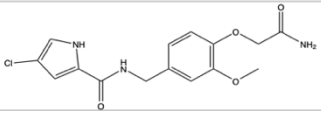	8%

Table 4. 3: Skeletal structures of inhibitory fragments

Skeletal structures of fragments that had reduced activity of MurD in initial screening and passed assay interference checks. Fragment ID, skeletal structure, and percentage activity of MurD are shown.

Seven of these fragments contain a five-membered ring structure attached to a six membered ring structure, with nitrogen present within the double ring structure. Comparison of the potential binding position of the fragments via VIDA showed that all inhibitory fragments have a nitrogen that has the potential to form

a hydrogen bond with the oxygen of Asn282 of MurD from *S. agalactiae* equivalent to Asn 271 of the *E. coli* enzyme. Eighteen fragments were predicted to be able to form hydrogen bonds to both the oxygen and nitrogen of Asn282 of MurD from *S. agalactiae*, with an example fragment in this binding mode shown in the predicted interaction in **Figure 4.18A**.

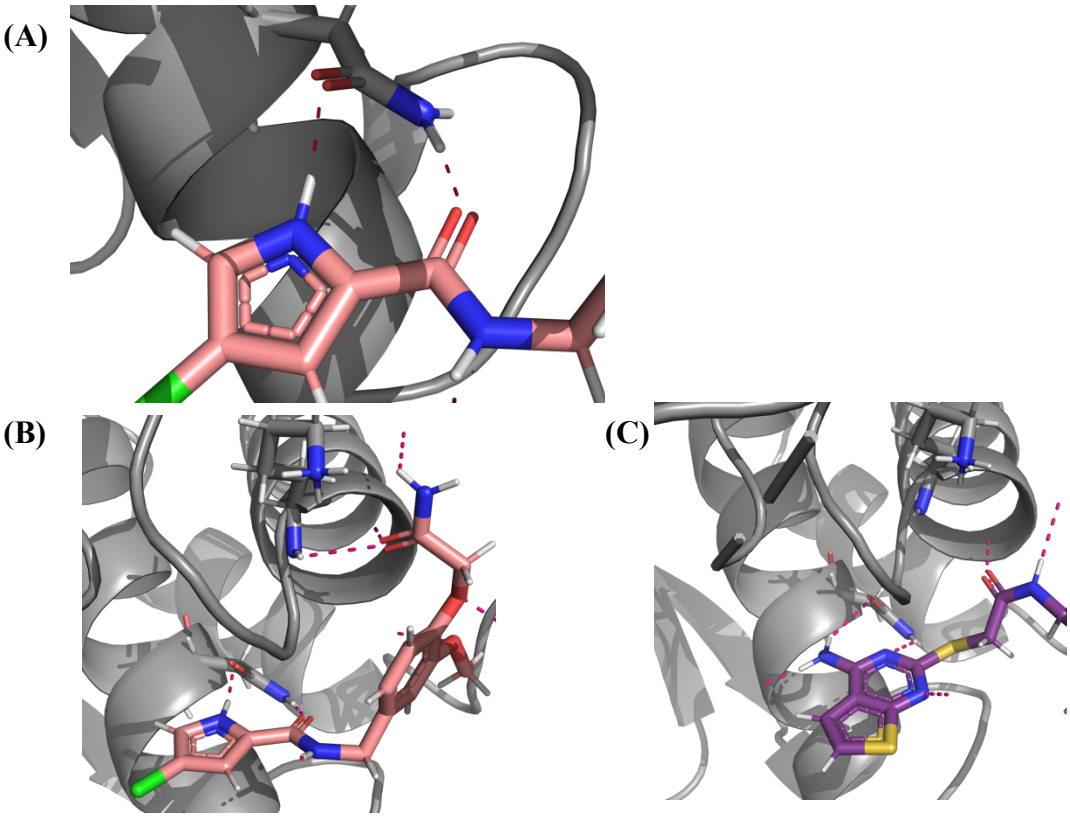

Figure 4. 18: Predicted binding of inhibitory fragments
The predicted binding of fragments that had reduced activity of MurD and passed assay interference checks was compared. Nitrogen is shown in blue, oxygen in red, sulphur in yellow and chloride in green. Polar contacts are shown in dotted red lines. (A) 18 fragments are predicted to be able to form hydrogen bonds with both the oxygen and nitrogen of Asn282. (B) Fragments were seen to kink towards the Lys123 involved in ATP binding. (C) Fragment G04.01 was the only fragment that is predicted to not kink towards the Lys123.

All inhibitory fragments, apart from G04.01, have a 'kink' within their structure, allowing them to potentially form interactions with the Lys123 (equivalent to Lys 115 of the *E. coli* enzyme) that interacts with the phosphate of ADP, as shown in the predicted interactions in **Figure 4.18B** and **Figure 4.18C**. The presence of these interactions may help provide information on why these fragments have inhibitory effects against MurD from *S. agalactiae*.

3.13 Identification of dual inhibitory fragments

The initial *in silico* screen was run against MurD from *S. agalactiae* and MurE from *E. coli*, with fragments identified as having the potential to be able to bind to both proteins. To determine if the fragments that had been identified as being able to reduce the activity of MurD from *S. agalactiae* by 70% or more were able to act as inhibitors of MurE as well, a stopped MESG assay was run in the presence of fragments against MurE from *S. agalactiae.* Fragments were incubated at a final concentration of 1 mM with 80 nM MurE from *S. agalactiae* prior to initiation of the activity assay. The activity rate of MurE in the presence of fragments was compared to a control assay where 10% ($^{v}/_{v}$) DMSO was added in place of a fragment, and the percentage activity of MurE in the presence of fragments relative to that in their

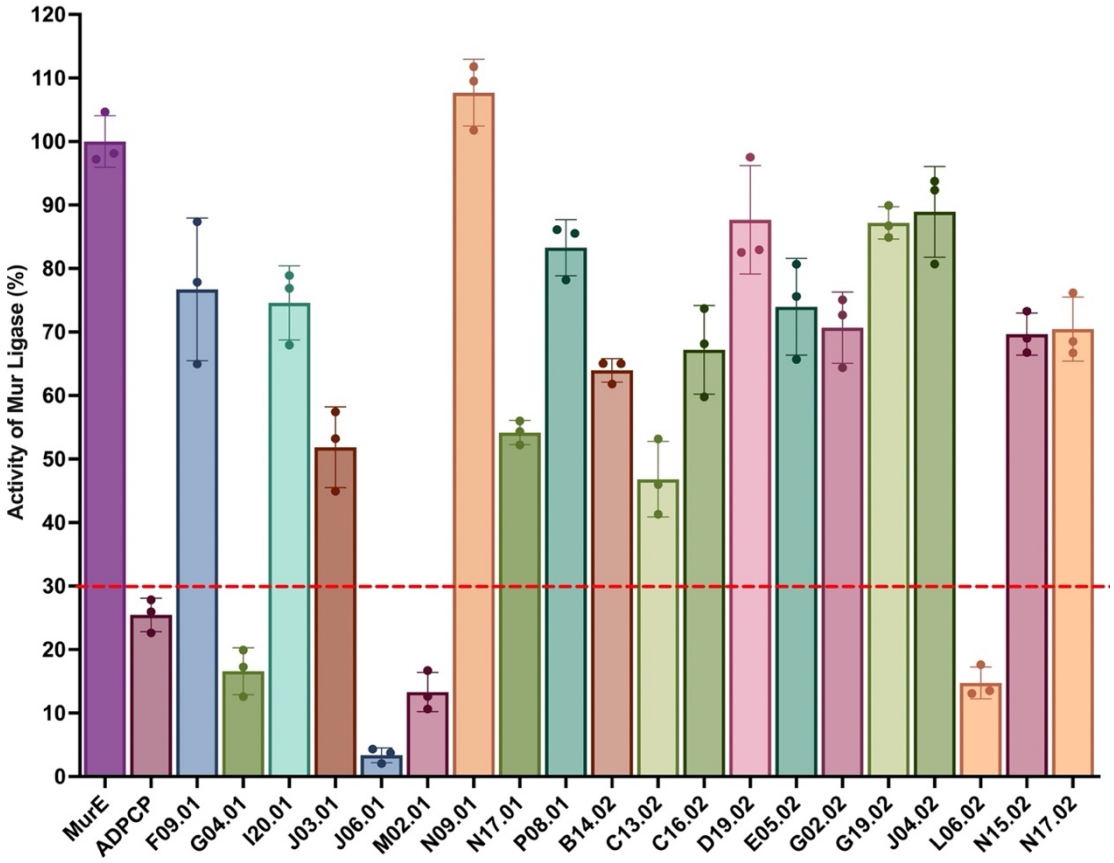

Figure 4. 19: Four fragments were able to inhibit the activity of MurE from S. agalactiae
Fragments that had reduced activity of MurD in initial screening were tested for their effect on MurE from *S. agalactiae*. Four fragments were able to reduce activity of MurE from *S. agalactiae* by 70% or more. All experiments were run in triplicate with mean results being plotted, with individual data points shown. Error bars show SD.

absence was determined, as shown in **Figure 4.19**. A positive control inhibitor of ADPCP at 5 μM was also used to confirm inhibition within the assay system. As can be seen in **Figure 4.19**, four fragments were able to reduce the activity of MurE from *S. agalactiae* by 70% or more. Fragment J06.01 was able to reduce activity by over 90%, with fragments G04.01, M02.01 and L06.02 able to reduce activity of MurE from *S. agalactiae* by around 80% or more. These four fragments were considered to be able to act as dual inhibitory fragments due to their ability to inhibit the activity of both MurD and MurE from *S. agalactiae.*

4. Conclusions and Future Direction

4.1 Targeting the ATP-binding site for antibacterial development

Within the initial stages of fragment screening, a specific region within the protein of interest can be selected to be specifically targeted by the fragment screen [116,117]. The ATP-binding site of Mur ligases was specifically targeted via the *in silico* fragment screen to allow for the potential of developing multi targeting inhibitors. The ATP-binding site within the Mur ligases was seen to have a high level of structural similarity, as well as having a high degree of sequence similarity across the four Mur ligases and across bacterial species. This level of similarity may allow for the development of a multitargeting inhibitor.

The ATP-binding site of bacterial enzymes was not considered in the development of new antibacterial compounds for many years due to the belief that inhibitory compounds would not be able to outcompete the ATP present within the bacterial cell [118]. Human cells contain an equivalent amount of ATP as to that found within bacterial cells, and so the emergence of protein kinase inhibitors, which mostly act upon the ATP-binding site of kinases within humans led to a change in that belief [118].

Due to their ability to target the ATP-binding site of kinases, protein kinase inhibitors have been used as the template for the design of novel inhibitors targeted towards the ATP-binding site of other proteins. Triola et al took a similar approach to our study, determining a similarity that existed between the ATP-binding site of kinases and D-Ala-D-Ala ligases, allowing them to use protein kinase inhibitors as scaffolds for the development of ATP competitive inhibitors with K_i*s* of 60 μM against D-Ala-D-Ala ligase[119]. Protein kinase inhibitors have also been used as the basis for the development of inhibitors targeted towards the Mur ligases. Hrast et al used a protein kinase inhibitor set within biochemical assays to identify a kinase inhibitor that was also able to act as a D-Glu competitive inhibitor of MurD with a K_i of 65 μM [102]. The use of kinase inhibitors as the basis for the fragment screen provides a solid foundation for the development of an inhibitory compound that has the potential to bind to the ATP-binding site of the Mur ligases, and potentially act in a competitive manner.

4.2 Use of *in silico* screens for fragment identification

In silico screening can act as a useful tool to provide an initial starting point for the development of inhibitory fragments [116,117]. *In silico* screening allows for the testing of large volumes of fragments without the requirement for protein crystals. Within our testing, 40,000 fragments were screened for their ability to bind to the Mur ligases. Much larger volumes of fragments can be tested though, with Azam et al testing 1.6 million fragments to identify potential hits against MurD from *Sta. aureus*[116].

However, certain limitations are present within the process of *in silico* screening. Use of the LigPrep software from Glide to generate a fragment library can lead to the docking of unnatural tautomers, due to the software considering different tautomers, sterochemistries and ring conformations when generating fragments [114]. Other limitations, such as flexibility within the backbone of the fragments can also lead to inclusion of fragments within the hits that are unlikely to be able to act effectively as inhibitors [120]. Limitations within the software can be mitigated against via the docking process but cannot be eliminated entirely and so fragment results require further screening before biochemical testing can be carried out.

4.3 Role of multi-targeting inhibitors within novel antibacterial compound design

Of the twenty fragments identified as having inhibitory effects against MurD from *S. agalactiae*, four were seen to have dual inhibitory effects, reducing the activity of MurE from *S. agalactiae* by 80% or more. These four fragments are good initial starting points, but further biochemical testing is required to determine if the fragments can target multiple Mur ligases across multiple bacteria. The ability of an inhibitory fragment to target multiple Mur ligases is essential for the development of a multitargeted antibacterial compound [73]. Development of a multitargeted antibacterial compound is becoming considered a better option for future drugs due to the reduced emergence of antibacterial resistance compared to single target drugs [121]. Due to their similarity in structure and catalytic mechanism, multi-targeted inhibitors against the Mur ligases are possible, and some have been

identified that are able to target the entire cascade of Mur ligases, with Hrast et al identifying inhibitors with IC_{50} values ranging from 157 μM to 39 μM across MurC-MurF of *E. coli* [102].

In order to continue to develop these fragments into multi-targeting compounds, the IC_{50} of these fragments against MurD and MurE from *S. agalactiae* would need to be determined to better understand the inhibitory effects of the fragments and their efficacy. Understanding the binding mode of these fragments would also need to be carried out to determine if these fragments are binding in a competitive manner to ATP. **Chapter 5** details further biochemical testing carried out on these inhibitory fragments.

Chapter 5

Identification of multitargeting inhibitors via a fluorometric assay

1. Introduction and Aims

In order to identify inhibitory fragments, biochemical testing is required. High throughput screening of fragments can be costly and time consuming. In **Chapter 2,** a stopped MESG assay was developed to reduce the time and cost involved in high throughput assay screening compared to a continuous assay of the same nature. However, limitations remained with this assay system that could be overcome with a different assay system, including the effect of natural absorbance of fragments at A360 and volume of fragment required for testing.

In the presence of hydrogen peroxide, amplex red can be converted to resorufin via HRP which can be coupled to the production of phosphate via PNP and Xanthine Oxidase [122], allowing it to act as a Mur ligase activity assay system. An amplex red assay can be followed spectrophotometrically at 555 nm or fluorometrically at 545 nm excitation and 585 nm emission wavelengths.

This chapter describes the optimization of an amplex red assay for use with Mur ligases for determining inhibition within an absorbance and fluorometric assay. Development of a stopped amplex red assay was then attempted. A continuous amplex red assay was used for the determination of the IC_{50} values of dual inhibitory fragments previously identified in **Chapter 4**, after which the mode of fragment inhibition was investigated.

2. Materials and Methods

2.1 Amplex Red assay

Mur ligase activity within an amplex red assay was confirmed. The amplex red assay was carried out in either a Cary 100 spectrophotometer at a total reaction volume of 200 μL at 37°c where absorbance was followed at 555 nm, or within a Varioskan Flash plate reader at 37°c at a total reaction volume of 10 μL. Fluorometric tracking was carried out at an emission of 545 nm and excitation of 585 nm. The reaction mixture contained the following components (final concentrations): 50 mM MOPs (pH 7.6), 10 mM $MgCl_2$, 2.5 U per mL PNP, 500 μM Inosine, 50 μM Amplex red, 25 U/mL Horse radish peroxidase (HRP), 1.25 U/mL Xanthine Oxidase, 100 μM ATP, 500 mM L-Lys, 50 μM UDP-MurNAc-L-Ala-D-Glu and 20 nM Mur ligase. To determine dependence on substrate, all components apart from one substrate were added and mixed and a background rate was determined. The substrate was added to start the reaction and the reaction was followed. The IC_{50} value for ADPCP was determined using this assay. ADPCP was added to the component mixture before the recording of the background rate of the reaction. Investigation into a stopped assay was carried out using this assay, with the $MgCl_2$ concentration decreased to 2 mM. All components were added barring one substrate, before the background rate was determined. Activity was initiated via the addition of a substrate and the initial rate period of the assay was allowed to proceed before 10 mM EDTA was added to the reaction. The assay was then allowed to proceed to allow determination of rate after addition of EDTA.

2.2 Amplex Red assay for IC_{50} determination and binding mode determination

Fragments were biochemically tested for IC_{50} determination via a continuous amplex red assay run using a Varioskan Flash plate reader. In a final volume of 10 μL, various concentrations of fragment were incubated with the relevant concentration of Mur ligase, in the presence of 50 mM MOPs (pH 7.6), 10 mM $MgCl_2$, 2.5 U per mL PNP, 500 μM Inosine, 50 μM Amplex red, 25 U/mL HRP, 1.25 U/mL Xanthine Oxidase and the relevant substrates without an amino acid for 10 minutes. The assay was then initiated with the relevant amino acid and allowed to

run past the initial rate period. A background absorbance was determined fluorometrically via the Varioskan plate reader (ThermoFisher) at 545 nm and 585 nm before the relevant amino acid was added. Fluorescent change was followed to allow the initial rate to be determined. The fluorescent change during the initial rate period was then determined. Each fragment concentration was run in triplicate in the presence and absence of the Mur ligase to determine background rate. Background rates were removed from the final activity rate for each fragment. The activity rate in the presence of fragment was compared to a control group of 10% $^{V}/_{V}$ DMSO. Assays were carried out at 37°c.

To determine the IC_{50} of fragments against MurD from *S. agalactiae*, 5 nM MurD was incubated with various fragment concentrations in the presence of 100 μM UDP-MurNAc-L-Ala and 15 μM ATP, before activity was initiated with 150 μM D-Glu. To determine the IC_{50} of fragments against MurE from *S. agalactiae,* 5 nM MurE was incubated with various fragment concentrations in the presence of 100 μM UDP-MurNAc-L-Ala-D-Glu and 20 μM ATP, before activity was initiated with 400 μM L-Lys. To determine the binding mode of J06.01, MurD was incubated with various fragment concentrations in the presence of 100 μM UDP-MurNAc-L-Ala and either 15 μM, 30 μM or 60 μM ATP, before activity was initiated with 150 μM D-Glu.

3. Results

3.1 Use of an amplex red assay to follow the activity of a Mur ligase

The amplex red assay can couple the activity of a Mur ligase reaction to a secondary coupling reaction via the formation of phosphate. In the same manner as the MESG coupled assay, the free phosphate formed during the Mur ligase reaction can be converted to ribose 1-phosphate via the actions of PNP. However, instead of acting upon MESG to convert it to 2-amino-6-mercapto-7-methylpurine, the PNP acts upon inosine to form hypoxanthine, as seen in **Figure 5.1.**

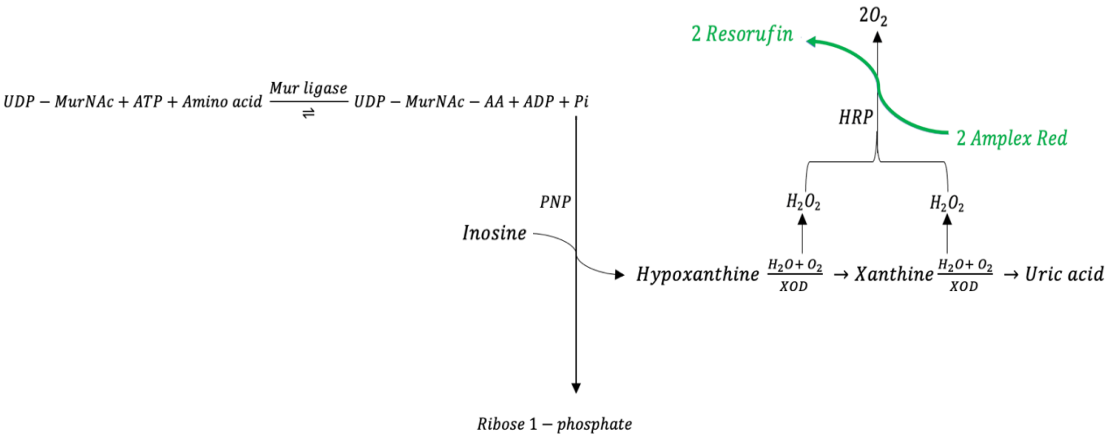

Figure 5. 1: Diagram to show the coupling reaction within an amplex red assay

The Mur ligase reaction results in the conversion of ATP to ADP and Phosphate. This free phosphate can be converted to ribose 1-phosphate via PNP, which also converts inosine to hypoxanthine. Hypoxanthine is converted to xanthine then uric acid by xanthine oxidase, generating hydrogen peroxide as a by-product. The hydrogen peroxidase can be converted to oxygen via HRP acting upon Amplex red to form resorufin. The accumulation of resorufin can be spectrophotometrically or fluorescently monitored, which can be equated to the activity of the Mur ligase during the initial rate period of the Mur ligase reaction.

The hypoxanthine generated via PNP acting upon inosine can be converted to xanthine and uric acid via xanthine oxidase. Hydrogen peroxidase is generated during this reaction and reacts with amplex red in a reaction catalysed by HRP to form resorufin [122], as seen in **Figure 5.1**. Resorufin has excitation and emission maxima of ~545 and 585 nm, allowing its production to be followed either spectrophotometrically at 555 nm or fluorometrically. An increase in absorbance or fluorescence corresponds to the conversion of amplex red to resorufin, which is taken to be twice the production of phosphate during the initial rate period of the Mur ligase reaction, thus allowing the following of the activity of the Mur ligase.

The amplex red assay was considered as an alternative to the MESG assay for several reasons. The amplex red assay follows the activity of the Mur ligases spectrophotometrically at 555 nm, while the MESG assay follows activity at 360 nm. Due to their composition, fragments may cause interference at lower wavelengths. The increase in wavelength of the amplex red assay should reduce the impact of this phenomenon. Spectrophotometrically, by virtue of the 4.7 times greater extinction coefficient of the amplex red assay relative to the MESG assay, it is intrinsically more sensitive to the presence of phosphate. Furthermore, the fluorescence properties of the amplex red product, resorufin, enables the assay to be performed at low volume because the assay depends upon emitted light, removing the impact of pathlength.

In order to determine if an amplex red assay could be used as a better biochemical assay for high throughput screening of fragments targeted towards the Mur ligases, the ability of the assay to follow the activity of MurE from *S. agalactiae* was determined both spectrophotometrically and fluorometrically. The sensitivity of the assay to inhibition was then determined via a positive control inhibitor and the determination of the Z prime score.

3.2 Activity of MurE within an amplex red assay is dependent on substrates being present

In order to establish whether an amplex red assay could be used for high throughput screening of the Mur ligases, the ability of the assay to follow the Mur ligase activity had to be established. The Mur ligases require the presence of three substrates to be active: the UDP intermediate, a nucleotide, and an amino acid. To determine whether the presence of all substrates was required for the activity of the Mur ligases within the amplex red assay, the assay was run with one substrate omitted on a spectrophotometer. The absorbance change was then followed and the omitted substrate introduced. As can be seen from **Figure 5.2**, no activity was seen within the assay until all substrates were present showing that within an amplex red assay, all substrates must be present for activity of the Mur ligases.

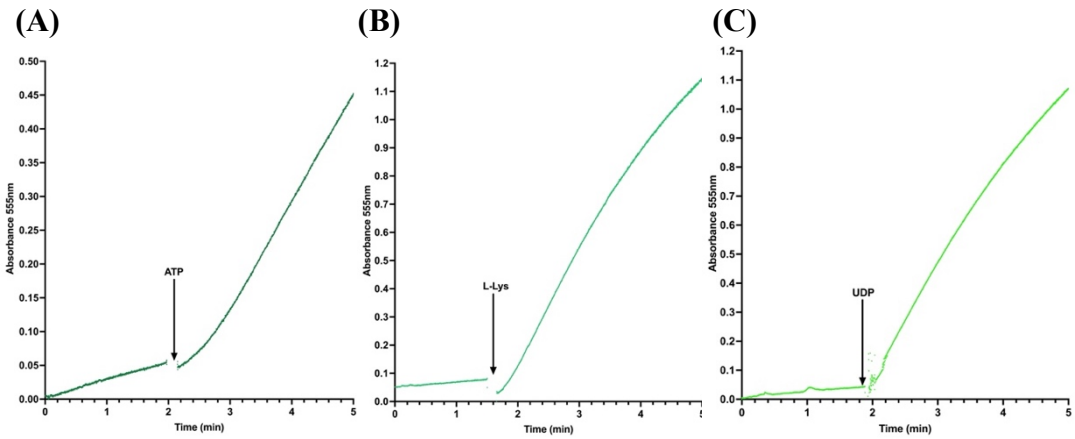

Figure 5. 2: The activity of S. agalactiae MurE relies on the presence of all three substrates

The activity of MurE was followed using an amplex red assay. All components of the assay were incubated at 37^0c barring one substrate which was added after 1 minute. No activity was seen within any of the assays until all three substrates were present. (A) ATP added after 2 minutes. (B) L-Lys added after 2 minutes. (C) UDP-MurNAc-L-Ala-D-Glu added after 2 minutes.

3.3 Amplex red assay is dependent on enzyme concentration

Within the amplex red assay, the absorbance change is dependent on the presence of phosphate. The Mur ligases generate phosphate when ATP is broken down into ADP and phosphate during the addition of an amino acid onto the UDP intermediate. The absorbance change of the amplex red assay should therefore be dependent on the concentration of the Mur ligase present. To confirm that this was the case, the enzyme concentration within the assay was varied and the initial rate determined using a Plate reader plate reader.

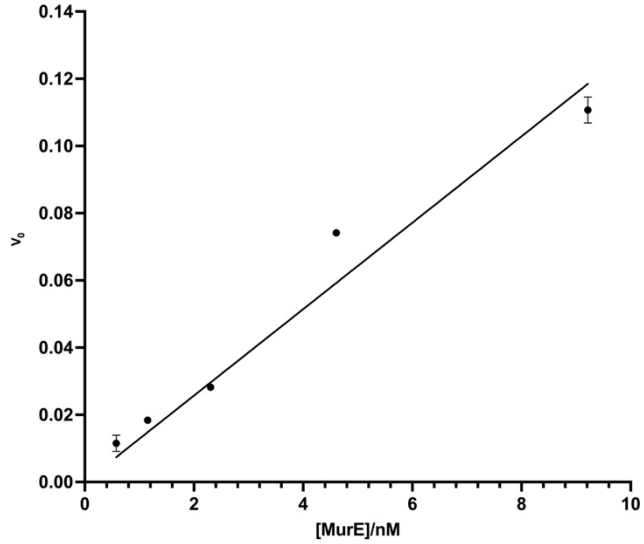

Figure 5. 3: Amplex red assay is dependent on Mur ligase concentration

The activity of *S. agalactiae* MurE was followed using an amplex red assay. The amplex red assay was run in the presence of various concentrations of MurE. The initial rate was determined and plotted against [MurE]. A linear relationship was seen. All data points were run in triplicate.

As can be seen from **Figure 5.3**, as the enzyme concentration was increased, the initial rate determined via the assay increased in a linear fashion. The amplex red assay was therefore dependent on the Mur ligase concentration within the assay, and so was able to track the activity of the Mur ligase.

3.4 Activity of MurE is dependent on presence of all substrates within a fluorometric amplex red assay

Within the amplex red assay, the product resorufin is produced from amplex red. Resorufin can be followed spectrophotometrically at 555 nm but can also be followed fluorometrically. Fluorometric assays have higher sensitivity than photometric assays, and so would be more ameanable for the detection of inhibition via fragments within high throughput screening.

In order to determine if the amplex red assay could be used fluorometrically for high throughput screening of fragments against the Mur ligases, the ability of the assay to follow the activity of the Mur ligases had to be established. Once again, the dependence of the assay on the presence of all three substrates was determined by running the assay with one substrate omitted before adding the latter and following the fluorometric change via a Plate reader. As can be seen from **Figure 5.4**, all three substrates were once again required for activity of the Mur ligase within the assay, showing that the amplex red assay in fluorometric form was able to follow the activity of the Mur ligase.

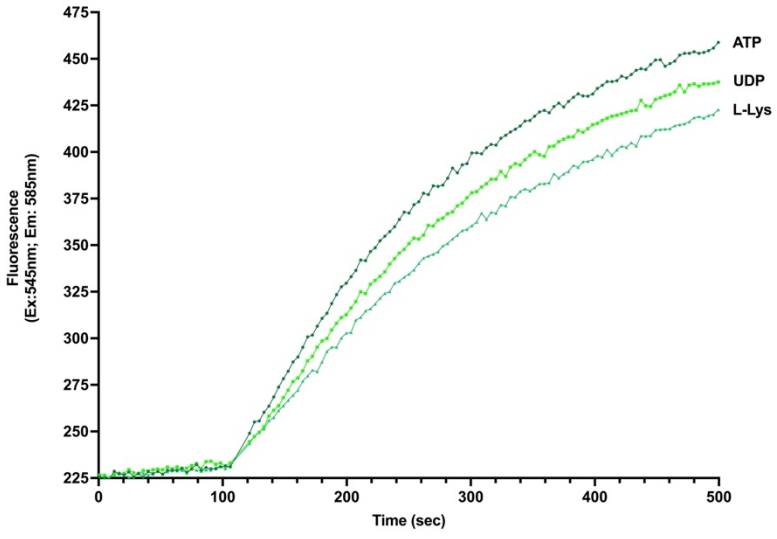

Figure 5. 4: Fluorometric amplex red assay is dependent on presence of all substrates

The activity of MurE was followed fluorometrically using an amplex red assay. All components barring one substrate were incubated before the final substrate was added. No activity was seen within any of the assays until all substrates were present.

3.5 Fluorometric amplex red assay is sensitive to inhibition via ADPCP

To be able to use the amplex red assay within high throughput screening of inhibitory fragments against the Mur ligases, the assay must be able to determine inhibition of the Mur ligases. ADPCP had previously been shown to act as an inhibitor of the Mur ligases, as well as previously being used as a positive control inhibitor of the Mur ligases within high throughput screens. To confirm the ability of the amplex red assay to identify Mur ligase inhibitors, and confirm ADPCP could still act as a positive control inhibitor of the Mur ligases within an amplex red assay, the determination of an IC_{50} of ADPCP against MurE from *S. agalactiae* was attempted. As can be seen from **Figure 5.5**, ADPCP was able to inhibit the activity of MurE within the amplex red assay.

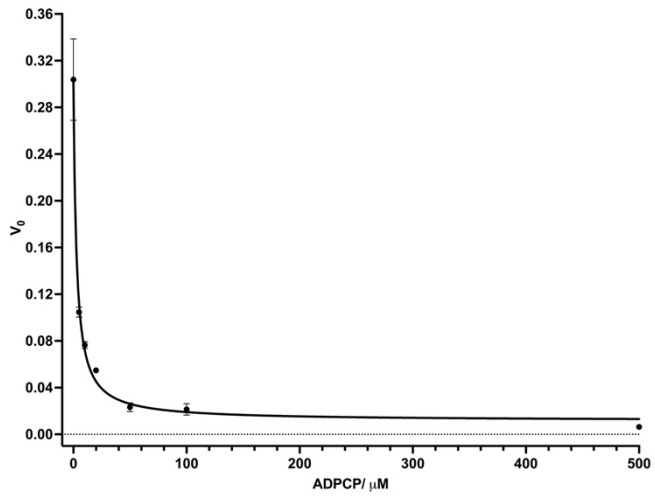

Figure 5. 5: ADPCP has an IC_{50} of 2.67μM against MurE within an amplex red assay

The IC_{50} of ADPCP for MurE from *S. agalactiae* was determined using an amplex red assay. The initial rate of MurE in the presence of various concentration of ADPCP was determined. The V_0 was determined and plotted against [ADPCP]. An IC_{50} of 2.67 μM was determined. All data points were run in triplicate.

ADPCP was seen to have an IC_{50} of 2.67 $^{+}/_{-}$ 0.7 μM against *S. agalactiae* MurE, which was not statistically different to the IC_{50} value previously seen for ADPCP against *S. agalactiae* MurE within a stopped MESG assay (**Supplementary 3**), allowing ADPCP to be effective as a positive control inhibitor against MurE within an amplex red assay.

To determine how effective the amplex red assay was at identifying inhibition, the Z prime score was determined. To determine the Z prime score of the amplex red assay, the initial rate for MurE from *S. agalactiae* in the presence and absence of ADPCP at its IC_{50} value were compared across 10 repeats. The mean value and

standard deviations were determined, to allow the determination of the Z prime score, as seen in **Table 5.1**. A Z prime score of 0.84 was seen when ADPCP was at its IC_{50} value within the amplex red assay, indicating that the activity assay could identify inhibitors accurately.

	MurE	MurE + ADPCP
Mean	0.24894	0.1276
Standard Deviation	0.00222	0.00423
Z prime Score	$Z = 1 - \frac{(3(0.00222) + 3(0.00423)}{(0.24894 - 0.1276)}$ $Z = 0.84$	

Table 5. 1: Determination of the Z prime score for ADPCP within an amplex red assay against MurE from S. agalactiae

The Z prime score was determined by calculating the mean V_0 for MurE in the presence and absence of ADPCP, along with the standard deviation of the means. The Z prime was then calculated. A Z prime score of 0.84 was determined for ADPCP against MurE from *S. agalactiae* within an amplex red assay.

3.6 Stopped activity assay

Development of a stopped MESG assay was previously carried out to reduce the time taken to complete a high throughput screening of inhibitory fragments against the Mur ligases and the amount of data that was required to achieve this goal. These issues are consistent with all continuous assays being used for high throughput screening, and so the development of a stopped amplex red assay was considered.

3.6.1 EDTA is unable to quench the reaction sufficiently

In **Chapter 2**, it was seen that within a stopped MESG assay, EDTA was able to quench the Mur ligase reaction within the initial rate stage, to allow the secondary reaction to be uncoupled from the Mur ligase reaction. To determine if EDTA could be used to uncouple the secondary reaction from the Mur ligase reaction within a stopped amplex red assay, the amplex red assay was run for the initial rate stage before 10 mM EDTA was added. As can be seen from **Figure 5.6**, after the addition of EDTA, the reaction rate was decreased but did not plateau. EDTA and EDTA in

complex with Mg do not absorb at 555 nm and so further investigations were required to determine why a plateau in absorbance was not achieved after the addition of EDTA.

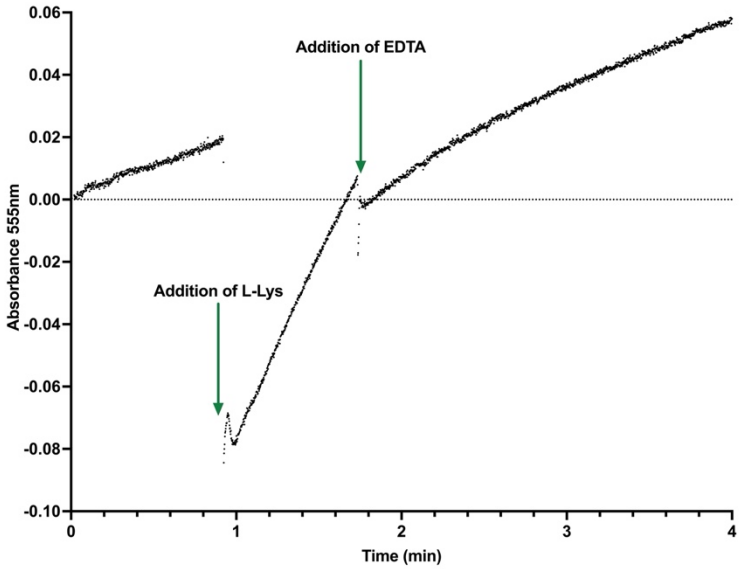

Figure 5. 6: EDTA is unable to quench the reaction within an Amplex red assay

To uncouple the secondary reaction from the Mur ligase reaction, a stopping agent is required. The amplex red assay was run, and EDTA was added after the initial rate stage. No plateau in rate was seen, meaning EDTA was unable to quench the reaction effectively for a stopped assay.

One reason why a plateau was not observed after the addition of EDTA could be due to EDTA interfering with the secondary coupling system. To determine if this was occurring, the secondary coupling system was run in the presence and absence of 10 mM EDTA at a set phosphate concentration. As can be seen from **Figure 5.7A**, in the presence of 10 mM EDTA the reaction rate of the secondary coupling system was increased, suggesting that EDTA was interfering with a component within the secondary coupling system.

To further determine what effect EDTA was having on the secondary coupling system, the absorption at 555 nm of the components of the secondary coupling system in the absence of phosphate were followed in the absence and presence of EDTA. As can be seen from **Figure 5.7B**, the addition of EDTA caused a greater increase in absorbance at 555 nm. To determine which component of the secondary coupling system EDTA was interfering with, a sequential addition experiment of the secondary coupling components was carried out. In order to be able to see any absorbance change at the point of interference the secondary coupling components were added in reverse order, starting with amplex red. As can be seen from **Figure 5.7C**, it was after the addition of amplex red that an absorption

rate was seen, suggesting that EDTA was causing the conversion of amplex red to resorufin in the absence of phosphate.

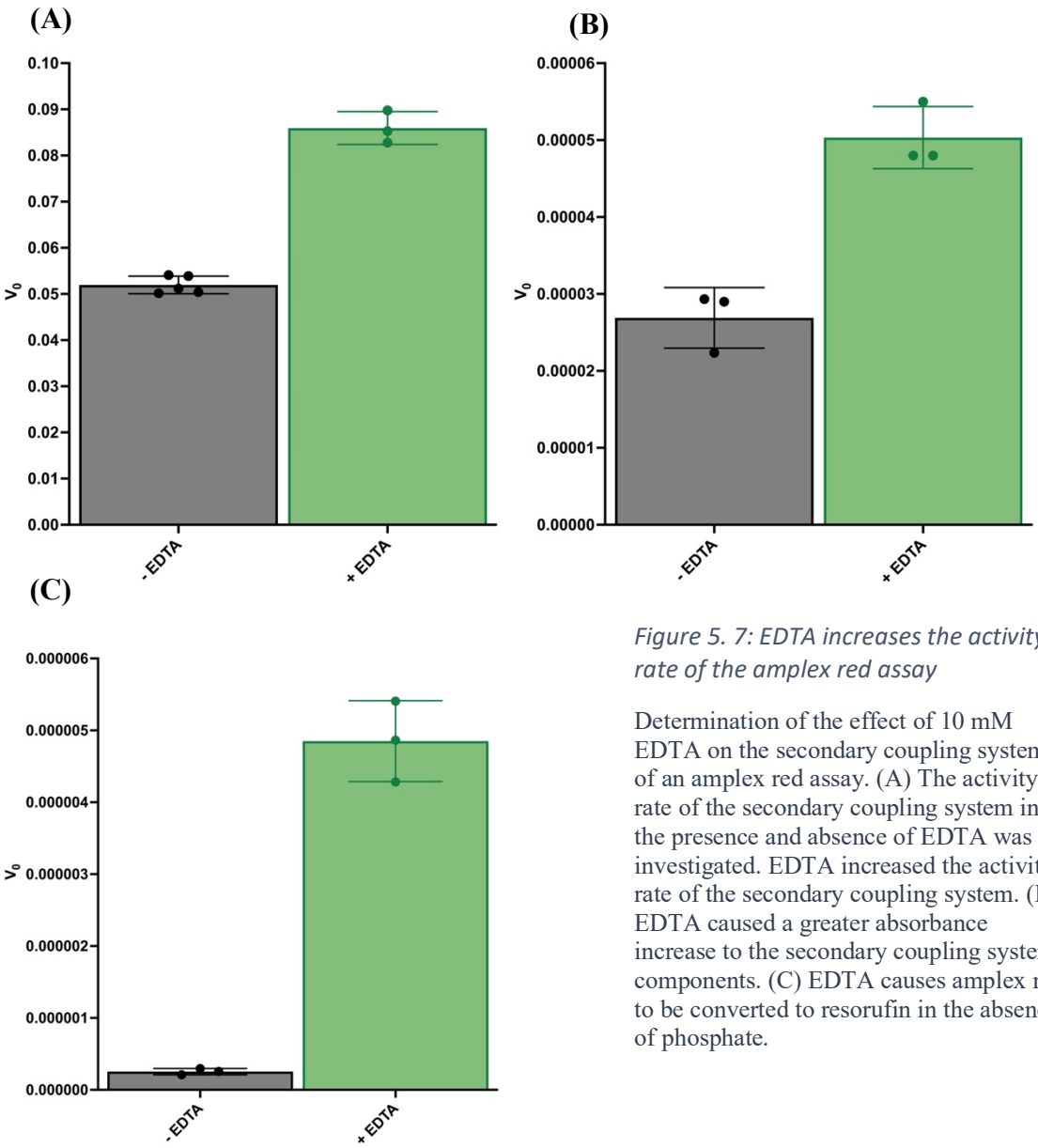

Figure 5. 7: EDTA increases the activity rate of the amplex red assay

Determination of the effect of 10 mM EDTA on the secondary coupling system of an amplex red assay. (A) The activity rate of the secondary coupling system in the presence and absence of EDTA was investigated. EDTA increased the activity rate of the secondary coupling system. (B) EDTA caused a greater absorbance increase to the secondary coupling system components. (C) EDTA causes amplex red to be converted to resorufin in the absence of phosphate.

As EDTA interfered with the secondary coupling system of the amplex red assay, EDTA could not be used to quench the Mur ligase reaction and allow for the uncoupling of the secondary reaction within an amplex red assay. This prevented the amplex red assay from being used for high throughput screening of fragments within this project. The amplex red assay could not be used for high throughput screening as a continuous assay as although the amplex red assay was able to be run at smaller final volumes than the MESG assay making it a cost-effective option,

the level of data analysis remained too high for high throughput screening. As the amplex red assay was able to effectively determine inhibition within a continuous assay system, had a Z prime score greater than that seen within the stopped MESG assay (**Chapter 2, Section 3.6.4.2**), and due to its increased sensitivity allowing it to be run at much smaller volumes than the MESG assay, the amplex red assay was an effective assay for the determination of the IC_{50} values of inhibitors previously identified within high throughput screens.

3.7 Screening of dual inhibitory fragments

Dual inhibitory fragments were previously identified against MurD and MurE from *S. agalactiae* using high throughput screening within **Chapter 4**. In order to better understand the inhibitory effects these fragments have on the Mur ligases, an amplex red assay was used to identify the IC_{50} values of these fragments against MurD and MurE from *S. agalactiae*, as well as try to better understand the binding mode of these fragments against MurD from *S. agalactiae*.

3.7.1 Identification of dual inhibitory fragments with micromolar IC_{50} values

Fragments J06.01, M02.01, G04.01 and L06.02 were identified to inhibit MurD and MurE from *S. agalactiae* at 1 mM concentration using a stopped MESG assay within **Chapter 4**. To develop a better understanding of the inhibitory potency of the fragments, dose response curves were generated to determine the concentration of fragment required to inhibit the activity of enzyme by half [100]. To determine the IC_{50} of the fragments, the amplex red assay was run at various concentrations of fragment against MurD and MurE from *S. agalactiae*. Previous work carried out by Dr Adrian Lloyd and Anita Catherwood identified no interference with the secondary components of the amplex red assay, apart from with J06.01 over 500 μM, allowing for the identification of IC_{50} values of these fragments using this assay system. The activity of the Mur ligase was determined in the absence and then presence of increasing concentrations of fragments, and the remaining activity, relative to that in the absence of fragment, was plotted against the log concentration of fragment.

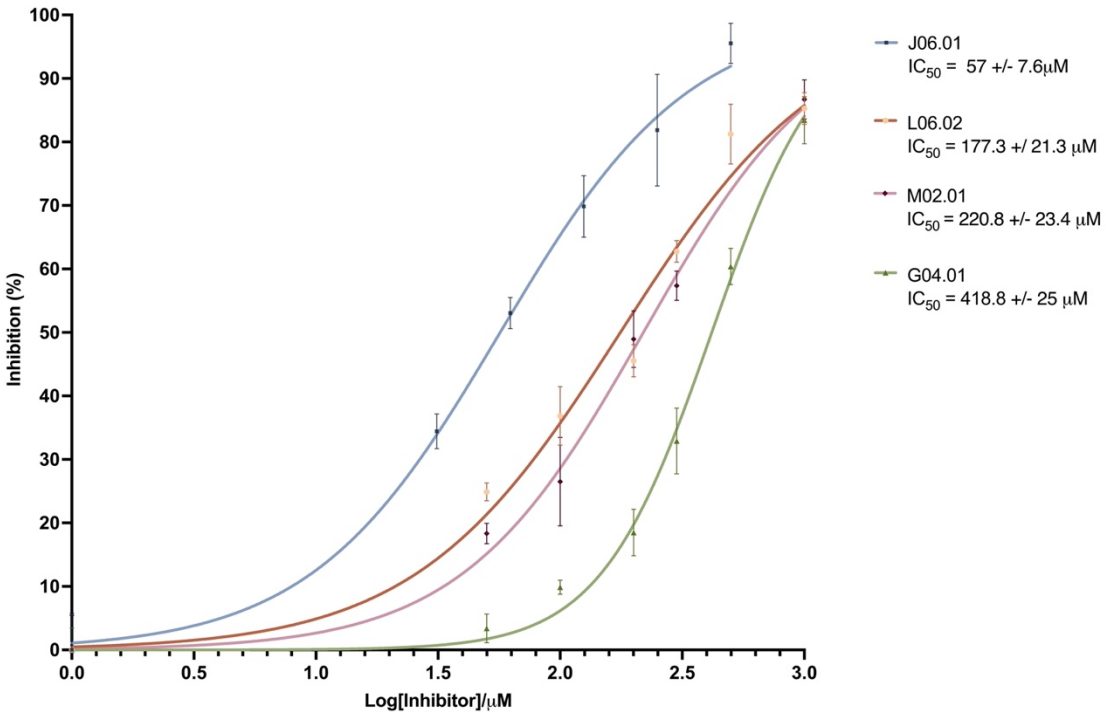

Figure 5. 8: IC_{50} determination against MurE from S. agalactiae

The IC_{50} of 4 fragments hits were identified using an amplex red assay. Various concentrations of fragment were incubated with MurE from *S. agalactiae* before activity of MurE was established. Activity was then plotted against log fragment concentration and the IC_{50} determined. All fragments were run in triplicate with a triplicate background rate being removed from the activity rate. The mean is plotted with error bars showing SD. A variable response curve was then plotted via PRISM.

As seen in **Figure 5.8**, the fragments IC_{50} values varied between 420 μM and 57 μM against MurE from *S. agalactiae*, with fragment J06.01 showing the greatest inhibitory effect, having an IC_{50} of 57 $^{+}/_{-}$ 7.6 μM. The fragments IC_{50} values were also varied against MurD from *S. agalactiae* with the fragments having IC_{50} values between 260 μM and 20 μM, as seen in **Figure 5.9**. J06.01 showed the greatest inhibitory effect against MurD as well, having an IC_{50} value of 21.6 $^{+}/_{-}$ 2.9 μM.

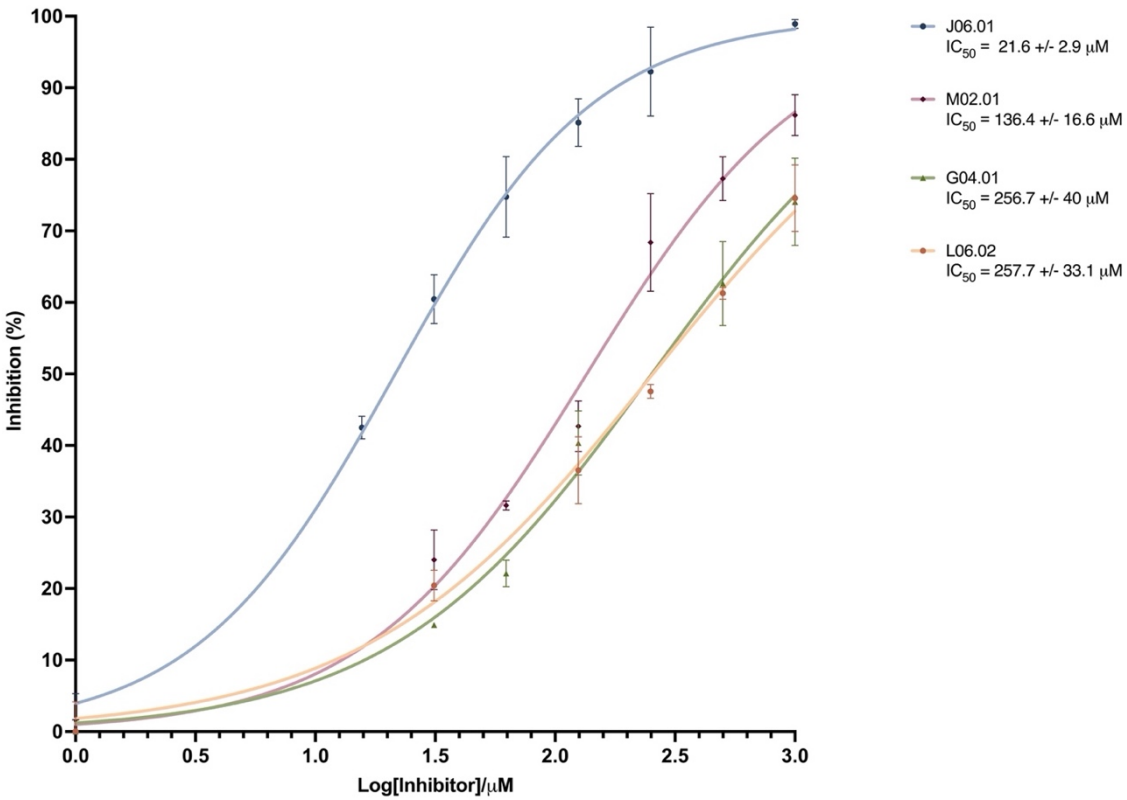

Figure 5. 9: IC_{50} determination against MurD from S. agalactiae

The IC_{50} of 4 fragments hits were identified using an amplex red assay. Various concentrations of fragment were incubated with MurD from *S. agalactiae* before activity of MurD was established. Activity was then plotted against log fragment concentration and the IC_{50} determined. All fragments were run in triplicate with a triplicate background rate being removed from the activity rate. The mean is plotted with error bars showing SD. A variable response curve was then plotted via PRISM.

3.7.2 J06.01 potentially binds to the ATP-binding site of Mur ligases

Fragments identified as having inhibitory effects against MurD and MurE from *S. agalactiae* were originally identified via *in-silico* screening which was targeted towards the ATP-binding site of the Mur ligases. J06.01 was identified as having an IC_{50} of 21.6 $^{+}/_{-}$ 2.9 μM and 57 $^{+}/_{-}$ 7.6 μM against MurD and MurE from *S. agalactiae* respectively, the lowest IC_{50} values of the identified dual inhibitory fragments. The binding mode of J06.01 was therefore investigated to determine if it was still targeting the ATP-binding site of the Mur ligases. To achieve this, IC_{50} determination was carried out using an amplex red assay at various ATP concentrations. As can be seen from **Figure 5.10**, as the ATP concentration increased, so did the IC_{50} for J06.01. The IC_{50} for J06.01 at 15 μM ATP was 21.6 $^{+}/_{-}$ 2.9 μM, whereas at 60 μM ATP the IC_{50} for J06.01 was 60.76 $^{+}/_{-}$ 40 μM. This suggests that J06.01 may be competing

with the ATP, and therefore is potentially binding within the ATP-binding site of the Mur ligases.

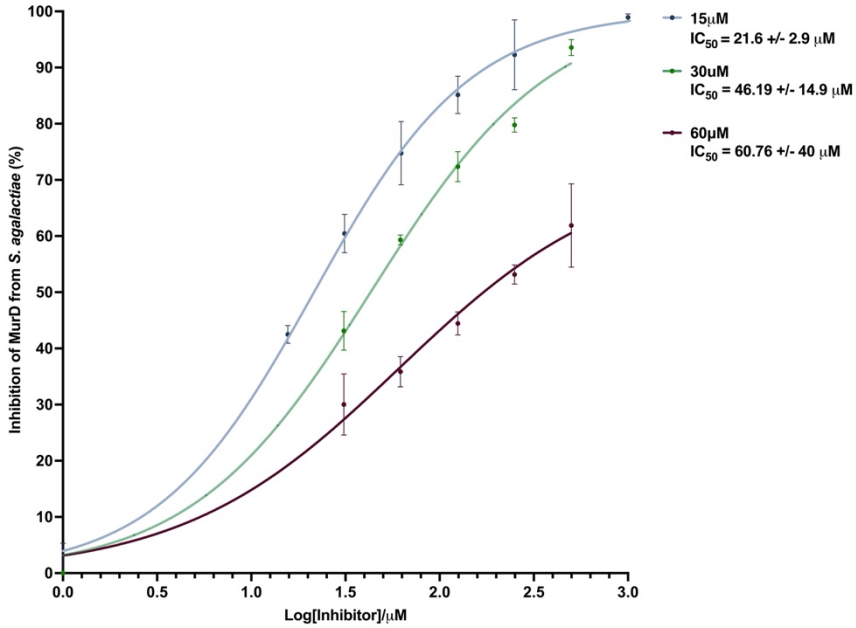

Figure 5. 10: The IC_{50} of J06.01 increases in the presence of increased ATP

The IC_{50} of J06.01 against MurD from *S. agalactiae* was determined in the presence of various concentrations of ATP. The initial rate of MurD was determined at various concentrations of J06.01 at three ATP concentrations. The initial rates were plotted against log J06.01 concentration and the IC_{50} determined. At higher concentrations of ATP, the IC_{50} of J06.01 increased.

If J06.01 is acting in a competitive manner with ATP, a K_i value for this fragment can be determined. The IC_{50} value for an inhibitor can vary based on enzyme and substrate concentration. To overcome this issue, the IC_{50} value can be related to the affinity of the inhibitor via an absolute inhibition constant, K_i [89]. The K_i value of J06.01 against MurD from *S. agalactiae* can be determined using the Cheng-Prusoff equation describing the relationship between IC_{50} and K_i for a simple competitive inhibitor [89]:

$$K_i = \frac{IC_{50}}{1+\frac{[S]}{K_m}}$$

where [S] is the fixed substrate concentration and K_m is the Michaelis constant. If J06.01 is acting in a competitive manner with ATP, then the K_m^{App} value for ATP (47.1 μM), the concentration of ATP used and the observed IC_{50} can be placed into the equation to allow for the computation of a K_i for J06.01. Using this equation

and the previously identified IC_{50} values, a K_i of 23.8 $^{+}/_{-}$ 18 μM can be determined for J06.01 against *S. agalactiae* MurD.

Potential interactions formed during the binding of J06.01 into the ATP-binding site of MurD from *S. agalcatiae* were predicted during the *in-silico* screen, and are shown in the predicted structure seen in **Figure 5.11**. As can be seen in the predicted binding in **Figure 5.11**, J06.01 has the potential to form three polar contacts within the ATP-binding site of MurD of *S. agalactiae*.

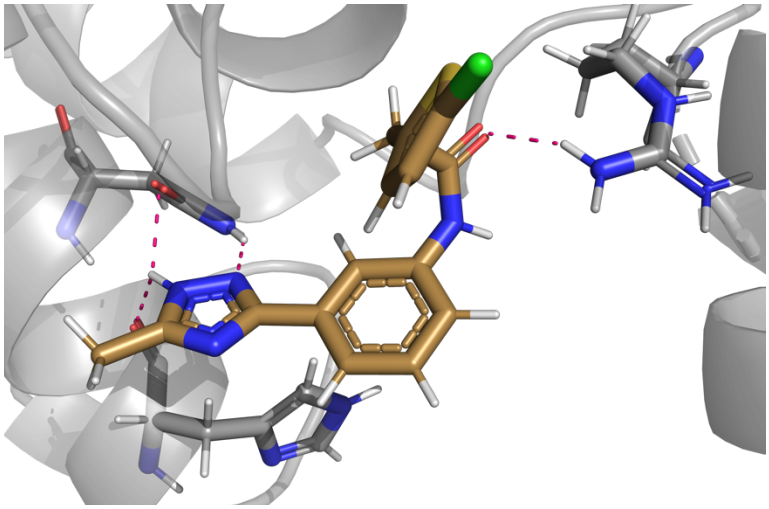

Figure 5. 11: Potential binding of J06.01 into the ATP-binding site of MurD from S. agalactiae

Potential binding location of J06.01 in the ATP-binding site of MurD of *S. agalactiae* based upon *in-silico* screening. Residues that form polar contacts with J06.01 are shown, with polar contacts shown in red. Chemicals are coloured according to standard Pymol schemes.

J06.01 has the potential to form a polar contact between a nitrogen within the pentose ring and the oxygen of His278, along with the oxygen of Asn282. Asn282 may also form a polar contact between its nitrogen and a nitrogen within the pentose ring of J06.01. J06.01 has the potential to 'kink' within the ATP-binding site towards the phosphate binding region, with the potential of an oxygen within J06.01 to bind with the nitrogen of Arg313.

4. Conclusions and Future Direction

4.1 Conversion of biochemical assays to a high-throughput assays

Many activity assays have been developed over the years to allow the activity of an enzyme to be followed [123]. The sensitivity of the assay and its ability to effectively follow the activity of the enzyme in the presence of an inhibitor can make an assay a better candidate for high throughput screening for inhibitory fragments [96]. An amplex red assay can effectively follow the activity of Mur ligases in the absence and presence of an inhibitor, and was shown to have a Z prime score of 0.8, consistent with other published assays used for the identification of inhibitors [93,94]. An amplex red assay is an attractive assay for high throughput screening due to its increased sensitivity compared to other absorbance assays, and its ability to be followed fluorometrically [96,101]. Its ability to be tracked fluorometrically removes the interference that coloured fragments exhibit in an absorbance assay [124], preventing as many false positive and false negative results during testing. However, fluorimetry does contain its own challenges for fragment screening, for example, fragment quenching of fluorescence can provide a real challenge to implementation of fluorescent assays. The amplex red assay has however previously been used in high throughput screening for the identification of NOX inhibitors [101].

Activity assays can either be run as continuous assays whereby the activity of the ligase is followed via a secondary reaction which is occurring concurrently with the activity assay, or via a stopped assay whereby the secondary reaction occurs after the activity assay. Stopped assays provide many benefits over continuous assays during high throughput screening; by reducing the amount of data analysis required by the scientist, removing the requirement for the secondary assay components to be present in excess and increasing the number of fragments that can be tested simultaneously. Sullivan et al used metal chelating agents to convert a continuous assay to a stopped assay to allow high throughput screening of inhibitors against purine biosynthesis enzymes [95]. In a similar fashion, EDTA was used to convert a continuous MESG coupled assay into a stopped MESG coupled assay within **Chapter 2**. However, EDTA interfered with the secondary coupling

system of the amplex red assay, preventing it from being useful as a stopping agent. Previously, Liu et al were able to use EDTA to quench Acetyl-Coenzyme A Carboxylases within a stopped amplex red assay [125]. EDTA was present in a high concentration, as within our stopped assays, but addition of amplex red was carried out after the addition of EDTA unlike within our assays. No interference with the assay system from the EDTA was mentioned within the study but absorbance readings were taken only after the addition of EDTA and amplex red [125].

Other stopping agents could be used to either quench the Mur ligase reaction or inhibit the activity of the secondary coupling system to allow the amplex red assay to be converted from a continuous assay to a stopped assay. One such agent is the Amplex Red Stop Reagent A33855, that can stop the assay via quenching of the HRP activity [126]. This reagent has been used to allow the enzymatic measurement of phosphatidic acid in cultured cells and determine the effect of a kinase inhibitor on levels of phosphatidic acid [127], and was present within the stopped assays used by Liu et al for high throughput screening of acetyl-coenzyme A carboxylase inhibitors [125]. This stopping agent has the potential to be able to convert the continuous amplex red assay to a stopped assay for high throughput screening of the Mur ligases.

4.2 Role of IC_{50} values in the determinations of the efficacy of novel inhibitory fragments

Within pharmacology IC_{50} values are used as a useful tool for measuring the potency and efficacy of an antagonist drug, as they describe the amount of substance required to reduce activity by 50% or more [100]. Determination of the IC_{50}s of the dual inhibitory fragments identified fragments with IC_{50}s ranging from 420 to 20 μM. Previous work by Hrast identified a kinase inhibitor that had IC_{50}s ranging from 368 to 59 μM against MurC-MurF from *E. coli* [102], suggesting that our dual inhibitory fragments are comparable to other kinase based Mur ligase inhibitors.

However, the IC_{50} value for an inhibitor can vary based on enzyme and substrate concentration, and so comparison between published IC_{50} data has its limitations. Within our study, the Mur enzymes were at 5 nM whereas Hrast et al did not reveal

the enzyme concentration employed and so a direct comparison of IC_{50} data is limited. To take substrate concentrations into account, the IC_{50} value can be related to the affinity of the inhibitor via an absolute inhibition constant, K_i [89], using the Cheng-Prusoff equation describing the relationship between IC_{50} and K_i for a simple competitive inhibitor [89]:

$$K_i = \frac{IC_{50}}{1+\frac{[S]}{K_m}}$$

Where K_i is the equilibrium constant of the dissociation of the inhibitor from the enzyme, [S] is the fixed substrate concentration and K_m is the Michaelis constant. J06.01 was seen to potentially be acting as a competitive inhibitor of MurD in respect to ATP, and had a K_i of 23.8 $^{+}/_{-}$ 18 μM. This value is similar to the K_i reported by Hrast et al for their compound that had mixed inhibition against ATP within MurD [102], suggesting that our dual inhibitory fragments are comparable to other kinase based Mur ligase inhibitors.

4.3 Repurposing old drugs for new purposes

J06.01 proved to be the most promising fragment identified within the screen, having dual inhibitory effects and the potential to bind to the ATP-binding site of MurD. Originally from an Enamine kinase inhibitor library, its ability to inhibit kinases will need to be investigated to determine its current level of specificity. Cross reactivity can be an issue when repurposing old drugs especially with protein kinase inhibitors as cross reactivity with a human kinase could lead to negative side effects of antibacterial compounds. Hrast et al eliminated a compound from their screen of kinase inhibitors due to its effect on human kinase activity [102]. One of the final steps taken by Le et al when repurposing human kinase inhibitors for antibacterial compounds against *Sta. aureus*was to confirm their lead compound possessed no affinity to kinases [128].

J06.01 has since been tested against other Mur ligases from different bacterial species and exhibits IC_{50} values of similar μM values. Due to its ability to inhibit multiple Mur ligases across multiple bacterial species, further development of

J06.01 needs to be carried out. Currently J06.01 has only been tested for its inhibitory effects against MurD and MurE; further testing against MurC and MurF would identify if J06.01 is able to target all the Mur ligases involved in the stepwise addition of amino acids. Crystallographic studies of J06.01 bound to MurD and MurE could confirm whether J06.01 is binding within the ATP-binding site of the Mur ligases and what residues are involved in this interaction. Understanding how J06.01 is binding to the Mur ligases could also provide a starting point for the development of J06.01 into a compound from a fragment [129], focusing on specificity for the Mur ligases over kinases and ability to cross the bacterial membrane.

Chapter 6

MurD and MurE from *S. agalactiae* form a binary complex

1. Introduction and Aims

Over the past 20 years, the Mur ligases have been the target of many drug discovery programmes. Inhibitory compounds targeted towards the Mur ligases have been identified, but virtually all lack the ability to act as an antibacterial agent. One hypothesis why inhibitory compounds are unsuccessful at targeting the Mur ligases *in vivo* is that the Mur ligases are forming a complex within the cytoplasm. Complex formation amongst the Mur ligases could prevent inhibitory compounds working *in vivo* either due to sequestering of intermediates or blocking of the site that the inhibitor is targeted towards. Determining if complex formation is occurring between the Mur ligases could give insight into how to design better inhibitory compounds in the future as well as potentially indicate how this part of the peptidoglycan pathway is regulated.

Biological evidence for potential complex formation among the Mur ligases can be found in the presence of a complex between the Mur enzyme MurT and GatD. MurT shares a similar C-terminal domain to the Mur ligases, which is required for complex formation with GatD [79]. Other biological evidence can be found in the presence of the fusion of the MurE and MurF proteins within *Bordetella pertussis*. A study by Laddomada and co-workers found that within *B. pertussis* the MurE and MurF proteins form a fusion protein with a 20 amino acid linker region. Once purified these proteins exist in a state that allows for activity of both proteins [83]. Further studies have been carried out to determine if the individual Mur ligases can form a complex, and if so what proteins are involved. A study by Dessen and co-workers investigating the Mur ligases from *T. maritima* concluded that the Mur ligase proteins are unable to interact with each other , but are able to interact with the structural protein MreB and the lipid 1 – glucosaminylating enzyme, MurG [81]. Interaction between the Mur ligases and MreB was also established by White and co-workers, who were able to show that the Mur ligases localised perpendicular to the long axis of the cell but only when MreB was present [80]. However, a more recent study carried out by Miyachiro and co-workers was able to identify direct interactions between the Mur ligase proteins in heterodimeric, binary complexes

from *S. pneumoniae* [82]. Analytical ultracentrifugation assays of MurC, MurD and MurF were able to identify binary globular compact complexes between all three pairings of proteins. This difference in interaction partners and the ability of the Mur ligases to directly interact with each other means it is still unknown if, or how a complex may be forming between the Mur ligases.

This chapter aimed to use a variety of experimental methods to determine if MurD and MurE from *S. agalactiae* are able to form a binary complex. Computational methods were then used to predict the ability of all the Mur ligase proteins from *E. coli* and *S. agalactiae* to form heterodimeric, binary complexes.

2. Materials and Methods

2.1 KEGG Database for Genomic Layouts

Using the KEGG Genome database, the genomes for *S. agalactiae, S. pneumoniae, T. martima, Caulobacter crescentus (C. crescentus)* and *B. pertussis* were identified. The genes identified for each bacterium were then searched for the location of the genes encoding the MurC, MurD, MurE and MurF proteins. Using the genome browser location facility, the exact location and surrounding genome sequences of each Mur ligase could be identified. The location of each Mur ligase gene within each genome was visualised using BioRender.

2.2 Cloning of MurE

2.2.1 Polymerase Chain Reaction

Manually designed DNA oligonucleotides were resuspended following the manufacturer's protocol (Integrated DNA Technologies). The reaction mixture contained the following components (final concentrations): 10 μM forward primer, 10 μM reverse primer, 250 μM dNTPs and 10 ng template DNA. *S. agalactiae* serotype V chromosomal DNA which was used as template DNA. Q5 DNA polymerase and reaction buffer (NEB) were used within the reaction mixture. Over a period of 30 cycles, a 30 second 95°C denaturing step was followed by a 30 second 55°C annealing step followed by a 72°C extension step. Extension length was determined for 1 minute per 1 kilobase of DNA. A final 10 minute extension was then carried out before samples were stored at 4°C.

2.2.2 Agarose Gel Electrophoresis

1% ($^{w}/_{v}$) agarose gels were prepared in TAE buffer, with GelRed Nucleic Acid Gel Stain (Biotium). PCR produced DNA was combined with 6x DNA loading dye (NEB) according to the manufacturer's instructions before being loaded onto the gel. A current of 100 V for 1 hour was applied to allow for separation. DNA was then visualised using a UV transilluminator.

2.2.3 Extraction of amplified DNA

Extraction of amplified DNA was carried out using a Gel Extraction kit (QIAGEN). DNA bands were removed from an agarose gel using a scalpel before DNA was extracted according to the manufacturer's instructions.

2.2.4 Restriction Digestion

Restriction digests of PCR products and plasmids were performed using the relevant restriction enzymes from NEB. Reaction mixtures contained plasmid DNA with restriction enzymes present a $1/10^{th}$ of the final reaction volume. Reactions were incubated at 37°C for 2 hours before DNA purification was carried out using a PCR purification kit (QIAGEN). DNA purification was carried out according to the manufacturer's instructions.

2.2.5 Restriction Cloning Ligation

Ligation mixtures contained approximately 50 ng of linearized vector along with 150 ng of purified DNA plasmid together with T4 DNA ligase (NEB) and ligation buffer. Reaction was incubated at room temperature overnight.

2.2.6 Transformation of Competent Cells

Transformation of chemically competent cells was carried out using NEB5 *E. coli* BL21 (DE3) and Top10 cells. Cryo-preserved competent cells were thawed on ice before being mixed with ligated DNA. Cells were incubated on ice for 30 minutes before being heat shocked via incubation at 42°C for 30 seconds. A further 5 minute incubation on ice was carried out before the cells were added to Super Optimal broth with Catabolite repression (SOC medium) to a final volume 10 times the original cell suspension volume. Cells were incubated at 37°C for one hour at 180 RPM before being plated on selective LB agar.

2.2.7 Construct Validation

Plasmid DNA constructs were verified via Genewiz sequencing. 80-100 ng of DNA was sent with relevant primers. Construct maps were then generated via Snapgene.

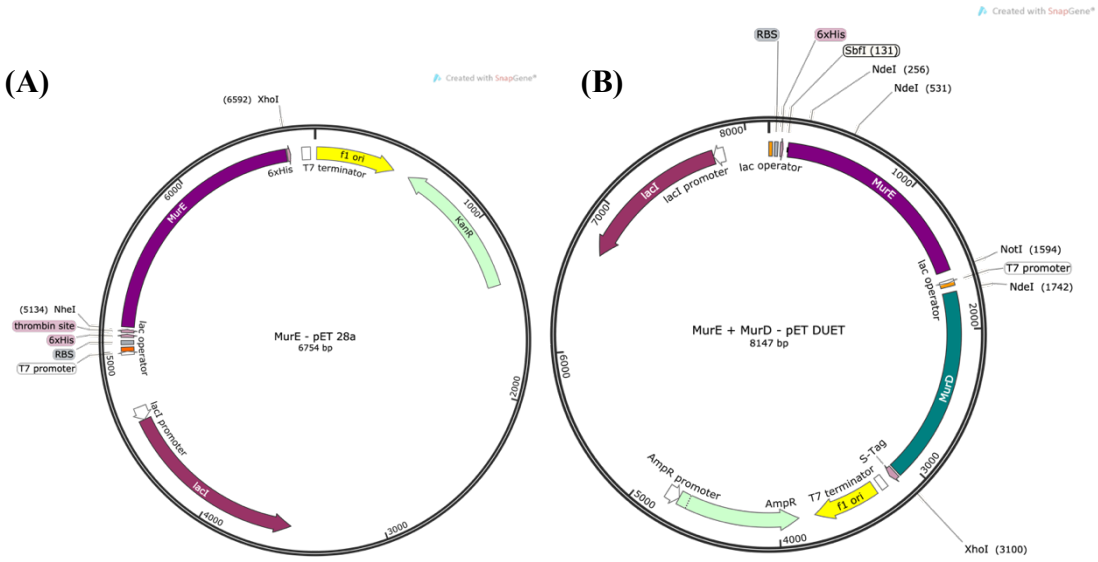

Figure 6. 1: Construct maps of MurE from S. agalactiae

Construct maps of *S. agalactiae* MurE. Construct maps were generated via Snapgene.(A) *S. agalactiae* MurE was cloned into open reading frame 1 of pET 28 using restriction enzyme digest. Restriction enzyme sites used were NheI and XhoI. (B) *S. agalactiae* MurE was cloned into His tagged site 1 of pET DUET using restriction enzyme digest. Restriction enzyme sites used were SbfI and NotI.

2.3 Protein Purification

Protein purification of MurE and the pET DUET system was carried out following the methodology previously described in **Chapter 2, Section 2.3**.

2.4 Size Exclusion Chromatography

To identify the presence of a MurD-MurE complex, size exclusion chromatography was employed. Individual proteins and their combined sample were separated by size using a Superdex 200 increase 10/300 GL column (GE Healthcare) on an AKTA pure system at room temperature where 100 µL of proteins, both at 2 mg/mL, were loaded via an injection system via a 100 µL loop. Separation of complex sample from lysate was carried out using a HiLoad 26/600 Superdex 200 pg (GE Healthcare) where 6 mL of protein sample was loaded via an

injection system via a 6 mL loop. The column was equilibrated with 1.5 column volumes of Buffer GF (as listed in **Chapter 2**). Elution was carried out with 1 column volume either at a flow rate of 0.75 mL min^{-1} and 0.5 mL fractions were collected, or at a flow rate of 2 mL min^{-1} and 1.2 mL fractions collected. Protein elution was monitored at 280 nm and 254 nm.

2.5 Cleavage of 6x His tag from MurD

Cleavage of the N-terminal 6x His tag from *S. agalactiae* MurD was carried out following protein purification of individual protein. Fractions containing pure protein identified via SDS-PAGE were pooled. Protein concentration was determined, and 1 unit of 3C protease per 100 μg of protein was incubated with the protein, along with a final concentration 1 mM DTT overnight. The sample was loaded into dialysis tubing and MurD digestion proceeded concurrently with overnight dialysis at 4°c into Buffer GF. Reverse IMAC was carried out on the digested and dialysed protein using a gravity fed His trap column. 2 mL of Ni resin was placed into a gravity column and washed with 3 column volumes of distilled water to remove storage buffer. The resin was washed with 3 column volumes of Buffer A (as listed in **Chapter 2**) before the dialysed protein was placed onto the column. Digested protein was eluted in 3 column volumes of Buffer A, before undigested protein was eluted using 3 column volumes of Buffer B. Cleaved protein was identified via SDS-PAGE.

2.6 Microscale Thermophoresis

Complex formation between MurD and MurE from *S. agalactiae* was analysed via microscale thermophoresis using a Monolith NT.115 (NanoTemper Technologies, Germany). MurE protein was labelled using Monolith NT protein labelling Blue according to the manufacturer's instructions via the 6x His tag present. 5 nM histidine tagged MurE and 400 μM MurD from which the tag had been removed were individually incubated with 1 mM $MgCl_2$ in Buffer GF for 30 minutes at room temperature, before incubation with the other protein was carried out. Protein incubations were carried out for 5 minutes at room temperature

before being loaded into standard capillaries (NanoTemper Technologies, Germany). Fluorescent readings were taken using Monolith NT.115 Blue conditions. K_D determinations were carried out using a doubling dilution series of unlabelled MurD in Buffer GF. Substrates were incubated with either labelled MurE or unlabelled MurD for 1 hour before incubation with the other protein sample. Substrate concentrations used were: 1 mM ADPCP, 100 μM UDP-MurNAc-L-Ala-D-Glu, 1 mM L-Lys, 100 μM UDP-MurNAc-L-Ala, and 1 mM D-Glu.

2.7 Mass Spectrometry

Mass spectrometry was carried out by Dr Cleidi Zampronio of WPH Proteomics Facility RTP. An aliquot containing 1 μL of extracted peptides (total sample volume 50 μL) was analysed by means of nanoLC-ESI-MS/MS using an Ultimate 3000/Orbitrap Fusion LC-MS (Thermo Scientific) using a 60 minute LC separation on a 50 cm column. The raw data were searched using MaxQuant against the E. coli database (www.uniprot.org/proteomes), the sequences provided, and the MaxQuant common contaminant database. Scaffold software was used for data analysis and visualisation of the results.

2.8 Activity assay for Mur ligases

Activity assays of the Mur ligases was carried out using an amplex Red coupled assay previously described in **Chapter 5**. The amplex red coupled assay was carried out in a Cary spectrophotometer at a total reaction volume of 200 μL at 37°c, and absorbance was tracked at 555 nm. The reaction mixture contained the following components (final concentrations): 50 mM MOPs (pH7.6), 10 mM $MgCl_2$, 2.5 U per mL PNP, 500 μM Inosine, 50 μM Amplex red, 25 U/mL HRP, 1.25 U/mL Xanthine Oxidase, 80 nM protein sample and the relevant substrates.

To determine dependence on substrate presence, all components apart from one substrate were added and mixed and a background rate was determined. To determine activity of the proteins, each substrate was added sequentially, and absorbance change tracked. To determine the ability of MurE to use UDP-MurNAc-

L-Ala-D-Glu produced by MurD, a MurD activity assay was run until a plateau was observed. L-Lys was then introduced to the assay and the absorbance tracked.

To determine the activity of MurD, 30 μM UDP-MurNAc-L-Ala, 1 mM D-Glu and 200 μM ATP were added to the reaction. To determine the activity of MurE, 30 μM UDP-MurNAc-L-Ala-D-Glu, 200 μM ATP and 500 μM L-Lys were added to the reaction.

2.9 Binary Complex Prediction

2.9.1 PRISM

Binary complex formation between *E. coli* Mur ligases was predicted using the PRISM 2.0 software, http://cosbi.ku.edu.tr/prism/. The PDB codes for the *E. coli* Mur ligases; 2F00 – MurC, 1E0D – MurD, 7B53 – MurE and 1GG4 – MurF were inputted as the target proteins. The template required for predicting complex formation was established by the software.

2.9.2 HADDOCK 2.4

Binary complex formation between the Mur ligases was predicted using the HADDOCK 2.4 software, https://wenmr.science.uu.nl/haddock2.4/. The Mur ligase structures were inputted via their PDB codes or homology model files. Residues of central importance for the interaction, active residues, were selected based on residues identified to potentially be involved with complex formation via PRISM or comparison between *E. coli* residues and *S. agalactiae* residues. Buried residues were removed by the software. Residues that contribute to the interactions but may not be directly involved in the interaction, passive residues, were defined by the software within a 6.5 angstrom radius of active residues. All other parameters were set to standard default settings. The runs were optimized for bioinformatic prediction.

2.9.3 AlphaFold 2

Binary complex formation between the *S. agalactiae* Mur ligases was predicted using the Alphafold2 software, available via Google Colab. The Mur ligase amino

acid sequences were taken from the KEGG database using the KEGG genome T00091 for *S. agalactiae* 2603 (serotype V) and inputted as the query sequence with a ':' used to specify inter-protein chainbreaks to model complexes. No template information was used. The MSA mode was set to MMseqs2 (UniRef + Environmental) with a pairing mode of unpaired+paired.

3. Results

3.1 The genomic layout of the Mur ligases differs between bacteria

Many proteins that form complexes are encoded close together in the bacterial genome and expressed together under the control of a single promoter. Such groups of genes are termed operons [130]. Identifying genes that fall in the same operon can therefore be a useful predictor that the encoded proteins might form a complex. Analysis of the genomic layout of the Mur ligases in various bacteria were compared. Using the KEGG database, the positioning of the four Mur ligases throughout the genomes of *S. agalactiae, S. pneumoniae, T. martima, C. crescentus,* and *B. pertussis* were compared, as seen in **Figure 6.2**.

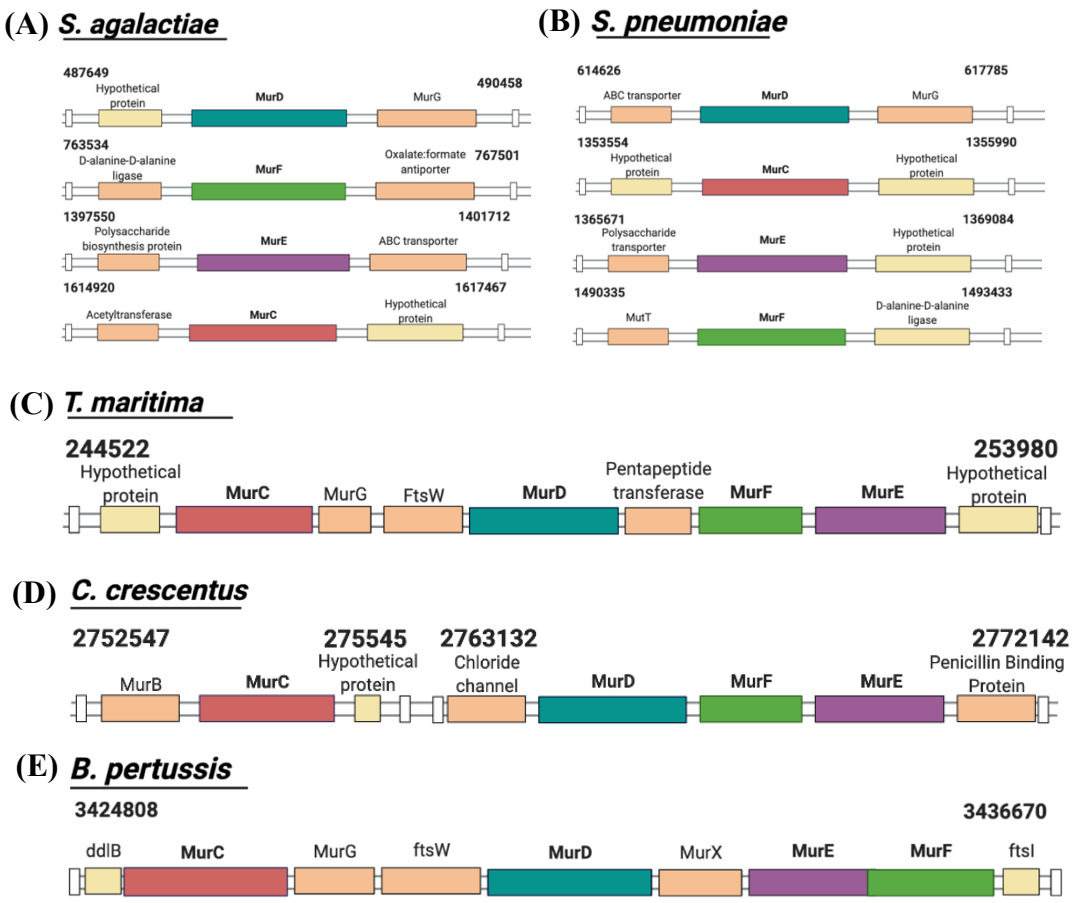

Figure 6. 2: Genomic layout of the Mur ligases differs across various bacteria

Using the KEGG database, the location of the 4 Mur ligases within the genome of various bacteria was determined. The positioning of the Mur ligases within the genome was then visualised and compared across different bacteria that have previously been studied in relation the Mur ligase complex formation, and *S. agalactiae*. (A) Genomic layout of the 4 Mur ligases within *S. agalcatiae.* (B) Genomic layout of the 4 Mur ligases within *S. pneumoniae.* (C) Genomic layout of the 4 Mur ligases within *T. maritima.* (D) Genomic layout of the 4 Mur ligases within *C. crescentus.*(E) Genomic layout of the 4 Mur ligases within *B. pertussis*

Within *S. agalactiae* and *S. pneumoniae* the Mur ligases are spread throughout the genome, whilst in *T. martima* and *C. crescentus* the Mur ligases are within a small section of the genome. Within *B. pertussis*, the MurE and MurF appear as a fusion protein, with MurC and MurD in close proximity. The appearance of a fusion of two Mur ligases and the Mur ligases within a small region of the genome may suggest a level of gene regulation that would be beneficial to complex formation. However, the Mur ligases from *T. martima* were previously shown to be unable to interact with each other [81] , while the Mur ligases from *S. pneumoniae* were able to form binary complexes [82] suggesting that close proximity of the Mur ligases within the genome is not an indicator of complex formation.

3.2 Experimental determination of a MurD-MurE binary complex

Previous studies have suggested that there may be the ability for the Mur ligases to form a complex. The presence of a fusion protein of two Mur ligases may suggest the ability for the Mur ligases to form complexes. The presence of a Mur ligase complex could explain some of the issues which have previously arisen when trying to observe antibacterial activity of Mur ligase inhibitors *in vivo*. Determining if the Mur ligases do form a complex could greatly affect future studies into Mur ligase inhibitors. The main focus of the *in-silico* screen and fragment studies presented within this thesis have been for MurD and MurE. Determining if a binary complex exists between these ligases could help focus future work on these projects.

3.3 Purification of MurE from *S. agalactiae*

In order to experimentally determine if a binary complex could exist between MurD and MurE from *S. agalactiae* an expression construct of MurE from *S. agalactiae* had to be produced. MurE from *S. agalactiae* serotype 5 was amplified by PCR and cloned into the *NheI* and *XhoI* sites of a pET-28a expression plasmid vector via restriction enzyme cloning. The sequence of the cloned *S. agalactiae* was confirmed, as seen in **Supplementary 6**. The vector was then transformed into *E. coli BL21 (DE3)* competent cells for protein expression. Protein purification was

carried out using IMAC purification via a nickel column and the purity of the purified protein was assessed via SDS-PAGE, as shown in **Figure 6.3A**.

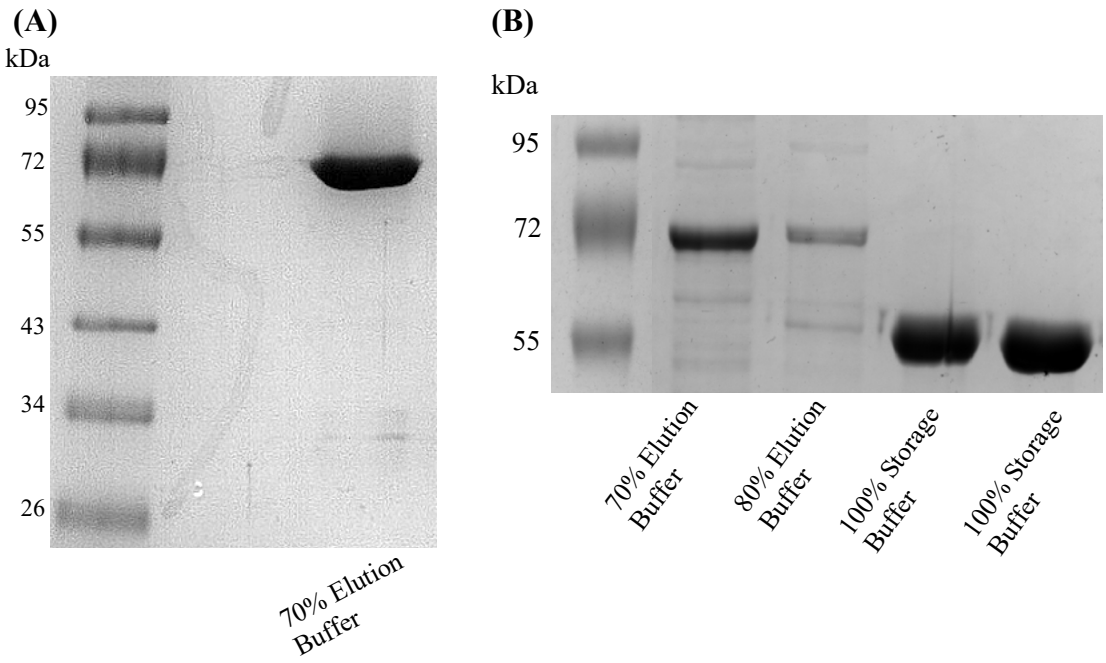

Figure 6. 3: SDS-PAGE gel of Purified MurE from S. agalactiae

cloning. The vector was then transformed into *E. coli BL21 (DE3)* competent cells. Protein purification was carried out using an IMAC nickel column and purity of the protein was assessed via SDS-PAGE. MurE has a MW of ~ 54 kDa. (A) SDS-PAGE gel of protein in elution buffer. (B) SDS-PAGE gel of protein in elution buffer, and after dialysis into storage buffer.

Electrophoretically homogeneous protein was obtained via this method with a clear band being seen at around 70 kDa. After dialysis to remove the imidazole present in the buffer and concentration of the protein, a pure protein band at 55 kDa can be seen, as shown in **Figure 6.3B**. MurE has a molecular weight of 55.319 kDa and a theoretical Pi of around 6.02. To confirm that the pure protein was MurE, mass spectrometry was carried out on the dialysed protein, along with activity assays to confirm the activity of the protein. As can be seen from **Figure 6.4A**, the activity of the protein was dependent on the presence of L-Lys, with the activity rate of the protein increasing in the presence of increasing concentrations of L-Lys. MurE from *E. coli* requires the amino acid DAP for activity, and so activity within the assay would be due to the presence of MurE from *S. agalactiae.* As can be seen from **Figure 6.4B**, mass spectrometry was able to confirm the presence of MurE from *S. agalactiae* within the protein sample with an 89% coverage and 60

exclusive unique peptides. These results confirm that MurE from *S. agalactiae* was purified, and suggest that MurE may have exhibited anomalous mobility within the gel prior to removal of the imidazole.

(A)

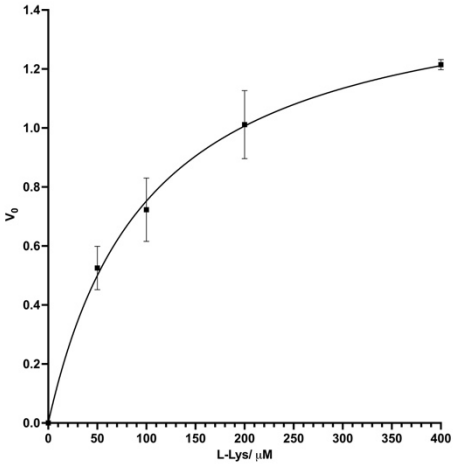

(B) MurE (100%), 56,367.9 Da
MurE (His tagged)
60 exclusive unique peptides, 131 exclusive unique spectra, 934 total spectra, 445/501 amino acids (89% coverage)

Figure 6. 4: Confirmation of presence of MurE from S. agalactiae in protein sample

Purified protein was further examined to confirm the presence of MurE from *S. agalactiae*. (A) Purified protein was active in the presence of L-Lys, and activity increased in the presence of increasing concentrations of L-Lys, an indicator for the presence of MurE from *S. agalactiae*. (B) Mass spectrometry confirmed the presence of MurE from *S. agalactiae* within the purified protein.

3.4 Size Exclusion Chromatography

In order to try and determine the ability of MurD and MurE to form a binary complex, size exclusion chromatography (SEC) was used. SEC works by separating molecules based on their size via filtration through a bead bed. Larger molecules are excluded from the beads and are able to pass through the column at a faster rate than smaller molecules which must pass through the beads themselves. When a complex occurs between proteins, the complex will travel through the column at a faster rate than that of the individual proteins due to its increased size.

3.4.1 Attempted demonstration of complex formation between MurD and MurE observed within a 1:1 mixture

In order to determine whether MurD and MurE from *S. agalactiae* are able to form a complex, the individual proteins and the proteins in a 1:1 ratio were passed through a SEC column and absorbance at 280 nm and 254 nm were tracked.

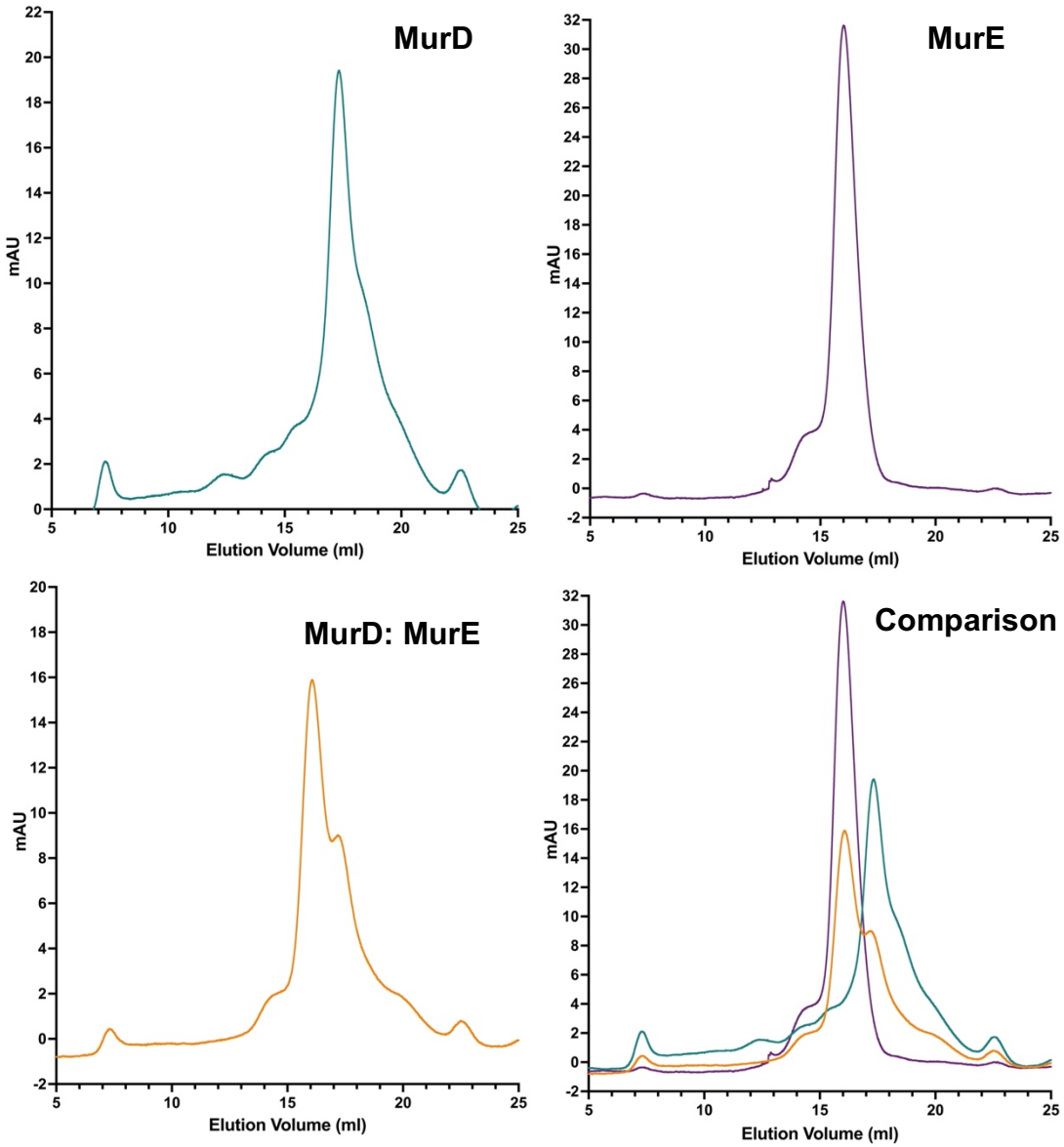

Figure 6. 5: 280 nm trace generated from SEC analysis of individual MurD, individual MurE and a 1:1 solution of MurD:MurE

MurD and MurE,at 2 mg/mL each, were chromatographed by SEC analysis as individual proteins and in a 1:1 molar ratio mixture. Traces were generated from the 280 nm absorbance change detected during the SEC run of MurD, MurE and 1:1 solution. MurD is shown in green, MurE in purple and 1:1 mixture in orange.

Absorbance changes at 280 nm were then plotted vs. elution volume and compared.

As can be seen from **Figure 6.5,** individual peaks for MurD and MurE were observed when the proteins were passed through the column as individual proteins. When the proteins were passed through the column in a 1:1 solution, a

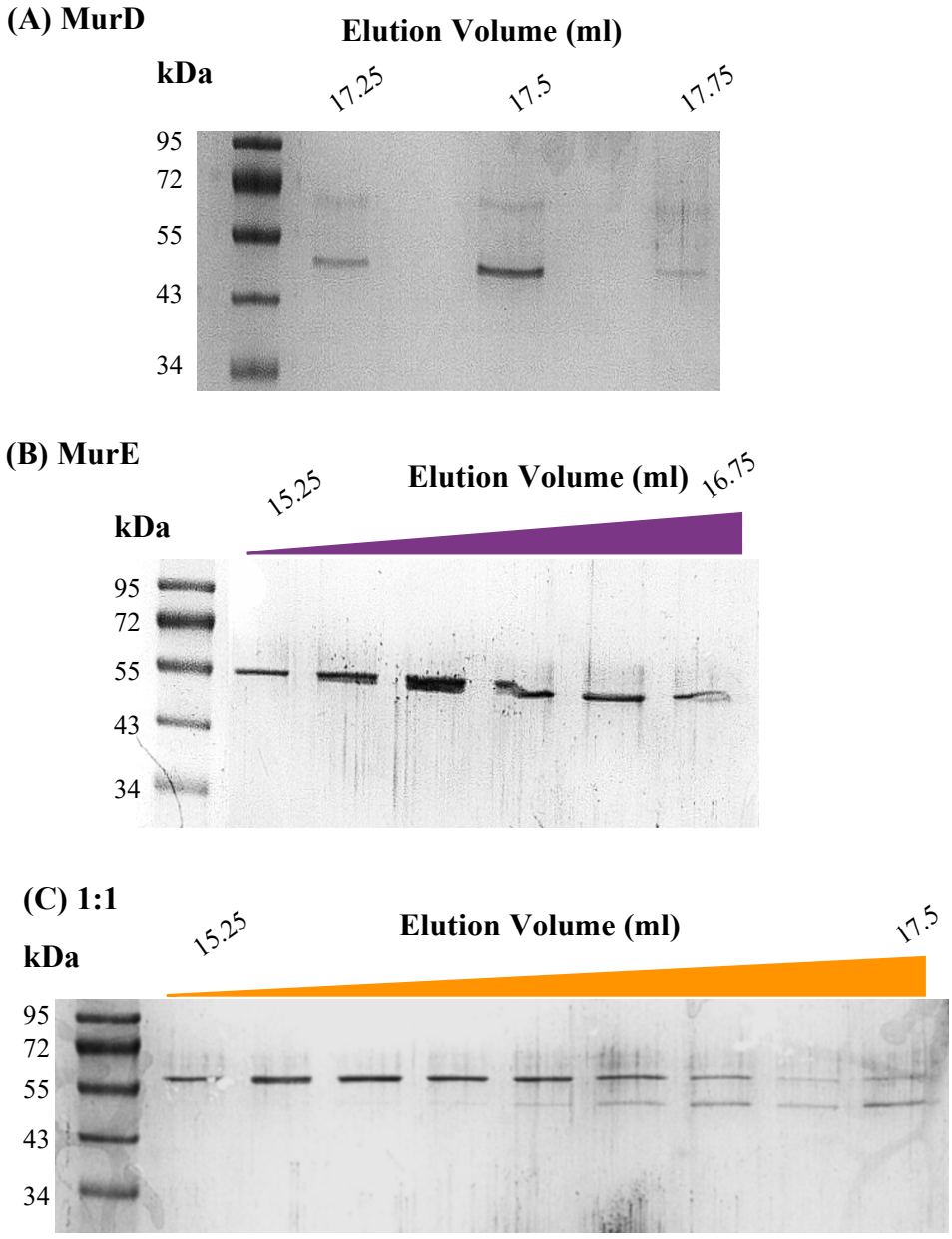

Figure 6. 6: SDS - PAGE shows the presence of MurD and MurE in eluted fractions

Fractions relating to increased absorbance at 280 nm from SEC analysis were run on SDS – PAGE gel before being visualised using Comassie blue staining. (A) Fractions relating to increased absorbance at 280 nm from SEC analysis of individual MurD. MurD is eluted between 17.25 mL and 17.75 mL. (B) Fractions relating to increased absorbance at 280 nm from SEC analysis of individual MurE. MurE is eluted between 15.25 mL and 16.75 mL. (C) Fractions relating to increased absorbance at 280 nm from SEC analysis of 1:1 solution of MurD and MurE. MurE is eluted between 15.25 mL and 17.5 mL. MurD is eluted between 16.25 mL and 17.5 mL.

large peak was seen with a secondary peak being observed on the falling edge of the first peak.

When overlayed with the individual traces of MurD and MurE, the 1:1 solution peaks corresponded to the protein peaks present for the individual proteins. To determine if any complex formation was occurring, the fractions from the SEC experiments that corresponded to increased absorbance at 280 nm were analysed electrophoretically by SDS gel to confirm the presence of proteins.

As can be seen from **Figure 6.6**, MurD was present in the fractions relating to the increased absorbance peak at 280 nm observed during its individual protein run in **Figure 6.5**, with the most protein being observed at an elution volume of 17.5 mL. MurE was also present in the fraction relating to the increased absorbance peak at 280 nm observed during its individual protein run, with the most protein being observed at an elution volume of 15.75 mL. As can be seen from **Figure 6.6C**, MurD and MurE were both present within certain fractions related to the increased absorbance peaks at 280 nm observed during the SEC fractionation of the 1:1 MurD/MurE mixture. MurE was mostly observed being eluted between 15.25 mL and 16.5 mL, but was still present at an elution volume of 17.5 mL. MurD was present in elution fractions from 16.5 mL to 17.5 mL.

The elution of MurD and MurE from the 1:1 mixture showed MurE eluting at a later elution stage than during its individual run, with MurD also being present at an earlier elution stage than during its individual run. This could suggest that some interaction between the proteins may have occurred, allowing them to be eluted at different elution volumes than during their individual protein runs. However, due to the very similar chromatographic profiles of MurD and MurE, it is also possible that the individual proteins are too close for complete resolution via a SEC column, and so the formation of a binary complex between MurD and MurE from *S. agalactiae* could not be confirmed via SEC analysis.

3.5 Microscale Thermophoresis (MST)

Due to the SEC experiments not being able to confirm complex formation between MurD and MurE, another technique had to be used in order to try and determine whether MurD and MurE are able to form a binary complex. There are

many techniques in which the interaction between two proteins can be investigated. MST is a fairly new technique for investigating protein-protein interaction. MST works via measuring the diffusion of molecules in a temperature gradient which has been induced by an infrared laser [131]. Before heating, an initial fluorescence of the sample is taken. The IR-laser is turned on which leads to a temperature jump within the sample, a *T*-jump, which leads to an abrupt change in fluorescence intensity, as seen in **Figure 6.7.**

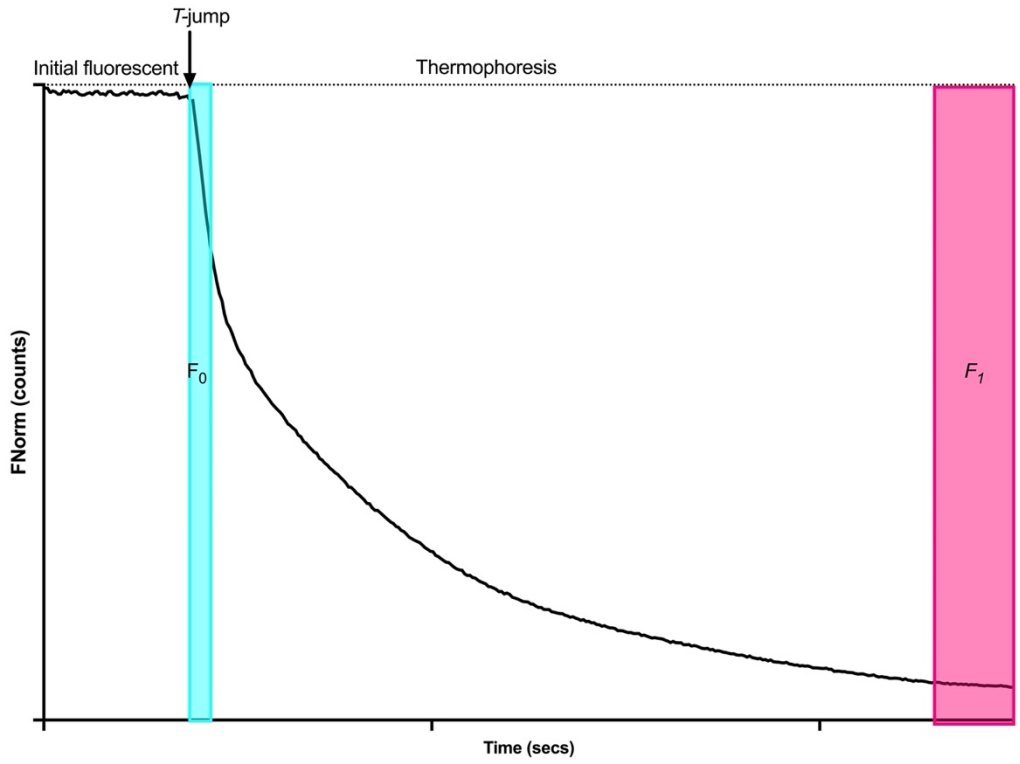

Figure 6. 7: Schematic diagram of MST fluorescent change due to temperature gradient

MST can be used to determine complex formation via tracking fluorescent changes of molecules within a temperature gradient. Initial fluorescent values are taken, before an IR-laser is switched on inducing a *T*-jump within the sample. A slow thermophoresis then occurs within the sample, before a plateau is reached.

Fluorescence around the *T*-jump focuses on the local surroundings of the fluorophore. A slow thermophoresis, which is a diffusion-limited process then occurs. This thermophoretic motion creates a fluorescent gradient which then reaches a plateau when thermodiffusion is counterbalanced by mass diffusion, as seen in **Figure 6.7**. The fluorescence after thermodiffusion is dependent on the properties of the entire molecule/ complex in regards to changes in the size and charge. The movement of the molecules through these temperature gradients can

be detected and quantified by fluorescence, and allows for the determination of the $F_{norm,}$ the normalized fluorescence. F_{norm} is calculated by dividing the fluorescence after thermodiffusion, F_1, by the fluorescence after the temperature jump, *T*-jump, F_0. [132]. F_{norm} can then be compared between samples to allow the determination of binding between proteins. When a complex forms, a change in the fluorescence after thermodiffusion and after the *T*-jump results in a change in the recordable F_{norm}.

The fluorescence detected can either be due to the inherent fluorescence of tryptophan residues present in the proteins, or via fluorescent labels that have been covalently linked to the protein via lysine, cysteine or polyhistidine residues. MST offers advantages over other protein-protein interaction analysis methods as it does not require large volumes of protein, with only a 10 μl final volume per capillary. MST does not require one of the proteins to be immobilised to a surface, allowing the whole protein to be accessible for binding, which is beneficial when the binding site is unknown.

3.5.1 MurD and MurE from *S. agalactiae* are able to form a binary complex

As the MurD and MurE proteins from *S. agalactiae* already had 6x polyhistidine tags, fluorescent labelling targeting the His tag was used to fluorescently label one of the proteins. The 6x polyhistidine tag had to be cleaved from the other protein to prevent cross-labelling when the two proteins were introduced. The 6x polyhistidine tag was cleaved from MurD via 3C and the cleaved MurD was purified via reverse IMAC, as shown in **Supplementary 7**. MurE was incubated with a fluorescent label that binds via a His tag prior to incubation with a secondary protein. Homogeneity checks between different capillaries of the labelled proteins was carried out by the Monolith system before initial fluorescent readings were taken. Once homogeneity was confirmed, the ability of MurE to bind to MurD could be established. A control protein was used to confirm that a difference in fluorescence between the single protein and the dual proteins would only be seen when binding between the proteins was occurring. As can be seen from **Figure 6.8A**, there was no difference in the recordable F_{norm} between MurE

and MurE in the presence of a control protein. However, there was an increase in the recordable F_{norm} between MurE and MurE in the presence of MurD. A change in the recordable F_{norm} suggests that MurD and MurE were able to interact.

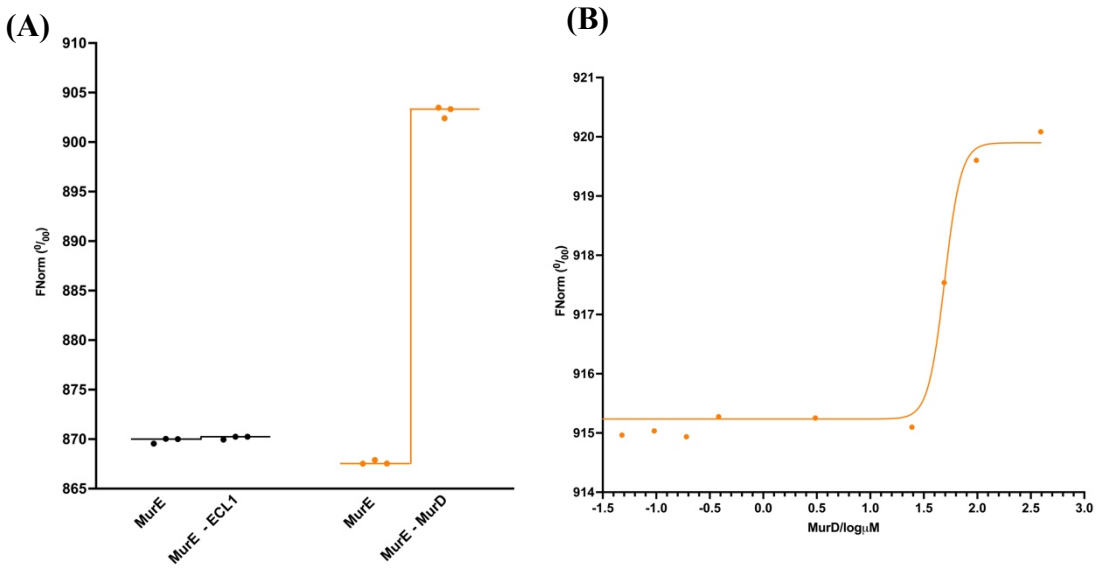

Figure 6. 8: Interaction between MurE and MurD from S. agalactiae was determined via MST

Fluorescently labelled MurE was incubated with MurD to establish complex formation. (A)Fluorescently labelled MurE was incubated with either ECL1 of FtsX from *S. pneumoniae* or MurD from *S. agalactiae*. The fluorescence of MurE and MurE in the presence of a secondary protein was recorded. All 4 data points were plotted and the mean FNorm shown with a line. (B) Fluorescently labelled MurE was incubated with a serial dilution of MurD from *S. agalcatiae*. The fluorescence of MurE bound to various MurD concentrations was recorded, and the plotted as a binding curve.

The binding affinity of MurD to MurE was then established using MST. A serial dilution of MurD was used to estimate the K_D of MurD against MurE. The binding curve can be seen in **Figure 6.8B.** A K_D of 49 µM was estimated based on this curve, suggesting that although the proteins can interact, it is not a favourable interaction.

3.5.2 The presence of substrates alters the binding and K_D of MurD to MurE

To further investigate the MurD:MurE interaction, various substrates for the two proteins were incubated with the proteins and the ability of the proteins to form a complex with each other was established via MST. As can be seen from **Figure 6.9**, MurD and MurE were able to still form a complex in the presence of all or only some of their substrates.

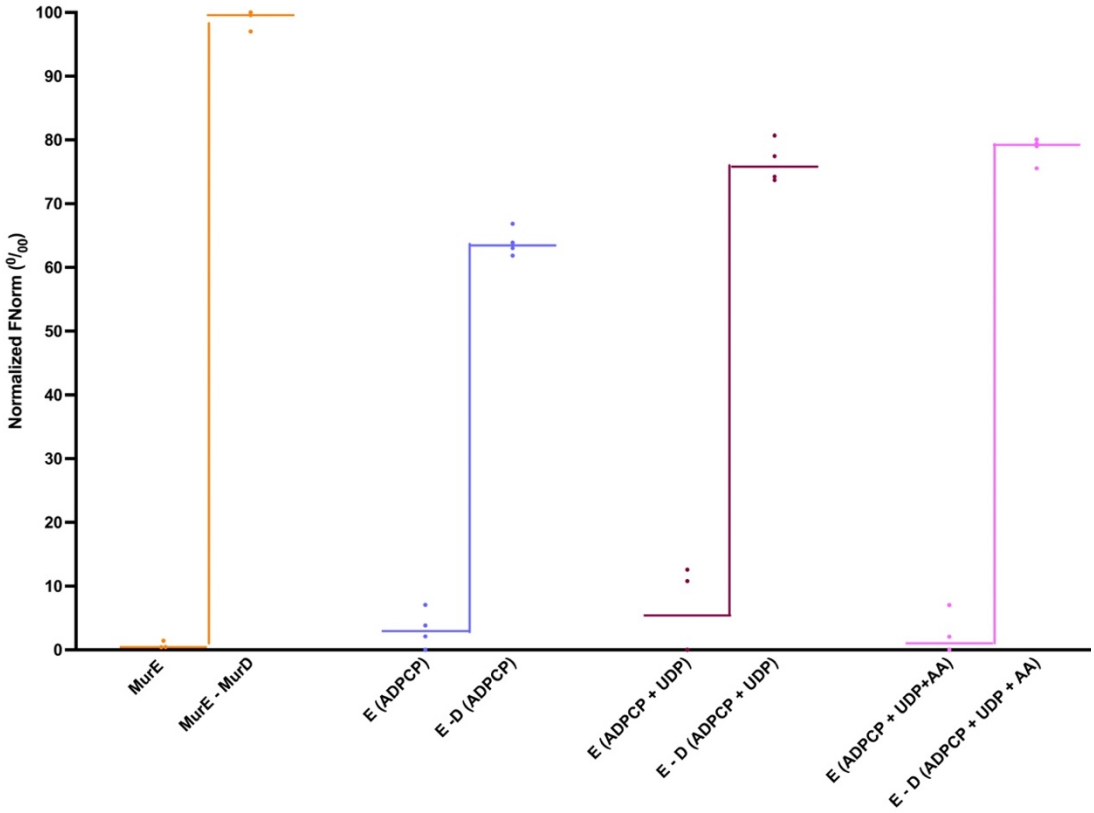

Figure 6. 9: MurD and MurE can form a binary complex in the presence of substrates

Fluorescently labelled MurE and MurD were incubated with various substrates for 1 hour before MST to determine the effect substrates have on complex. MurE was incubated with a combination of 1 mM ADPCP, 100µM UDP-MurNAc-L-Ala-D-Glu, and 1 mM L-Lys. MurD was incubated with a combination of 1 mM ADPCP, 100µM UDP-MurNAc-L-Ala, and 1 mM D-Glu. All 4 data points were plotted and the mean FNorm shown with a line.

The K_D of these interactions were then investigated to determine the effect substrates have on the binding of MurD to MurE. As can be seen from **Figure 6.10**, the binding of substrates increased the estimated K_D of MurD binding to MurE. The presence of ADPCP, and ADPCP and the UDP intermediates increased the K_D to an extent that a true estimated K_D could not be calculated as the curve was unable to plateau. The curve was able to plateau in the presence of all 3 substrates allowing an estimated K_D to be calculated that is close to the estimated apo K_D.

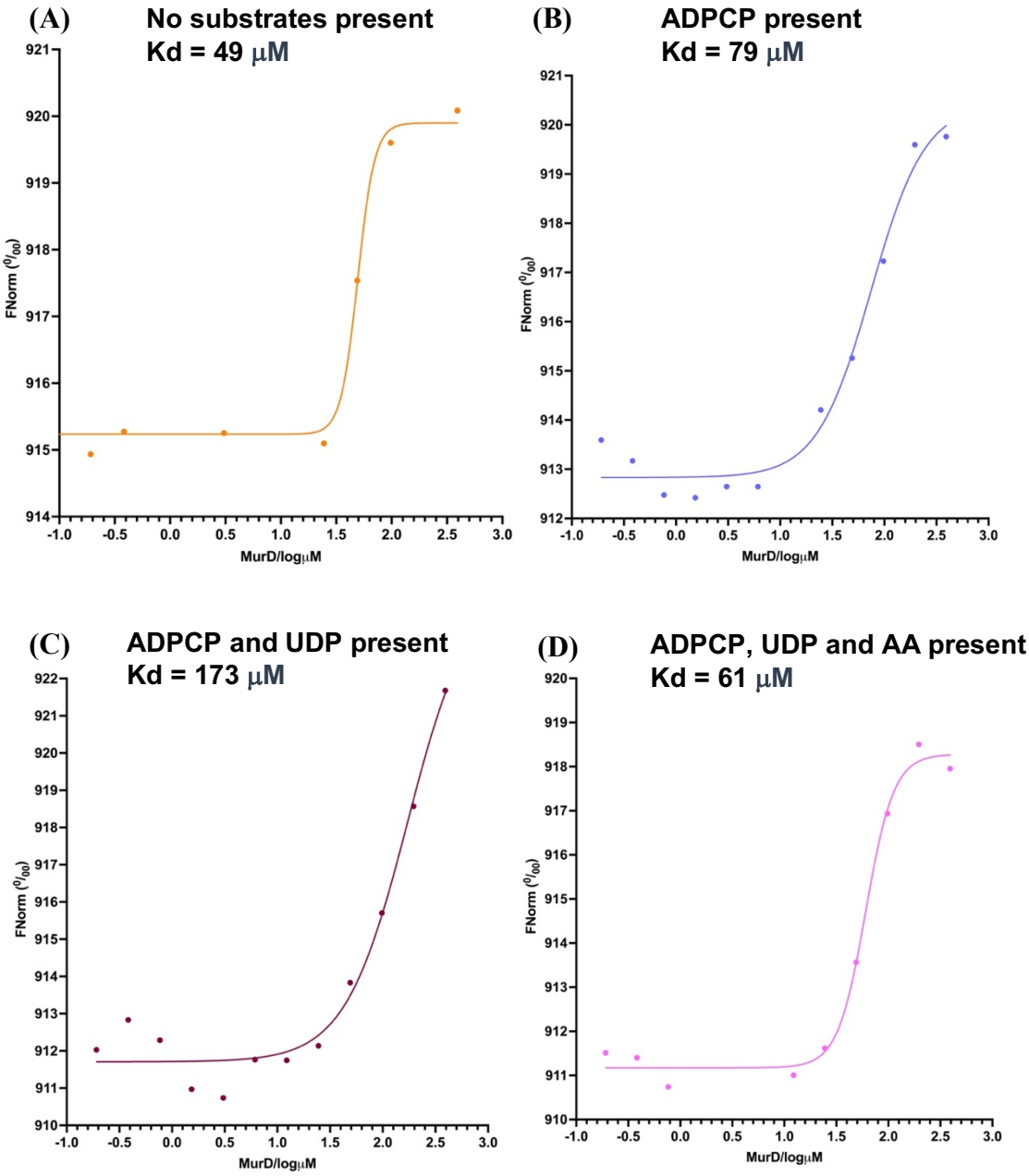

Figure 6. 10: The binding of substrates increases the Kd of MurD to MurE

Fluorescently labelled MurE and MurD were incubated with various substrates for 1 hour before MST to determine the effect substrates have on the complex Kd. The fluorescently labelled MurE in the presence or absence of substrates was then incubated with a serial dilution of MurD in the presence or absence of substrates. The fluorescence of MurE bound to various MurD concentrations was recorded, and the plotted as a binding curve. (A) No substrates present. Estimated Kd of 49 μM. (B) MurE was incubated with 1 mM ADPCP, MurD was incubated with 1 mM ADPCP. Estimated Kd of 79 μM. (C) MurE was incubated with 1 mM ADPCP and 100μM UDP-MurNAc-L-Ala-D-Glu, MurD was incubated with 1 mM ADPCP and 100μM UDP-MurNAc-L-Ala. Estimated Kd of 173 μM. (D) MurE was incubated with 1 mM ADPCP,100μM UDP-MurNAc-L-Ala-D-Glu, and 1 mM L-Lys. MurD was incubated with 1 mM ADPCP, 100μM UDP-MurNAc-L-Ala, and 1 mM D-Glu. Estimated Kd of 61 μM.

The change in K_D in the presence of substrates suggests that the binding of the substrates is weakening but not breaking the complex between MurD and MurE. A hypothesis as to why this may be occurring relates to the domain movement that occurs within the C-terminal domain of the Mur ligases upon binding of the substrates. As can be seen from the known structures of MurC shown in **Figure 6.11**, an average distance of 28 Å within the C-terminal domain of MurC can be seen when a molecule binds to the ATP-binding site. An average distance of 4 Å can be seen in the same region of MurC when a molecule binds to the UDP intermediate binding site. This flexibility and movement of the C-terminal region can be seen across all four Mur ligases. If the C-terminal of MurD or MurE are involved in the formation of the complex then movement within this region, upon the binding of first ADPCP and then the UDP intermediate could result in the complex weakening, but not fully breaking, resulting in the increased K_D data seen within the MST experiments. This movement and changing of the complex may allow the proteins to remain active while within a complex.

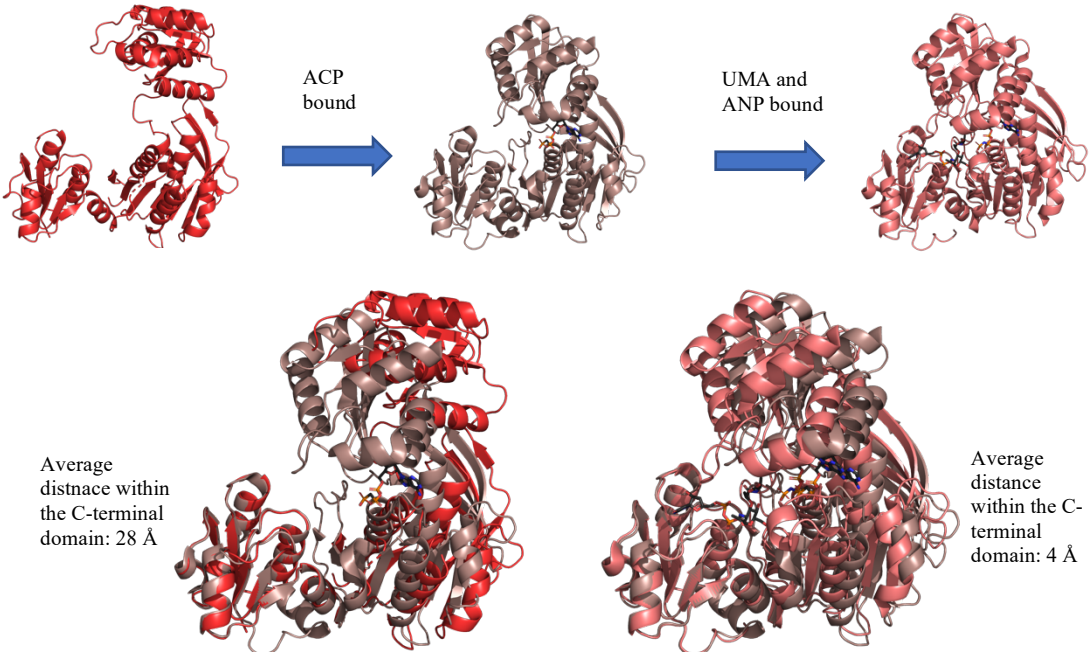

Figure 6. 11: C-terminal domain movement upon binding of substrates within MurC

Upon binding of substrates, the C-terminal domain of MurC from *Haemphilus influenzae* undergoes domain movement. Apo MurC structure (1GQQ – red), MurC with ACP bound (1GQY – brown), and MurC with UMA and ANP bound (1P3D - pink) were all taken from PDB and compared within Pymol. The structures were aligned and any movement in the domain was measured using the measurement tool within Pymol. The C-terminal domain undergoes domain movement with the binding of ACP, and further domain movement occurs with the binding of UMA.

3.6 pET DUET Expression System

MurD and MurE were shown to be able to form a binary complex within MST. MST determines interaction between proteins *in vitro,* which may allow complex formations that do not occur *in vivo* to be seen. To investigate whether MurD and MurE can form a complex within a bacterial cell, a pET DUET expression system was produced. A pET DUET expression system allows two proteins to be co-expressed from one vector, with only one protein containing a polyhistidine tag. After expression, purification of the proteins can be carried out using a standard IMAC purification via a nickel column. The polyhistidine tagged protein will bind to the nickel on the column and be present in the eluted fractions. If the secondary protein can form a complex with the polyhistidine tagged protein, both proteins will be present in the same eluted fractions. If no complex occurs, the untagged protein will be present in the flowthrough or washes of the column, but not within the elution stages.

3.6.1 MurD and MurE can be purified within a complex

To determine if MurD and MurE can form a complex within a bacterial cell, MurD and MurE from *S. agalactiae* serotype 5 were cloned into the pET DUET expression plasmid vector via restriction enzyme cloning. MurE was cloned into cloning site 1 which contains a 6x polyhistidine tag, while MurD was cloned into cloning site 2 which contains an S-tag. The vector was then transformed into *E. coli BL21 (DE3)* competent cells for protein expression following sequence conformation. Protein purification was carried out using IMAC purification via a nickel column and the presence of MurD and MurE was established using SDS-PAGE, as shown in **Figure 6.12**. As can be seen from **Figure 6.12**, both MurE and MurD were seen in the same eluted fractions. MurD was seen to not bind to the nickel column independently of MurE as shown in **Supplementary 8**. This suggests that MurE and MurD from *S. agalactiae* were able to form a complex within a bacterial cell.

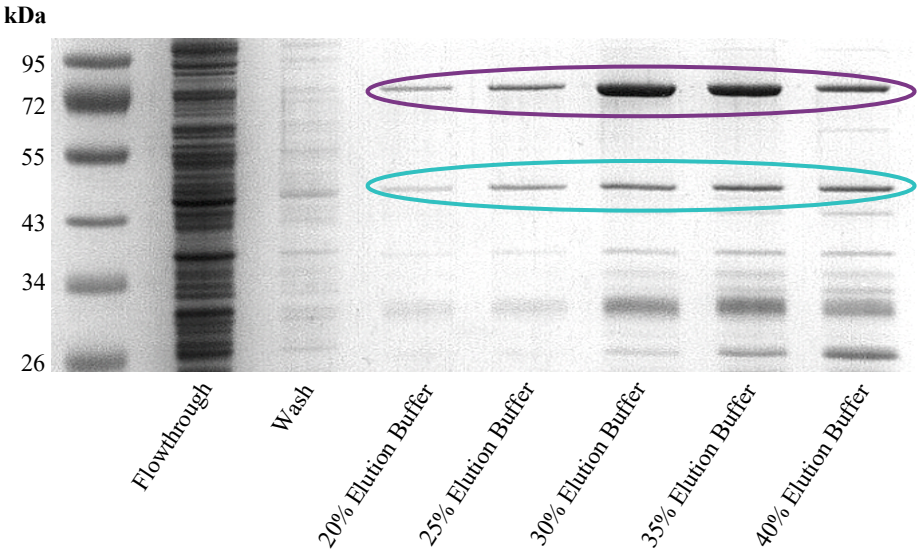

Figure 6. 12: MurD and MurE can be co-purified in a complex formation via a pET-DUET system

Using a pET DUET expression system, MurE and MurD from *S. agalactiae* were co-purified together. A pET DUET vector, with a polyhistidine tagged MurE and an S-tagged MurD was expressed in *E. coli BL21 (DE3)* competent cells. Purification was carried out using IMAC purification via a nickel column. The presence of MurE and MurD was confirmed in the same elution fractions. MurE and MurD are highlighted on the gel. MurD is highlighted with blue, MurE is highlighted in purple.

3.6.2 Presence of MurD and MurE confirmed via Mass spectrometry

Using a pET DUET vector, MurE and MurD were believed to have been co-purified together within a complex. However, as seen in **Figure 6.12**, there were other bands present within the elution fractions containing MurD and MurE. These bands could correspond to other proteins that are also involved within the complex or could correspond to breakdown products of the two proteins of interest, or could be due to contamination with native *E. coli* proteins. To confirm that the proteins identified via the SDS-PAGE were *S. agalactiae* MurE and MurD, and to try and identify any other proteins that were present within the samples, the elution fractions were subjected to mass spectrometry analysis via the WPH Proteomics RTP department at the University of Warwick. The fractions that may have contained *S. agalactiae* MurD and MurE were pooled before the proteins were digested overnight with trypsin. The resulting peptides were then de-salted before being subjected to mass spectrometry analysis. Results were analysed using

Scaffold software with a set 95% protein threshold and a 95% peptide threshold. The presence of *S. agalactiae* MurE and MurD were confirmed via mass spectrometry, as seen in **Figure 6.13.**

Figure 6. 13: The presence of MurD and MurE was confirmed via Mass spectrometry

Using mass spectrometry, the presence of MurD and MurE from *S. agalactiae* within the pET DUET fractions was confirmed. A sample of the fractions previously shown to contain MurD and MurE from a pET DUET expression were analysed via mass spectrometry to confirm the protein identification and identify any contaminating proteins. One contaminating protein, 50s ribosomal subunit L17 was identified.

The presence of *S. agalactiaae* MurE was confirmed via the presence of 21 exclusive unique peptides with a 28% coverage. The presence of *S. agalactiae* MurD was confirmed via the presence of 17 exclusive unique peptides with a 26% coverage. A 50s ribosomal protein L17 was also seen to be present within the sample. The 50s ribosomal protein L17 forms part of the 50s ribosomal subunit [133].

It is unlikely that this the protein is involved within the formation of the complex between *S. agalactiae* MurD and MurE, and so was treated as a contaminant within the sample. Two other contaminants were also present within the sample; trypsin which was present from the digestion step required for mass spectrometry analysis, and human keratin. These results suggest that *S. agalactiae* MurE and MurD were able to form a binary complex.

3.7 Dual expression of MurD and MurE

MurD and MurE from *S. agalactiae* were shown to be able to be purifiable as a complex with each other when co-expressed within a bacterial cell. However, the yield from this method was low. To try and improve the yield of the protein complex, a His tagged *S. agalactiae* MurE and an untagged *S. agalactiae* MurD were expressed separately before the lysates were combined and purified. Protein purification was carried out using IMAC purification via a nickel column and fractions were dialysed into Buffer GF before the presence of *S. agalactiae* MurD and MurE was established using SDS-PAGE, as shown in **Figure 6.14.**

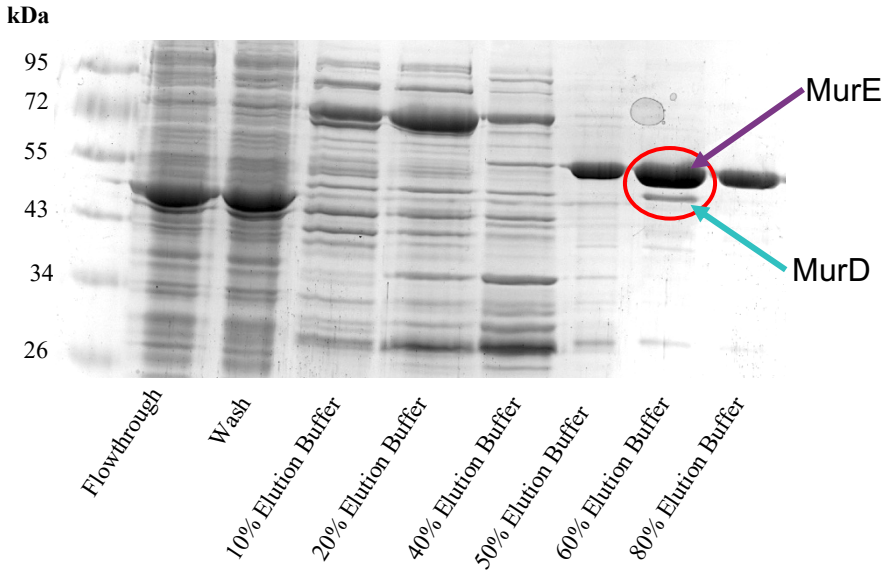

Figure 6. 14: MurD and MurE can be co-purified in a complex formation via dual protein expression
Using two protein expression systems, MurE and MurD from *S. agalactiae* were co-purified together. A polyhistidine tagged MurE and an un-tagged MurD were separately expressed in *E. coli BL21 (DE3)* competent cells before the cell lysates were combined. Purification was carried out using IMAC purification via a nickel column. The presence of MurE and MurD was confirmed in the same elution fractions. MurE and MurD are highlighted on the gel.

As can be seen from **Figure 6.14**, MurD was present within the wash and flowthrough of the column. However, MurD was also present within one elution stage where MurE was also present. As was established in **Supplementary 8**, untagged *S. agalactiae* MurD did not bind to a nickel column independently and so the presence of MurD in an elution stage suggests that MurE and MurD from *S. agalactiae* were able to form a complex.

As can be seen in **Figure 6.14**, the elution fraction contained a higher proportion of *S. agalactiae* MurE compared to *S. agalactiae* MurD. The appearance of a higher proportion of MurE within the elution fraction could suggest that some MurE present within the elution fraction was not complexed to MurD. To try and purify the protein complex, the elution fractions containing both MurD and MurE were passed through a SEC column and absorbance at 280 nm and 254 nm were tracked. The fractions from the SEC experiment that corresponded to increased absorbance at 280 nm were analysed electrophoretically by SDS gel to confirm the presence of proteins. As can be seen from **Figure 6.15**, *S. agalactiae* MurE was seen in various fractions across the SEC experiment, but *S. agalactiae* MurD was only seen in the final fraction. MurD and MurE were not present within any of the same fractions from the SEC experiment, as seen in **Figure 6.15**. This suggests that the protein complex between MurD and MurE was broken during the SEC column, which prevented the purification of the protein complex.

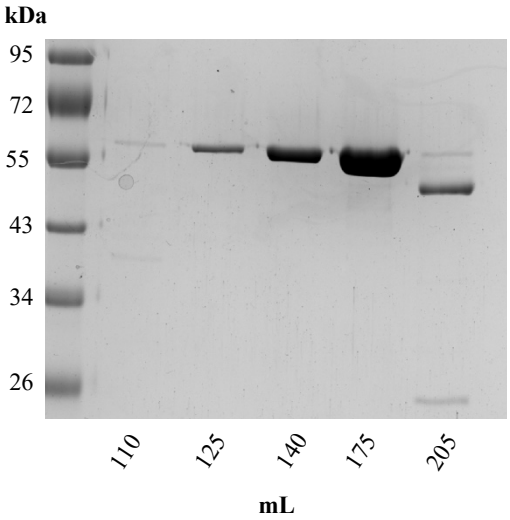

Figure 6. 15: SEC results in breakage of protein complex between S. agalactiae MurD and S. agalactiae MurD

Fractions relating to increased absorbance at 280 nm from SEC analysis were run on SDS – PAGE gel before being visualised using Coomassie blue staining. *S. agalactiae* MurE was present across multiple fractions. *S. agalactiae* MurD was present at an elution volume of 200 mL. Complex formation between MurD and MurE was not seen after the SEC experiment.

3.7.1 MurD is active within a complex

MurD and MurE from *S. agalactiae* were shown to be able to be purifiable as a complex with each other when co-expressed within a bacterial cell, or when purified together from cell lysates. The Mur ligases are responsible for the addition of amino acids onto the UDP-MurNAc intermediate within the cytoplasm. Whether these proteins still retained the ability to carry out this function while within a complex would provide further information on the biological relevance of a Mur ligase complex.

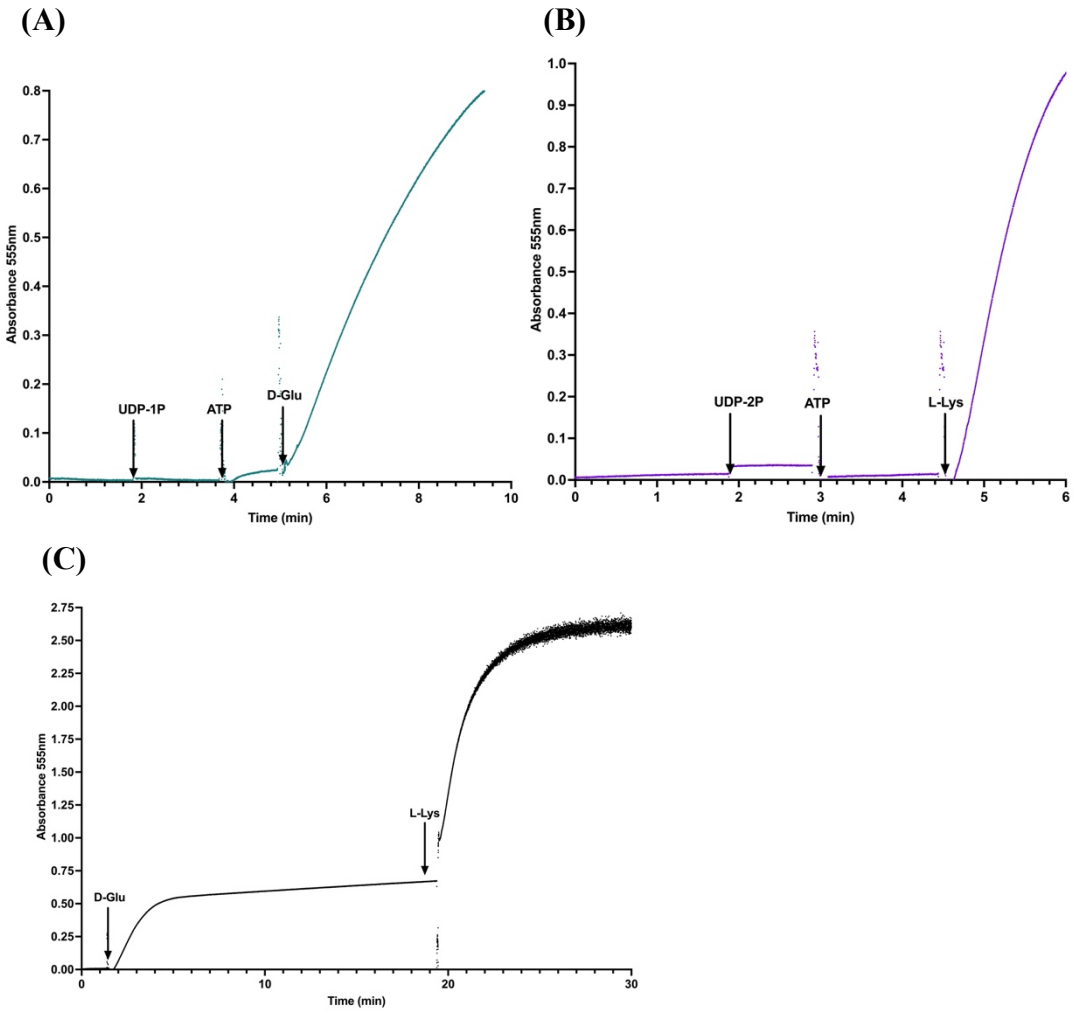

Figure 6. 16: Activity of proteins within a complex was identified via an amplex red assay

Using an amplex red assay the activity of MurD and MurE in complex was investigated. (A) MurD was active while in complex formation and required the presence of all substrates. (B) MurE was active within the protein sample and required the presence of all substrates. (C) MurE was able to use the UDP-MurNac-L-Ala-D-Glu produced by MurD while in complex.

The activity of *S. agalactiae* MurD while within a complex was investigated using an amplex red assay. Initial experiments were carried out into the dependence of activity of MurD upon the addition of all three substrates. To determine whether the presence of all substrates was required for the activity of *S. agalactiae* MurD, an amplex red assay was run via a spectrophotometer, in the absence of a substrate or the ligase. The absorbance change was followed and the initial rate determined. No initial rate was seen upon the addition of only one substrate or in the absence of the protein sample. As can be seen from **Figure 6.16A**, only after the addition of all three substrates was an initial rate for *S. agalactiae* MurD seen.

The true activity of *S. agalactiae* MurE while within a complex could not be established as the protein complex could not be purified, potentially resulting in MurE being present within the sample that was not in complex with MurD. As can be seen from **Figure 6.16B**, the *S. agalactiae* MurE present within the sample was active. However, this activity could relate to free MurE or MurE in complex with MurD.

Within complex formation, channelling of substrates may occur between the proteins present. To determine whether the *S. agalactiae* MurE present within the sample could accept the UDP-MurNAc-L-Ala-D-Glu produced by the *S. agalactiae* MurD while within a complex, an activity assay of MurD while within a complex was allowed to run to completion with UDP-MurNAc-L-Ala acting as the limiting factor. L-Lys was then added to the assay and the activity of the sample tracked via a spectrophotometer. As can be seen from **Figure 6.16C**, after the addition of the L-Lys, activity was seen as the *S. agalactiae* MurE converted the UDP-MurNAc-L-Ala-D-Glu to UDP-MurNAc-L-Ala-D-Glu-L-Lys. This suggested that the MurE was able to use the product of MurD while within a complex, suggesting that channelling of substrates within a Mur ligase complex may be possible.

3.8 Computational modelling of predicted Mur ligase complex

Experimental work carried out into the formation of a binary complex between MurD and MurE from *S. agalactiae* suggested that there may be the ability for

these two proteins to exist in a binary complex. To better understand how this complex may exist, and if other Mur ligases may be able to exist in binary complexes, computational modelling of the binary complexes of the Mur ligases of *E. coli* and *S. agalactiae* were undertaken.

3.9 Binary complex prediction of the *E. coli* Mur ligases via PRISM

To investigate the ability of MurC, MurD, MurE and MurF to form binary complexes, the PRISM software was used. PRISM is a prediction algorithm that uses structural similarity and evolutionary conservation in template interfaces to predict protein-protein interactions [134].

Experimental work into binary complex formation between MurD and MurE determined that the presence of substrates may alter the ability of the Mur ligases to form binary complexes. The Mur ligases also undergo a conformational change in the presence of substates. To make sure all proteins were in the same conformation and remove the potential effects of different substrates on the formation of binary complexes, PDB files of the Mur ligases in their apo form were used for binary complex predictions.

Using the known structures of the four apo *E. coli* Mur ligases, PRISM was able to predict whether binary complexes could form between all pairings of the four Mur ligases based on template interfaces. All four Mur ligases were predicted to be able to form a binary complex with all other Mur ligases. For each binary complex, the top hit predicted by PRISM is listed in **Table 6.1**, with the global energy binding score (GEBS), and the template interface used to predict the binding shown.

Target 1	Target 2	GEBS (kcal/mol)	Template
MurC	MurD	-35.98	3synAD
MurD	MurE	-4.32	1t8qBC
MurF	MurE	-9.75	3aq0EH
MurC	MurE	-4.63	3qu2AD
MurC	MurF	-19.97	2fw7AB

Table 6. 1: PRISM top hit score for binary complex formation amongst the E. coli Mur ligases

Using PRISM, binary complex formation amongst the Mur ligases from *E. coli* was predicted. The GEBS and template identification for each hit is listed.

MurC-MurD was predicted to form the strongest binary complex, while MurD-MurE was predicted to form the weakest binary complex.

3.9.1 Binary complex prediction of the *E. coli* Mur ligases via HADDOCK

PRISM was able to predict that the Mur ligases of *E. coli* would be able to form binary complexes based on existing templates of interactions from PDB files. To further investigate the ability of the Mur ligases to form binary complexes, another computational program was used to predict the interactions between the Mur ligases in complex formation. Complex formation between pairs of Mur ligases that fall before and after each other within the pathway of peptidoglycan precursor synthesis were investigated. Using the interfaces determined by PRISM, the residues that may potentially be involved in complex formation were inputted into HADDOCK 2.4 as active residues. Passive residues were determined by the software, and the run was optimised for bioinformatic predictions, which automatically sets the distance restraints and sampling parameters to settings that favour bioinformatic predictions. The final models produced by HADDOCK were then clustered based on similarity before the top hit model from each cluster was provided as a Pymol file by the software. HADDOCK 2.4 was able to predict interactions between all the pairs of Mur ligases using the residues provided. The top hit from the top cluster, as determined by HADDOCK 2.4., for each pair is shown in **Figure 6.17**.

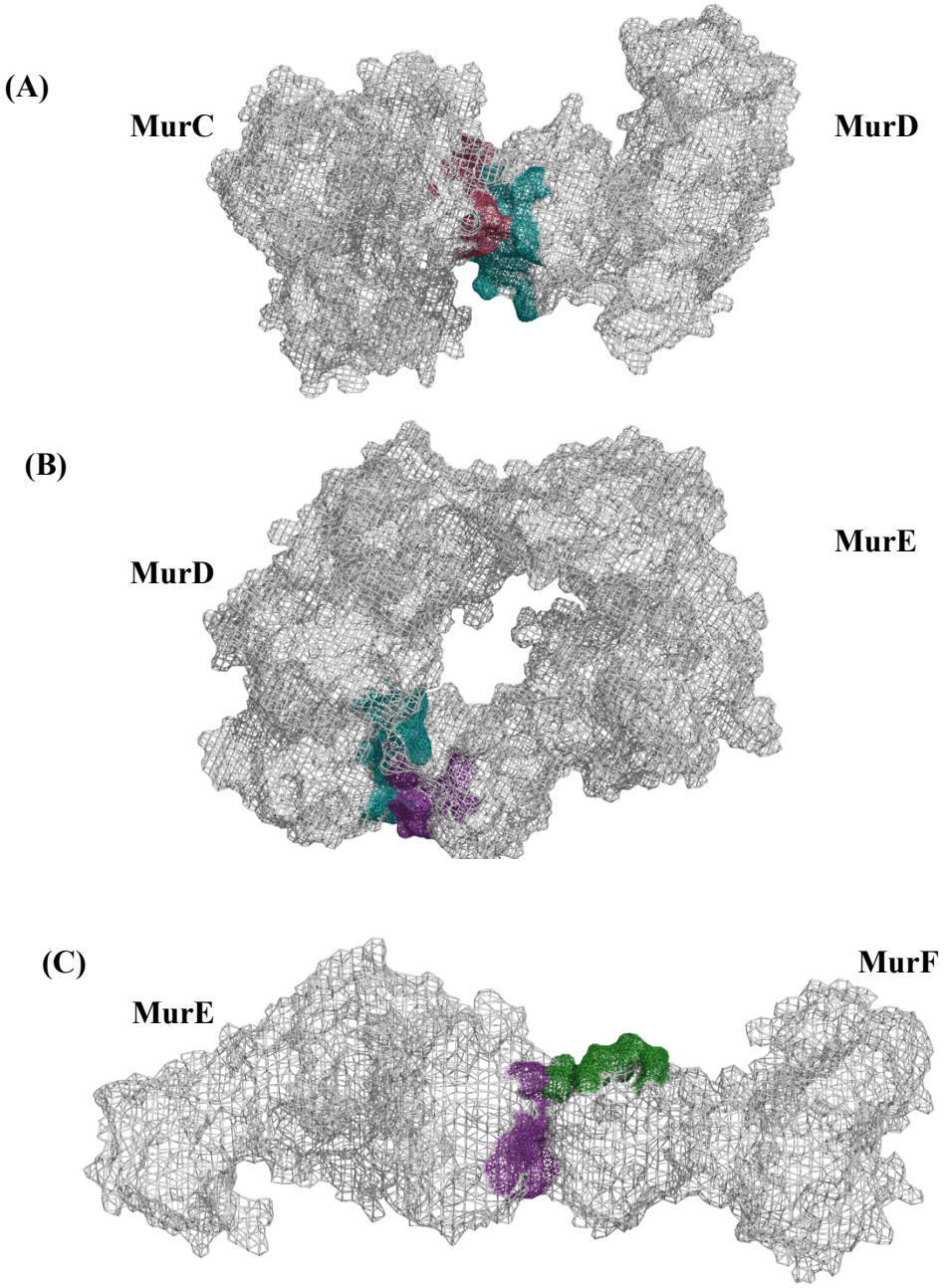

Figure 6. 17: Structural diagrams to show the interaction areas between pairs of Mur ligases

Using HADDOCK 2.4, and the residues identified by PRISM, pairs of Mur ligases were analysed for their ability to form binary complexes. The top hit for each of these pairings is shown. The residues previously identified by PRISM, and used as active residues by HADDOCK are highlighted in the structures. MurC residues are shown in red, MurD residues are shown blue, MurE residues are shown in purple and MurF residues are shown in green. (A) Predicted binary complex between MurC and MurD. (B) Predicted binary complex between MurD and MurE. (C) Predicted binary complex between MurE and MurF.

HADDOCK provides a score for the interactions predicted based on the equation:

$$HADDOCK\ score = \\ 1 \times Van\ der\ Waals\ energy \\ +0.2 \times Intermolcular\ electrostatic\ energy \\ +1 \times Desolvation\ energy \\ +\ 0.1 \times\ Ambiguous\ Interaction\ Restraint\ energy$$

These scores, along with the Z score provided by HADDOCK are shown in **Table 6.2**. The Z score indicates how many standard deviations from the average cluster this cluster is in terms of Z score.

	MurC-MurD	MurD-MurE	MurE-MurF
HADDOCK score	-74.3 +/- 1.1	-86.4 +/- 1.0	-64.6 +/-5.4
Van der Waals	-50.6 +/- 3.1	-52.9 +/- 4.6	-23.2 +/- 2.6
Electrostatic	-130.7 +/- 32.8	-195.8+/-40	-183.9 +/-30.8
Z score	-1.9	-2.1	-1.8

Table 6. 2: HADDOCK top hits for binary complex formation between the Mur ligases from E. coli

Using HADDOCK 2.4, binary complex formation between the Mur ligases from *E. coli* was predicted. The HADDOCK score, Van der Waals energy score, electrostatic energy score and Z score are listed.

The energy values provided by HADDOCK suggest that the interactions predicted were feasible. Visual inspection of the predicted interactions also suggested that the predicted binary complex formations were feasible as no predicted complex formation blocked the active site of the proteins involved, forced the proximity of repulsive charge:charge interactions or twisted the protein into an unnatural state. These results, along with the PRISM results suggest that the *E. coli* Mur ligases may be able to form binary complexes in which they are active.

3.10 Production of homology models of the *S. agalactiae* Mur ligases

The ability of the *E. coli* Mur ligases to form binary complexes was predicted via PRISM and HADDOCK. Currently, *E. coli* is the only bacterium for which all the Mur

ligase structures are known. To predict the ability of the *S. agalactiae* Mur ligases to form binary complexes, homology models of the ligases would need to be produced. One way to produce homology models is via the software SWISS-MODEL. SWISS-MODEL generated homology models by generating a pair-wise alignment to the template sequence provided. Backbone only models were then formed using an average of the atom positions of the template structure, with constraint space programming providing coordinates for regions of insertions or deletions that could not be determined from the template. Side chain modelling was the final stage carried out using weighted positions of corresponding residues within the template structure [135]. To generate the homology models, the amino acid sequence of the

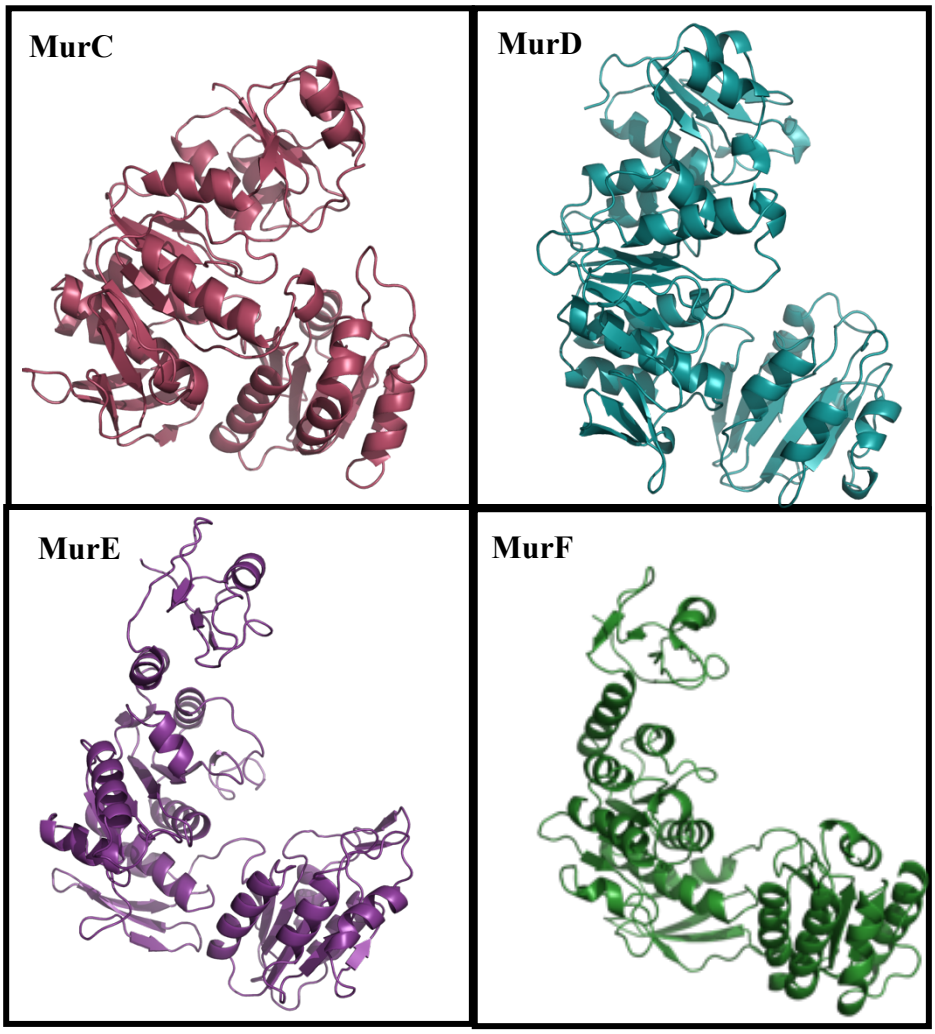

Figure 6. 18: Homology models of the Mur ligase from S. agalactiae
Using SWISS-MODEL, homology models of the four Mur ligases from *S. agalactiae* were generated using 'open' *E. coli* structures as templates. The homology models were then visualised via Pymol.

four Mur ligases were taken from the KEGG database using the KEGG genome T00091 for *S. agalactiae* 2603 (serotype V).

A user template modelling mode on SWISS-MODEL was then used to model the sequences, with the previously used *E. coli* structures acting as templates. The homology models for the four Mur ligases from *S. agalactiae* generated via SWISS-MODEL are shown in **Figure 6.18**. 98% of the *S. agalactiae* MurC sequence was modelled against *E. coli* MurC (2F00). 94% of the *S. agalactiae* MurD sequence was modelled against *E. coli* MurD (1E0D). 91% of the *S. agalactiae* MurE sequence was modelled against *E. coli* MurE (7B53). 89% of the *S. agalactiae* MurF sequence was modelled against *E. coli* MurF (1GG4). The homology models produced had high levels of sequence modelling, suggesting that the predicted structures would be very similar to the actual 'open' structure of these proteins. This means the homology models could be used to help predict the interaction areas for binary complex formation amongst the Mur ligases from *S. agalactiae.*

3.11 Binary complex prediction of the *S. agalactiae* Mur ligases via HADDOCK

Using the homology models of the *S. agalactiae* Mur ligases, and the previously generated binary complex formation models from PRISM and HADDOCK, the residues potentially involved in complex formation within the *S. agalactiae* Mur ligases were identified. By aligning the homology models of the *S. agalactiae* Mur ligases to the binary complex formation models, residues within the *S. agalactiae* Mur ligases that corresponded to interacting residues within the *E. coli* Mur ligases were identified. If the residues were comparable, or still could form an interaction with its partnering amino acid, residues were considered to be potential interacting residues. HADDOCK was then used to identify if binary complex formation could exist between the *S. agalactiae* proteins using the homology models generated via SWISS-MODEL. Active residues were listed as the residues identified via alignment with the *E. coli* ligases, and passive residues were identified by the software. The software was optimized for bioinformatic predictions. HADDOCK was able to predict the interaction between all the pairs of *S. agalactiae* Mur ligases using the

residues provided. The top hit for each pair is shown in **Figure 6.19,** and the scores for each hit provided in **Table 6.3**.

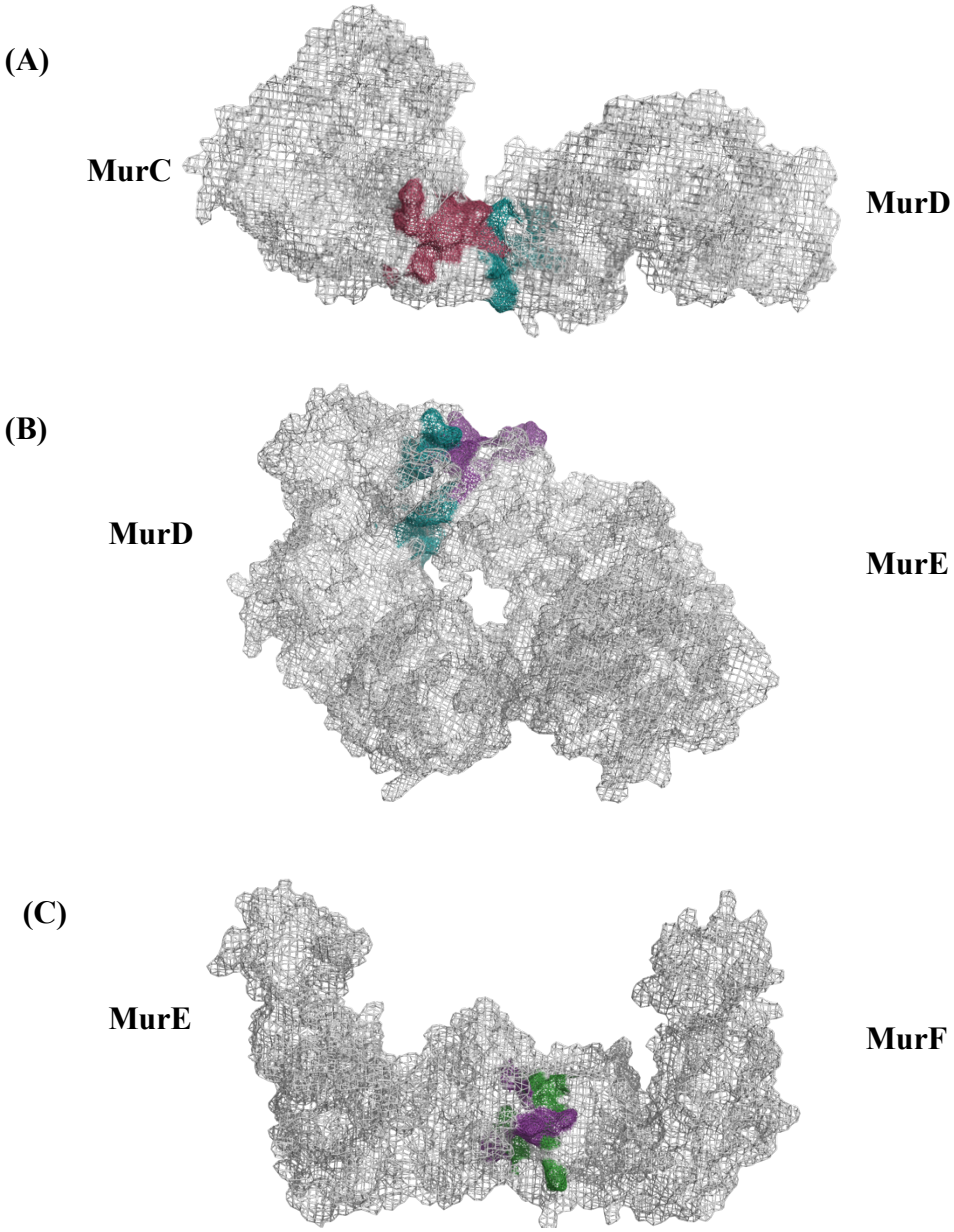

Figure 6. 19: Structural diagrams to show the interaction areas between pairs of Mur ligases from S. agalactiae using HADDOCK

Using HADDOCK 2.4, and the residues identified as corresponding to *E. coli* interacting residues, pairs of *S. agalactiae* Mur ligases were analysed for their ability to form binary complexes. The top hit for each of these pairings is shown. The residues previously identified by PRISM, and used as active residues by HADDOCK are highlighted in the structures. MurC residues are shown in red, MurD residues are shown blue, MurE residues are shown in purple and MurF residues are shown in green. (A) Predicted binary complex between MurC and MurD. (B) Predicted binary complex between MurD and MurE. (C) Predicted binary complex between MurE and MurF.

	MurC-MurD	MurD-MurE	MurE-MurF
HADDOCK score	-75.9 +/-3.4	-96.4 +/-1.8	-85.4 +/-4.1
Van der Waals	-19.1 +/-5.9	-38.5 +/-7.2	-33.6 +/-4.9
Electrostatic	-321.9 +/-19.7	-213.1 +/-20.1	-336.1 +/-20.2
Z score	-2.1	-1.7	-2.1

Table 6. 3: HADDOCK top hits for binary complex formation between the Mur ligases from S. agalactiae

Using HADDOCK 2.4, binary complex formation between the Mur ligases from *S.agalactiae* was predicted. The HADDOCK score, Van der Waals energy score, electrostatic energy score and Z score are listed.

The energy values provided by HADDOCK suggest that the interactions predicted were feasible. Visual inspection of the predicted interactions was also able to determine that the predicted binary complex formations were feasible as no complex formation blocked the active site of the proteins involved or twisted the protein into an unnatural state which forced the proximity of repulsive charge: charge interactions. These results suggested that the *S. agalactiae* Mur ligases may be able to form binary complexes in which they are active.

3.12 Alphafold for binary complex prediction

Alphafold is an AI system that was recently developed by DeepMind to help predict a proteins 3D structure from its amino acid sequence [136]. Alphafold works by generating multiple sequence alignments (MSA) from a query amino acid sequence via several databases of protein sequences. Alongside this, Alphafold also identifies proteins that have similar structures to the inputted sequence and uses these as templates to generate an initial structure [136]. A final structure is generated via the creation of a 3D backbone structure, before the prediction of side chain placements occurs. Throughout the stages of structure prediction, Alphafold is continuously applying outputs from its own modules back into the structure prediction, allowing refinement of the structure. Due to its ability to assess its own predicted structures, Alphafold has been shown to be able to predict protein

structures with a high level of accuracy, even when no similar structure is known [136].

As well as being able to predict protein structures, Alphafold has been developed to allow for the prediction of protein complexes [137]. This uses the same learning system based on MSAs and pair representation as standard Alphafold with minor changes to allow for cross-chain genetic information to be incorporated into the system. Alphafold does not require previous experimental data to identify the region of the protein or specific residues that may be involved in complex formation, allowing Alphafold to predict complex structures for previously unidentified complexes.

Alphafold predictions can be evaluated by a variety of means. Firstly, the sequence coverage of the predicted Alphafold models can provide information on how accurate the folding of the individual proteins are. Secondly, comparison of the models produced by Alphafold for their similarity and the variations between models can provide information on how confident Alphafold is within the modelling. Thirdly, Alphafold generates PAE scores that can provide information on how likely the residues are to be in to within the region of the structure that Alphafold has predicted [138].

A control Alphafold run was carried out with a known binary complex structure of HisF-HisH to determine how accurately Alphafold can predict binary complex formation [139]. As can be seen from **Figure 6.20A**, Alphafold predicted a structure within 5 angstroms of the known structure of the complex. Sequence coverage was high over the two proteins and comparison of the five models showed highly similar predictions, as seen in **Figure 6.20B and C.** Co-evolution data for the top model showed low PAE scores for residues within each protein along with residues across the two proteins, as seen in **Figure 6.20D**.

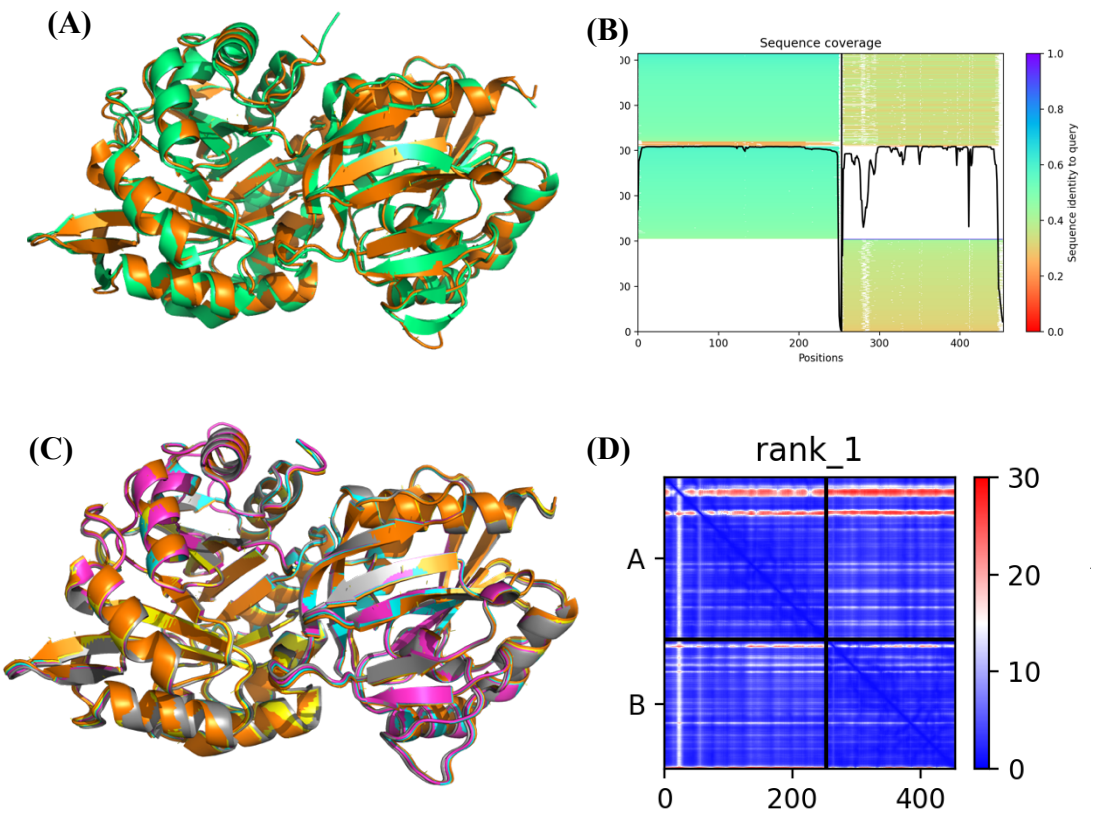

Figure 6. 20: Alphafold prediction of the HisF-HisH binary complex

Using Alphafold 2, the structure of the HisF-HisH complex was predicted to act as a control for future binary complex predictions. (A) The Alphafold predicted structure of HisF-HisH (shown in orange) was compared to the known structure of the HisF-HisH structure (PDB: 1GPW, shown in green). (B) Sequence coverage of residues in HisH and HisF predicted by Alphafold (C) Comparison of 5 models predicted by Alphafold for the binary complex of HisH and HisF. (D) PAE score for the top model predicted by Alphafold.

3.12.1 Binary complex prediction of the *S. agalactiae* Mur ligases via Alphafold

Using Alphafold2, binary complex formation between the *S. agalactiae* Mur ligases was predicted. The protein sequences previously used to generate the homology models of the *S. agalactiae* Mur ligases were inputted into the Alphafold2 Google Colab in their respective pairs. The five models produced were then viewed in Pymol and compared to determine similarity. Along with comparison of the five models produced, the sequence coverage and PAE score of the models were considered when determining the accuracy of the predicted binary complex.

Alphafold was able to produce five models of the binary complex formation of MurC-MurD from *S. agalactiae*. The sequence coverage of the two proteins was high, with around 2000 sequences used to predict the structure of the two proteins as seen in **Figure 6.21A**. As can be seen in **Figure 6.21C**, comparison of the five predicted models from Alphafold showed that there were was a high level of consensus in the predicted structure of the top three ranked structures, while rank 4 and 5 models were in a different arrangement.

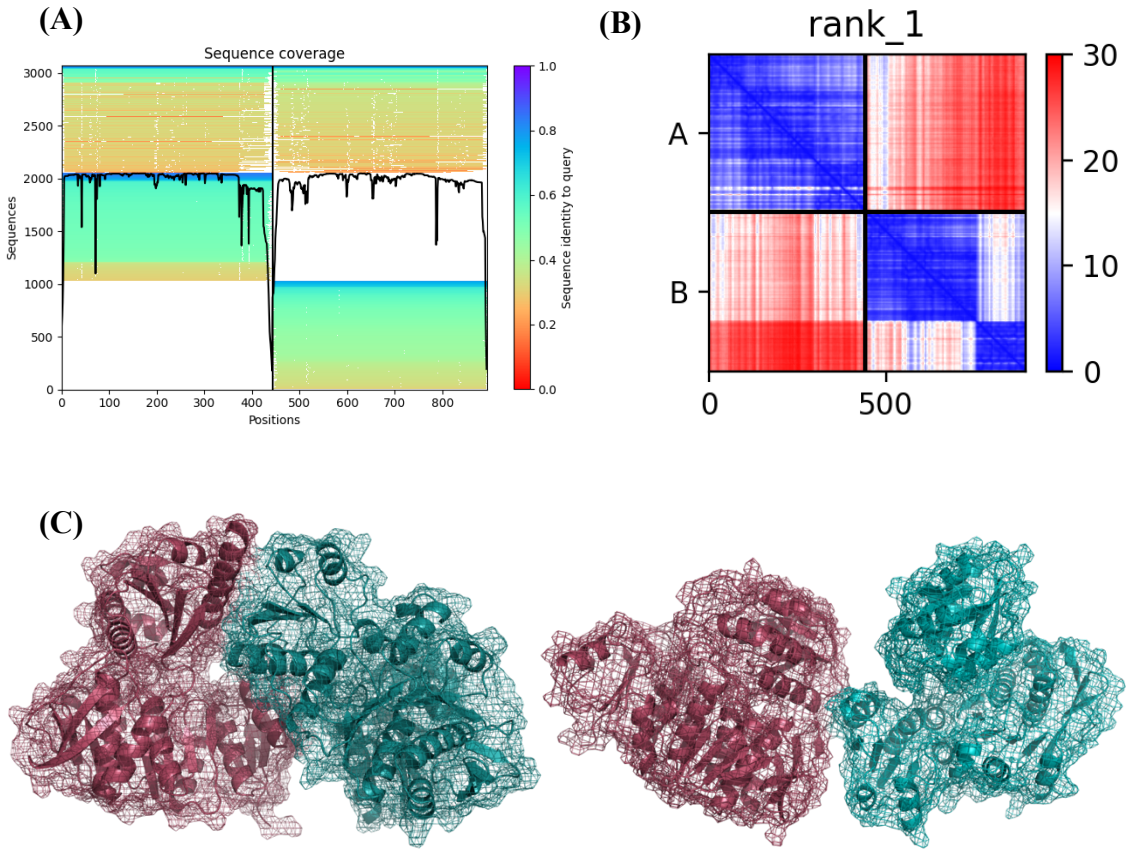

Figure 6. 21: Alphafold predicted binary complex between MurC and MurD from S. agalactiae

Using Alphafold2, MurC and MurD from *S. agalactiae* were analysed for their ability to form a binary complex. (A) Sequence coverage of predicted structures of MurC and MurD. (B) PAE scores of rank 1 model of binary complex formation between MurC and MurD. (C) Comparison of predicted structures of binary complex formation of MurC-MurD. Two complex formations were predicted via Alphafold for the binary complex formation between MurC and MurD. Rank 1,2 and 3 predicted structure is shown on the left, rank 4 and 5 predicted structure is shown on the right. MurC is shown in red and MurD is shown in blue.

The PAE data for the top ranked model is shown in **Figure 6.21B.** The PAE scores for the individual proteins was low, suggesting a confidence in the prediction

of the structures of the individual proteins. However, there were very high PAE scores for the location of residues while in binary complex formation, showing poor confidence in the way in which the proteins relate to each other within the model, suggesting a high level of confidence in the intramolecular predictions but low intermolecular predictions.

The presence of multiple complex predictions combined with high PAE scores for intermolecular predictions suggested that the predicted binary complex between MurC and MurD from *S. agalactiae* may not be an accurate representation of binary complex formation.

Alphafold was able to produce five models of the binary complex formation of MurD-MurE from *S. agalactia*e. The sequence coverage of the two proteins was high, with around 2000 sequences used to predict the structure of the two proteins as seen in **Figure 6.22A**. The PAE data for the top ranked model is shown in **Figure 6.22B.** The PAE scores for the individual proteins was low, suggesting a confidence in the prediction of the structures of the individual proteins, although the PAE data for the top ranked model showed regions of higher PAE scores for the location of residues within MurD, suggesting a less accurate prediction of the structure of MurD. There were very high PAE scores for the location of residues while in binary complex formation, showing poor confidence in the way in which the proteins relate to each other within the model, suggesting a low level of confidence in the intermolecular predictions.

Comparison of the five predicted models from Alphafold showed that there was no interaction in models ranked 4 and 5 by Alphafold as seen in **Figure 6.22C**. Models ranked 1, 2 and 3 showed interaction between MurD and MurE, but interaction zones differed between the three models. A lack of consistency between the models showed a lack of accuracy in the model predictions, which when combined with the high PAE scores for intermolecular interactions suggested that the predicted binary complex between MurD and MurE from *S. agalactiae* may not be an accurate representation of binary complex formation.

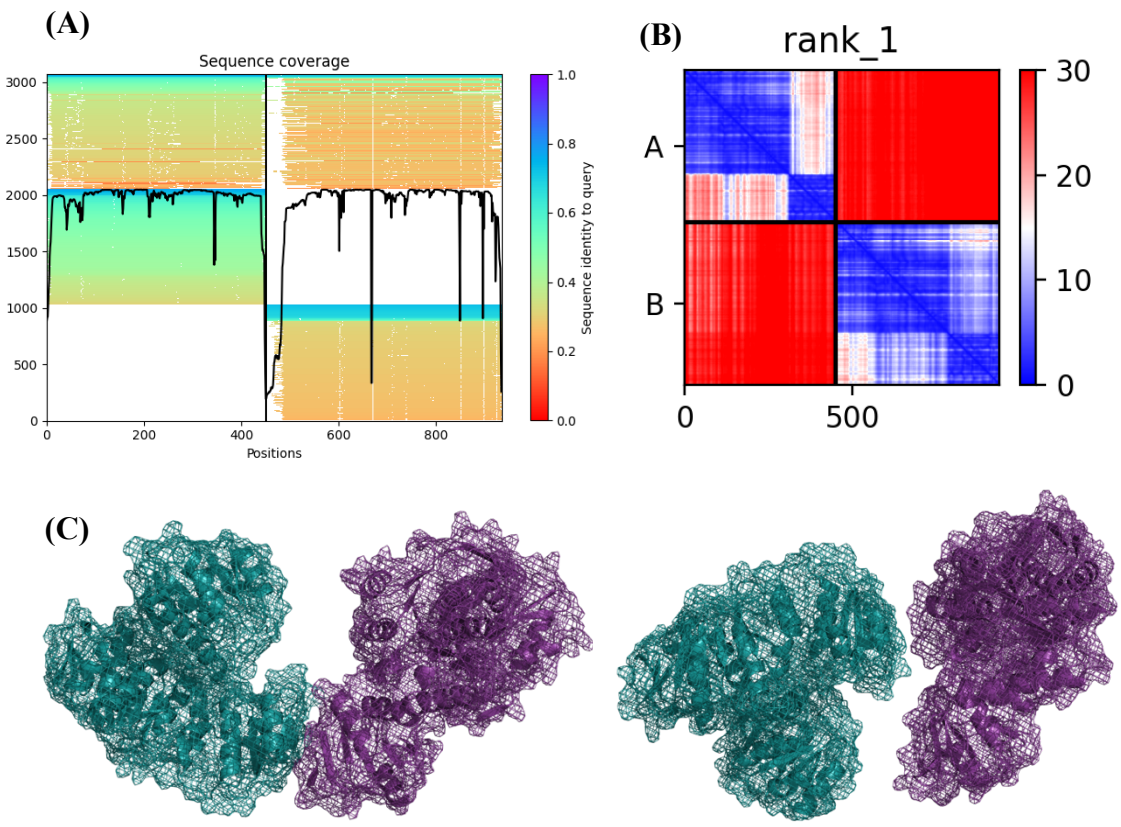

Figure 6. 22: Alphafold predicted binary complex formation between MurD and MurE

Using Alphafold2, MurD and MurE from *S. agalactiae* were analysed for their ability to form a binary complex. (A) Sequence coverage of predicted structures of MurD and MurE. (B) PAE scores of rank 1 model of binary complex formation between MurD and MurE. (C) Comparison of predicted structures of binary complex formation of MurD-MurE. Three complex formations were predicted via Alphafold for the binary complex formation between MurD and MurE, with two models showing no interaction. Rank 1 predicted structure is shown on the left, rank 4 predicted structure is shown on the right. MurD is shown in blue and MurE is shown in purple.

Alphafold was able to produce five models of the binary complex formation of MurE-MurF from *S. agalactiae*. The sequence coverage of the two proteins was high, with around 2000 sequences used to predict the structure of the two proteins as seen in **Figure 6.23A**. The PAE data for the top ranked model showed regions of high PAE scores for the location of residues within both MurE and MurF, suggesting a less accurate prediction of the intramolecular predictions within these Mur ligases as seen in **Figure 6.23B**. There was also high PAE scores for the location of residues while in binary complex formation, as seen in **Figure 6.23B,** showing poor confidence in the way in which the proteins relate to each other within the model, suggesting a low level of confidence in the intermolecular predictions. As can be

seen in **Figure 6.23C**, comparison of the five predicted models from Alphafold showed that there was a high level of consensus in the predicted structure of the top two ranked structures, while rank 3,4 and 5 models were in different arrangements. However, visual inspection of the predicted models showed a lack of interaction between MurE and MurF in these arrangements, with no interaction in models 3, 4 and 5.

A lack of interaction between MurE and MurF within the predicted models, combined with the appearance of multiple complex predictions and high PAE scores for intermolecular interactions suggested that the predicted binary complex between MurE and MurF from *S. agalactiae* may not be an accurate representation of binary complex formation.

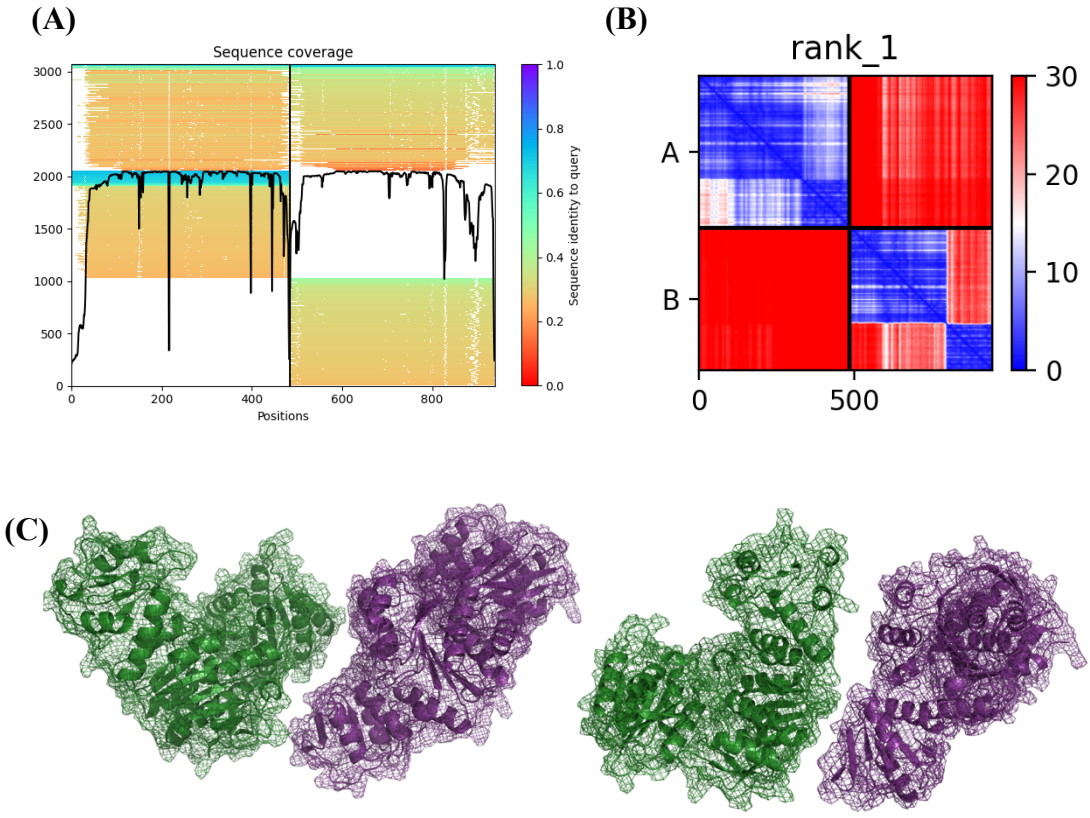

Figure 6. 23: Alphafold predicted binary complex formation between MurE and MurF

Using Alphafold2, MurE and MurF from *S. agalactiae* were analysed for their ability to form a binary complex. (A) Sequence coverage of predicted structures of MurE and MurF. (B) PAE scores of rank 1 model of binary complex formation between MurE and MurF. (C) Comparison of predicted structures of binary complex formation of MurE-MurF. A complex formations were predicted via Alphafold for the binary complex formation between MurE and MurF, while three models showed no interaction. Rank 1,and 2 predicted structure is shown on the left, rank 3 predicted structure is shown on the right. MurE is shown in purple and MurF is shown in green.

3.13 Alphafold predictions present in only one state

Complex predictions of binary complex formation between the *S. agalactiae* Mur ligases generated via Alphafold lack similarity amongst models, along with high PAE scores for the models. The lack of interaction between the Mur ligases within certain models also suggests that these binary complex formation predictions may not be biologically present. Alphafold predictions are produced in only one state [140], which may affect its ability to accurately predict the binary complex formation of the Mur ligases due to the conformational changes that occur upon binding of substrates. To better understand how conformational change may affect Alphafold's ability to predict binary complex formation, the binary complex of MurT/GatD was predicted via Alphafold and compared to the known complex formation (PDB: 6GS2) [79].

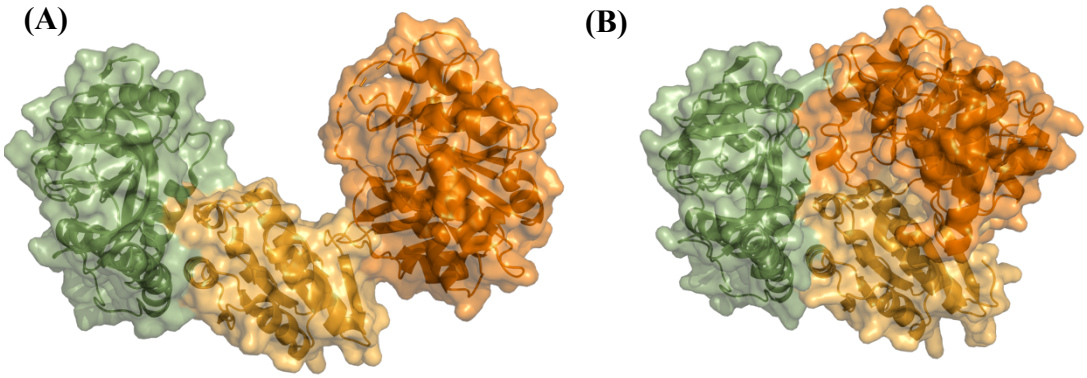

Figure 6. 24: Alphafold predicts the MurT/GatD complex in a different conformational state to known complex

Using Alphafold2, the MurT/GatD binary complex was predicted and compared to the known complex formation. MurT C-terminal is shown in yellow, MurT middle domain is shown in orange, GatD is shown in green. (A) Known complex formation of MurT/GatD. PDB: 6GS2 (B) Alphafold predicted complex formation of MurT/GatD.

As can be seen from **Figure 6.24**, the Alphafold prediction of the binary complex of MurT/GatD differs from the known complex formation. Alphafold was able to predict the same interaction of GatD to the C-terminal domain of MurT. However, the N-terminal domain and middle domain of MurT were in a different position within the Alphafold prediction compared to the known complex structure, resulting in a new interaction area of MurT to GatD. The middle domain of MurT

moved a distance of around 20 Å between the known complex structure and the Alphafold prediction, resulting in a 'closed' MurT conformation within the Alphafold prediction. MurT binds to Lipid II to allow for amidation [26]. The binding of Lipid II has been predicted to induce a conformational change within MurT similar to that seen within the Mur ligases upon binding of ATP [79], resulting in a 'closed' conformation of MurT. The difference of the layout of the middle domain and N-terminal domain of MurT between the known complex structure and predicted Alphafold structure could be due to this conformational change. A conformational change within MurT may have led to a different Alphafold prediction of complex formation between MurT to GatD to that previously identified, suggesting that conformational changes within proteins may have a large effect on the binary complex formation that Alphafold is able to predict.

4. Conclusions and Future Direction

4.1 Formation of a binary complex between the Mur ligases

The ability of the Mur ligases to form a complex, either independently or in the presence of additional structural proteins is still a debated topic. Complex formation between MurD and MurE from *S. agalactiae* was seen experimentally via MST and two protein expression systems. These protocols were able to identify a complex formation between MurD and MurE from *S. agalactiae* that occurred independently of other proteins. MST was able to estimate a dissociation constant for the interaction of MurD and MurE at 49 μM. Miyachiro et al had previously identified K_D values ranging from 283 nM to 23 nM [82] for binary complex formations between the Mur ligases of *S. pneumoniae* using MST, with MurD – MurE having a K_D of 40 nM [82]. Miyachiro et al employed MurE as the ligand while MurD was employed as the ligand within our studies. The binding of the fluorophore to MurE rather than MurD within our studies may have prevented as tight a binary complex formation as that previously seen. However, the difference in K_D does suggest that further investigation into the formation of the binary complex formation between the *S. agalactiae* Mur ligases is required. Analytical ultracentrifugation (AUC) is an analytical technique that allows the study of macromolecules in solution. AUC would allow for the determination of complex formation between MurD and MurE in solution, while also providing data on the number of molecules present within the complex [82], providing further insight into the formation of the complex between MurD and MurE.

4.2 Role of substrates within binary complex formation

The Mur ligases are multi substrate enzymes, having three unique substrates required for activity of the enzyme. Upon binding of these substrates the Mur ligases undergo a conformational change; the C-terminal domain of the Mur ligases undergoes a rigid body rotation allowing it to be brought towards the N-terminal and central domain. The capping of ATP by the C-terminal domain appears to induce this conformational change, and allows for the binding of the nucleotide substrate. A final rotation of the C-terminal domain then causes the enzyme to

enter its active 'closed' conformation [63]. This domain movement that occurs due to the binding of substrates may play a role in complex formation between the Mur ligases. The K_D of the complex formation between MurD and MurE was seen to change in the presence of substrates, suggesting that substrates may affect the complex formation between the Mur ligases.

The effect of substrates on the stability of the complex would need further investigation, potentially via AUC which can provide information on the shape of macromolecules and conformational changes within macromolecules [141], allowing AUC to be used to investigate the effect substrates have on complex formation.

4.3 Complex formation effect on enzyme activity

MurD from *S. agalactiae* was seen to be active while in complex formation via an activity assay. Activity assays were also able to determine that MurE was able to use the UDP-MurNAc-L-Ala-D-Glu formed by MurD. One hypothesis for why the Mur ligases may form a complex within the cytoplasm is to allow for the channelling of the UDP intermediates [82,83]. Channelling of substrates can provide kinetic advantages as seen with polyketide synthase modules where the K_{cat} was increased 10 to 100 fold when channelling was available [142]. The ability of the Mur ligases to channel UDP intermediates while in complex formation could be established by using a heavy labelled UDP-MurNAc-L-Ala within an activity assay of the complex proteins. Tracking of the production of heavy labelled UDP-MurNAc-L-Ala-D-Glu-L-Lys in comparison to unlabelled UDP-MurNAc-L-Ala-D-Glu-L-Lys would allow for the determination of whether MurE preferentially turned over the product of MurD to free substrate [143]. Channelling of the UDP intermediates could provide an explanation into the lack of inhibitors that are able to work *in vivo* against the Mur ligases, due to increased substrate concentrations.

However, the Mur ligases can become inhibited by their UDP substrates, as shown with MurE from *P. aeruginosa* becoming inhibited by UDP-MurNAc-L-Ala-D-Glu at concentrations higher than 300 μM [52]. Complex formation of the Mur ligases could result in a regulation of the Mur ligases that results in a decrease of enzyme activity. Further biochemical testing via activity assays could determine if complex formation causes a downregulation of enzyme activity.

4.4 Role of computational predictions for structure determination

Computational software can provide predictions for structures which have not yet been solved. HADDOCK predicted the formation of binary complexes between the Mur ligases of *E. coli* and *S. agalactiae,* based on the residues predicted via PRISM, suggesting potential structures for the binary complexes of the Mur ligases. Computational modelling is constantly evolving, and therefore interaction predictions can shift depending on the software used. Alphafold is an artificial intelligence program designed around a deep learning system that is able to predict a protein's 3D structure from its amino acid sequence [136]. Binary complex predictions for the Mur ligases via Alphafold greatly differed from the predicted structures generated via HADDOCK. Alphafold could be viewed as a preferable software for the prediction of complex formation amongst the Mur ligases due to its ability to predict complex formation without previous knowledge of residues involved in the complex, allowing an unbiased prediction. However, Alphafold's ability to predict complexes is limited. Alphafold is only able to predict structures in a single state [140]. The inability of Alphafold to reproduce the MurT/GatD binary complex suggests that conformational changes within the proteins does affect the ability of Alphafold to predict complex formation. The Mur ligases are known to undergo a conformational change upon the binding of substrates, allowing them to be present in multiple conformational states. MST K_D data suggested that the binding of substrates may play an important role in the formation of the binary complex between MurD and MurE from *S. agalactiae*, potentially limiting the ability of Alphafold to accurately predict binary complex formation between the Mur ligases.

The models produced via HADDOCK and Alphafold provide potential interaction regions within the Mur ligases that may be involved in complex formation. However, these are only predictions and require experimental procedures to identify how the binary complexes are forming. One way to determine how the binary complex formations are forming between the Mur ligases is to use carbene footprinting [144]. Carbene is introduced to the proteins and labels areas of the protein that are accessible. Mass spectrometry is then used to identify the residues

to which the carbene was unable to bind, due to them being involved within complex formation [144]. Mutation of these residues could then be carried out to identify the residues that are essential for complex formation. Identification of the specific regions and residues involved in complex formation could allow for targeted fragment screens that would inhibit the formation of the Mur ligase complex, allowing the development of antibiotics targeted towards the Mur ligases.

Chapter 7

Discussion and Final Conclusion

1. Impact of fragment screening on the development of novel inhibitors

The development of novel inhibitors is a task that scientists have been attempting to tackle for many years. One newer approach to this problem is the screening of fragments. Fragments are small chemical scaffolds, generally smaller than 250 Da, that can act as the basis for the development, in this instance, of an antibacterial compound [129]. There are a number of different techniques that allow for the screening of fragments. X-ray crystallography allows for the structural characterisation of the binding ability of fragments to a protein of interest [98], as seen within **Chapter 3**, while *in silico* screening can allow for the targeted screening of fragments to a specific region of interest within a protein as carried out in **Chapter 4**.

Both X-ray crystallography and *in silico* screening can act as a starting point for the development of a fragment screen that can then be tested for inhibitory effects against a protein of interest, as seen in **Chapter 3** and **Chapter 4**. Development of hit fragments can then be carried out to improve their efficacy and cell permeability to allow for the development of an antibacterial compound that can enter clinical trials. Currently six fragment derived drugs have passed through clinical trials and been approved for clinical use. Most recently the novel kinase inhibitor compound, Asciminib, was approved for the treatment of chronic myeloid leukaemia [145]. The process of discovering Asciminib began with an NMR fragment screen of 500 diverse fragments [146]. Erdafitinib, a drug approved for the treatment of urothelial carcinomas with genetic alterations in the FGFR2 or FGFR3 genes, began in the lab via the repurposing of compounds from a previous fragment screen into a virtual screen, allowing for the identification of a compound that bound within the intended target [147]. These success stories show that fragment screening can play a pivotal role in the development of novel compounds, and potentially could be used for the discovery of a novel antibacterial compound.

2. Role of multi-targeting in inhibitor design

Multi-targeted inhibitors are a more attractive approach for the development of novel antibacterial compounds, due to their ability to reduce the emergence of resistance. Single targeted antibacterial compounds are prone to the emergence of resistance, with many single targeted antibacterial compounds developing resistance before they can make it through clinical trials. Recently, a promising antibacterial compound GSK 052, an inhibitor of bacterial leucyl tRNA-synthetase, rapidly selected resistance in bacteria within phase II clinical trials, with resistance emerging in patients against the new antibacterial compound within 2 days [148]. Many long-established antibacterial compounds such as β-lactams and quinolones are able to effectively target multiple proteins and so confer resistance at a slower rate [121].

Due to the reduction in the emergence of resistance to multi-targeting antibacterial compounds, the Mur ligases are a very attractive target for the development of antibacterial compounds. Due to their similar catalytic mechanism and similar domain topology, it is possible that novel multi-targeting inhibitors can be designed and developed to act against the Mur ligases. Within **Chapter 3** and **Chapter 4**, inhibitory fragments that were able to target both MurD and MurE were identified via high throughput biochemical screens.

3. Role of complex formation of the Mur ligases within the design of inhibitory fragments

The formation of a complex involving the Mur ligases has been suggested as one potential reason why a suitable *in vivo* antibacterial compound against the Mur ligases has yet to be identified. Previous studies have identified the potential for the Mur ligases to interact either with each other in binary complex formations [82], or with structural proteins such as MreB and MurG [149]. The ability of MurD and MurE from *S. agalactiae* to form a binary complex was investigated within **Chapter 6,** with evidence suggesting that these two proteins can form a binary complex independent of other proteins.

The identification of a complex formation between the Mur ligases could greatly affect the development of antibacterial compounds targeted towards the Mur ligases. Previous fragment screens against the Mur ligases have focused on the known structures of the individual proteins; identifying areas of interest such as that used within the X-ray crystallography screen of **Chapter 3**. These sites however may become inaccessible to antibacterial compounds in the presence of a complex formation between the Mur ligases, preventing previously identified inhibitory fragments from having *in vivo* activity [102,116]. Understanding how the Mur ligases form complexes would provide structural data that would guide future inhibitory screens to prevent this issue arising.

Along with allowing for better predictions of the binding ability of inhibitory compounds within fragment screening, better understanding of complex formation between the Mur ligases could provide a greater understanding of the kinetics of the Mur ligases. The ability of the Mur ligases to potentially channel intermediates within a complex could greatly affect the IC_{50} values of inhibitory fragments [150], preventing them from being effective antibacterial compounds. The development of biochemical assays that consider the formation of Mur ligase complexes could allow for the identification of inhibitory fragments that have antibacterial effects *in vivo* [151].

4. Final conclusions

Antibacterial resistance is increasing, and new antibacterial compounds are desperately required to fight the rising number of antibacterial resistant infections [152]. Proteins involved in peptidoglycan formation are an attractive target, with the Mur ligases presenting a unique target due to the ability to design a multi-targeted inhibitor with the potential to act upon all four Mur ligases, potentially reducing the emergence of antibacterial resistance to newly developed drugs.

Fragment screening provides an attractive starting point for the development of new antibacterial compounds due to its ability to identify potential fragment scaffolds from large screens [129]. Biochemical testing then allows for the identification of the functional effect of fragments identified via fragment screens

on the proteins of interest [150]. These two techniques work hand in hand to allow for the development and optimization of antibacterial compounds from small chemical fragments. Fragment screens and biochemical testing have been used to produce effective new antibacterial compounds [145], but for the development of new antibacterial compounds targeted towards the Mur ligases, we must have a greater understanding of the ability of the Mur ligases to form complexes to develop antibacterial compounds that are effective *in vivo*.

Supplementary Data

Supplementary 1

Skeletal diagrams of elaborated fragment screen

373

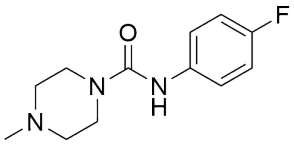

PIPERAZINE ANALOGUES	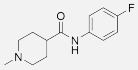 OSA_000738	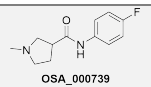 OSA_000739	
ARYL ANALOGUES	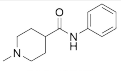 OSA_000740	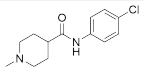 OSA_000741	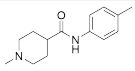 OSA_000742
	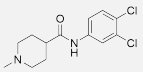 OSA_000743	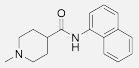 OSA_000744	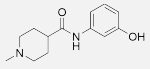 OSA_000745
	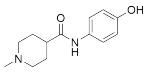 OSA_000746	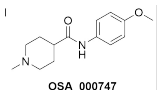 OSA_000747	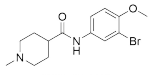 OSA_000748
	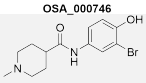 OSA_000749	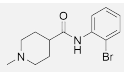 OSA_000750	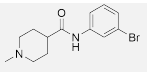 OSA_000751
	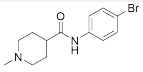 OSA_000752		
EXTENDED ANALOGUES	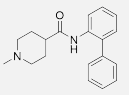 OSA_000753	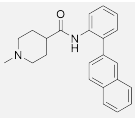 OSA_000754	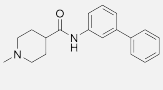 OSA_000755
	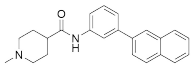 OSA_000756	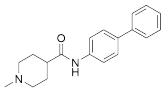 OSA_000757	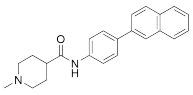 OSA_000758
	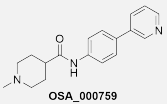 OSA_000759	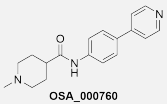 OSA_000760	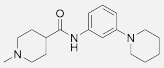 OSA_000761
	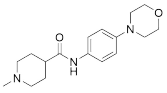 OSA_000762	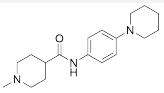 OSA_000763	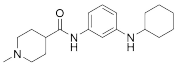 OSA_000764
	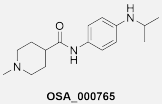 OSA_000765	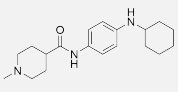 OSA_000766	

349

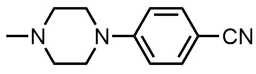

PIPERAZINE ANALOGUES	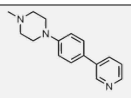 FI132-1 OSA_000771	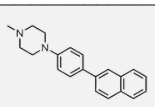 FI144-1 OSA_000780	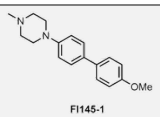 FI145-1 OSA_000781
	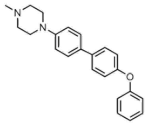 FI150-1 OSA_000784	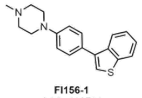 FI156-1 OSA_000790	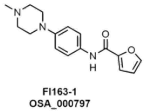 FI163-1 OSA_000797

	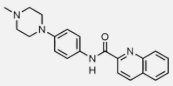 FI164-1 OSA_000798	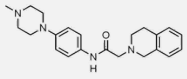 FI166-1 OSA_000799	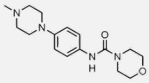 FI167-1 OSA_000800
	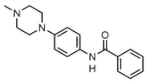 FI168-1 OSA_000801	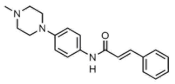 FI171-1 OSA_000802	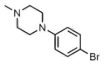 FI71-1 OSA_000808
	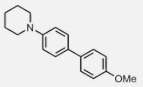 FI179-1 OSA_000809	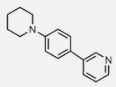 FI180-1 OSA_000810	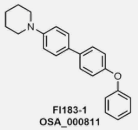 FI183-1 OSA_000811
MORPHOLINE ANALOGUES	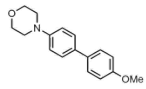 FI173-1 OSA_000803	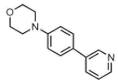 FI174-1 OSA_000804	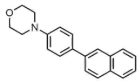 FI175-1 OSA_000805
	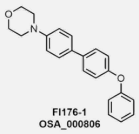 FI176-1 OSA_000806	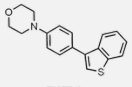 FI177-1 OSA_000807	
COMBINED FRAGMENT	 FI112-2 OSA_000767		

378

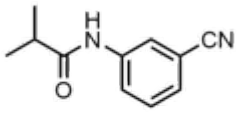

META ANALOGUES	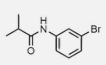 FI124-2 OSA_000768	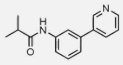 FI131-1 OSA_000770	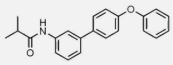 FI137-1 OSA_000776
	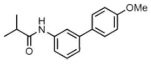 FI138-1 OSA_000777	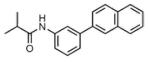 FI151-1 OSA_000785	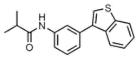 FI152-1 OSA_000786
PARA ANALOGUES	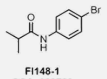 FI148-1 OSA_000783	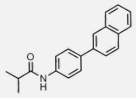 FI153-1 OSA_000787	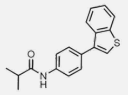 FI154-1 OSA_000788
	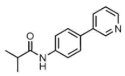 FI155-1 OSA_000789	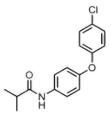 FI157-1 OSA_000791	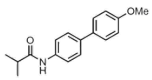 FI158-1 OSA_000792
	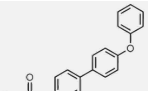 FI159-1 OSA_000793	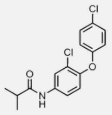 FI160-1 OSA_000794	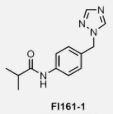 FI161-1 OSA_000795
	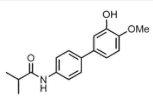 FI162-1 OSA_000796		

SULFONAMIDE ANALOGUES	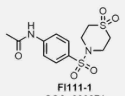 FI111-1 OSA_000071	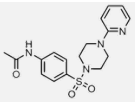 FI130-1 OSA_000769	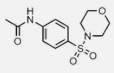 FI133-1 OSA_000772
	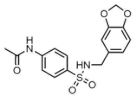 FI134-1 OSA_000773	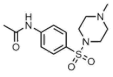 FI135-1 OSA_000774	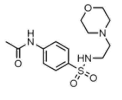 FI136-1 OSA_000775
	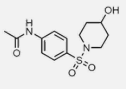 FI139-1 OSA_000778	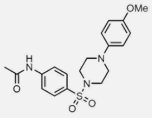 FI145-1 OSA_000781	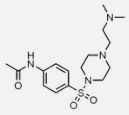 FI146-1 OSA_000782

Supplementary 2

Activity of MurD in the presence of elaborated fragments

Activity of MurD (%)							
Fragment ID	1	2	3	**Fragment ID**	1	2	3
1	83.88	77.63	77.43	**773**	17.25	14.29	26.86
2	123.35	131.61	127.54	**774**	31.94	39.83	35.44
4	74.79	76.21	66.23	**775**	87.49	78.11	81.99
71	108.09	83.91	195.42	**776**	25.00	18.77	22.75
738	-26.99	-18.03	-21.64	**777**	-275.11	-77.22	-290.36
739	31.72	19.65	22.80	**778**	61.37	108.11	35.78
740	36.27	12.11	18.94	**779**			
741	125.32	149.16	134.86	**780**	-8.14	-20.97	0.05
742	10.32	2.81	9.65	**781**	-446.09	-523.26	-622.96
743	85.47	96.87	139.61	**782**	102.43	94.15	107.48
744	113.56	116.99	112.33	**783**	29.19	37.50	34.12
745	70.02	87.14	56.99	**784**			
746	24.09	35.25	29.54	**785**	148.63	148.63	148.63
747	113.91	87.33	107.54	**786**	0.67	1.30	0.25
748	131.07	156.15	89.50	**787**	-38.10	-70.50	-28.91
749	19.54	11.55	22.56	**788**	24.76	15.05	17.17
750	132.40	166.99	100.86	**789**	12.24	12.74	24.02
751	50.12	30.08	39.17	**790**			
752	78.22	81.34	77.12	**791**	-14.49	-29.69	-24.23
753	45.13	44.39	36.03	**792**	2191.22	-134.96	737.47
754	1.40	0.84	0.40	**793**	717.68	-80.36	128.09
755	7.96	18.28	19.67	**794**	100.99	75.35	59.62
756	86.30	86.36	102.94	**795**	54.47	53.66	73.15
757	32.52	30.71	43.74	**796**	10.51	9.36	14.63
758	6.82	7.66	5.11	**797**	70.34	70.32	70.32
759	10.64	10.77	19.21	**798**	644.21	679.62	679.62
760	100.74	98.82	117.73	**799**			
761	125.65	94.34	129.37	**800**	94.03	111.29	156.47
762	60.88	71.78	55.54	**801**	51.78	75.27	67.80
763	107.00	89.13	97.41	**802**	563.83	736.34	518.88
764	84.34	118.92	95.39	**803**	-1756.60	-1779.28	-1742.42
765	18.48	22.78	22.31	**804**	150.72	158.73	142.07
766	103.40	89.52	84.35	**805**	167.52	82.05	95.71
767	65.34	33.01	55.60	**806**			
768	259.73	131.09	200.67	**807**	-76.59	-110.41	-3.48
769	108.46	263.05	238.89	**808**	92.49	193.31	138.85
770	48.45	52.09	42.93	**809**	-11.45	-45.29	-28.38
771	19.32	28.08	41.94	**810**	-4.67	-0.92	-4.24
772	35.79	42.46	34.91	**811**	1585.64	68.75	-336.97

Supplementary 3

Validation of an MESG coupled assay with MurE from *S. agalactiae*

Assay was dependent on presence of all substrates and ligase

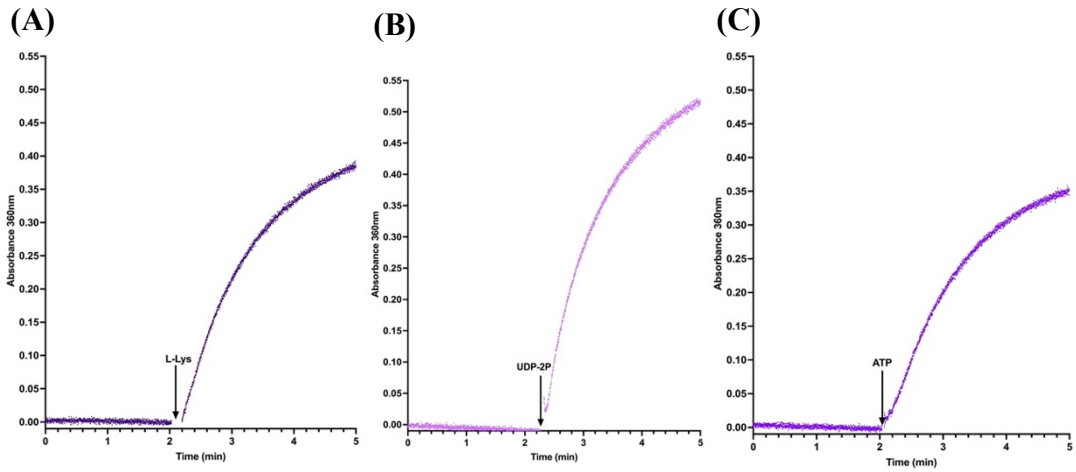

Figure S3. 1: The activity of MurE relies on the presence of all three substrates

The activity of MurE was tracked using a MESG coupled assay. All components of the assay were incubated at 37^0c barring one substrate which was added after 2 minutes. No activity was seen within any of the assays until all three substrates were present. (A) Comparison of initial rate when individual substrates were omitted and when all substrates were present. (B) L-Lys added after 1 minute. (C) UDP-MurNAc-L-Ala-D-Glu (UDP-2P) added after 1 minute. (D) ATP added after 1 minute.

Assay was linear to protein concentration

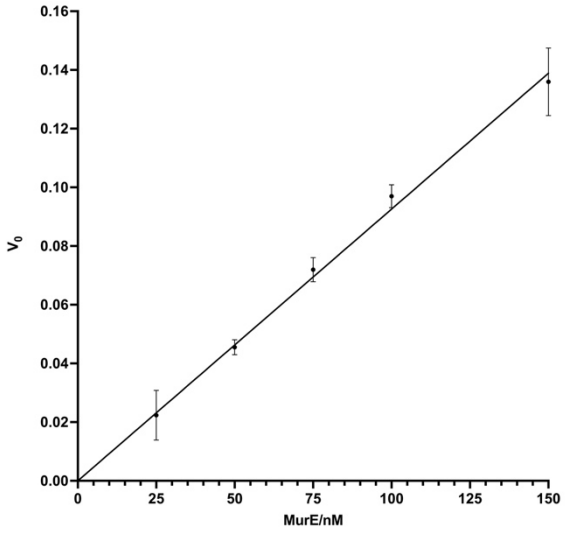

Figure S3. 2: MESG coupled reaction is reliant on MurE concentration

The activity of *S. agalactiae* MurE was determined via the MESG coupled assay. The assay was tracked in the presence of various MurE concentrations. The initial rate of the reaction was determined and plotted against MurE concentration. A linear relationship was observed between MurE concentration and initial rate.

ADPCP IC_{50}

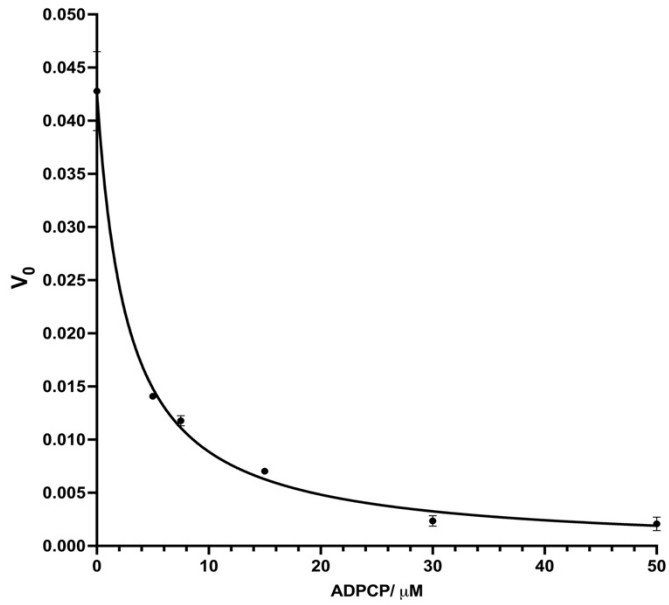

Figure S3. 3: ADPCP has an IC_{50} value of 2.7 μM against MurE from S. agalactiae

The IC_{50} of ADPCP against MurE was determined using a stopped MESG coupled assay. Substrate concentrations were at their K_m values. The concentration of ADPCP was increased and the initial rate of MurE determined. The IC_{50} value was determined as the concentration of ADPCP that reduced activity of MurE by 50%. All experiments were run in triplicate with error bars indicating SD.

Z prime

	MurE	MurE + ADPCP
Mean	0.1387	0.02708
Standard Deviation	0.00922	0.00381
Z prime Score	$Z = 1 - \frac{(3(0.00922) + 3(0.00381)}{(0.1387 - 0.02708)}$ $Z = 0.65$	

Supplementary 4

Enamine fragment screen IDs and SMILES

Plate 01		
Well ID	**Enamine ID**	**Smile**
A02	Z31428352	O=C(NCC=1C=CC=2OCOC2C1)C3=NNC=4C=CC=CC34
B02	Z1742686736	COC=1C=CC(OCC2=CC=3C=CC=CC3C(=O)N2)=C(C1)C(=O)N
C02	Z27695286	O=C(NCC=1C=CC=2OCOC2C1)C3=NNC(=O)C=4C=CC=CC34
D02	Z1230415721	COC=1C=C2N=C(CN(C)C=3C=CC=C(O)C3)NC(=O)C2=CC1OC
E02	Z31717432	OC=1C=CC=C(NC(=O)CCC2=NC=3C=CC=CC3C(=O)N2)C1
F02	Z1754180927	CC1=NN=C(O1)C2CN(CCO2)C(=O)CN3C(=O)NC=4C=CC=CC34
G02	Z57339412	COC=1C=CC(OCC2=NNC(=N2)C=3C=CC=NC3)=CC1
H02	Z1381367571	COC(C)(C)C1=NOC(CC2=CSC(=N2)N3CCNC3=O)=N1
I02	Z16225295	COCCNC(=O)CSC1=NN=C2NC=3C=CC=CC3N12
J02	Z1407882427	O=C1NCCN1C2=NC(CC3=NC(=NO3)C4CCOC4)=CS2
K02	Z94789885	COC=1C=CC(CNC(=O)C2=C(C)OC=3N=CNC(=O)C23)=CC1
L02	Z1172208621	Cl.Cl.CCN1CCN(CC1)C=2C=NC=C(Br)C2
M02	Z31129458	NC=1NN=C(CCCCCNC=2N=CN=C3SC=CC23)C1C#N
N02	Z365298776	CCC=1C=C(NN1)C(=O)NCC(N(C)C)C=2C=CC(OC)=CC2
O02	Z17559315	CC(SC=1N=C(N)N=C(N)N1)C(=O)NCC=2C=CC=3OCOC3C2
P02	Z1824274849	COC=1C=CC(=CC1)C2=CC(=NN2)N(C)CC3=NNC(=O)S3
A03	Z82184050	COC=1C=CC(CNC(=O)C2=C(C)OC=3N=CNC(=O)C23)=CC1OC
B03	Z56831588	NS(=O)(=O)C=1C=CC=C(NC(=O)C2=CC=3CCCC3S2)C1
C03	Z373770778	CC1=NN(C)C=2NC(=O)C(CCC(=O)NC=3C=NN(C)C3)=C(C)C12
D03	Z19126119	C(SC=1N=NC=2C=3C=CC=CC3NC2N1)C4=NC=5C=CC=CC5S4
E03	Z641206860	NC=1N=C(NCC=2C=CC=3OCOC3C2)N=CC1[N+](=O)[O-]
F03	Z56936356	COC=1C=CC(NC(=O)CSC=2N=CN=C3NN=CC23)=CC1
G03	Z1530946344	CC1=NC(=NN1)C=2C=CC=C(CNC(=O)C3=CC=CS3)C2
H03	Z217737566	COC=1C=CC=CC1C=2C=C(CSC=3N=C(N)N=C(N)N3)ON2
I03	Z1478432600	CS(=O)C=1C=CC(CNC=2C=CC(NC(=O)C3CC3)=NC2)=CC1
J03	Z29885103	O=C(NCC1COC=2C=CC=CC2O1)C3=NNC(=O)C=4C=CC=CC34
K03	Z1005269362	CS(=O)(=O)NC=1C=C(C=CC1F)C(=O)NC=2C=CC3=CNN=C3C2
L03	Z165645656	NC(=O)C=1C=CC(CSC=2N=C(N)C=C(N)N2)=C(C1)[N+](=O)[O-]
M03	Z1469057666	NC=1N=C(CN(CC2CCCO2)CC=3C=CC=NC3)N=C4C=CC=CC14
N03	Z110096110	CC1OC=2C=CC(NC(=O)CC3=CNC=4C=CC=CC34)=CC2NC1=O
O03	Z1557592893	CC=1C=C(NC(=O)NCCNC(=O)C2=CC=CN2C)C=C3NN=CC13
P03	Z48851300	OC=1C=CC(C2=CSC(NC=3C=CC=4OCCOC4C3)=N2)=C(O)C1
A04	Z103860258	NC(=O)CN1CCCC1C=2C=CC=3OCCOC3C2
B04	Z1685134911	CN1N=CC=C1CC2=NOC(=N2)C3=NNC(=O)C=4C=CC=CC34
C04	Z203053480	Cl.NC(=O)C=1C=C(C=CC1O)C2=CSC(NC3CC3)=N2
D04	Z2028214363	CC1(CCNC(=O)CC1)C=2C=CC=CC2
E04	Z167849056	COC=1C=CC(OCC=2N=C(N)C=3C=CC=CC3N2)=C(C1)[N+](=O)[O-]
F04	Z1443594996	CCC1=CC(=NN1)C(=O)NCC=2C=CC(=CC2)C(=O)O
G04	Z166467790	CN(C)C(=O)CNC(=O)CSC=1N=C(N)C=2C=CSC2N1
H04	Z1835954542	O=C(CC=1C=CC=2C=NNC2C1)N3CCN(CC3)C=4N=CC=CN4
I04	Z167838862	NC=1N=C(COC=2C=CC(=CC2)[N+](=O)[O-])N=C3C=CC=CC13
J04	Z1952865255	CC1(CC1)C=2C=C(NN2)N3CCN(CC3)C(=O)C=4C=CN=CC4F
K04	Z166468496	NC=1N=C(SCC2=COC(=N2)C3=CC=CS3)N=C4SC=CC14
L04	Z1852075533	NC(=O)C=1C=NN2CCC(CNC(=O)C=3C=CC=4NC=NC4C3)CC12
M04	Z166465770	CC(C)CNC(=O)NC(=O)CSC=1N=C(N)C=2C=CSC2N1
N04	Z191126564	CC(NC(=O)C1=NNC=2C=CC=CC12)C=3C=CC=C(C3)S(=O)(=O)N
O04	Z167801970	NC=1N=C(CSC=2N=CC=CN2)N=C3SC=4CCCCC4C13
P04	Z2033609726	CC(C)C1=NSC(=N1)N2CCCC(C2)C3=NNC(=O)O3
A05	Z1357256284	CS(=O)C=1C=CC(CNC=2N=CC([N+](=O)[O-])=C(N)N2)=CC1
B05	Z83017152	CC(NC(=O)CC1=NNC(=O)C=2C=CC=CC12)C=3C=CC=NC3
C05	Z1231837049	NC(=O)C=1C=CC=CC1N2CCC(C2)NC(=O)C=3C=CC(Cl)=CN3
D05	Z167856942	NC=1N=C(COC=2C=CC=NC2[N+](=O)[O-])N=C3C=CC=CC13
E05	Z1589570777	NC(=O)C=1C(Cl)=CC=CC1NCC=2C=CC=C(C#N)C2F
F05	Z30612234	CC(C)C(=O)NC=1C=CC(C#N)=CC1
G05	Z1347877672	CC(C(=O)NC=1C=NN(CC(=O)N)C1)C2=CC=C(Cl)S2
H05	Z48861640	CCOC=1C=CC(NC2=NC(=CS2)C=3C=CC(O)=CC3O)=CC1
I05	Z1315026747	CC1=NN(C=2C=CC(F)=CC2)C=3NN=C(NC(=O)CC=4C=CON4)C13
J05	Z990856154	COC=1C=CC(CNC=2N=CN=C3N(CCO)N=CC23)=CN1
K05	Z1426335808	NC(=O)C(CC=1C=CC=CC1)NC(=O)CN2C=C(N=N2)C=3C=CC=CC3

L05	Z643599154	COC=1C=CC(CNC=2N=CC([N+](=O)[O-])=C(N)N2)=CN1
M05	Z442692294	COC(C(=O)NC=1C=CC=2OC(C)C(=O)NC2C1)C=3C=CC=CC3
N05	Z776735836	CCCCC1=NN=C(NC(=O)CN(C)C=2N=CN=C3N=CNC23)S1
O05	Z1419679430	CN1C=C(C=N1)C2=NC(CNC=3C=C(Cl)C=CC3C(=O)N)=CS2
P05	Z1137690688	NC=1N=C(CSCC(=O)NC=2C=CC=CC2)N=C3C=CC=CC13
A06	Z112433702	OC=1C=CC(=CC1)C(=O)CSC2=NNC3=NC=4C=CC=CC4N23
B06	Z1889528746	O=C(NC=1C=CN(CC=2C=CN=CC2)N1)NC=3C=CN=CN3
C06	Z126474000	COC=1C=CC(=CC1)C2CCCCCN2CC=3N=C(N)N=C(N)N3
D06	Z2014289995	CC=1C=C(COCC(=O)NC2=NNC=3C=C(F)C=CC23)ON1
E06	Z32388176	COC=1C=CC(CNC(=O)C2=NNC=3C=CC=CC23)=CC1
F06	Z1996872008	CCCC1=CC(NS(=O)(=O)C=2C=CC(=CC2)C(=O)N(C)C)=NN1
G06	Z25777642	NC(=O)C=1C=CC=CC1OCC2=NN=C(O2)C=3C=CC=CC3
H06	Z1982323353	CC(CC=1C(C)=NN(C)C1C)NC(=O)C=2C=C(Cl)C=C(F)C2N
I06	Z44585618	CCN1CCN(CC1)C(=O)NC=2C=CC(C)=CC2
J06	Z2010503124	CC1=NC(=NN1)C=2C=CC=C(NC(=O)CC3=CC=C(Cl)S3)C2
K06	Z56800698	Cl.O=C1CCN(CC=2C=CC=CC2)CCN1
L06	Z1231798863	O=C(NC=1C=CC=C(C1)C2=NC=CN2)C=3NN=C4CCCCC34
M06	Z167718922	CC=1C=C(C)N2N=C(SCC=3N=C(N)C=4C=CC=CC4N3)N=C2N1
N06	Z25714070	OCCNC1=NC=2C=CC=CC2N1CC(=O)NCC3CCCO3
O06	Z99551913	COC=1C=CC(OCCSCC=2N=C(N)N=C(N)N2)=CC1
P06	Z647382560	CC1=CC=C(C(=O)NCC2=NC(=NO2)C=3C=CC=NC3)C(=O)N1
A07	Z1422042115	NC(=O)C1CCCCC1NC=2C=CC=3N=CC=NC3N2
B07	Z1165168528	CC1=C(N=NN1C=2C=CC=C3C=CC=NC23)C(=O)NCC=4C=CC=NC4
C07	Z1325974399	CC1=NOC(CNC=2C=CC=C(OC=3C=CC=CC3C(=O)N)C2)=N1
D07	Z990878262	OCCN1N=CC=2C(NCC=3C=CNN3)=NC=NC12
E07	Z1203680577	CN(CCO)C1(CNC2=NN3C(=O)C=CN=C3S2)CCCCC1
F07	Z1165227098	OC=1C=CC(Cl)=CC1NC(=O)C=2C=NC=3NC(=O)NC(=O)C3C2
G07	Z1219888793	CCNC(=O)CN1C=CC(NC(=O)C=2C=CC=C(C2)N3C=CC=N3)=N1
H07	Z1167942545	O=C(NC=1C=CC=C(CN2C=NC=3C=CC=CC23)C1)C4CCC(=O)N4
I07	Z1189016073	CN1N=CC(NCC=2C=CNN2)=C(Br)C1=O
J07	Z915390666	NC=1N=CN=C2N(CCCSC=3N=CN=C4C=CC=CC34)C=NC12
K07	Z1410243144	FC=1C=CC=C(F)C1C2=CC(NC(=O)C3CCCC=4NN=CC34)=NN2
L07	Z1141203222	CC1=NN(C)C(C)=C1C2CCCN2CC=3N=C(N)C=4C=CC=CC4N3
M07	Z1544591530	CC(=O)C=1C=CC(CNC(=O)C2=NNC=3C=CC=CC23)=NC1C
N07	Z57472297	CC(CO)(CO)NC(=O)NC=1C=CC=CC1
O07	Z1601701772	CC1=NNC=2N=CC(NS(=O)(=O)CC=3C=CC(C#N)=CC3)=CC12
P07	Z2295601457	CNC=1N=C(C)C=C(N1)C(=O)N[C@H](CC=2C=CC=CC2)C(=O)O
A08	Z167849604	CN1C(SCC=2N=C(N)C=3C=CC=CC3N2)=NN=C1C(F)(F)F
B08	Z107289492	CC1=NN(CC=2N=C(N)N=C(NC=3C=CC=CC3)N2)C(=O)C(C#N)=C1C
C08	Z195626578	CN(CC(=O)NC=1C=CC(F)=CC1)CC=2N=C(N)C=3C=CC=CC3N2
D08	Z438021866	NC(=O)C1CCN(C1)C(=O)CCC=2C=NN(C2)C=3C=CC=CC3
E08	Z89105592	CCOC=1C=CC(OCCN2CC(OC=3C=CC=CC23)C(=O)N)=CC1
F08	Z645593308	CC=1C=C(NCCOC=2C=CC=3OCOC3C2)N=C(N)N1
G08	Z17559309	CC(SC=1N=C(N)N=C(N)N1)C(=O)NC=2C=CC=3OCCOC3C2
H08	Z666973398	NC(=O)C1CCN(C1)C(=O)CCCC2=NN=C(O2)C=3C=CC=CC3
I08	Z193663186	CC1CCC2=C(C1)SC=3N=C(CSC4=NN=NN4C)N=C(N)C23
J08	Z167529348	CN1N=C(C=CC1=O)C(=O)N(CCC(=O)N)CC=2C=CC=CC2
K08	Z193603654	COC=1C=CC(NC(=O)C(SC=2N=C(N)N=C(N)N2)C(C)C)=CC1
L08	Z98622786	CC=1OC=2N=CNC(=O)C2C1C(=O)NCC=3C=CC=4OCCOC4C3
M08	Z193659230	CC=1SC=2N=C(CSC3=NN=C(N)S3)N=C(N)C2C1C
N08	Z1037453586	NS(=O)(=O)NCC1CCCN(C1)C=2N=CN=C3C=CSC23
O08	Z228466476	CC=1C=CC(NC2=NC(CN3C=NC(C#N)=N3)=CS2)=CC1C
P08	Z666969462	NC(=O)C1CCN(C1)C(=O)COC=2C=CC=C(OC=3C=CC=CN3)C2
A09	Z1606797477	CC1=NN(CCO)C(C)=C1CNC2=NC=3C=CC(=CC3S2)[N+](=O)[O-]
B09	Z1148797578	N#CC=1C=CC(NC2CCC2)=CC1
C09	Z1443672196	OC(=O)CC(NC(=O)C1=NNC=2CCCCC12)C=3C=CC(F)=CC3
D09	Z373231540	N#CC=1C=CC(NCC2CC2)=CC1
E09	Z1587166764	CN1N=CC=C1CNC=2C=C(N=CN2)N3CCCC(CO)C3
F09	Z1834766073	O=C(NCC1=CSC(=O)N1)C2=NNC=3CCCCCC23
G09	Z1537141848	CN(CCOC=1C=CC=C(C#N)C1)C=2N=CN=C3N=C(N)C=CC23
H09	Z928369420	CC=1C=CC=2NN=C(C(=O)N3CCCC(C3)C(=O)O)C2C1
I09	Z1238969821	CC(C)NC(=O)C=1C=CC=C(CNC=2N=C3C=CC=CC3=CC2CO)C1
J09	Z1757791520	NC(=O)C=1C=NN2CCC(CNC=3N=CC(C#N)=CC3Cl)CC12
K09	Z1445326541	OC(=O)C(CNC(=O)C=1C=CC=2C=CNC2C1)CC=3C=CC=CC3F
L09	Z1672660229	OC(=O)C=1C=CC=CC1NS(=O)(=O)C=2C=CC=3CCNC(=O)C3C2
M09	Z1537055266	NC=1C=CC=2C(NCCNC=3C=CC(=CC3)[N+](=O)[O-])=NC=NC2N1
N09	Z1594722049	CCN1C(NC(=O)CCC2=NN=CN2)=NC=3C=C(C)C=CC13

O09	Z1610792820	CCS(=O)(=O)C=1C=CC(CNC(=O)C=2NN=C3CCCCC23)=CC1
P09	Z2053817169	CN1CCN(CC2=CC=3C=CC=CC3NC2=O)CC1C4=NC(C)=NO4
A10	Z166464456	COC(=O)C=1C=CC(CSC=2N=C(N)C=3C=CSC3N2)=CC1
B10	Z968578484	CC=1OC(=NC1CC(=O)N2CCCCC2CC(=O)N)C=3C=CC=CC3
C10	Z87528924	COC=1C=CC(C(=O)NC=2C=CC=C(C2)S(=O)(=O)N)=C(F)C1
D10	Z1127121867	CCC1=CC(=O)N2N=C(NC(CO)CC=3C=CC=CC3)SC2=N1
E10	Z139931614	O=C(NCC=1C=CC=NC1)C=2C=CC=3N4CCCC4C(=O)NC3C2
F10	Z1021200422	CC(NC(=O)C=1NN=C2C=CC=CC12)C(=O)NC=3C=CC=CN3
G10	Z195604552	NC=1N=C(CN2CCNC(=O)C2)N=C3SC=4CCCCC4C13
H10	Z283996420	BrC1=CNC(=C1)C(=O)NC2CCCC=3NC(=O)C=CC23
I10	Z167819734	NC=1N=C(CSC=2C=CC=CN2)N=C3SC=4CCCCC4C13
J10	Z908578022	CC1=NN(C)C=2NC(=O)C(CCC(=O)N3CCNC(=O)CC3)=C(C)C12
K10	Z167849398	CC1=NN=C(SCC=2N=C(N)C=3C=CC=CC3N2)S1
L10	Z1141172409	CC=1C=NN(CC2CN(CC=3N=C(N)C=4C=CC=CC4N3)CCO2)C1
M10	Z229763982	CN(CC1=NC=2C=CSC2C(=O)N1)C(=O)CCC=3C=CC=CC3O
N10	Z1120822018	CN(CC(=O)NC=1C=C(C)C=CN1)CC=2N=C(N)C=3C=CC=CC3N2
O10	Z228468632	NC=1N=C(CN2C=NC(C#N)=N2)N=C3SC=4CCCCCC4C13
P10	Z1139263618	CC=1C=CC(=NN1)N2CCCN(CC2)C(=O)C3=NNC=4CCCC34
A11	Z1665269287	NC(=O)C=1C=CC=C(CN2CCCC=3C=C(C=CC23)C(=O)N)C1
B11	Z2058042499	C[C@H]1OCCN(CC2=CC(=NO2)C=3C=NN(C)C3C)[C@@H]1C(=O)N
C11	Z1607387226	COCC1=NN(CC=2N=C(N)C=3C(C)=C(C)OC3N2)C(=O)O1
D11	Z1981382941	O=C(NCC1=NC=2C=CC=NC2N1)C3=NC=4C=CC=CC4C(=O)N3
E11	Z1420563641	NC(=O)C=1C=CC=CC1OC=2C=CC(NC(=O)C=3C=CNC(=O)C3)=CC2
F11	Z1841030291	CC1=NC(=NN1)C(NCC2=CN(N=N2)C(C)(C)C)C=3C=CC=CC3
G11	Z1603499135	OC(=O)C1CCC(CC1)NC(=O)C=2C=CC=C3C=CNC23
H11	Z2061995932	COC=1C=CC=2C(NC(=O)[C@@H]3CCO[C@H]3C4=NC=CN4C)=NNC2C1
I11	Z1646203992	OCCOC=1C=CC=C(N1)C2=NC=3C=CC(Cl)=CC3C(=O)N2
J11	Z1952676944	CC1=NNC=2C=C(NC(=O)CCC3=CNC=N3)C=CC12
K11	Z1654253541	O=C(NC1CCCN(C1=O)C=2C=CC=NC2)C3=NNC=4C=CC=CC34
L11	Z283994004	O=C(NC1CCCC=2NC(=O)C=CC12)C3=NNC=4C=CC=CC34
M11	Z1298880666	CN(CC1=NC(CS(=O)(=O)C)=NO1)C=2C=C(NN2)C=3C=CC=CC3
N11	Z219152228	CC(OC=1C=C(C)C=CC1C(=O)N)C2=NC(=NO2)C=3C=CC=CC3
O11	Z1658117319	COCC1=NSC(NC(=O)C=2C=CC=C3C=NNC23)=N1
P11	Z1185890576	FC=1C=C(C#N)C=CC1CNC=2C=C(C=CC2Cl)N3CCNC3=O
A12	Z241744900	CC1CCCN(C1)C=2N=C(NCCOCCO)N=C(N)C2[N+](=O)[O-]
B12	Z1139290388	CC(C)N1C=C(CN2CCCN(CC2)C(=O)C3=CC(Cl)=CN3)C=N1
C12	Z245296262	NC=1N=C(NCCOCCO)N=C(NCC2CCCO2)C1[N+](=O)[O-]
D12	Z1116579229	CC=1C=C(NC(=O)CSC=2N=C(N)C=3C(C)=C(C)SC3N2)ON1
E12	Z217923492	CC=1C=CC(C(=O)N)=C(OCC=2C=CC(C#N)=CC2F)C1
F12	Z1032350050	NC(=O)C1CCCN1CC2=NC(=NO2)C=3C=CC=4OCOC4C3
G12	Z32864072	NS(=O)(=O)C1=CC=C(CNC(=O)C2=NNC=3C=CC=CC23)S1
H12	Z1095449427	C(SC1=NNC(=N1)C=2C=CC=NC2)C3=NOC(=N3)C=4C=CSC4
I12	Z116884932	FC=1C=CC=CC1CNC(=O)C=2C=C(NN2)C=3C=CC=CC3
J12	Z642600410	NC=1NN=C(CCCNC2=NC=3C=CC=CC3O2)C1C#N
K12	Z190123430	CN(CC1=NC=2C=CC=CC2C(=O)N1)C(=O)CCC=3C=CC=CC3O
L12	Z1171353464	NC(=O)CCNC(=O)C=1C=CC=CC1NCC(=O)NC=2C=CC=CC2
M12	Z237580922	COC=1C=CC=2C=C(CNC=3N=CN=C4NN=CC34)C=CC2C1
N12	Z1137690489	COCCNC(=O)C(C)SCC=1N=C(N)C=2C=CC=CC2N1
O12	Z101496686	CN(CC1=NC=2C=CC=CC2C(=O)N1)C(=O)C3=CNC(=O)N3
P12	Z990878264	N#CCCN1N=CC=2C(NCC=3C=CNN3)=NC=NC12
A13	Z1559477505	NC=1N=C(N)N=C(CN(CC=2C=CC=C(C2)C=3C=CC=NC3)C4CC4)N1
B13	Z1139198022	OCC1CCCN1C=2C=C(NCCNC(=O)C=3C=NC=CN3)N=CN2
C13	Z928843496	OC(=O)CC(NC(=O)C=1C=CC=C2C=NNC12)C3=CC=CS3
D13	Z1272715826	CN1N=C2CCN(CC=3N=C(N)C=4C=CC=CC4N3)CC2=CC1=O
E13	Z1515325641	NC=1N=C(CSCC(=O)O)N=C2C=CC=CC12
F13	Z737359742	NC(=O)CCOC=1C=CC=CC1NC(=O)C2=CC=3C=CC=CC3N2
G13	Z1603697552	CC(C)C1=CC(=NN1)C(=O)NC(CC(=O)O)C=2C=CC=CC2C
H13	Z1184934107	COC(=O)C=1N=CN(CC=2N=C(N)C=3C=CC=CC3N2)N1
I13	Z1614820320	NC=1N=CN=C2N(CCCOC3=NN=C(O3)C=4C=CC=CC4)C=NC12
J13	Z1227794655	[O-][N+](=O)C1=CC(CSC=2N=CN=C3NC=NC23)=CS1
K13	Z1443672224	OC(=O)CC(NC(=O)CC1=NNC=2C=CC=CC12)C=3C=CC(F)=CC3
L13	Z1139194703	OCC1CCCN1C=2C=C(NCC=3C=CC=4OCOC4C3)N=CN2
M13	Z1646424827	NC=1N=C(CN2CCCCC2C3CNC(=O)C3)N=C4C=CC=CC14
N13	Z1205112089	CC1=NN(C)C=2NN=C(NC(=O)CC=3C=CC(=CC3)[N+](=O)[O-])C12
O13	Z929744756	OC(=O)CC(NC(=O)C=1C=CC=C2C=NNC12)C=3C=CC(F)=CC3
P13	Z366649676	CCCC=1C=C(NN1)C(=O)NCC=2C=CN=C(C2)N3C=CC=N3
A14	Z295464032	NC=1N=C(NCCOCCO)N=C(N2CCCCCC2)C1[N+](=O)[O-]

B14	Z1137690726	NC=1N=C(CSCC(=O)NC=2C=CC=C(F)C2)N=C3C=CC=CC13
C14	Z95764039	NC(=O)C=1C=CC=C(NC(=O)CC2=CSC(=N2)N3CCCC3=O)C1
D14	Z1137690592	NC=1N=C(CSCC(=O)NCC2=CC=CS2)N=C3C=CC=CC13
E14	Z335929974	COC=1C=CC(=CC1)C(=O)C(C)SC=2N=C(N)C=3C=CSC3N2
F14	Z1203333452	NC(=O)C=1C=CN(N1)C=2C=CC=CC2NC(=O)C=3C=CC=4OCCC4C3
G14	Z26325497	COC=1C=CC(OCCOC=2C=C(OC)C=CC2C(=O)N)=CC1
H14	Z1024558214	CC(C)OC=1C=CC(CSC2=NC=3NN=CC3C(=O)N2)=CC1
I14	Z107057210	COC=1C=C(C=CC1OCC=2N=C(N)N=C(N)N2)C(=O)C
J14	Z1137690422	CC(SCC=1N=C(N)C=2C=CC=CC2N1)C(=O)NC=3C=C(C)ON3
K14	Z211302198	NC=1N=CC=NC1C(=O)NCC=2C=CC=3OCOC3C2
L14	Z1126905076	NC(=O)CCSC=1C=CC=CC1NC(=O)C=2C=CC=3OCOC3C2
M14	Z165420976	NC(=O)C=1C=CC(COC=2C=CC=CC2C(=O)N)=CC1
N14	Z959434124	COC=1C=CC(OCCSCC2=CC(=O)N3N=C(N)NC3=N2)=CC1
O14	Z99465328	O=C(CC1=NOC=2C=CC=CC12)NC=3C=CC=4OCC(=O)NC4C3
P14	Z1162797985	NC(=O)CC=1C=CC=C(OCC2=NOC(=N2)C=3C=CC(F)=CC3)C1
A15	Z1587738637	CC1=NNC=2N=CC(NS(=O)(=O)C=3C=NC=4C=CSC4C3)=CC12
B15	Z1212628432	CCC1=NN(C)C=2NN=C(NC(=O)CCN3C=C(C=N3)[N+](=O)[O-])C12
C15	Z1603513793	OC(=O)C(CNC(=O)C=1C=CC=C2C=CNC12)CC=3C=CC=CC3
D15	Z1287588443	CC=1NN=C(NC(=O)C=2C=CC=NC2O)C1C=3C=CC=4OCOC4C3
E15	Z1603697938	CC=1C=CC=CC1C(CC(=O)O)NC(=O)CC2=NNC=3C=CC=CC23
F15	Z1172756805	COC=1C=C2N=C(NCC=3C=CC(C)=NC3)N=C(N)C2=CC1OC
G15	Z1646361792	CCCCN(CC=1N=C(N)C=2C=CC=CC2N1)C3CCS(=O)(=O)C3
H15	Z1272279212	OC=1C=CC=C(CCNC=2C=C3N=CNC(=O)C3=CC2[N+](=O)[O-])C1
I15	Z1603657201	OC(=O)C(CC=1C=CC(F)=CC1)NC(=O)C=2C=CC=C3C=NNC23
J15	Z1137690433	NC=1N=C(CSCC(=O)NCC(F)(F)F)N=C2C=CC=CC12
K15	Z1603232613	OC(=O)CC(NC(=O)C=1C=CC=C2C=CNC12)C3=CC=CS3
L15	Z1137689711	NC=1N=C(CSCCN2C(=O)CNC2=O)N=C3C=CC=CC13
M15	Z1697026833	O=C1NC(SCC2=NN=C(S2)C=3C=CC=CC3)=NC=4NN=CC14
N15	Z1143316964	NC=1N=CN=C2N(CC(=O)NC=3C=CC=4OCCOC4C3)C=NC12
O15	Z1385487152	CN1N=CN=C1CNC=2C=CC=C(OC=3C=CC=CC3C(=O)N)C2
P15	Z1252790211	NC=1N=C(CSCC=2C=CON2)N=C(NC=3C=CC(F)=CC3)N1
A16	Z199215096	CC(NC=1C=CC=C(C1)C(=O)N)C(=O)NC=2C=C(C)ON2
B16	Z1137690438	NC=1N=C(CSCC(=O)NC2CCCC2)N=C3C=CC=CC13
C16	Z193670946	CC=1SC=2N=C(COC=3C=CC=CC3C#N)N=C(N)C2C1C
D16	Z1222455261	NC(=O)C=1C=CC=CC1OCCN2C=NC=3C=CC=CC3C2=O
E16	Z195767192	CC(N(C)CC=1C=NN(C)C1)C=2N=C(N)N=C(N2)N(C)C
F16	Z1139323858	CC=1C=C(C)N(CC2CCCN2C(=O)CC3=NNC=4C=CC=CC34)N1
G16	Z46335179	CC=1C=CC(NC2=NC(CN3CCNC(=O)C3)=CS2)=CC1
H16	Z434059434	CC1=CC(NC(=O)C(N2CCC(C2)C(=O)N)C=3C=CC=CC3)=NO1
I16	Z368759930	NC(=O)C=1C=CC(Cl)=CC1NCC=2C=CC(=CC2)N3C=CC=N3
J16	Z990848554	OCCN1N=CC=2C(NCCC=3C=CC=4OCOC4C3)=NC=NC12
K16	Z367145654	O=C(NC=1C=CC=C(OC=2C=NC=CN2)C1)C3=CC=4C=CC=CC4N3
L16	Z990845858	NC=1NN=C(CCCNC=2N=CN=C3N(CCO)N=CC23)C1C#N
M16	Z370757596	COCC(C)NC(=O)CCC1=C(C)C=2C(C)=NN(C)C2NC1=O
N16	Z370820222	CC1=NN(C)C=2NC(=O)C(CCC(=O)NCCC3=CC=CO3)=C(C)C12
O16	Z370478790	ClC=1C=CC=C(C1)C2=CC(=NN2)C(=O)NC3=NN=C(S3)C4CC4
P16	Z1213670840	OC=1C=CC=CC1C=2C=C(NN2)C(=O)NCC=3C=CC=4OCOC4C3
A17	Z1716589504	NC=1N=C(NC2CCCN(CCO)C2=O)N=CC1[N+](=O)[O-]
B17	Z1192076899	COC=1C=CC(NC(=O)C2CCCN2C=3N=CN=C4NN=CC34)=CC1
C17	Z757978954	CS(=O)(=O)CC=1C=CC(CNC(=O)C=2N=CC=NC2N)=CC1
D17	Z1267773828	CN1CCCN(CC1)C=2C=CC(C#N)=CC2Cl
E17	Z1633947241	O=C(CC1=NOC=2C=CC=CC12)NCCNC(=O)C3=CC=NN3
F17	Z1268793772	CCC1=NC(=NO1)C2CCCN2C(=O)CC3=NNC=4C=CC=CC34
G17	Z98478092	COC=1C=CC(OC)=C(C1)C2CCCN2CC=3N=C(N)N=C(N)N3
H17	Z1281746494	CC(NC=1N=CC([N+](=O)[O-])=C(N)N1)C=2C=CC(=CC2)N3C=CC=N3
I17	Z1646280879	CCS(=O)(=O)CC(C)N(C)CC=1N=C(N)C=2C=CC=CC2N1
J17	Z1272649563	CC(NC=1N=CC([N+](=O)[O-])=C(N)N1)C=2C=CC=C(C2)N3C=CN=C3
K17	Z1656606541	O=C(CNC(=O)C1=CC(=NN1)C2=CC=CS2)C3=CC=CO3
L17	Z1172987081	COC=1C=C2N=C(NCC=3C=C(C)ON3)N=C(N)C2=CC1OC
M17	Z1609713553	CC(C)CC=1C=C(NN1)C(=O)NC2CCC(C2)C(=O)O
N17	Z1137690090	NC(=O)CCSCC=1N=C(N)C=2C=CC=CC2N1
O17	Z727556306	O=C(CCCC1=NC=2C=CC=CC2C(=O)N1)NC3CCCCNC3=O
P17	Z1170065052	FC=1C=CC(CNC(=O)C2=NOC(CN3C=CC(=O)NC3=O)=N2)=CC1
A18	Z361977892	CC=1N=CNC(=O)C1CCC(=O)NC2=NC(=CS2)C=3C=CC=NC3
B18	Z48856940	COC=1C=CC(NC2=NC(=CS2)C=3C=CC(O)=CC3O)=CC1
C18	Z370478792	FC=1C=CC(=CC1)C2=CC(=NN2)C(=O)NC3=NN=C(S3)C4CC4
D18	Z1213673036	CC=1C=CC(CNC(=O)C2=CC(=NN2)C=3C=C(C)C=C(C)C3O)=CC1

E18	Z370477906	CCC1=NN=C(NC(=O)C=2C=C(NN2)C=3C=CC=CC3Cl)S1
F18	Z1456352580	NC=1N=C(CN2N=CC=C2[N+](=O)[O-])N=C3C=CC=CC13
G18	Z301140786	CC(C)C=1C=CC=C(NC(=O)C2=CC=3C=C(F)C=CC3N2)C1
H18	Z228468614	CC=1SC=2N=C(CN3C=NC(C#N)=N3)N=C(N)C2C1C
I18	Z425548762	CC(NC(=O)C=1C=C(NN1)C=2C=CC=CC2)C3=NN=CN3C
J18	Z167927522	NC=1N=C(CSC2=NN=C(NC3CC3)S2)N=C4C=CC=CC14
K18	Z316734936	O=C(NC=1C=CC=C(NC(=O)C2=CC=3C=CC=CC3N2)C1)C4CC4
L18	Z238018648	CC(NC(=O)CCC1=C(C)NC(=O)NC1=O)C=2C=CC=CN2
M18	Z423955510	OC=1N=CC=CC1C(=O)NCC=2C=CC=NC2N3C=NC=N3
N18	Z415212312	O=C(NCC=1C=CC=2OCOC2C1)C=3C=CC=C(C3)N4CCNC4=O
O18	Z408136572	NC(=O)C=1C=CC=C(C1)C(=O)NC(C2CCCC2)C3=CC=CS3
P18	Z415223258	O=C(NCC=1C=CC=NC1)C=2C=CC=C(C2)N3CCNC3=O
A19	Z1783424244	O=C1NC(SCCC=2C=CC=3OCCC3C2)=NC=4NN=CC14
B19	Z1324017370	CC(NC=1N=CC([N+](=O)[O-])=C(N)N1)C=2C=CC=C(C2)N3C=NC=N3
C19	Z1783475778	NC(=O)C=1C(F)=CC=CC1OCCC=2C=CC=3OCCC3C2
D19	Z1329975813	O=C(NC=1C=CC=C2C=NNC12)C=3C=CC=C(C3)N4CCCNC4=O
E19	Z1637285222	CCC=1C=C(NN1)C(=O)NC2=NNC(CC=3C=CC=C(F)C3)=N2
F19	Z1268777463	CCCC1=NNC(=N1)C2CN(CCO2)C(=O)CC=3C=CC=NC3
G19	Z1656164992	CC1=NN(C)C=2NN=C(NC(=O)C=3C=CC=CC3N4C=CN=N4)C12
H19	Z1269668088	NC(=O)C1=CC(=NN1)C2CCCN(C2)C(=O)CCC=3C=CN=CC3
I19	Z1700536967	COC=1C=CN=C(CSCC=2N=C(N)C=3C=CC=CC3N2)C1
J19	Z1269676814	COCC1=NC(=CS1)C(=O)N2CCCC(C2)C=3C=C(NN3)C(=O)N
K19	Z1695813672	CS(=O)CC=1C=CC=CC1NC(=O)C2=CC=3C=C(F)C=CC3N2
L19	Z642326440	CCN(C)C(=O)NC=1C=CC(C#N)=CC1
M19	Z1696936165	CC=1OC=2N=C(CN3C=NC(C#N)=C3C#N)N=C(N)C2C1C
N19	Z1269691328	CC=1C=C(ON1)C(=O)N2CCCC(C2)C=3C=C(NN3)C(F)(F)F
O19	Z283666198	CS(=O)(=O)N1CCCN(CC=2N=C(N)N=C(N)N2)CC1
P19	Z1268776368	CC(C)C1=NNC(=N1)C2CN(CCO2)C(=O)CCN3C=CN=N3
A20	Z256910566	NC(=O)CC1=CSC(NC(=O)CN2C=CC=CC2=O)=N1
B20	Z375691710	CN(CC=1C=C(C)ON1)C(=O)C=2C=CC=CC2OCC(=O)N
C20	Z595802756	OC=1C=CN=CC1NC(=O)C=2C=CC=C(NC(=O)C=3C=CC=NC3)C2
D20	Z812954026	OC(=O)C=1C=CC=CC1CC(=O)NC=2C=CC=C(C2)N3CCNC3=O
E20	Z359630092	CN1C(CSC2=NC=3NN=CC3C(=O)N2)=CC(=O)N(C)C1=O
F20	Z372731156	OC(=O)CC(NC(=O)C=1C=C(NN1)C2CC2)C=3C=CC=CC3Cl
G20	Z221489362	NC(=O)CC1=CSC(NC(=O)CN2N=NC=3C=CC=CC23)=N1
H20	Z463320776	CC(C)C1=CC(=NN1)C(=O)NC2CCN(CC2)C(=O)C
I20	Z605714984	CC1=NC(=NN1)C=2C=CC=C(NC(=O)CC3=NOC=4C=CC=CC34)C2
J20	Z728964912	CC(C)(C)C1=CN2N=C(NCCCC3=NNC(N)=C3C#N)SC2=N1
K20	Z366489576	O=C(NC=1C=CC=C(CN2C(=O)CNC2=O)C1)C3=CC=CS3
L20	Z230019828	NC(=O)CN1CCC(CC1)NC(=O)CC2=NNC(=O)C=3C=CC=CC23
M20	Z763366252	CN1CCN(CC1)C(=O)C=2C=CC(N)=CC2
N20	Z666621402	O=C1CNC(=O)N1CC=2C=CC(=CC2)C3=NC=4C=CSC4C(=O)N3
O20	Z369188228	CC=1C=CC(=CC1C(=O)N)S(=O)(=O)N2CCNC(=O)C2
P20	Z415230368	CC(NC(=O)C=1C=CC=C(C1)N2CCNC2=O)C=3C=CC=NC3
A21	Z1464284046	CCNC1=NC=C(S1)C(=O)NC2=NC=3C=C(F)C=CC3N2C
B21	Z1269695557	FC(F)(F)C1=CC(=NN1)C2CCCN(C2)C(=O)C3=CSN=N3
C21	Z1728584311	CC=1C=CN2C(NCC3=CC(C#N)=CS3)=NN=C2C1
D21	Z1430528865	NC=1C=CN=C(CNC=2N=CN=C3N(N=CC23)C=4C=CC=CC4)N1
E21	Z1603698477	CC=1C=CC=CC1C(CC(=O)O)NC(=O)C=2C=CC=C3C=NNC23
F21	Z666182210	CC(NC(=O)CSC=1C=CC(O)=CC1)C=2C=CC=3NC(=O)CC3C2
G21	Z1679672955	CN(CCCC1=NNC(N)=C1C#N)C2=NN=C(S2)C=3C=CC=CN3
H21	Z1434151429	CN(C)C(=O)N1CCN(CC=2N=C(N)C=3C(C)=C(C)OC3N2)CC1
I21	Z1646281215	CC(C(C)S(=O)(=O)C)N(C)CC=1N=C(N)C=2C=CC=CC2N1
J21	Z1434063702	CCC=1NN=C(NCC2=CN(C)N=C2C=3C=CC=NC3)C1C
K21	Z1725291463	COC=1C=CC=CC1CN(C)C2=NC(=O)C=3C=NNC3N2
L21	Z1269659108	CC1=NC(CC(=O)N2CCCC(C2)C=3C=C(NN3)C(=O)N)=CS1
M21	Z1754369356	CCOC=1C=NC=C(N1)N2CCC(C2)N3C=CC(NC(=O)C)=N3
N21	Z336006826	CC=1SC=2N=C(SCC=3C=CC=C(C3)[N+](=O)[O-])N=C(N)C2C1C
O21	Z1757876196	CCCN1C=C(CN2CCCC2C3=NC(=NO3)C(=O)N)C=N1
P21	Z1381360106	COCC1=NOC(=N1)C=2C=CC=C(C2)C3=NNC(C)=N3
A22	Z195558914	CCOC(=O)C1CCN(CC=2N=C(N)C=3C=CC=CC3N2)CC1
B22	Z650324494	CN(CC1=CN=C(C)S1)CC=2N=C(N)C=3C=CC=CC3N2
C22	Z730527164	CC(O)CNC(=O)C1=CC(C)=NC2=C(C=NN12)C(=O)N
D22	Z414644216	CC=1C=CC(=CC1C(=O)N)S(=O)(=O)NCC2CCOC2
E22	Z195777550	CC(C=1N=C(N)N=C(N1)N(C)C)N2N=NC(=N2)C=3C=CC(C)=CC3
F22	Z640965314	O=C(NCCC1CCCO1)C=2C=CC=C(C2)N3CCNC3=O
G22	Z402670418	COC=1C=CC(=CC1)C2CCCN2C(=O)CC3=C(C)N=C(C)NC3=O

H22	Z336009532	CCC1=NOC(CSC=2N=C(N)C=3C(C)=C(C)SC3N2)=N1
I22	Z195777918	CC(C=1N=C(N)N=C(N1)N(C)C)N2N=NC(=N2)C=3C=CC(Cl)=CC3
J22	Z402773276	CC(C)(C)C1=NOC(CCC(=O)NC2=NN=CN2)=N1
K22	Z108232150	COC=1C=CC(NC(=O)C=2C=CC(C)=C(F)C2)=CC1S(=O)(=O)N
L22	Z271357426	O=C1COC=2C=CC(=CC2N1)S(=O)(=O)NCCN3C=CN=C3
M22	Z359630102	CC=1OC(=NC1CSC2=NC=3NN=CC3C(=O)N2)C=4C=CC=CC4
N22	Z505783438	O=C(NCCNC1=NC=2C=CC=CC2S1)NC3CCCCNC3=O
O22	Z649943484	CC(NCC=1C=NC=2NN=C(C)C2C1)C=3C=CC=4OCCCOC4C3
P22	Z372657268	NC(=O)C=1C=CC=C(C1)C(=O)NCCNC=2C=NC=CN2
A23	Z1757134012	CN1C=NC=2CN(CCC2C1=O)C(=O)C=3C=CC=C4C=NNC34
B23	Z1381359081	COCCC1=NOC(=N1)C=2C=CC=C(C2)C3=NNC(C)=N3
C23	Z1833927283	CC(C(=O)NC1=NNC=2C=CC(=CC12)C(F)(F)F)S(=O)(=O)C
D23	Z1430614303	CC=1C=CC(NC(=O)CCCC2=NC=3C=CC=CC3C(=O)N2)=CC1O
E23	Z1756530754	CN1C=C(C=N1)[C@H]2OCC[C@@H]2NC(=O)C3=CC(Cl)=CN3
F23	Z220516810	NC=1N=C(CSCC=2C=CC(=CC2)N3C=CC=N3)N=C4C=CC=CC14
G23	Z1757876820	NC(=O)C1=NOC(=N1)C2CCCN2CC=3C=NN4C=CC=CC34
H23	Z940779128	CC(C)(CNC=1N=CC([N+](=O)[O-])=C(N)N1)C=2C=CC=3OCOC3C2
I23	Z1725304079	COC=1C=CC(=CC1)C(NC2=NC(=O)C=3C=NNC3N2)C(C)C
J23	Z1205112321	CC1=NN(C)C=2NN=C(NC(=O)CN3CCC=4SC=CC4C3)C12
K23	Z1599318716	OC(=O)C=1C=CC=C(CNC(=O)C=2NN=CC2Br)C1
L23	Z1269732229	CC(=O)NC1=NC(=CS1)C(=O)N2CCCC(C2)C=3C=C(C)NN3
M23	Z646130978	CN(C)C(=O)COC=1C=CC=C(CNC=2N=CN=C3N=CNC23)C1
N23	Z1230738271	COC=1C=CC(=CC1)C2=NN(CC(=O)N)C(=O)C=3C=CC=CC23
O23	Z1444935286	OC(=O)C=1C=CC=C(CNC(=O)CC2=NNC=3C=CC=CC23)C1
P23	Z1420694225	O=C(NC=1C=CC=2NN=NC2C1)C=3C=CC=CC3CN4C=NC=N4
Plate 02		
Well ID	**Enamine ID**	**Smile**
A02	Z55002275	N#CC=1C=CC=CC1CN2CCCC2
B02	Z1003932498	O=C1NCCCC1NCC=2C=CC=C(OCC=3C=CC=CN3)C2
C02	Z1029460372	COC=1C=CC(NC(C)C2CC2)=CC1
D02	Z644911980	C(NC=1N=C(N=C2C=CC=CC12)C=3C=CC=NC3)C=4C=CNN4
E02	Z1837077123	CN1CCN(CC1)C=2C=CC=NC2
F02	Z1157795830	FC=1C=CC(CNC2=NC=CN(C=3C=CC=C(Cl)C3)C2=O)=CC1
G02	Z1626044416	C(NC=1C=CC=C(OC=2C=CC=CN2)C1)C=3C=CNN3
H02	Z1212626878	CCC1=NN(C)C=2NN=C(NC(=O)CC=3C=CC(=CC3)N4C=CC=N4)C12
I02	Z1603063499	O=C(N1CCCCC1C=2N=CNN2)C3=CN=C4C=CC=CN34
J02	Z1731807231	NC(=O)C1COCCN1CC=2C=CC(OCC=3C=CC=CC3F)=NC2
K02	Z1756624842	O=C(N[C@H]1CCO[C@@H]1C=2C=CC=NC2)C3=NNC=4CCCC34
L02	Z1778594783	CC1OC=2C=CC(NC(=O)CC3=CN=CS3)=CC2NC1=O
M02	Z1444478080	CC1=CC(=NN1)C(=O)NC(CCC(=O)O)C=2C=CC=CC2
N02	Z2027574086	CC(C(=O)NC(C(=O)NC=1C=CNN1)C=2C=CC=CC2)C=3C=CC=CN3
O02	Z908179396	CC(C)C(NC(=O)C=1C=CNN1)C2=NC(=NO2)C=3C=CC=CC3
P02	Z2056670311	O=C(NC=1C=CC(=CC1)C2=NC=CO2)N3CCOCC3C=4N=CNN4
A03	Z229769862	CN(CC1=NC=2C=CSC2C(=O)N1)C(=O)C3=NNC=4C=CC=CC34
B03	Z1174947567	CC(NC(=O)C=1C=CNN1)C2=NC(=CS2)C=3C=CC=NC3
C03	Z98624459	CC=1OC=2N=CNC(=O)C2C1C(=O)NCCC=3C=CC=4OCOC4C3
D03	Z1205112379	COC=1C=CC(=CC1)C2CC2C(=O)NC3=NNC=4N(C)N=C(C)C34
E03	Z167725780	COC=1C=CC(=CC1)C2=NN=C(COC=3C=CC=CC3C(=O)N)O2
F03	Z1462270658	CC(C(=O)NC=1C=CC=C(NCC=2C=CNN2)C1)N3C=CC=N3
G03	Z193733986	NC=1N=C(SCC=2N=CON2)N=C3SC=4CCCCC4C13
H03	Z1396661910	COC=1C=CC(=CC1)N2C=C(CNC=3C=NNC(=O)C3Cl)N=N2
I03	Z84959970	CCN(CC1=NC=2C=CC=CC2C(=O)N1)C(=O)C3=NNC=4C=CC=CC34
J03	Z1467080296	CCC=1C=C(NN1)C(=O)NC2CCN(C2)C(=O)C=3C=CC=CN3
K03	Z466715476	CNS(=O)(=O)CC=1C=CC(CNC(=O)C=2C=CNN2)=CC1
L03	Z1081524668	CC1=NC(COC=2C=CC=CC2C(=O)NC=3C=CC4=CNN=C4C3)=NO1
M03	Z301431984	NC(=O)COC=1C=CC=C(NC(=O)C2=CC=3C=C(Cl)C=CC3N2)C1
N03	Z1127124609	CCC1=CC(=O)N2N=C(OC=3C=C(C=CC3C)C(=O)N)SC2=N1
O03	Z224062218	OC(=O)C1=CC=C(CSC2=NN=C3NC=4C=CC=CC4N23)O1
P03	Z1445591698	CC1(CCN(C1)C(=O)CCN2C(=O)NC(=O)C=3C=CC=CC23)C(=O)O
A04	Z1269729596	CC1=CC(=NN1)C2CCCN(C2)C(=O)CCN3C=CC=CC3=O
B04	Z1549126187	O=C(NCC1=NC(=CN1)C=2C=CC=C(C#N)C2)C3CCCC=4NN=CC34
C04	Z1544958954	COCC1=NN(CC2=CSC(NC=3C=CC=CC3)=N2)C(=O)O1
D04	Z1498266805	CC(C)C(NC1=NN2C=C(C)N=C2S1)C3=NC(=NO3)C4=NN=CN4
E04	Z1269657050	CCC1=NC(CN2CCCC(C2)C=3C=C(NN3)C(=O)N)=NO1
F04	Z1317591805	CC1=CN2N=C(NCCC3=NNC(=O)N3)SC2=N1
G04	Z1649198766	C1CC(C2=NOC(=N2)C=3C=CC=C4C=CNC34)C=5C=CC=CC5C1
H04	Z228468538	NC(=O)CCN(C(=O)CN1C=NC(C#N)=N1)C=2C=CC(F)=CC2

I04	Z1139419618	CCC1=NN=C2CCC(CNC(C(=O)N)C=3C=CC=CC3)CN12
J04	Z168931710	CN(C)C=1N=C(N)N=C(CN2C=NC=3C=CC=CC3C2=O)N1
K04	Z1443671489	CCC1=CC(=NN1)C(=O)NC(CC(=O)O)C=2C=CC(F)=CC2
L04	Z816643200	O=C(NCCN1N=C2C=CC=CN2C1=O)C=3C=C(NN3)C4CC4
M04	Z1757700501	CC(=O)NC=1C=CN(N1)C2CCN(CC=3SC=NC3C)C2
N04	Z840914790	O=C1CNC(=O)N1CC2=NC(=CS2)C=3C=CC=4OCCOC4C3
O04	Z1756623868	O=C(N[C@H]1CCO[C@@H]1C=2C=CC=NC2)C3=NNC=4C=CC=CC34
P04	Z356378012	CN(C)C=1N=C(N)N=C(COC=2C=CC=C(C2)C3=NN=CO3)N1
A05	Z646004850	FC=1C=CC(OC=2C=CC(CNC=3N=CN=C4N=CNC34)=CN2)=CC1
B05	Z1231741282	CCC=1C=CC(NC(=O)C=2C=CC(Cl)=CN2)=CC1S(=O)(=O)N
C05	Z645320010	OCCN1N=CC=2C(CCCC21)NC=3N=CN=C4SC=CC34
D05	Z1833765715	CN(C)C(=O)C1CCC(CNC(=O)C2=NNC=3CCCCCC23)O1
E05	Z786122912	O=C(NCCN1N=C2C=CC=CN2C1=O)C=3C=C(NN3)C=4C=CC=CC4
F05	Z1838746682	CC=1C=CC(NS(=O)(=O)C=2C=CC(=CC2)C(=O)O)=C(O)N1
G05	Z435533268	COC=1C=CC(NC(=O)C=2C=NC=CN2)=CC1OCC(=O)N
H05	Z1414196069	NC(=O)C[C@@H](NC(=O)C=1C=NC=C(F)C1)C=2C=CC=C(Cl)C2
I05	Z18357537	O=C(NC=1C=CC=CC1)C=2C=CC(CN3C(=O)CNC3=O)=CC2
J05	Z1175169619	CC(C)CC=1C=C(NN1)C(=O)NCC2=NC(=NO2)C=3C=CC=CN3
K05	Z167812982	NC=1N=C(COC=2C=CC=CC2C#N)N=C3C=CC=CC13
L05	Z1603549284	OC(=O)CC1CN(CCO1)C(=O)C=2C=C(NN2)C3=CC=CS3
M05	Z991890658	CC(C)N(CC1=NC=2C=CC=CC2C(=O)N1)C(=O)C=3C=CC=NC3O
N05	Z324593550	CC(SC=1N=C(N)C=2C(C)=C(C)SC2N1)C(=O)NC(=O)N
O05	Z1081521234	CCS(=O)(=O)NC=1C=CC=CC1C(=O)NC=2C=CC3=CNN=C3C2
P05	Z199942268	COC=1C=CC(COC=2C=CC=CC2C(=O)N)=CC1
A06	Z1756622000	CC(C)C1=CC(=NN1)C(=O)N[C@H]2CCO[C@@H]2C=3C=CC=NC3
B06	Z278162754	COC=1C=C(OC)C=2NC(=CC2C1)C(=O)NC=3C=CC=C(C)N3
C06	Z1756696623	CC(C)C1=CC(=NN1)C(=O)N[C@H]2CCCO[C@@H]2C=3C=NN(C)C3
D06	Z757937068	CC(CN1CCCC1=O)NC(=O)C2=NNC=3C=CC=CC23
E06	Z1546781983	NC=1N=C(N=C2C=CC=CC12)N3CCC(CN4C=CC=N4)CC3
F06	Z910730878	O=C(CC=1C=CC(=CC1)N2C=NN=N2)NC=3C=CNN3
G06	Z1756222265	CCC1=NC(=NN1)C(C)NC(=O)C2=CNN=C2C3CCOC3
H06	Z872961304	O=C(CNC(=O)C1CCCO1)NC=2C=CC=C3C(=O)NNC(=O)C23
I06	Z1360871768	CC=1C=C(NN1)C(=O)N2CC(CCN3CCCC3=O)C=4C=CC=CC24
J06	Z649748444	CC1=NN(C)C=2NC(=O)C(CCC(=O)NCC=3C=COC3)=C(C)C12
K06	Z960343492	CCN(CC=1C=CC=2OCOC2C1)C(=O)CC3=NNC=4C=CC=CC34
L06	Z838498424	CC(C(=O)NC=1C=C(C=C(F)C1C)C(=O)N)N2N=C(C)C=C2C
M06	Z1268749945	CC=1NN=C2N=CC(=CC12)C(=O)N3CCCC3C4=NOC(=N4)C5CC5
N06	Z1837067471	CCNC1=NC=2N(C)C(=O)N(C)C(=O)C2N1
O06	Z1268770697	CC1=NNC(=N1)C2CN(CCO2)C(=O)CC=3N=C4N=CC=CN4N3
P06	Z3225843160	Cl.FC=1C=CC=C(C1)N2CCNCC2=O
A07	Z827321112	CC1=NN(C)C=2NC(=O)C(CCC(=O)NC=3C=CNN3)=C(C)C12
B07	Z226769910	CC1=NN=C(SCC=2N=C(N)N=C(N)N2)N1
C07	Z370743754	CC1=NN(C)C=2NC(=O)C(CCC(=O)NCC=3C=CC=NC3)=C(C)C12
D07	Z110096298	CC1OC=2C=CC(NC(=O)CC=3C(F)=CC=CC3Cl)=CC2NC1=O
E07	Z1126979163	CC=1C=NC(=CN1)C(=O)NC(C(=O)NC=2C=CNN2)C=3C=CC=CC3
F07	Z226188078	NC(=O)CC1=CSC(NC(=O)CCC=2C=CC=3OCCOC3C2)=N1
G07	Z1119645172	COC=1C=CC(=CC1)C2=NC(CNC(=O)C=3C=CC=CN3)=NN2
H07	Z356355054	CC(SC1=NN=C(O1)C2=CC=CN2)C3=NC(=NO3)C4=CC=CO4
I07	Z1171354243	NC(=O)C=1C=CC(Cl)=C(NCC(=O)NC=2C=CC=3OCOC3C2)C1
J07	Z319736250	CCC(=O)NC=1C=CC=C(NC(=O)C2=CC=3C=C(F)C=CC3N2)C1
K07	Z1139301323	CCC1=NN=C2CN(CCN12)C(=O)C3=CC(C)=CC4=CNN=C34
L07	Z335888748	NC(=O)C=1C=C(Cl)C=CC1OCC2=NOC(=N2)C3=CC=CO3
M07	Z56984548	OC(=O)C=1C=CC=CC1OCC2=CSC(NC=3C=CC=CC3)=N2
N07	Z324593526	COC(=O)C1=CC=C(CSC=2N=C(N)C=3C(C)=C(C)SC3N2)O1
O07	Z19126364	FC=1C=CC=C(CSC=2N=NC=3C=4C=CC=CC4NC3N2)C1
P07	Z335929862	NC=1N=C(SCC(=O)C=2C=CC=3OCOC3C2)N=C4SC=CC14
A08	Z1268778158	CCCC1=NNC(=N1)C2CN(CCO2)C(=O)CCC=3C=CC=NC3
B08	Z997948526	NC(=O)CC1=CSC(=N1)C=2C=CC=3OCOC3C2
C08	Z1269691768	FC(F)(F)C1=CC(=NN1)C2CCCN(C2)C(=O)CC=3C=CC=NC3
D08	Z594976072	COC=1C=CC(=CC1)C(NC(=O)C2=CC=C(C)NC2=O)C=3C=CC=CC3
E08	Z224125774	CC=1C=CC(=CC1)C(CC(=O)O)NC(=O)CC2=CNC=3C=CC=CC23
F08	Z1168169445	CN(CCCC1=NNC(N)=C1C#N)C=2N=CC(=CC2Cl)C(=O)N
G08	Z1329036659	CC(NC=1C=CC=C(OC=2C=CC=CC2C(=O)N)C1)C3=NN=C(C)O3
H08	Z1269729284	CC1=CC(=NN1)C2CCCN(C2)C(=O)C3=CNC(C)=N3
I08	Z1269733339	CC1=CC(=NN1)C2CCCN(C2)C(=O)CCCOC=3C=CC=CC3
J08	Z990848676	COC=1C=CC(=CC1F)C(C)NC=2N=CN=C3N(CCO)N=CC23
K08	Z1704527216	CCCN1C=C(NC(C)CCCOC=2C=CC=CC2C(=O)N)C=N1

L08	Z324593374	CC1=CC(NC(=O)CSC=2N=C(N)C=3C(C)=C(C)SC3N2)=NO1
M08	Z1625982458	FC=1C=CC(NCC=2C=CNN2)=CC1NC(=O)CC=3C=CC=CC3
N08	Z1250804313	COC=1C=CC(NC2=NC(=CS2)C(=O)N3CCCC3)=CC1
O08	Z1756705867	CCN1C=C(C=N1)[C@H]2OCCC[C@@H]2NC(=O)C=3C=C(NN3)C(C)C
P08	Z1185890746	CCC1=NOC(CNC=2C=C(C=CC2Cl)N3CCNC3=O)=N1
A09	Z990871800	CN(C)C(=O)C=1C=CC=C(CNC=2N=CN=C3N(CCO)N=CC23)C1
B09	Z336009536	CCCC1=NOC(CSC=2N=C(N)C=3C(C)=C(C)SC3N2)=N1
C09	Z654149278	CC=1C=CC(NC(=O)C=2C=CC=CC2)=CC1NC(=O)C=3C=CC=NC3O
D09	Z241403990	CC(=O)NC=1C=CC(CNC(=O)C2=NNC=3C=CC=CC23)=CC1
E09	Z82184085	COC=1C=CC(CCNC(=O)C2=C(C)OC=3N=CNC(=O)C23)=CC1
F09	Z1225468526	C(CC1=NN=C(N1)C2=CC=CO2)NC=3C=NC=4C=CC=CC4N3
G09	Z51086702	CCOC(=O)C1=C(C)OC=2N=C(CSC=3N=CC=CN3)N=C(N)C12
H09	Z728986548	CC(NC=1N=CC(=CC1Cl)C(=O)N)C=2C=CC=3OCOC3C2
I09	Z215307148	CN1C(CSC=2N=C(N)C=3C=CSC3N2)=CC(=O)N(C)C1=O
J09	Z1149453302	CC1=NC=C(CNC(=O)CC=2C(C)=NC3=NC(N)=NN3C2C)S1
K09	Z1223491308	CCOC=1C=CC=2C=C(NC2C1)C(=O)NC=3C=CC=4CCNC(=O)C4C3
L09	Z980548268	O=C(NCC=1C=CNN1)C2CCCN2C(=O)C=3C=CC=4OCOC4C3
M09	Z256913326	CNC=1SN=C(C)C1C(=O)NC2=NC(CC(=O)N)=CS2
N09	Z1252215658	CS(=O)(=O)C1CCCC(C1)NC(=O)C=2C=CC=C3C=NNC23
O09	Z1116849613	CC1=NC(=NN1)C(NC(=O)CNC(=O)C=2C=CC=CC2)C=3C=CC=CC3
P09	Z1269322079	COC=1C=CC(COC=2C=CC(Cl)=CC2C(=O)N)=C(Cl)C1
A10	Z1756695442	CN1C=C(C=N1)[C@H]2OCCC[C@@H]2NC(=O)C=3C=CC=C(C3)C(=O)N
B10	Z228468438	NC=1N=C(CN2C=NC(C#N)=N2)N=C(NC=3C=CC(F)=CC3)N1
C10	Z1759859744	CCC=1C=C(NN1)C(=O)N2CCC(CN(C)CC=3C=CC=NC3)C2
D10	Z407940970	O=C(NCC=1C=CC=C(C1)N2CCCC2=O)C=3C=CC=C4C=NNC34
E10	Z1756708067	CCN1C=C(C=N1)[C@H]2OCCC[C@@H]2NC(=O)C3=NNC=4CCCC34
F10	Z649822922	CN1C=C(C=N1)C2=NC(=CS2)C(=O)NCC=3C=CNN3
G10	Z1216403474	CCOC(C)C1=NOC(CC2=CSC(=N2)N3CCNC3=O)=N1
H10	Z26325537	COC=1C=CC(C(=O)N)=C(OCC2=CC(=O)N3C=CC(C)=CC3=N2)C1
I10	Z1444360403	OC(=O)CN(CC=1C=CC=CC1)C(=O)CC2=NNC=3C=CC=CC23
J10	Z168760202	CC=1C=C(CN2CCN(CC2)C(=O)C3=NNC=4C=CC=CC34)ON1
K10	Z1759563032	CCC=1C=C(NN1)C(=O)NC[C@@H]2C[C@H](F)CN2CC3=CC(C)=NO3
L10	Z649978136	Cl.CC1=NNC=2N=CC(CNCCOC=3C=CC=4OCOC4C3)=CC12
M10	Z1434063749	CCC=1NN=C(NCC=2C=CC=CC2OCC=3C=CC=NC3)C1C
N10	Z649748576	CC1=C(CCC(=O)NCC=2C=COC2)C(=O)NC=3N(C)NC(=O)C13
O10	Z1343180792	CC1=NN=C(S1)N2CCN(CC=3N=C(N)C=4C=CC=CC4N3)CC2
P10	Z131516146	CC(NC(=O)C1=NNC(=O)C=2C=CC=CC12)C3=NN=C4C=CC=CN34
A11	Z1033101872	C(SC1=NN=C(N1)C=2C=CC=CC2)C3=NC=4C=CC=NC4N3
B11	Z1177707334	O=C(CC=1C=CC=NC1)NC2=CC(=NN2)C3=CC=4C=CC=CC4O3
C11	Z1233140741	CC=1NN=CC1S(=O)(=O)NC=2C=CC=CC2N3C=CC(=N3)C(=O)O
D11	Z1462566362	CN(C)C(=O)CC=1C=CC=CC1NCC=2C=C3C=CC=CC3=NC2O
E11	Z996066116	NC(=O)CCCNC(=O)CC1=CSC(=N1)C=2C=CC=3OCOC3C2
F11	Z1314059453	CC1=CC(C)=C(C(=O)NCCNC=2N=CN=C3C=CC=CC23)C(=O)N1
G11	Z980349258	O=C(NC=1C=CC=CC1OCC2=CSC=N2)C3=CC=4C=CC=CC4N3
H11	Z1212628882	CCC1=NN(C)C=2NN=C(NC(=O)C3CC=4C=CC=CC4O3)C12
I11	Z25777174	NC(=O)C=1C=CC=CC1OCC=2C=CC(C#N)=CC2
J11	Z826696564	CCC=1C=CC(=CC1S(=O)(=O)NC=2C=NN(CCO)C2)C(=O)O
K11	Z1119643286	COC=1C=CC(=CC1)C2=NC(CNC(=O)C=3C=CC=C4C=NNC34)=NN2
L11	Z729127304	CC=1C=C(NN1)C(=O)N2CCN(CC=3C=CC=CN3)CC2
M11	Z1126978940	CC=1C=C(ON1)C(=O)NC(C(=O)NC=2C=CNN2)C=3C=CC=CC3
N11	Z1233958166	CC=1C=C(NCC=2C=CC(C#N)=CC2F)C(=CC1F)C(=O)N
O11	Z1126978346	CC1=NC=C(S1)C(=O)NC(C(=O)NC=2C=CNN2)C=3C=CC=CC3
P11	Z1445443572	OC(=O)CC1CN(CCO1)C(=O)C=2C=C(NN2)C=3C=CC=CC3
A12	Z1480757085	CC1=NC(=NN1)C=2C=CC=C(NCC=3C=CC(=C(C)C3)N4C=NC=N4)C2
B12	Z228464920	CC=1C=CC(NC2=NC(CN3C=NC(C#N)=N3)=CS2)=CC1
C12	Z1443750597	OC(=O)CC(NC(=O)CC1=CNC=2C=C(F)C=CC12)C3=CC=CS3
D12	Z968561832	COC=1C=CC(=CC1F)S(=O)(=O)NC=2C=CC=NC2O
E12	Z1281831612	CN1C=C(C=N1)N2CCCC(NC=3C=CC(Cl)=C(C3)C(=O)N)C2=O
F12	Z733210418	CC=1C=C(NN1)C(=O)NCCNC2=NC=3C=CC=CC3S2
G12	Z1348386359	CCC1=NSC(NCC=2C=CC=CC2N3CCCC(C3)C(=O)N)=N1
H12	Z821291704	CNC1=NN=C(SCCC2=NC=3C=CC=CC3C(=O)N2)S1
I12	Z1546688605	NC=1N=C(N=C2C=CC=CC12)N3CCCC3C4=NN=C5CCCCCN45
J12	Z816646802	CC=1C=C(NN1)C(=O)NCCN2N=C3C=CC=CN3C2=O
K12	Z1269731298	CC1=CC(=NN1)C2CCCN(C2)C(=O)C=3C=CC=C(C3)S(=O)(=O)C
L12	Z644970508	CCOCCOCC=1C=CC=C(CNC=2N=CN=C3N=CNC23)C1
M12	Z224125208	OC(=O)CC(NC(=O)CC1=CNC=2C=CC=CC12)C=3C=CC(F)=CC3
N12	Z963434718	COC=1C=CC(OCC2=CC(=O)N3C=C(C)C=CC3=N2)=C(C1)C(=O)N

O12	Z1444207363	CC(CN(CC=1C=CC=CC1)C(=O)C2=NNC=3CCCCC23)C(=O)O
P12	Z816645476	CC(C)C1=CC(=NN1)C(=O)NCCN2N=C3C=CC=CN3C2=O
A13	Z1127288512	CC(C)NC(=O)N1CCN(CC1)C(=O)C2=C(C)OC=3N=CNC(=O)C23
B13	Z1021209608	CCC1=NN=C(NC(=O)C(C)NC(=O)C=2NN=C3C=CC=CC23)S1
C13	Z1119645160	COC=1C=CC(=CC1)C2=NC(CNC(=O)C=3C=NC(C)=CN3)=NN2
D13	Z1231976709	ClC=1C=CC=C(C1)C2=NN=C(NC(=O)C3CC3C=4C=CC=NC4)N2
E13	Z1120825959	CCC1=NOC(CN(C)CC=2N=C(N)C=3C=CC=CC3N2)=N1
F13	Z1084534512	COC=1C=CC(CNC(C2=NNC(C)=N2)C=3C=CC=CC3)=CC1
G13	Z1149164411	O=C(NCCNC(=O)C1=NC=2C=CC=CC2C(=O)N1)C=3C=CC=NC3
H13	Z1191230807	CC1=CC(=NN1C)C(=O)NC(C(=O)NC=2C=CNN2)C=3C=CC=CC3
I13	Z1119645296	COC=1C=CC(=CC1)C2=NC(CNC(=O)C=3C=CC(O)=NC3)=NN2
J13	Z1172581671	NC(=O)C1=CC(=NN1C=2C=CC=CC2)C(=O)NC3CCC=4C=CC=CC34
K13	Z241567956	NC=1N=C(N)N=C(SCC2=CSC(=N2)C3=CC=CO3)N1
L13	Z1158308049	CC(C)(C)C1=NOC(=N1)C=2C=CC=CC2C(=O)N3CCC(C3)C(=O)N
M13	Z361929940	CC1=CN=C(NC(=O)CCC2=C(C)C=3C(C)=NN(C)C3NC2=O)S1
N13	Z217920818	CC=1C=CC(C(=O)N)=C(OCC=2C=CC(C#N)=CC2)C1
O13	Z883400278	NC(=O)C=1C=CC=CC1OCCCOC=2C=CC=3OCOC3C2
P13	Z358274380	FC(F)(F)C=1C=CC(CNC(=O)C=2NN=C3CCCCC23)=CC1
A14	Z1758013572	CS(=O)C=1C=CC(CNC2CCCN(C2)C3=NC=CNC3=O)=CC1
B14	Z666232532	CC=1C=C(NC(=O)CCC2=C(C)C=3C(C)=NN(C)C3NC2=O)NN1
C14	Z1756824711	COC=1C=C(C=CN1)[C@H]2OCCC[C@@H]2NC(=O)C=3C=C(NN3)C(C)C
D14	Z109305448	CC(NC(=O)C1=CC(Cl)=CN1)C=2C=CC(=CC2)N3C=CN=C3
E14	Z1754197948	CC(C)C1=NN=C(O1)C2CN(CCO2)C(=O)C=3C=CC=C4C=NNC34
F14	Z666586994	O=C1CNC(=O)N1CC=2C=CC(=CC2)C3=NC=4C=CC=CC4C(=O)N3
G14	Z1139198732	CNC=1C=C(N=CN1)N2CCCC2CNC=3C=CC4=NN=NN4N3
H14	Z3228283128	OC=1C=CC(CNC2=CC=CC3=CNN=C23)=CC1
I14	Z221228892	COC=1C=CC(CNC(=O)C2=NNC=3C=CC=CC23)=CN1
J14	Z166467536	CC(SC=1N=C(N)C=2C=CSC2N1)C=3C=CC=C(C3)[N+](=O)[O-]
K14	Z1432909170	NC(=O)C=1C=CC(=CN1)C(=O)N2CCC(C2)OC=3C=CC=CN3
L14	Z441212406	CC=1C(CSC=2N=C(N)C=3C=CSC3N2)=CC=CC1[N+](=O)[O-]
M14	Z1614131615	CC1=NN=C(CN2CCCC(C2)C3=NNC(=N3)C=4C=CC=CC4)S1
N14	Z981111724	OC=1C=CC(=CN1)C(=O)NCCNC(=O)C=2NN=C3C=CC=CC23
O14	Z1802347005	CC1=NNC=2N=CC(NCC=3C=CC(C#N)=CC3)=CC12
P14	Z1262404550	COC(=O)CN1N=CC=2C(NCC=3C=NC(O)=NC3O)=NC=NC12
A15	Z132931720	NC(=O)C=1C=CC(NS(=O)(=O)C2=CC(=CS2)C(=O)O)=CC1
B15	Z324593544	CNC(=O)NC(=O)C(C)SC=1N=C(N)C=2C(C)=C(C)SC2N1
C15	Z821301506	NC=1N=C(SCCCC2=NC=3C=CC=CC3O2)N=C4SC=CC14
D15	Z1396653646	CCC(CCO)CNC1=NN2C(=O)C=CN=C2S1
E15	Z371624082	CC1=NN(C)C=2NC(=O)C(CCC(=O)NCC3=CC=NN3C)=C(C)C12
F15	Z1341629225	CC(C)(C)C1=CN2N=C(NCCCC3=NC(=O)NN3)SC2=N1
G15	Z886909616	CC1=NC2=NC(N)=NN2C(C)=C1CC(=O)N3CCOC4CCCCC43
H15	Z223671374	O=C(CCC1CC=2C=CC=CC2NC1=O)NCC=3C=CC=NC3
I15	Z666645730	CC(NC(=O)C=1C=CC=NC1O)C=2C=CC=3NC(=O)NC3C2
J15	Z1185124459	ClC=1C=CC(=CC1NC(=O)CCC=2C=CC=NC2)N3CCNC3=O
K15	Z650414262	CN1C=C(C=N1)C2=NC(COC=3C=CC=CC3C(=O)N)=CS2
L15	Z1192820437	CCC=1C=CC(NC(=O)C2=COC=3C=CC=CC23)=CC1S(=O)(=O)N
M15	Z645321080	CCC1=CC=2C(NC3CCCC4=C3C=NN4CCO)=NC=NC2S1
N15	Z1282105741	CC(C)C1=NOC(=N1)C(C)NC=2C=CC=C(C2)N3CCCNC3=O
O15	Z910731756	O=C(CC1=CSC(=N1)C=2C=CC=NC2)NC=3C=CNN3
P15	Z1328965766	CS(=O)C1=NN=CN1CC2=CSC(NC=3C=CC=CC3C)=N2
A16	Z1400890685	O=C(CC1=CNC=2N=CC=CC12)N3CCCC(C3)N4CCNC4=O
B16	Z1126979295	CC1=CC(=NO1)C(=O)NC(C(=O)NC=2C=CNN2)C=3C=CC=CC3
C16	Z1141132968	NC=1N=C(CN2CCCCC2CN3C=NC=N3)N=C4C=CC=CC14
D16	Z2242917793	COC=1C=CC(CN2C=C(C=N2)C(=O)N3CCCC3CN)=CC1
E16	Z1958483455	OCC1CCCN(C1)C=2C=C(NCC=3C=CC=4N=CC=CC4C3)N=CN2
F16	Z2376880965	C[C@@H]1CN(C[C@H]1C(=O)O)C(=O)CC=2C=CC=3C=NNC3C2 |&1:1,5,r|
G16	Z1455155305	OC(=O)C=1C=CC(CNC(=O)C2CCC(=O)N2)=CC1
H16	Z1570104769	CC=1C=CC=2NN=C(C(=O)NC3CCC(CC3)C(=O)O)C2C1
I16	Z1869684220	OC(=O)CCC(NC(=O)CC1=CNC=2N=CC=CC12)C=3C=CC=CC3
J16	Z645390922	NC(=O)COC=1C=CC(CCNC2=NC=3C=CC=CC3O2)=CC1
K16	Z1757022852	CC=1C=CC=2NN=C(C(=O)N3CCOC(C3)C4=NN=CN4C)C2C1
L16	Z1528727319	Cl.CC=1C=CC=2NN=C(C(=O)N3CCC(C3)C(=O)O)C2C1
M16	Z1455199553	CN1C=C(C=C1C(=O)NC(C)(C)CCC(=O)O)C(=O)N
N16	Z2242912768	CN(C1CCNC1)C(=O)CN2C(=O)NC=3C=CC=CC3C2=O
O16	Z752254022	CN(CC=1C=CC(OC(F)F)=CC1)C(=O)C=2C=NC3=NNC(C)=C3C2
P16	Z769794590	CN(CC(=O)NCC1=NN=C2CCCCN12)C=3N=CN=C4N=CNC34
A17	Z733239458	CC=1C=C(NN1)C(=O)NCC=2C=CN=C(C2)N3C=CC=N3

B17	Z243563742	COC=1C=C(CNC(=O)C2=NNC=3C=CC=CC23)C=CN1
C17	Z666947144	NC(=O)C1CCN(C1)C(=O)CCC2=NC=3C=CC=CC3C(=O)N2
D17	Z26395418	O=C(NCCC1=CNC=2C=CC=CC12)C3=NNC(=O)C=4C=CC=CC34
E17	Z1127139266	CC1=CC(NC(=O)CN(CC=2C=CNN2)CC=3C=CC=CC3)=NO1
F17	Z228468604	NC=1N=C(CN2C=NC(C#N)=N2)N=C3C=CC=CC13
G17	Z845333020	NC(=O)CN1CCCN(CC1)C(=O)CC=2C=NN(C2)C=3C=CC=CC3
H17	Z92636259	CC=1C=C(C)C=C(C1)C2=NN=C(SCC=3N=C(N)N=C(N)N3)O2
I17	Z103948276	CCN(CC=1C=CC(OC)=C(F)C1)CC=2N=C(N)N=C(N)N2
J17	Z1270084123	CNC1=NC(CNC2=NN3C=C(C)N=C3S2)=CS1
K17	Z51853629	CC(=O)NC=1C=CC=C(NC(=O)CN2C=CC=CC2=O)C1
L17	Z1274121018	CC(C(=O)NCC1=NNC(C)=N1)N2N=NC(=N2)C=3C=CC=CC3
M17	Z317045196	CC=1SC=2N=C(CSC=3N=CC=CC3C(=O)O)N=C(N)C2C1C
N17	Z224221052	OC(=O)C=1C=CC(CCNC(=O)CC2=CNC=3C=CC=CC23)=CC1
O17	Z224264812	COC=1C=CC(CNC(=O)C2=NNC=3C=CC=CC23)=CC1C(=O)O
P17	Z1138020853	COC=1C=CC(NC(=O)CS(=O)CC=2C=CC=C(C2)C(=O)N)=CC1
A18	Z2379492132	CNS(=O)(=O)C=1C=CC(=CN1)C(=O)NC(C)C=2C=CNN2
B18	Z1787637438	CN1N=CC=2C(N)=NC(=NC12)N3CCC(CN4C=CN=N4)CC3
C18	Z1411438547	CC(C)C1=NC(CN(C)C2CCN(C2)C(=O)C3=CC(C)=NN3)=NO1
D18	Z1759277492	CC1=NC(=CN1)C(=O)NC[C@@H]2C[C@H](F)CN2CC=3C=NN(C)C3
E18	Z729805042	CCN(CC=1C=CC=2OCOC2C1)C(=O)C=3C=NC4=NNC(C)=C4C3
F18	Z1671598133	CCC=1N=CC(NC(=O)N2CCCCC2C=3N=CNN3)=CN1
G18	Z1204553247	CNC(=O)C=1C=C(OC2CCN(C2)C(=O)C3=CC=CN3)C=CN1
H18	Z1984528335	CC(C)N1C=C(CNC=2C=CC(Cl)=C(C2)N3CCNC3=O)C=N1
I18	Z1614129093	C(N1CCCC(C1)C2=NNC(=N2)C=3C=CC=CC3)C=4C=CON4
J18	Z2204483625	CN1CCC(O)(CC1)C=2C=CC=C(Cl)N2
K18	Z2054653686	CC1=NOC(=N1)C2CCN(CC=3C=C4C=CC=CC4=NC3O)C2
L18	Z3243694072	CN1CCC(O)(CC1)C=2C=CC(Cl)=NC2
M18	Z381616952	CCCN(CC1=NC=2C=C(Cl)C=CC2C(=O)N1)C(=O)C=3C=CNN3
N18	Z3242731200	CN1CC(NCC1=O)C=2C=CC=CC2
O18	Z1928111543	FC(F)OC=1C=CC(CCC(=O)N2CCCC3=NNC=C23)=CC1
P18	Z2491498223	COC=1C=CC(CN2CCC2CN)=CC1
A19	Z285688150	CC(=O)NC=1C=CC(SC=2C=CC3=NN=C(N)N3N2)=CC1
B19	Z220420794	NC=1NN=C(CCCNC=2C=CC3=NN=NN3N2)C1C#N
C19	Z226215246	COC=1C=CC(CNC(=O)C2=CC(=NN2)C=3C=CC(C)=CC3)=CN1
D19	Z954441040	COC=1C=CC(=CC1)C2CCCN2C=3C=C(C=CN3)C(=O)N
E19	Z232515128	NC(=O)C=1C=CC=CC1NCC=2C=CC(C#N)=CC2
F19	Z1314018002	CNC=1C=C(C(=O)NCCNC(=O)C(C)(C)C)C=2C=CC=CC2N1
G19	Z666250770	COC=1C=C(CNC(=O)C2=CC(Cl)=CN2)C=CC1OCC(=O)N
H19	Z139942108	COC(=O)C=1C=CC(CNC(=O)C2=C(C)OC=3N=CNC(=O)C23)=CC1
I19	Z991004054	CN(CC1=NC=2C=CC=CC2C(=O)N1)CC3=NC=4C=CC=CC4NC3=O
J19	Z1376464081	NC(=O)C=1C=CC=CC1OCC2=CN(N=N2)C=3C=CC(Cl)=CC3
K19	Z804108370	CC1=CC(C)=C(CNC(=O)C2=CNC=3N=CC=CC23)C(=O)N1
L19	Z1389502856	CC1=CC(CC(=O)NC=2C=CC=C(OC=3C=NC=CN3)C2)=NN1
M19	Z1438836112	COC=1C=CC(=CC1)C(C)(C)C(=O)NCCC=2C=CC=C(C2)C(=O)N
N19	Z1191230926	O=C(CCN1C=CC=N1)NC(C(=O)NC=2C=CNN2)C=3C=CC=CC3
O19	Z1523053611	ClC1=CC=C(S1)C2=CC(NC(=O)CC=3C=CC=NC3)=NN2
P19	Z1174872997	CC(C)CC=1C=C(NN1)C(=O)NCCC2=NOC(=N2)C=3C=CC=CN3
A20	Z2400432799	O[C@@H]1COC[C@H]1N2C=C(N=N2)C(=O)NCC=3C=CC=4OCCC4C3
B20	Z1169033594	CN(CC=1C=CC(Cl)=NC1)C2CC2
C20	Z1273698874	O=C(N1CCCC(C1)N2CCNC2=O)C=3C=CC=C4C=CNC34
D20	Z1642151030	Cl.CCCC(C)NC=1C=CC=C(C#N)C1
E20	Z2440418079	CC=1C=CC=2NN=C(C(=O)NC(CN)C3CC3)C2C1
F20	Z1653394708	CN1CCNC(=O)C1C=2C=CC=CC2Cl
G20	Z1984528451	ClC=1C=CC(NCC=2C=CC=NC2)=CC1N3CCNC3=O
H20	Z1119625807	O=C(N1CCCC(C1)N2C=NC=3C=CC=CC23)C4=NNC=5CCCC45
I20	Z1651729217	NC(=O)C(NC1CCCN(C1=O)C=2C=CC=NC2)C=3C=CC=CC3
J20	Z826871136	O=C(CC1=NNC=2C=CC=CC12)NC=3C=CC=NC3
K20	Z1234098811	OC=1N=C2C=CC=CC2=CC1CNC3CCCN(C3)C=4C=CC=NN4
L20	Z445986708	CC=1NN=CC1CCCNC(=O)NC2CCS(=O)(=O)C2
M20	Z1445272300	OC(=O)C1CN(CCO1)C(=O)C=2C=C(NN2)C=3C=CC(F)=CC3
N20	Z1607385949	COCC1=NN(CC=2N=C(N)C=3C=4CCCCC4SC3N2)C(=O)O1

Supplementary 5

Activity of MurD in the presence of Enamine fragments

Activity of MurD (%)							
Plate 01							
Fragment ID	1	2	3	Fragment ID	1	2	3
A02	75.46	85.66	68.17	**C08**	79.62	91.68	81.82
A03	7.47	14.40	12.76	**C09**	82.39	103.83	81.82
A04	59.17	68.93	67.92	**C10**	135.27	101.72	105.70
A05				**C11**	53.57	51.34	46.80
A06	66.54	52.11	44.52	**C12**			
A07				**C13**	117.07	123.65	98.72
A08	32.09	36.32	35.49	**C14**	110.04	114.16	120.09
A09				**C15**	106.75	100.77	81.03
A10				**C16**			
A11	56.09	55.21	62.02	**C17**			
A12				**C18**			
A13	122.52	94.50	140.85	**C19**			
A14				**C20**	81.27	106.40	90.67
A15	82.85	94.47	71.92	**C21**	30.08	46.97	34.51
A16	75.38	105.98	93.12	**C22**	35.58	43.82	11.66
A17				**C23**	70.55	103.92	106.93
A18				**D02**			
A19	68.34	54.23	58.29	**D03**			
A20	70.35	88.84	102.71	**D04**	57.72	93.21	131.71
A21				**D05**	106.73	186.73	102.16
A22	57.69	56.98	58.29	**D06**			
A23	95.18	86.53	103.35	**D07**	56.02	71.47	49.12
B02	36.09	42.86	39.19	**D08**	60.13	82.48	62.43
B03				**D09**	59.47	43.37	57.50
B04	565.19	480.93	267.92	**D10**	63.25	50.44	51.42
B05	63.85	60.94	65.13	**D11**	47.68	48.12	43.10
B06	80.97	100.71	77.71	**D12**	76.44	60.04	53.53
B07	30.89	38.44	50.60	**D13**	78.57	79.98	79.32
B08				**D14**	127.21	154.25	139.66
B09	48.14	47.15	50.11	**D15**			
B10	84.01	89.92	81.01	**D16**	69.98	96.64	77.12
B11	88.27	75.33	77.30	**D17**	116.91	115.88	109.70
B12	79.83	85.87	95.61	**D18**			
B13	107.24	123.79	137.94	**D19**	48.91	56.75	51.12
B14	137.17	203.35	137.42	**D20**	67.87	65.01	60.84
B15	90.26	88.53	87.69	**D21**	7.24	15.88	31.76
B16	72.46	67.79	86.07	**D22**	100.30	107.94	83.82
B17	109.44	106.09	87.30	**D23**	81.71	156.08	107.64
B18				**E02**	125.21	-6.20	56.68
B19				**E03**			
B20	55.14	75.44	62.38	**E04**			
B21	63.99	78.46	65.19	**E05**	22.96	24.42	20.98
B22	116.98	123.42	120.84	**E06**			
B23	72.71	90.95	69.25	**E07**	47.32	69.33	68.67
C02				**E08**			
C03	128.25	99.09	102.92	**E09**	66.70	84.45	81.16
C04	30.26	18.01	6.56	**E10**	49.29	28.42	54.71
C05	40.28	41.19	40.64	**E11**	42.62	40.15	44.32
C06	68.67	95.62	86.74	**E12**			
C07	72.67	72.95	76.89	**E13**	81.50	107.73	85.48

Fragment ID	1	2	3	Fragment ID	1	2	3
E14				**F19**	90.59	97.82	90.94
E15	74.07	50.25	62.82	**F20**	62.51	70.15	67.64
E16	68.19	65.88	65.90	**F21**	64.42	135.58	202.91
E17	109.61	155.45	108.07	**F22**	99.36	95.34	95.54
E18				**F23**			
E19				**G02**	137.79	174.97	117.74
E20	87.84	65.33	72.16	**G03**	64.09	64.09	65.55
E21	132.60	120.94	96.82	**G04**	22.48	25.58	21.02
E22				**G05**	23.57	42.16	35.67
E23	67.60	93.13	102.78	**G06**	85.32	76.12	84.90
F02	81.04	90.89	83.71	**G07**	61.45	60.79	66.33
D17	116.91	115.88	109.70	**G08**	41.07	65.72	55.86
D18				**G09**			
D19	48.91	56.75	51.12	**G10**	103.18	97.59	88.82
D20	67.87	65.01	60.84	**G11**	64.28	74.59	68.45
D21	7.24	15.88	31.76	**G12**	108.20	213.22	145.31
D22	100.30	107.94	83.82	**G13**	99.39	122.45	105.52
D23	81.71	156.08	107.64	**G14**	43.78	83.43	54.94
E02	125.21	-6.20	56.68	**G15**	88.25	86.08	76.79
E03				**G16**	94.01	103.82	91.76
E04				**G17**	86.35	99.74	85.06
E05	22.96	24.42	20.98	**G18**			
E06				**G19**	150.45	158.29	110.65
E07	47.32	69.33	68.67	**G20**	60.77	57.35	67.60
E08				**G21**			
E09	66.70	84.45	81.16	**G22**	65.63	61.81	50.55
E10	49.29	28.42	54.71	**G23**	88.38	109.68	112.09
E11	42.62	40.15	44.32	**H02**	103.04	92.65	93.99
E12				**H03**	18.23	33.35	25.94
E13	81.50	107.73	85.48	**H04**	66.16	134.14	158.02
E14				**H05**			
E15	74.07	50.25	62.82	**H06**	66.05	51.92	46.33
E16	68.19	65.88	65.90	**H07**	24.97	29.29	26.94
E17	109.61	155.45	108.07	**H08**	42.88	59.97	43.54
E18				**H09**	64.07	58.16	40.42
E19				**H10**	61.45	50.27	50.27
E20	87.84	65.33	72.16	**H11**	58.25	63.73	45.30
E21	132.60	120.94	96.82	**H12**	102.74	101.98	116.12
E22				**H13**	92.51	92.06	87.60
E23	67.60	93.13	102.78	**H14**	176.22	140.94	155.28
F02	81.04	90.89	83.71	**H15**			
F03	66.59	90.58	43.01	**H16**	79.32	72.90	83.96
F04	85.78	70.53	162.88	**H17**			
F05	98.24	96.23	83.84	**H18**			
F06	62.25	72.95	52.25	**H19**	79.33	63.65	55.21
F07				**H20**	68.61	66.20	78.86
F08	31.00	23.77	17.85	**H21**	56.97	57.22	59.43
F09	19.38	24.82	21.99	**H22**			
F10	84.23	78.64	81.60	**H23**			
F11	62.23	80.01	55.65	**I02**	91.86	94.17	82.50
F12	116.29	198.85	94.71	**I03**	58.26	51.34	58.99
F13				**I04**			
F14				**I05**			
F15	121.82	115.57	107.69	**I06**	58.60	52.35	62.87
F16	71.10	75.02	73.88	**I07**	71.52	81.38	79.18
F17	83.91	76.57	87.64	**I08**			
F18				**I09**	44.03	45.66	43.70

Fragment ID	1	2	3	Fragment ID	1	2	3
I10				**K23**	95.06	92.19	114.30
I11				**L02**	138.70	111.54	66.89
I12				**L03**	11.85	59.23	34.75
I13	118.81	196.83	130.27	**L04**	32.08	31.85	30.44
I14	46.17	58.71	33.99	**L05**			
I15	94.84	91.72	88.10	**L06**	127.60	17.20	71.74
I16				**L07**	59.91	68.46	30.67
I17	81.80	85.28	102.92	**L08**			
I18	62.63	64.12	60.70	**L09**	68.13	42.06	31.98
I19	33.17	40.80	56.28	**L10**	32.20	69.00	93.98
I20	22.81	24.52	25.03	**L11**	35.54	57.92	47.10
I21	79.90	75.78	80.60	**L12**	103.81	107.18	104.41
I22				**L13**	92.79	105.10	112.30
I23	130.95	136.98	143.02	**L14**	108.28	156.95	109.57
J02	78.61	91.01	82.16	**L15**	69.45	90.24	71.03
J03	22.46	25.47	26.86	**L16**	99.17	85.82	68.94
J04	66.28	16.16	49.19	**L17**	26.82	18.54	25.06
J05	75.03	50.61	67.19	**L18**	108.27	82.14	73.50
J06	12.49	11.83	13.39	**L19**	65.23	74.17	61.71
J07				**L20**	66.57	50.99	69.48
J08	84.61	58.75	63.25	**L21**	68.94	58.29	52.26
J09	57.39	32.42	47.21	**L22**	50.45	13.87	28.54
J10	59.69	51.81	55.42	**L23**	114.37	140.30	116.78
J11	69.47	80.60	78.69	**M02**	19.96	22.24	35.09
J12	31.54	80.08	43.84	**M03**	80.74	102.61	81.11
J13	72.42	75.04	74.50	**M04**	-14.88	-17.80	-21.63
J14	54.21	28.71	41.12	**M05**	12.76	27.89	42.65
J15	70.88	110.39	81.51	**M06**	117.31	54.87	89.38
J16	92.77	64.68	101.61	**M07**	-141.79	-19.55	-65.88
J17				**M08**			
J18	42.21	55.88	33.02	**M09**			
J19	85.23	100.90	55.68	**M10**	52.03	73.38	73.06
J20	94.97	95.58	93.62	**M11**	77.15	99.97	64.21
J21	75.28	98.39	78.94	**M12**	89.67	125.26	145.33
J22	118.86	105.39	107.02	**M13**	60.46	52.83	43.99
J23	91.32	90.12	91.73	**M14**	100.09	94.68	113.99
K02				**M15**	67.08	87.26	47.90
K03	71.81	62.33	72.72	**M16**	129.79	107.58	86.14
K04				**M17**	87.38	80.17	95.88
K05	66.16	60.02	63.79	**M18**	73.37	64.92	86.43
K06	67.47	58.60	62.20	**M19**	82.51	89.55	109.65
K07	75.61	77.33	73.38	**M20**	59.90	70.35	56.48
K08	46.00	51.26	46.33	**M21**	22.26	16.28	43.02
K09	71.63	62.10	87.73	**M22**			
K10	68.51	63.64	60.95	**M23**			
K11	74.65	72.62	79.64	**N02**	131.41	91.68	25.52
K12	109.46	153.88	176.70	**N03**	51.37	76.67	32.75
K13	120.26	127.96	125.61	**N04**	66.28	92.75	118.77
K14				**N05**			
K15	79.26	108.49	103.22	**N06**	120.92	112.71	62.10
K16				**N07**	34.06	82.04	58.05
K17				**N08**	72.29	81.16	21.03
K18				**N09**	31.07	29.57	27.60
K19				**N10**	84.34	67.91	59.04
K20	90.45	72.16	71.91	**N11**			
K21	91.93	92.73	100.97	**N12**	125.21	98.36	109.08
K22				**N13**	155.44	130.19	115.86

				Plate 02			
Fragment ID	1	2	3	Fragment ID	1	2	3
N14	48.50	41.29	40.26	**A02**	106.71	93.96	100.84
N15				**A03**	78.63	103.89	75.85
N16	89.13	93.67	100.93	**A04**	76.54	82.80	78.05
N17	17.56	12.27	19.74	**A05**			
N18	53.67	60.10	41.21	**A06**	113.43	129.18	154.67
N19	72.96	71.76	69.75	**A07**			
N20	67.00	319.26	122.08	**A08**	102.65	95.93	92.46
N21				**A09**	101.96	135.79	100.57
N22	97.89	111.96	155.78	**A10**	51.26	43.55	45.10
N23				**A11**	111.42	48.94	94.62
O02	48.00	72.96	45.44	**A12**	129.00	153.19	123.29
O03	108.87	113.79	101.00	**A13**	135.72	116.57	109.52
O04	13.65	16.40	18.98	**A14**	9.07	14.12	5.81
O05				**A15**	150.62	86.11	97.54
O06	111.39	129.46	95.62	**A16**	107.50	126.32	145.46
O07				**A17**	59.16	49.73	74.08
O08				**A18**	119.42	97.05	81.47
O09	18.29	88.94	82.04	**A19**			
O10				**A20**	85.67	82.60	63.08
O11	266.34	236.95	-32.69	**B02**	108.14	135.25	176.49
O12	118.90	135.50	139.21	**B03**	38.23	75.54	56.77
O13	132.85	139.54	127.76	**B04**	95.08	99.72	90.95
O14				**B05**			
O15	106.62	84.28	83.47	**B06**			
O16				**B07**	79.94	86.43	66.74
O17	89.27	107.55	93.13	**B08**	87.36	116.32	125.13
O18				**B09**			
O19	95.78	104.02	90.35	**B10**	22.39	64.81	42.44
O20	70.22	82.28	69.82	**B11**	23.18	22.84	16.01
O21	75.78	61.51	62.91	**B12**			
O22	48.24	71.96	108.94	**B13**	97.09	117.25	120.27
O23	90.45	83.22	85.83	**B14**	9.41	3.34	0.34
P02	81.41	61.18	37.85	**B15**			
P03				**B16**	99.27	79.45	124.80
P04	72.90	82.00	123.39	**B17**	40.28	37.15	47.68
P05	65.86	44.11	94.41	**B18**	98.84	54.30	91.16
P06	84.78	102.52	92.33	**B19**	124.54	113.57	102.82
P07	45.25	47.65	40.09	**B20**	34.99	44.65	44.21
P08	21.80	27.10	32.64	**C02**			
P09	52.35	28.70	43.50	**C03**			
P10	46.77	81.27	71.41	**C04**			
P11				**C05**			
P12	118.16	133.19	149.24	**C06**	89.21	102.19	158.96
P13	106.17	86.89	82.83	**C07**	78.24	45.34	59.94
P14	23.18	47.38	34.91	**C08**	86.87	87.71	85.85
P15	84.50	98.39	100.54	**C09**			
P16				**C10**	68.02	75.42	70.54
P17	113.48	116.05	85.67	**C11**	132.92	198.43	168.87
P18	102.85	102.04	82.55	**C12**	155.21	141.10	208.62
P19	103.82	130.35	69.45	**C13**	20.83	11.53	18.38
P20	77.45	89.11	60.97	**C14**	98.88	64.61	132.70
P21	133.13	135.34	139.16	**C15**			
P22	89.58	75.31	80.74	**C16**	24.75	23.54	21.39
P23	85.33	133.17	89.75	**C17**	69.26	62.02	61.14
				C18	95.66	107.72	73.28
				C19			

Fragment ID	1	2	3	Fragment ID	1	2	3
C20	65.96	47.97	60.04	**F20**	60.99	54.85	31.81
D02	86.66	66.74	93.85	**G02**	28.73	21.09	39.62
D03	61.25	53.37	46.88	**G03**			
D04	86.74	107.36	137.26	**G04**			
D05	63.47	73.50	86.00	**G05**	36.55	33.79	34.52
D06	70.67	81.57	72.73	**G06**	90.29	71.76	108.14
D07				**G07**	76.78	74.38	81.57
D08				**G08**	63.88	77.37	76.85
D09				**G09**	33.52	32.64	43.56
D10	26.89	55.17	40.94	**G10**	78.52	66.95	70.84
D11	55.10	40.65	47.37	**G11**			
D12	77.04	91.49	86.45	**G12**	60.30	103.98	81.13
D13				**G13**	167.97	118.92	43.34
D14	36.94	32.47	48.38	**G14**			
D15	141.88	72.00	111.98	**G15**	164.95	102.46	104.82
D16	60.25	88.47	73.35	**G16**	99.78	84.66	56.77
D17	10.53	10.10	8.78	**G17**	54.48	47.24	47.24
D18	99.17	86.88	55.73	**G18**	75.03	72.84	52.00
D19	27.43	25.23	26.77	**G19**	10.24	7.23	6.73
D20				**G20**	43.81	42.93	40.08
E02	131.54	175.80	95.39	**H02**	184.84	146.37	155.18
E03				**H03**			
E04	136.17	135.25	108.14	**H04**	120.65	69.67	77.09
E05	23.26	22.82	23.91	**H05**	118.33	61.50	82.78
E06	52.91	70.98	67.04	**H06**	366.23	154.90	-37.42
E07	87.36	47.73	77.63	**H07**			
E08	128.37	132.08	83.42	**H08**	89.68	92.46	104.74
E09				**H09**	159.89	469.46	55.15
E10	83.13	84.74	82.76	**H10**	103.16	51.42	76.64
E11	110.86	105.82	108.20	**H11**	100.22	164.05	162.04
E12	137.96	134.27	86.90	**H12**	35.05	65.96	67.97
E13	96.98	81.96	83.20	**H13**	136.90	60.64	99.94
E14	135.72	59.46	110.19	**H14**	111.20	118.59	152.18
E15	94.40	83.99	71.22	**H15**	142.89	72.68	77.04
E16	123.07	106.27	101.22	**H16**	94.51	97.20	73.35
E17	46.73	70.43	56.38	**H17**			
E18	83.30	107.87	56.75	**H18**	50.57	48.16	55.40
E19				**H19**			
E20	75.11	60.85	53.61	**H20**	44.76	66.26	60.82
F02				**I02**	99.06	76.70	103.00
F03	110.18	132.43	69.63	**I03**	75.64	104.39	45.30
F04	79.63	70.60	98.40	**I04**	90.76	119.49	88.44
F05	70.43	45.63	97.63	**I05**			
F06	77.32	99.33	124.82	**I06**	156.02	85.35	183.14
F07	39.04	37.42	55.03	**I07**			
F08	53.30	120.96	85.27	**I08**	151.78	112.85	78.78
F09	357.08	139.50	38.93	**I09**	234.89	182.98	182.98
F10	77.88	74.99	76.54	**I10**	50.13	86.45	67.82
F11	65.85	93.06	93.06	**I11**	98.32	101.01	74.80
F12	79.17	79.84	108.73	**I12**	56.22	106.94	142.89
F13	63.38	90.59	98.66	**I13**	112.99	134.49	122.73
F14				**I14**	76.15	54.98	111.20
F15	62.79	71.39	59.63	**I15**	62.49	100.78	86.00
F16	97.93	58.62	122.12	**I16**	64.95	68.76	64.95
F17	49.00	42.42	34.52	**I17**	55.07	44.10	57.92
F18	92.58	85.78	65.38	**I18**	70.75	65.71	68.56
F19	54.19	46.51	41.25	**I19**	11.55	14.76	8.63

Fragment ID	1	2	3	Fragment ID	1	2	3
I20	75.54	54.48	74.45	**L20**	46.40	45.78	53.02
J02	96.51	96.05	90.25	**M02**	59.09	47.73	91.76
J03	164.52	78.78	89.68	**M03**			
J04	22.09	17.31	16.68	**M04**	78.44	98.60	63.14
J05	71.85	67.68	93.13	**M05**	69.00	76.24	94.01
J06	64.53	25.14	44.84	**M06**	72.64	63.61	133.35
J07	143.67	-9.04	85.97	**M07**	86.43	90.75	98.02
J08	102.65	69.98	97.55	**M08**	105.28	66.12	116.40
J09	76.31	76.78	92.53	**M09**	34.18	96.51	92.57
J10	52.60	191.75	128.64	**M10**	44.19	62.51	54.17
J11	59.57	94.18	76.71	**M11**	111.42	64.39	123.52
J12	108.96	108.29	96.53	**M12**	167.30	163.27	91.04
J13				**M13**	81.19	97.98	97.31
J14				**M14**	59.80	32.92	38.75
J15	41.38	42.33	50.39	**M15**	62.71	62.37	65.73
J16	74.58	112.88	105.82	**M16**	25.87	46.14	40.65
J17	24.24	26.44	25.69	**M17**			
J18	64.87	77.81	112.70	**M18**	105.32	107.94	61.21
J19				**M19**	83.81	77.45	96.09
J20	48.27	56.16	52.00	**M20**	42.12	29.03	36.05
K02	87.05	106.51	114.62	**N02**	129.99	142.74	135.32
K03	72.76	101.49	73.92	**N03**	51.44	45.73	44.49
K04	60.02	103.35	113.77	**N04**	176.96	218.67	84.27
K05				**N05**			
K06	52.14	101.49	149.46	**N06**	45.34	55.77	53.91
K07	85.35	52.45	109.22	**N07**			
K08	78.48	109.76	94.70	**N08**	92.57	118.76	74.27
K09				**N09**	102.96	103.66	92.53
K10	107.34	85.81	97.15	**N10**			
K11	148.82	525.76	264.73	**N11**			
K12	64.61	106.61	177.83	**N12**	92.83	97.87	66.97
K13	13.70	23.30	26.96	**N13**			
K14	101.12	165.29	143.45	**N14**	141.21	120.38	96.42
K15	120.10	109.69	133.54	**N15**	20.72	14.86	6.61
K16	116.69	74.36	103.25	**N16**	135.05	100.45	51.40
K17	49.99	51.78	40.81	**N17**	11.08	8.70	4.97
K18	54.48	79.27	51.19	**N18**	110.36	84.91	94.56
K19	76.42	140.49	70.50	**N19**	109.55	111.09	107.36
K20	53.02	53.68	65.09	**N20**			
L02	152.55	109.22	123.82	**O02**	140.04	156.95	123.58
L03				**O03**	119.34	120.74	125.36
L04	101.84	59.90	67.31	**O04**	139.15	94.89	97.44
L05	38.39	44.54	32.47	**O05**	1.97	3.51	2.72
L06	12.94	20.26	14.97	**O06**	121.27	124.51	107.83
L07				**O07**			
L08				**O08**	96.94	79.09	78.86
L09	132.66	112.04	120.61	**O09**	123.04	163.59	147.37
L10	42.45	42.31	42.97	**O10**	-4.98	183.99	80.75
L11	107.73	146.70	208.51	**O11**	153.30	176.48	111.65
L12	97.87	164.39	93.17	**O12**	189.36	146.70	134.94
L13	134.94	126.20	87.57	**O13**			
L14				**O14**	591.27	284.21	-112.21
L15				**O15**	71.89	102.80	32.92
L16	69.32	59.91	60.92	**O16**	39.98	49.38	48.61
L17	66.62	72.18	77.15	**O17**	47.68	47.90	35.62
L18	89.51	57.48	73.28	**O18**	103.19	111.53	76.64
L19	84.91	74.81	84.47	**O19**			

Fragment ID	1	2	3
P02	74.27	113.89	120.84
P03	122.46	62.45	80.75
P04	253.62	129.18	120.15
P05	92.22	132.15	110.43
P06	91.30	98.71	60.25
P07			
P08	69.98	80.87	55.15
P09	182.83	440.50	282.47
P10	32.14	138.51	85.43
P11	86.00	73.24	104.14
P12	98.99	69.76	35.83
P13	29.23	32.25	32.05
P14	445.58	120.72	53.42
P15	64.33	62.65	96.58
P16	91.15	136.84	143.23
P17	34.88	32.87	31.59
P18	100.12	72.25	108.67
P19	78.84	83.22	88.49

Supplementary 6

Sequence of MurE from *S. agalactiae*

```
-
          10        20        30        40        50        60        70        80        90        100
           *         *         *         *         *         *         *         *         *         *
   1 ATGATTACAATAGATAAAATTTTAGAAATTTTAAAAAATGACCATAATTTCAGAGAGATTTTGTTTCATGAGCATTATTATTATAACTGGACACAAAATG 100

          110       120       130       140       150       160       170       180       190       200
           *         *         *         *         *         *         *         *         *         *
 101 TAACTTTTAATGCCTTATCATATGATAGTCGTCAAATTTCATCTGATACTTTATTTTTCGCTAAGGGTGCTACTTTTAAAAAAGAATATCTAGATTCTGC 200

          210       220       230       240       250       260       270       280       290       300
           *         *         *         *         *         *         *         *         *         *
 201 AATCACAGCAGGCCTTTCTTTTTACGTTTCTGAGATAGATTACGGCGCCGATATTCCAGTGATATTAGTCAATGATATCAAAAAAGCCATGAGTTTGATA 300

          310       320       330       340       350       360       370       380       390       400
           *         *         *         *         *         *         *         *         *         *
 301 TCTATGTCTTTCTATAATAACCCACAAAACAAACTTAAACTTCTAGCTTTTACTGGAACAAAAGGAAAAACAACTGCGGCTTACTTTGCTTATCATATGT 400

          410       420       430       440       450       460       470       480       490       500
           *         *         *         *         *         *         *         *         *         *
 401 TAAAAGTAAACCATCGTCCTGCTATGCTCTCAACTATGAACACAACATTAGATGGTAAATCTTTCTTTAAATCACATCTCACAACCCCCGAGAGTCTTGA 500

          510       520       530       540       550       560       570       580       590       600
           *         *         *         *         *         *         *         *         *         *
 501 TTTATTTCGGATGATGGCTACAGCTGTTGAGAATCAAATGACACACTTAGTTATGGAAGTATCAAGCCAAGCATACCTAACCAAACGTGTTTATGGTTTA 600

          610       620       630       640       650       660       670       680       690       700
           *         *         *         *         *         *         *         *         *         *
 601 ACCTTTGACGTTGGCGTTTTCTTAAATATTAGTCCCGATCATATTGGTCCTATCGAGCACCCTACATTCGAAGATTATTTTTTCCACAAACGGCTCTTGA 700

          710       720       730       740       750       760       770       780       790       800
           *         *         *         *         *         *         *         *         *         *
 701 TGGAGAATAGCAATGCTGTTGTTGTAAATAGTCAGATGGATCATTTTAATATTGTCAAAGAACAGGTAGAATATATTCCTCATGATTTCTATGGAGATTA 800

          810       820       830       840       850       860       870       880       890       900
           *         *         *         *         *         *         *         *         *         *
 801 TTCTGAAAATGTTATCACAGAATCACAGGCCTTTTCTTTCCATGTCAAAGGAAAGTTGGAGAACACCTACGATATCAAGCTGATTGGAAAATTCAATCAA 900

          910       920       930       940       950       960       970       980       990      1000
           *         *         *         *         *         *         *         *         *         *
 901 GAAAATGCTATCGCAGCTGGACTTGCTTGTCTCCGACTTGGTGTTTCAATTGAAGATATAAAAAACGGAATTGCACAAACTACCGTTCCTGGCCGCATGG 1000

         1010      1020      1030      1040      1050      1060      1070      1080      1090      1100
           *         *         *         *         *         *         *         *         *         *
1001 AAGTCCTAACACAAACCAACGGCGCAAAGATTTTCGTTGACTATGCCCACAACGGAGACAGTTTGAAGAAATTATTAGCTGTTGTTGAGGAACACCAAAA 1100

         1110      1120      1130      1140      1150      1160      1170      1180      1190      1200
           *         *         *         *         *         *         *         *         *         *
1101 AGGGGATATTATATTAGTGCTCGGAGCTCCTGGTAATAAAGGTCAAAGCCGTCGTAAAGACTTCGGAGATGTCATTAATCAACATCCTAATCTACAAGTG 1200

         1210      1220      1230      1240      1250      1260      1270      1280      1290      1300
           *         *         *         *         *         *         *         *         *         *
1201 ATACTCACTGCAGATGATCCTAATTTTGAAGATCCCTTAGTTATCTCACAAGAAATAGCAAGCCATATTAATCGTCCGGTTACTATCATCATTGATCGAG 1300

         1310      1320      1330      1340      1350      1360      1370      1380      1390      1400
           *         *         *         *         *         *         *         *         *         *
1301 AAGAAGCAATTGCTAATGCCAGTACTCTTACTAATTGCAAACTAGATGCAATTATTATCGCTGGTAAAGGGGCAGATGCTTATCAAATTATCAAAGGAAA 1400

         1410      1420      1430      1440      1450
           *         *         *         *         *
1401 TCATGACAATTACTCTGGAGATTTAGAAGTTGCGAAAAAATACCTTAAACGATAA 1455
```

Supplementary 7

Cleavage of His tag from *S. agalactiae* MurD

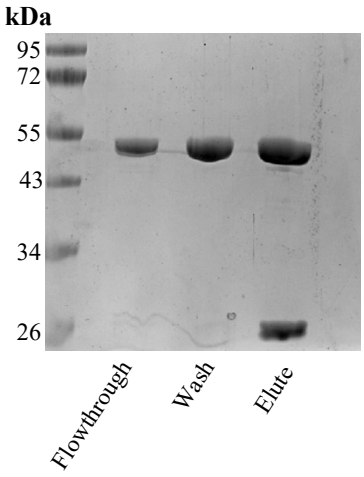

Figure S7. 1: Cleavage of His tag from MurD from S. agalactiae

MurD from *S. agalactiae* was purified via IMAC Ni column. Overnight dialysis was carried out into Buffer GF in the presence of 3C to cleave the His tag. The sample was then purified via reverse IMAC and the cleaved protein present in the flow-through was stored for use within MST.

Supplementary 8

pET DUET MurD does not bind to Ni IMAC column

MurD was cloned into the second open reading frame of pET DUET with no tag. Expression and purification of MurD was carried out using the same condiitions as the duel pET DUET system. MurD was seen within the flow-through and wash steps, but was not present within the elution.

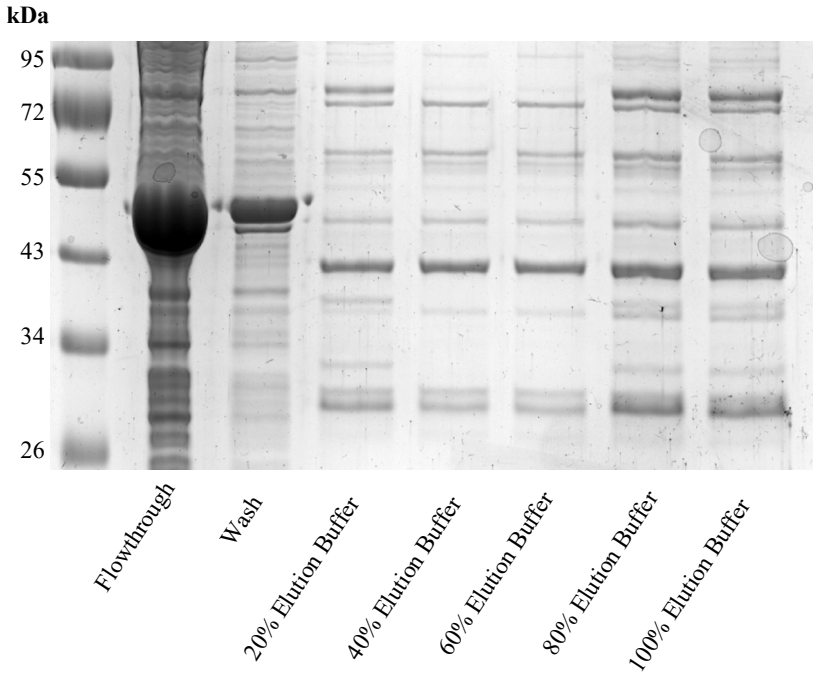

Figure S8. 1: MurD does not bind an IMAC Ni column without a His tag

MurD without a His tag does not bind to a Ni IMAC column. pET DUET MurD was expressed and purified via an Ni IMAC column. MurD was present within the flow-through and wash steps. MurD was not present within the elution steps.

Bibliography

1. Brochet, M. *et al.* Genomic diversity and evolution within the species Streptococcus agalactiae. *Microbes Infect.* **8**, 1227–1243 (2006).
2. Raabe, V. N. & Shane, A. L. Group B Streptococcus (Streptococcus agalactiae). *Microbiol. Spectr.* **7**, (2019).
3. Glaser, P. *et al.* Genome sequence of Streptococcus agalactiae, a pathogen causing invasive neonatal disease. *Mol. Microbiol.* **45**, 1499–1513 (2002).
4. Hanson, B. R. *et al.* Functional analysis of the CpsA protein of Streptococcus agalactiae. *J. Bacteriol.* **194**, 1668–1678 (2012).
5. Collin, S. M., Shetty, N. & Lamagni, T. Invasive Group B Streptococcus Infections in Adults, England, 2015–2016. *Emerg. Infect. Dis.* **26**, 1174 (2020).
6. Farley, M. M. Group B streptococcal disease in nonpregnant adults. *Clin. Infect. Dis.* **33**, 556–561 (2001).
7. Vergnano, S., Sharland, M., Kazembe, P., Mwansambo, C. & Heath, P. T. Neonatal sepsis: an international perspective. *Arch. Dis. Child. Fetal Neonatal Ed.* **90**, F220 (2005).
8. Camacho-Gonzalez, A., Spearman, P. W. & Stoll, B. J. Neonatal Infectious Diseases: Evaluation of Neonatal Sepsis. *Pediatr. Clin. North Am.* **60**, 367–389 (2013).
9. Benjamin Cailes, Christina Kortsalioudaki, Jim Buttery, Santosh Pattnayak, Anne Greenough, Jean Matthes, Alison Bedford Russell, Nigel Kennea, P. T. H. Epidemiology of UK neonatal infections: the neonIN infection surveillance network. *Arch. Dis. Child. - Fetal Neonatal Ed.* **103**, F547–F553 (2018).
10. Giannoni, E. *et al.* Neonatal Sepsis of Early Onset, and Hospital-Acquired and Community-Acquired Late Onset: A Prospective Population-Based Cohort Study. *J. Pediatr.* **201**, 106-114.e4 (2018).
11. R Tiskumara, S H Fakharee, C Q Liu, P Nuntnarumit, K M Lui, M Hammoud, J K F Lee, C B Chow, A Shenoi, R Halliday, D. I. Neonatal infections in Asia. *Arch. Dis. Child. - Fetal Neonatal Ed.* **94**, F144–F148 (2009).

12. Shane, A. L. & Stoll, B. J. Neonatal sepsis: progress towards improved outcomes. *J. Infect.* **68 Suppl 1**, (2014).
13. Singh, T., Barnes, E. H. & Isaacs, D. Early-onset neonatal infections in Australia and New Zealand, 2002-2012. *Arch. Dis. Child. Fetal Neonatal Ed.* **104**, F248–F252 (2019).
14. Velaphi, S. C. *et al.* Surveillance for incidence and etiology of early-onset neonatal sepsis in Soweto, South Africa. *PLoS One* **14**, (2019).
15. Chaurasia, S. *et al.* Neonatal sepsis in South Asia: huge burden and spiralling antimicrobial resistance. *BMJ* **364**, (2019).
16. Dr L Ratnayake. Empirical Antibiotic Guideline for Neonates. (2015).
17. Cailes, B. *et al.* Antimicrobial resistance in UK neonatal units: NeonIN infection surveillance network. *Arch. Dis. Child. Fetal Neonatal Ed.* **103**, F474–F478 (2018).
18. EUCAST. eucast: Clinical breakpoints and dosing of antibiotics. https://www.eucast.org/clinical_breakpoints/ (2022).
19. Stoll, B. J. *et al.* Early onset neonatal sepsis: the burden of group B Streptococcal and E. coli disease continues. *Pediatrics* **127**, 817–826 (2011).
20. Garland, S. M. *et al.* Antimicrobial resistance in group B streptococcus: the Australian experience. *J. Med. Microbiol.* **60**, 230–235 (2011).
21. Lamagni, T. L. *et al.* Emerging Trends in the Epidemiology ofInvasive Group B Streptococcal Disease inEngland and Wales, 1991–2010. *Clin Infect Dis* **57**, 682–8 (2013).
22. Höltje, J.-V. Growth of the Stress-Bearing and Shape-Maintaining Murein Sacculus of Escherichia coli . *Microbiol. Mol. Biol. Rev.* **62**, 181–203 (1998).
23. El Zoeiby, A., Sanschagrin, F. & Levesque, R. C. Structure and function of the Mur enzymes: development of novel inhibitors. *Mol. Microbiol.* **47**, 1–12 (2003).
24. Sobhanifar, S., King, D. T. & Strynadka, N. C. J. Fortifying the wall: synthesis, regulation and degradation of bacterial peptidoglycan. *Curr. Opin. Struct. Biol.* **23**, 695–703 (2013).
25. Van Heijenoort, J. Recent advances in the formation of the bacterial peptidoglycan monomer unit. *Nat. Prod. Rep.* **18**, 503–519 (2001).

26. Münch, D. *et al.* Identification and in vitro Analysis of the GatD/MurT Enzyme-Complex Catalyzing Lipid II Amidation in Staphylococcus aureus. *Plos Pathog.* **8**, e1002509 (2012).
27. Lloyd, A. J. *et al.* Characterization of tRNA-dependent Peptide Bond Formation by MurM in the Synthesis of Streptococcus pneumoniae Peptidoglycan * □ S. *J. Biol. Chem.* **283**, 6402–6417 (2008).
28. Kuk, A. C. Y., Hao, A. & Lee, S. Y. Structure and Mechanism of the Lipid Flippase MurJ. *https://doi.org/10.1146/annurev-biochem-040320-105145* **91**, 705–729 (2022).
29. Pazos, M. & Vollmer, W. Regulation and function of class A Penicillin-binding proteins. *Curr. Opin. Microbiol.* **60**, 80–87 (2021).
30. Otten, C., Brilli, M., Vollmer, W., Viollier, P. H. & Salje, J. Peptidoglycan in obligate intracellular bacteria. *Mol. Microbiol.* **107**, 142–163 (2018).
31. Dowson, A. J. *et al.* Plant peptidoglycan precursor biosynthesis: Conservation between moss chloroplasts and Gram-negative bacteria. *Plant Physiol.* **190**, 165–179 (2022).
32. Skarzynski, T. *et al.* Structure of UDP-N-acetylglucosamine enolpyruvyl transferase, an enzyme essential for the synthesis of bacterial peptidoglycan, complexed with substrate UDP-N-acetylglucosamine and the drug fosfomycin. *Structure* **4**, 1465–1474 (1996).
33. Batson, S. *et al.* Inhibition of D-Ala:D-Ala ligase through a phosphorylated form of the antibiotic D-cycloserine. *Nat. Commun. 2017 81* **8**, 1–7 (2017).
34. Hakulinen, J. K. *et al.* MraY–antibiotic complex reveals details of tunicamycin mode of action. *Nat. Chem. Biol.* **13**, 265–267 (2017).
35. Wang, B. *et al.* Total Synthesis of Mannopeptimycins α and β. *J. Am. Chem. Soc.* **138**, 3926–3932 (2016).
36. Wang, J. *et al.* Total Synthesis of Mannopeptimycin β via β-Hydroxyenduracididine Ligation. *Cite This J. Am. Chem. Soc* **143**, (2021).
37. Prince, A. *et al.* Lipid-II Independent Antimicrobial Mechanism of Nisin Depends On Its Crowding And Degree Of Oligomerization. *Sci. Reports 2016 61* **6**, 1–15 (2016).
38. Brötz, H. *et al.* Role of lipid-bound peptidoglycan precursors in the formation

of pores by nisin, epidermin and other lantibiotics. *Mol. Microbiol.* **30**, 317–327 (1998).

39. Viel, J. H., Jaarsma, A. H. & Kuipers, O. P. Heterologous Expression of Mersacidin in Escherichia coli Elucidates the Mode of Leader Processing. *ACS Synth. Biol.* **10**, 600–608 (2021).
40. Butler, M. S., Hansford, K. A., Blaskovich, M. A. T., Halai, R. & Cooper, M. A. Glycopeptide antibiotics: Back to the future. *J. Antibiot. 2014 679* **67**, 631–644 (2014).
41. Hamburger, J. B. *et al.* A crystal structure of a dimer of the antibiotic ramoplanin illustrates membrane positioning and a potential Lipid II docking interface. *Proc. Natl. Acad. Sci. U. S. A.* **106**, 13759–13764 (2009).
42. Vollmerhaus, P. J., Breukink, E. & Heck, A. J. R. Getting closer to the real bacterial cell wall target: Biomolecular interactions of water-soluble lipid II with glycopeptide antibiotics. *Chem. - A Eur. J.* **9**, 1556–1565 (2003).
43. Kang, H. K. & Park, Y. Glycopeptide Antibiotics: Structure and Mechanisms of Action. *J. Bacteriol. Virol.* **45**, 67–78 (2015).
44. Cheng, T. J. R. *et al.* Domain requirement of moenomycin binding to bifunctional transglycosylases and development of high-throughput discovery of antibiotics. *Proc. Natl. Acad. Sci. U. S. A.* **105**, 431–436 (2008).
45. Ostash, B. & Walker, S. Moenomycin family antibiotics: chemical synthesis, biosynthesis, biological activity. *Nat. Prod. Rep.* **27**, 1594 (2010).
46. Macheboeuf, P., Contreras-Martel, C., Job, V., Dideberg, O. & Dessen, A. Penicillin Binding Proteins: key players in bacterial cell cycle and drug resistance processes. *FEMS Microbiol. Rev.* **30**, 673–691 (2006).
47. Bush, K. & Bradford, P. A. β-Lactams and β-Lactamase Inhibitors: An Overview. *Cold Spring Harb. Perspect. Med.* **6**, a025247 (2016).
48. Boniface, A., Bouhss, A., Mengin-Lecreulx, D. & Blanot, D. The MurE Synthetase from Thermotoga maritima Is Endowed with an Unusual D-Lysine Adding Activity *. (2006) doi:10.1074/jbc.M506311200.
49. Mizyed, S., Oddone, A., Byczynski, B., Hughes, D. W. & Berti, P. J. UDP-N-acetylmuramic acid (UDP-MurNAc) is a potent inhibitor of MurA (enolpyruvyl-UDP-GlcNAc synthase). *Biochemistry* **44**, 4011–4017 (2005).

50. Dhalla, A. M. *et al.* Steady-State Kinetic Mechanism of Escherichia coli UDP-Af-Acetylenolpyruvylglucosamine Reductase. *Biochemistry* **34**, 5390–5402 (1995).
51. Walsh, A. W. *et al.* Comparison of the d-Glutamate-Adding Enzymes from Selected Gram-Positive and Gram-Negative Bacteria. *J. Bacteriol.* **181**, 5395 (1999).
52. Paradis-Bleau, C. *et al.* Pseudomonas aeruginosa MurE amide ligase: enzyme kinetics and peptide inhibitor. *Biochem. J.* **421**, 263–272 (2009).
53. Michaud, C., Blanot, D., Flouret, B. & Heijenoort, Van, J. Partial purification and specificity studies of the d-glutamate-adding and d-alanyl-d-alanine-adding enzymes from Escherichia coli K12. *Eur. J. Biochem.* **166**, 631–637 (1987).
54. Mengin-Lecreulx, D., Flouret, B. & Van Heijenoort, J. Cytoplasmic steps of peptidoglycan synthesis in Escherichia coli. *J. Bacteriol.* **151**, 1109–1117 (1982).
55. Munshi, T. *et al.* Characterisation of ATP-Dependent Mur Ligases Involved in the Biogenesis of Cell Wall Peptidoglycan in Mycobacterium tuberculosis. *PLoS One* **8**, 60143 (2013).
56. Fiuza, M. *et al.* The MurC ligase essential for peptidoglycan biosynthesis is regulated by the serine/threonine protein kinase PknA in Corynebacterium glutamicum. *J. Biol. Chem.* **283**, 36553–36563 (2008).
57. Emanuele, J. J., Jin, H., Yanchunas, J. & Villafranca, J. J. Evaluation of the kinetic mechanism of Escherichia coli uridine diphosphate-N-acetylmuramate:L-alanine ligase. *Biochemistry* **36**, 7264–7271 (1997).
58. Bertrand, J. A. *et al.* Determination of the MurD mechanism through crystallographic analysis of enzyme complexes. *J. Mol. Biol.* **289**, 579–590 (1999).
59. Mol, C. D. *et al.* Crystal structures of active fully assembled substrate- and product-bound complexes of UDP-N-acetylmuramic acid:L-alanine ligase (MurC) from Haemophilus influenzae. *J. Bacteriol.* **185**, 4152–4162 (2003).
60. Gordon, E. *et al.* Crystal Structure of UDP-N-acetylmuramoyl-l-alanyl-d-glutamate:meso-Diaminopimelate Ligase from Escherichia Coli *. *J. Biol.*

Chem. **276**, 10999–11006 (2001).

61. Yan, Y. *et al.* Crystal structure of Escherichia coli UDPMurNAc-tripeptide D-alanyl-D-alanine-adding enzyme (MurF) at 2.3 Å resolution. *J. Mol. Biol.* **304**, 435–445 (2000).
62. Deva, T., Baker, E. N., Squire, C. J. & Smith, C. A. Structure of Escherichia coli UDP-N-acetylmuramoyl:l-alanine ligase (MurC). *Acta Crystallogr. Sect. D Struct. Biol.* **62**, 1466–1474 (2006).
63. Bertrand, J. A. *et al.* "Open" structures of MurD: domain movements and structural similarities with folylpolyglutamate synthetase. *J. Mol. Biol.* **301**, 1257–1266 (2000).
64. Smith, C. A. Structure, Function and Dynamics in the mur Family of Bacterial Cell Wall Ligases. *J. Mol. Biol.* **362**, 640–655 (2006).
65. Perdih, A., Kotnik, M., Hodoscek, M. & Solmajer, T. Targeted molecular dynamics simulation studies of binding and conformational changes in E. coli MurD. *Proteins Struct. Funct. Genet.* **68**, 243–254 (2007).
66. Šink, R. *et al.* Crystallographic Study of Peptidoglycan Biosynthesis Enzyme MurD: Domain Movement Revisited. *PLoS One* **11**, (2016).
67. Bugg, T. D. H. & Walsh, C. T. Intracellular steps of bacterial cell wall peptidoglycan biosynthesis: enzymology, antibiotics, and antibiotic resistance. *Nat. Prod. Rep.* **9**, 199–215 (1992).
68. Eveland, S. S., Pompliano, D. L. & Anderson, M. S. Conditionally Lethal Escherichia coli Murein Mutants Contain Point Defects That Map to Regions Conserved among Murein and Folyl Poly-γ-glutamate Ligases: Identification of a Ligase Superfamily. *Biochemistry* **36**, 6223–6229 (1997).
69. Bouhss, A., Mengin-Lecreulx, D., Blanot, D., Van Heijenoort, J. & Parquet, C. Invariant Amino Acids in the Mur Peptide Synthetases of Bacterial Peptidoglycan Synthesis and Their Modification by Site-Directed Mutagenesis in the UDP-MurNAc:l-Alanine Ligase from Escherichia coli†. *Biochemistry* **36**, 11556–11563 (1997).
70. Tomašictomašic´, T. *et al.* 5-Benzylidenethiazolidin-4-ones as Multitarget Inhibitors of Bacterial Mur Ligases. *ChemMedChem* **5**, 286–295 (2010).
71. Tanner, M. E., Vaganay, S., Van Heijenoort, J. & Blanot, D. Phosphinate

Inhibitors of the D-Glutamic Acid-Adding Enzyme of Peptidoglycan Biosynthesis. *J. Org. Chem.* **61**, 1756–1760 (1996).

72. Štrancar, K., Boniface, A. & Gobec, S. Phosphinate Inhibitors of UDP-N-Acetylmuramoyl-L-Alanyl-D-Glutamate: L-Lysine Ligase (MurE). *Arch. Pharm. Chem. Life Sci* **340**, 127–134 (2007).
73. Perdih, A. *et al.* Benzene-1,3-dicarboxylic acid 2,5-dimethylpyrrole derivatives as multiple inhibitors of bacterial Mur ligases (MurC-MurF). *Bioorganic Med. Chem.* **22**, 4124–4134 (2014).
74. Longenecker, K. L. *et al.* Structure of MurF from Streptococcus pneumoniae co-crystallized with a small molecule inhibitor exhibits interdomain closure. *Protein Sci* **14**, 3039–3047 (2005).
75. Hrast, M. *et al.* Structure-activity relationships of new cyanothiophene inhibitors of the essential peptidoglycan biosynthesis enzyme MurF. *Eur. J. Med. Chem.* **66**, 32–45 (2013).
76. Nikaido, H. Preventing drug access to targets: Cell surface permeability barriers and active efflux in bacteria. *Semin. Cell Dev. Biol.* **12**, 215–223 (2001).
77. Hameed, P. S. *et al.* Pyrazolopyrimidines establish MurC as a vulnerable target in Pseudomonas aeruginosa and Escherichia coli. *ACS Chem. Biol.* **9**, 2274–2282 (2014).
78. Jukič, M., Gobec, S. & Sova, M. Reaching toward underexplored targets in antibacterial drug design. *Drug Dev. Res.* **80**, 6–10 (2019).
79. Nöldeke, E. R. *et al.* Structural basis of cell wall peptidoglycan amidation by the GatD/MurT complex of Staphylococcus aureus. *Sci. Reports 2018 81* **8**, 1–15 (2018).
80. White, C. L., Kitich, A. & Gober, J. W. Positioning cell wall synthetic complexes by the bacterial morphogenetic proteins MreB and MreD. *Mol. Microbiol.* **76**, 616–633 (2010).
81. Favini-Stabile, S., Contreras-Martel, C., Thielens, N. & Dessen, A. MreB and MurG as scaffolds for the cytoplasmic steps of peptidoglycan biosynthesis. *Environ. Microbiol.* **15**, 3218–3228 (2013).
82. Miyachiro, M. M. *et al.* Complex Formation between Mur Enzymes from

Streptococcus pneumoniae. *Biochemistry* **58**, 3314–3324 (2019).

83. Laddomada, F. *et al.* the MurG glycosyltransferase provides an oligomeric scaffold for the cytoplasmic steps of peptidoglycan biosynthesis in the human pathogen Bordetella pertussis. *Sci Rep* **9**, (2019).
84. O'Neill, J. *TACKLING DRUG-RESISTANT INFECTIONS GLOBALLY: FINAL REPORT AND RECOMMENDATIONS*. (2016).
85. Sangshetti, J. N., Joshi, S. S., Patil, R. H., Moloney, M. G. & Shinde, D. B. Mur Ligase Inhibitors as Anti-bacterials: A Comprehensive Review. *Curr. Pharm. Des.* **23**, (2017).
86. Dawson, R.M.C.; Elliot, D.C.; Elliot, W.H.; Jones, K. M. *Data for biochemical research (Third Edition)*. *Clarendon Press, Oxford* (1986).
87. Lloyd, A. J., Thomann, H.-U., Ibba, M. & Soil, D. *A broadly applicable continuous spectrophotometric assay for measuring aminoacyl-tRNA synthetase activity*. *Nucleic Acids Research* vol. 23 https://academic.oup.com/nar/article/23/15/2886/1111818 (1995).
88. Pelley, J. W. Enzymes and Energetics. in *Elsevier's Integrated Review Biochemistry* 29–37 (W.B. Saunders, 2012). doi:10.1016/B978-0-323-07446-9.00004-0.
89. Yung-Chi, C. & Prusoff, W. H. Relationship between the inhibition constant (KI) and the concentration of inhibitor which causes 50 per cent inhibition (I50) of an enzymatic reaction. *Biochem. Pharmacol.* **22**, 3099–3108 (1973).
90. Zhang, J. H., Chung, T. D. Y. & Oldenburg, K. R. A simple statistical parameter for use in evaluation and validation of high throughput screening assays. *J. Biomol. Screen.* **4**, (1999).
91. Birmingham, A. *et al.* Statistical methods for analysis of high-throughput RNA interference screens. *Nature Methods* vol. 6 (2009).
92. Acker, M. G. & Auld, D. S. Considerations for the design and reporting of enzyme assays in high-throughput screening applications. *Perspect. Sci.* **1**, 56–73 (2014).
93. Hall, M. D. *et al.* Fluorescence polarization assays in high-throughput screening and drug discovery: a review. *Methods Appl. Fluoresc.* **4**, 022001 (2016).

94. Klingler, F. M. *et al.* Approved drugs containing thiols as inhibitors of metallo-β-lactamases: Strategy to combat multidrug-resistant bacteria. *J. Med. Chem.* **58**, 3626–3630 (2015).

95. Sullivan, K. L., Huma, L. C., Mullins, E. A., Johnson, M. E. & Kappock, T. J. Metal stopping reagents facilitate discontinuous activity assays of the de novo purine biosynthesis enzyme PurE. *Anal. Biochem.* **452**, 43–45 (2014).

96. Mayr, L. M. & Bojanic, D. Novel trends in high-throughput screening. *Curr. Opin. Pharmacol.* **9**, 580–588 (2009).

97. Tsai, J. *et al.* Discovery of a selective inhibitor of oncogenic B-Raf kinase with potent antimelanoma activity. *Proc. Natl. Acad. Sci. U. S. A.* **105**, 3041–3046 (2008).

98. Patel, D., Bauman, J. D. & Arnold, E. Advantages of crystallographic fragment screening: Functional and mechanistic insights from a powerful platform for efficient drug discovery. *Prog. Biophys. Mol. Biol.* **116**, 92–100 (2014).

99. Cox, O. B. *et al.* A poised fragment library enables rapid synthetic expansion yielding the first reported inhibitors of PHIP(2), an atypical bromodomain. *Chem. Sci.* **7**, 2322–2330 (2016).

100. Aykul, S. & Martinez-Hackert, E. Determination of half-maximal inhibitory concentration using biosensor-based protein interaction analysis. *Anal. Biochem.* **508**, 97–103 (2016).

101. Zielonka, J. *et al.* Mitigation of NADPH oxidase 2 activity as a strategy to inhibit peroxynitrite formation. *J. Biol. Chem.* **291**, 7029–7044 (2016).

102. Hrast, M. *et al.* Evaluation of the published kinase inhibitor set to identify multiple inhibitors of bacterial ATP-dependent mur ligases. *J. Enzyme Inhib. Med. Chem.* **34**, 1010–1017 (2019).

103. Tomašić, T. *et al.* Virtual screening for potential inhibitors of bacterial MurC and MurD ligases. *J. Mol. Model.* **18**, 1063–1072 (2012).

104. Zidar, N. *et al.* New 5-benzylidenethiazolidin-4-one inhibitors of bacterial MurD ligase: Design, synthesis, crystal structures, and biological evaluation. *Eur. J. Med. Chem.* **46**, 5512–5523 (2011).

105. Christopeit, T., Carlsen, T. J. O., Helland, R. & Leiros, H. K. S. Discovery of Novel Inhibitor Scaffolds against the Metallo-β-lactamase VIM-2 by Surface

Plasmon Resonance (SPR) Based Fragment Screening. *J. Med. Chem.* **58**, 8671–8682 (2015).

106. Friesner, R. A. *et al.* Extra precision glide: Docking and scoring incorporating a model of hydrophobic enclosure for protein-ligand complexes. *J. Med. Chem.* **49**, 6177–6196 (2006).
107. Prlić, A. *et al.* Pre-calculated protein structure alignments at the RCSB PDB website. *Bioinformatics* **26**, 2983–2985 (2010).
108. Eniyan, K. *et al.* Screening of Antitubercular Compound Library Identifies Inhibitors of Mur Enzymes in Mycobacterium tuberculosis. *Acta Crystallogr. Sect. D Struct. Biol.* **25**, 70–78 (2020).
109. Alhadrami, H. A., Abdulaal, W. H., Hassan, H. M., Alhakamy, N. A. & Sayed, A. M. In Silico-Based Discovery of Natural Anthraquinones with Potential against Multidrug-Resistant E. coli. *Pharmaceuticals* **15**, (2022).
110. Miller, J. R. *et al.* A class of selective antibacterials derived from a protein kinase inhibitor pharmacophore. *Proc. Natl. Acad. Sci. U. S. A.* **106**, 1737 (2009).
111. Wu, P., Nielsen, T. E. & Clausen, M. H. FDA-approved small-molecule kinase inhibitors. *Trends Pharmacol. Sci.* **36**, 422–439 (2015).
112. Castillo, M. *et al.* Highly potent aminopyridines as Syk kinase inhibitors. *Bioorg. Med. Chem. Lett.* **22**, 5419–5423 (2012).
113. buildbot. Schrödinger Press Canvas User Manual Canvas 2.4 User Manual Canvas User Manual. (2015).
114. Schrodinger. *Schrödinger Press Glide User Manual Glide 6.7 User Manual Glide User Manual*. (2015).
115. Benfenati, E. *et al.* Characterization of chemical structures. in *Quantitative Structure-Activity Relationships (QSAR) for Pesticide Regulatory Purposes* 83–109 (Elsevier, 2007). doi:10.1016/B978-044452710-3/50005-7.
116. Azam, M. A. & Jupudi, S. Structure-based virtual screening to identify inhibitors against Staphylococcus aureus MurD enzyme. *Struct. Chem.* **30**, 2123–2133 (2019).
117. Perdih, A. *et al.* Discovery of novel benzene 1,3-dicarboxylic acid inhibitors of bacterial MurD and MurE ligases by structure-based virtual screening

approach. *Bioorg. Med. Chem. Lett.* **19**, 2668–2673 (2009).

118. Škedelj, V., Tomašić, T., Mašič, L. P. & Zega, A. ATP-binding site of bacterial enzymes as a target for antibacterial drug design. *J. Med. Chem.* **54**, 915–929 (2011).
119. Triola, G. *et al.* ATP competitive inhibitors of d-alanine–d-alanine ligase based on protein kinase inhibitor scaffolds. *Bioorg. Med. Chem.* **17**, 1079–1087 (2009).
120. Rognan, D. The impact of in silico screening in the discovery of novel and safer drug candidates. *Pharmacol. Ther.* **175**, 47–66 (2017).
121. Gray, D. A. & Wenzel, M. Multitarget Approaches against Multiresistant Superbugs. *ACS Infect. Dis.* **6**, 1346 (2020).
122. Vazquez, M. J., Rodriguez, B., Zapatero, C. & Tew, D. G. Determination of phosphate in nanomolar range by an enzyme-coupling fluorescent method. *Anal. Biochem.* **320**, 292–298 (2003).
123. Goddard, J. P. & Reymond, J. L. Enzyme assays for high-throughput screening. *Curr. Opin. Biotechnol.* **15**, 314–322 (2004).
124. Simeonov, A. & Davis, M. I. Interference with Fluorescence and Absorbance. *Assay Guid. Man.* (2018).
125. Liu, Y., Zalameda, L., Ki, W. K., Wang, M. & McCarter, J. D. Discovery of acetyl-coenzyme A carboxylase 2 inhibitors: comparison of a fluorescence intensity-based phosphate assay and a fluorescence polarization-based ADP Assay for high-throughput screening. *Assay Drug Dev. Technol.* **5**, 225–235 (2007).
126. Morita, S. Y., Ueda, K. & Kitagawa, S. Enzymatic measurement of phosphatidic acid in cultured cells. *J. Lipid Res.* **50**, 1945 (2009).
127. Morita, S. Y., Ueda, K. & Kitagawa, S. Enzymatic measurement of phosphatidic acid in cultured cells. *J. Lipid Res.* **50**, 1945–1952 (2009).
128. Le, P. *et al.* Repurposing human kinase inhibitors to create an antibiotic active against drug-resistant Staphylococcus aureus, persisters and biofilms. *Nat. Chem. 2019 122* **12**, 145–158 (2019).
129. Lamoree, B. & Hubbard, R. E. Using Fragment-Based Approaches to Discover New Antibiotics. *Slas Discov.* **23**, 495 (2018).

130. Wells, J. N., Bergendahl, L. T. & Marsh, J. A. Operon Gene Order Is Optimized for Ordered Protein Complex Assembly. *Cell Rep.* **14**, 679–685 (2016).
131. Seidel, S. A. I. *et al.* Microscale thermophoresis quantifies biomolecular interactions under previously challenging conditions. *Methods* **59**, 301–315 (2013).
132. Jerabek-Willemsen, M. *et al.* MicroScale Thermophoresis: Interaction analysis and beyond. *J. Mol. Struct.* **1077**, 101–113 (2014).
133. Rombauts, W., Feytons, V. & Wittmann-Liebold, B. The primary structure of protein L17 from the Escherichia coli ribosome. *FEBS Lett.* **149**, 320–327 (1982).
134. Baspinar, A., Cukuroglu, E., Nussinov, R., Keskin, O. & Gursoy, A. PRISM: a web server and repository for prediction of protein–protein interactions and modeling their 3D complexes. *Nucleic Acids Res.* **42**, W285 (2014).
135. Schwede, T., Kopp, J., Guex, N. & Peitsch, M. C. SWISS-MODEL: an automated protein homology-modeling server. *Nucleic Acids Res.* **31**, 3381 (2003).
136. Jumper, J. *et al.* Highly accurate protein structure prediction with AlphaFold. *Nat. 2021 5967873* **596**, 583–589 (2021).
137. Evans, R. *et al.* Protein complex prediction with AlphaFold-Multimer. *bioRxiv* 2021.10.04.463034 (2022) doi:10.1101/2021.10.04.463034.
138. Guo, H. B. *et al.* AlphaFold2 models indicate that protein sequence determines both structure and dynamics. *Sci. Reports 2022 121* **12**, 1–15 (2022).
139. Douangamath, A. *et al.* Structural evidence for ammonia tunneling across the (βα)8 barrel of the imidazole glycerol phosphate synthase bienzyme complex. *Structure* **10**, 185–193 (2002).
140. Perrakis, A. & Sixma, T. K. AI revolutions in biology. *EMBO Rep.* **22**, e54046 (2021).
141. Brautigam, C. A., Tso, S. C., Deka, R. K., Liu, W. Z. & Norgard, M. V. Using modern approaches to sedimentation velocity to detect conformational changes in proteins. *Eur. Biophys. J.* **49**, 729 (2020).
142. Wu, N., Tsuji, S. Y., Cane, D. E. & Khosla, C. Assessing the Balance between Protein-Protein Interactions and Enzyme-Substrate Interactions in the

Channeling of Intermediates between Polyketide Synthase Modules. (2001) doi:10.1021/ja010219t.

143. Kuo, Y. M., Henry, R. A. & Andrews, A. J. Measuring specificity in multi-substrate/product systems as a simple tool to investigate selectivity in vivo. *Biochim. Biophys. Acta* **1864**, 70 (2016).

144. Manzi, L. *et al.* Carbene footprinting accurately maps binding sites in protein–ligand and protein–protein interactions. *Nat. Commun. 2016 71* **7**, 1–9 (2016).

145. NICE. *Asciminib for treating chronic myeloid leukaemia after 2 or more tyrosine kinase inhibitors Technology appraisal guidance*. www.nice.org.uk/guidance/ta813 (2022).

146. Schoepfer, J. *et al.* Discovery of Asciminib (ABL001), an Allosteric Inhibitor of the Tyrosine Kinase Activity of BCR-ABL1. *J. Med. Chem.* **61**, 8120–8135 (2018).

147. Murray, C. W., Newell, D. R. & Angibaud, P. A successful collaboration between academia, biotech and pharma led to discovery of erdafitinib, a selective FGFR inhibitor recently approved by the FDA. *Medchemcomm* **10**, 1509–1511 (2019).

148. Gupta, A. *et al.* A Polymorphism in leuS Confers Reduced Susceptibility to GSK2251052 in a Clinical Isolate of Staphylococcus aureus. *Antimicrob. Agents Chemother.* **60**, 3219 (2016).

149. Favini-Stabile, S., Contreras-Martel, C., Thielens, N. & Dessen, A. MreB and MurG as scaffolds for the cytoplasmic steps of peptidoglycan biosynthesis. (2013) doi:10.1111/1462-2920.12171.

150. Holdgate, G. A., Meek, T. D. & Grimley, R. L. Mechanistic enzymology in drug discovery: a fresh perspective. *Nat. Rev. Drug Discov. 2017 172* **17**, 115–132 (2017).

151. Boes, A., Olatunji, S., Mohammadi, T., Breukink, E. & Terrak, M. Fluorescence anisotropy assays for high throughput screening of compounds binding to lipid II, PBP1b, FtsW and MurJ. *Sci. Reports 2020 101* **10**, 1–8 (2020).

152. Manesh, A. & Varghese, G. M. Rising antimicrobial resistance: an evolving epidemic in a pandemic. *The Lancet Microbe* **2**, e419–e420 (2021).